The challenges of multi-mineral assemblages in the reverse cationic flotation of iron ores

Carlos Henrique Veloso de Melo

Université de Lorraine
UMR 7359 GeoRessources CNRS-UL
École Doctorale SIReNa

Thèse CIFRE financée par :
ArcelorMittal Global R&D Mining

The challenges of multi-mineral assemblages in the reverse cationic flotation of iron ores

Les défis des assemblages multi-minéraux dans la flottation cationique inverse des minerais de fer

par
Carlos Veloso

Thèse présentée pour l'obtention du titre de
Docteur de l'Université de Lorraine en Géosciences

Soutenance publique le 11 Octobre 2019

Membres du Jury

Saija Luukkanen	Professeur, Université de Oulu, Finlande	Rapporteur
Rosa M. F. Lima	Professeur, Université de Ouro Preto, Brésil	Rapporteur
Vanessa Fierro	Directrice de Recherche, Université de Lorraine, France	Examinateur
Armando C. Araujo	Principal Scientist Mining, ArcelorMittal Global R&D, France	Examinateur
Daniel Fornasiero	Professeur associé, Université de South Australia, Australie	Invité
Michael Badawi	Maître de conférence, Université de Lorraine, France	Invité
Inna Filippova	Chargée de Recherche, Université de Lorraine, France	Co-Directrice de Thèse
Lev Filippov	Professeur, Université de Lorraine, France	Directeur de Thèse

Abstract

Iron ore is the main raw material for the steel production and generally it must be processed to reach the specifications required by the steel industry. The iron ore mining industry is now facing increasingly lean-grade deposits with complex mineral assemblages. This study addresses the upgrade of a magnetic concentrate from Peña Colorada mine in Mexico by reverse cationic flotation.

Peña Colorada deposit is an iron skarn with an average iron content of 36%. It is composed by several mineral phases that were identified in a detailed mineralogical characterisation programme. Iron-bearing silicates such as chamosite and epidote are the problematic minerals to draw attention to. They present certain properties that are like the iron oxides.

The current processing of this ore is made by magnetic separation and yet the silica content of the final concentrate remains between 4 and 5%, too high for the upstream process. Traditional techniques like magnetic separation or gravity separation are not capable to promote further separation. The intrinsic properties of these minerals do not have enough contrast and the liberation is reached only at micrometre sizes. Flotation is proposed in this study as a technique capable of playing with those properties to make this separation possible. The surface chemistry study of the minerals coupled with comparative adsorption isotherms with depressants, has shown that corn starch does not promote selectivity for such a complex iron ore, adsorbing on all minerals. The testing of alternative depressants highlighted humic acid as a viable depressant to sponsor the required level of selectivity in the separation by flotation.

Micro-flotation experiments with pure minerals show that chamosite behaves very similar to iron oxides, not presenting good floatability with amines, like the other two silicates. Bench flotation tests with a material previously screened at 53 µm leads to a high-quality concentrate with 1.82% of silica and 84% of iron recovery, when humic acid is selected as depressant. Locked cycle tests trying to simulate a continuous process gave an excellent response of a concentrate with 2.78% of silica and 85% of iron recovery, with an altered natural polysaccharide as depressant. Pilot tests also confirmed the feasibility of the method with a concentrate with 2.06% of silica content and 64% of iron recovery, that should be improved by the addition of more scavenger stages. The use of column flotation for this stage is entirely possible, considering that its tests indicated a high iron recovery of 96%.

A concentration route combining fine screening at 53 µm and reverse cationic flotation of silicates using alternative depressant as humic acid or altered natural polysaccharides has proven to be effective in achieving the desired quality levels for the iron concentrate at high iron recovery levels. Finally, molecular modelling identified that the strange behaviour of chamosite is mainly because it is less hydrophilic than the other minerals involved in flotation.

Résumé

Le minerai de fer est la principale matière première utilisée dans la production d'acier et doit en général être traité de manière à répondre aux spécifications requises par l'industrie de l'acier. L'industrie du minerai de fer fait désormais face à des gisements de plus en plus pauvres avec des assemblages de minéraux complexes. L'objective de cette étude est de valoriser un concentré magnétique de la mine de Peña Colorada (Mexique) via flottation cationique inverse.

La mine de Peña Colorada est un gisement de type skarn ayant une teneur moyenne en fer de 36%. Il est composé de plusieurs phases minérales identifiées dans un programme détaillé de caractérisation minéralogique. Les silicates de fer tels que la chamosite et l'épidote sont les minéraux les plus problématiques car ils présentent certaines propriétés proches des oxydes de fer.

Le traitement actuel de ce minerai se fait par séparation magnétique et pourtant la teneur en silice du concentré final reste comprise entre 4 et 5%, ce qui est trop élevé pour le traitement en amont. Les techniques traditionnelles telles que la séparation magnétique ou la séparation par gravité ne peuvent pas entrainer une séparation plus poussée. Les propriétés physiques de ces minéraux associés à la libération fine, atteinte seulement au niveau du micromètres, n'ont pas assez de contraste pour que cette séparation aye lieu. La flottation est proposée dans cette étude comme une technique capable de jouer plus finement avec ces propriétés pour rendre cette séparation possible. L'étude de la chimie de surface des minéraux, associée à des isothermes comparatifs d'adsorption avec des déprimants, a montré que l'amidon de maïs ne favorise pas la sélectivité pour un minerai de fer aussi complexe, puisqu'il s'adsorbe sur tous les minéraux. L'essai de déprimants alternatifs a montré que l'acide humique était un déprimant viable permettant de garantir le niveau de sélectivité requis dans la séparation par flottation.

Des expériences de micro-flottation avec des minéraux purs montrent que la chamosite se comporte de manière très similaire aux oxydes de fer, ne présentant pas de bonnes capacités de flottabilité avec les amines, comme les deux autres silicates. Les tests de flottation à l'échelle du laboratoire avec un matériau préalablement tamisé à 53 µm conduisent à un concentré de haute qualité avec 1,82% de silice et 84% de récupération de fer, lorsque l'acide humique est sélectionné comme déprimant. Des essais en circuit fermé (locked cycle test) tentant de simuler un processus continu ont donné une excellente réponse d'un concentré contenant 2,78% de silice et 85% de récupération de fer, avec un polysaccharide naturel modifié comme déprimant. Des essais pilotes ont également confirmé la faisabilité de la méthode avec un concentré contenant 2,06% de silice et 64% de récupération de fer, ce qui devrait être amélioré en ajoutant davantage d'étapes d'épuisage. L'utilisation de la flottation en colonne pour cette étape est tout à fait possible, étant donné que ses tests ont indiqué une récupération de fer élevée de 96%.

Une voie de concentration combinant un tamisage fin à 53 µm ainsi qu'une flottation cationique inverse des silicates en utilisant un déprimant alternatif comme l'acide humique ou des polysaccharides naturels modifiés s'est révélée efficace pour atteindre les niveaux de qualité souhaités pour le concentré de fer à des taux de récupération élevés. Enfin, la modélisation moléculaire a révélé que le comportement particulier de la chamosite est principalement dû au fait qu'elle est moins hydrophile que les autres minéraux impliqués dans la flottation.

Avant-propos

Le présent manuscrit de thèse est intégralement rédigé en anglais pour plusieurs raisons. D'une part, les objets à l'étude sont issus de la collaboration avec Arcelor-Mittal Global R&D, notamment par l'intermédiaire de son expert mines Armando Corrêa de Araujo. D'autre part, le jury est composé de membres internationaux, notamment les deux rapporteurs de la thèse, Prof. Saija Luukkanen (Université de Oulu, Finlande) et Prof. Rosa M. F. Lima (Université de Ouro Preto, Brésil). Un résumé étendu en français est inclus au manuscrit.

Acknowledgements

I would like to express my gratitude to my supervisors Prof. Lev Filippov and Dr. Inna Filippova for the support, guidance and valuable discussions they have provided during the course of my studies. My sincere thanks should also be extended to my mentor Dr. Armando Corrêa de Araujo for the encouragement and advice provided throughout my studies and also for his enthusiasm and confidence in my research, that motivates me a lot. I am very grateful to Dr. Michael Badawi who spared no effort in contributing to the study of molecular modelling, even not belonging to the same laboratory.

My deep appreciation goes to my reading committee members: Prof. Saija Luukkanen and Prof. Rosa M. F. Lima, for their time, interest and helpful comments. I would also like to thank the other two members of my oral defense committee: Prof. Vanessa Fierro and Dr. Daniel Fornasiero, for accepting to participate in the evaluation of this work and for their time.

I acknowledge Dr. Stéphanie Ouvrard from LSE laboratory for her help during my TOC measurements, Prof. Philippe Marion for sharing his vast knowledge in mineralogy, Prof. Paulo Viana from UFMG, Brazil and LIEC laboratory through Celine Caillet and Yves Waldvogel for the help with the electrophoresis measurements. I owe a sincere thank you to all my colleagues of "Bâtiment A". Fred, Pierric, Eric, Cédric, Jérôme, Bob, for the help during the pilot tests and Pabla for sharing her laboratory and tools when necessary. Special thanks are reserved for my fellow labmates Antony Geneyton and Yann Foucaud for the stimulating discussions we have had in the last three years. I also would like to extend thanks to all my colleagues at ArcelorMittal Maizières-lès-Metz. Yves for all the help with the characterisation. Arnaud, Marine and Géraldine for sharing their strong background in mineralogy. Rémi for all the technical help and the discussions about the life of a PhD student. Filipe, Josué and Lucas for all the support, discussions and advice that were essential during that time. Marcela for believing in my potential back at the time of my internship. Matthias, Marjolaine and Quentin for the help in the daily life of the laboratory. Audrey for organising the whole administrative part of the activities in such a dedicated way. Thanks also to all the interns who have helped me over these three years. Especially to Wilker for his excellent work and to Louis, currently my co-worker, who has always been willing to help.

Getting through my thesis required more than academic support, and I have many friends to thank for supporting me over the past three years. Thank you to all my Brazilian friends living in Metz, for being present during this time, it helped me a lot. Nathalie Fick for making me feel so good in France back in 2013 when I first arrived here. In addition, all my friends back home (Brazil) that even being physically far away, were present with their sense of care. Paloma and Paulinha, thank you for staying by me side. Thanks to Dr. José Ricardo Chaves for having started my French teaching, and for his sincere friendship.

The financial support from ArcelorMittal Global R&D and the ANRT (Association Nationale de la Recherche et de la Technologie) is gratefully acknowledged.

Por último e mais importante, agradeço à toda minha família, em especial minha avó, minha mãe e minha irmã. Obrigado por me apoiarem durante todos os desafios ao longo da minha vida, mesmo se isso significasse ficarmos longes. Amo muito vocês!

Résumé des travaux

Introduction

Le fer est le métal le plus employé au quotidien (e.g., construction, transport, objets de consommation). Les minéraux porteurs de fer les plus couramment rencontrés dans la nature et exploités de manière économique sont la magnétite [Fe_3O_4], l'hématite [Fe_2O_3], la goethite [FeO(OH)] et la sidérite [$FeCO_3$] (Filippov et al., 2014). Les minéraux porteurs de fer sont généralement associés à d'autres minéraux, dits de gangue, la plupart du temps non exploités économiquement, formant ce que l'on appelle du minerai de fer. Le minerai de fer est la principale source de fer pour les industries sidérurgiques mondiales. C'est traditionnellement le deuxième marché des commodités après le pétrole brut (US Geological Survey, 2018). Les minerais de fer consommés dans l'industrie sidérurgique exigent un certain niveau de qualité en fonction des usages, à savoir, une teneur en fer élevée (58–65% Fe en général) et inversement, une faible teneur en impuretés (e.g., Si, Al, P, S). Rares sont les minerais de fer qui ont déjà la qualité physico-chimique nécessaire pour être utilisés directement dans l'industrie sidérurgique. La plupart des minerais doivent être enrichis pour atteindre la qualité souhaitée. L'industrie du minerai de fer est de plus en plus confrontée à un déclin de ses gisements de haute qualité ; elle fait face à des minerais de moins en moins riches en fer et plus complexes en termes de minéralogie et de textures, qui nécessitent des procédés minéralurgiques adaptés pour être enrichis. ArcelorMittal est le plus grand producteur d'acier au monde et par conséquent l'un des plus gros consommateurs de minerai de fer. Une partie de sa consommation provient de la production des mines du groupe, situées dans le monde entier, et doit également faire face à cette problématique de dégradation de qualité des minerais.

Ce projet concerne spécifiquement un actif important de la société située dans l'ouest du Mexique : la mine de Peña Colorada. Une expansion de l'usine de traitement a débuté en 2017 afin de maintenir les mêmes niveaux de production en raison de la diminution de la teneur en fer du tout-venant de la mine. Cependant, le procédé de séparation magnétique actuellement utilisé ne permet pas de générer un concentré de qualité suffisante pour alimenter le procédé de pelletisation en aval. Plus particulièrement, la teneur en silice (SiO_2) du produit final, qui devrait être en moyenne à 2,5%, a augmenté jusqu'à environ 3,5% ces dernières années, avec des valeurs parfois supérieures en fonction de la partie du gisement exploité. L'objectif de la société est de faire en sorte que la qualité du produit soit maintenue aux mêmes niveaux de spécification (i.e., x% Fe minimum, y% SiO_2, z% Al_2O_3, ..., maximum) avec une récupération maximale de fer.

Le gisement de Peña Colorada est un skarn composé de trois corps minéralisés (Tritlla et al., 2003) : *magnétite massive*, *magnétite disséminée* et *brèche polymitique*. Le corps massif est composé principalement de magnétite, mais également d'hématite, de pyroxènes, de chlorite, de pyrite, d'apatite et de carbonates. Le corps disséminé se situe à environ 40 mètres sous le corps principal et se compose de magnétite, pyrite, pyroxènes, feldspaths-K, épidote, calcite, plagioclases, kaolinite. Le troisième corps minéralisé représente le dernier stade de minéralisation dans le gisement après l'intrusion des deux corps minéralisés précédents. Il est composé de blocs de roche andésitique cimentée par de la magnétite et est vertical avec une épaisseur d'environ 5 mètres.

L'usine de traitement minéralurgique actuellement en opération à Peña Colorada est composée essentiellement d'un circuit de broyage autogène, suivi d'une série de séparateurs magnétiques à basse intensité. Ce projet vise à explorer de nouvelles possibilités de techniques de traitement pour la valorisation du minerai complexe de Peña Colorada et, par conséquent, d'autres gisements du même type

Stratégie d'étude

Une revue de la littérature sur les minerais de fer met en évidence les principaux problèmes liés au traitement des minerais complexes, notamment lorsque des silicates de fer sont présents en tant que minéraux de gangue. Chaque minéral joue un rôle important dans le processus de traitement du minerai de fer car ses caractéristiques intrinsèques sont utilisées pour favoriser leur séparation. La concentration par gravité pourrait être une possibilité pour la séparation des oxydes de fer de ces silicates complexes, car leurs densités spécifiques sont relativement différentes. Cependant, la taille du matériel utilisé dans cette étude (80% inférieur à 53 µm) ne permet pas l'utilisation de cette technique. La concentration magnétique, une technique largement utilisée dans la concentration de minerais de fer magnétique, s'est déjà révélée inefficace à l'usine de traitement au Mexique, car les susceptibilités magnétiques des silicates contenant du fer sont suffisamment élevées pour pouvoir être attirés par un champ magnétique. La flottation est en revanche plus appropriée grâce à un fort potentiel de séparation : l'ajout de réactifs (e.g., déprimants, collecteurs) peut créer un contraste important en modifiant les propriétés de surface des minéraux, en les rendant hydrophobe ou hydrophile. Parmi les voies possibles de flottation des minerais de fer, la flottation cationique inverse est la plus utilisée, compte tenu de la facilité avec laquelle les silicates simples, comme le quartz, flottent. Les collecteurs s'adsorbent à la surface des minéraux et les rendent hydrophobes, générant une affinité favorable à la flottation par bulles d'air. Les déprimants, à leur tour, s'adsorbent sur les minéraux, les empêchant de devenir hydrophobes et les empêchant ainsi de flotter. Lors de la flottation cationique inverse des minerais de fer magnétitiques, les déprimants, ne sont généralement pas nécessaires en raison de la faible flottabilité de la magnétite en présence de

collecteurs cationiques. Cependant, ce processus manque de sélectivité, même avec l'utilisation de déprimant, puisque la magnétite finit par flotter avec certains collecteurs.

Pour les raisons exposées ci-dessus, la flottation cationique inverse présente un fort potentiel pour la séparation des oxydes de fer (i.e., *hématite* et *magnétite* des assemblages complexes de silicates de gangue. Compte tenu de la proximité des propriétés physico-chimiques entre oxydes de fer et silicates de fer, l'utilisation de déprimants semble importante pour l'étude en raison de la forte concentration de magnétite dans le concentré étudié, ainsi que la nécessité de réaliser une flottation la plus sélective possible. La recherche d'un déprimant sélectif est une problématique abordée dans cette thèse, à travers une étude complète des déprimants alternatifs pour la flottation des minerais de fer magnétitiques. Compte tenu de la quasi-inexistence de recherches fondamentales sur les silicates de fer étudiés, une étude expérimentale sur l'interaction des oxides et silicates de fer avec les réactifs a été menée. Une caractérisation de la charge de surface, des études d'équilibres d'adsorption, et de micro-flottations ont été réalisées sur des minéraux purs, ainsi qu'une recherche appliquée sur la flottation cationique inverse d'un concentré de fer contenant de tels minéraux. Enfin, compte tenu des développements récents sur la modélisation moléculaire appliquée à la flottation, une approche *ab-initio* a été utilisée pour comprendre mieux la propriété de surface du silicate de fer plus problématique étudié, la chamosite.

Caractérisation minéralogique

La caractérisation d'un échantillon de minerai est essentielle pour fournir des informations utiles pour savoir quelles méthodes utiliser pour approfondir des recherches sur la manière de générer le contraste nécessaire entre les minéraux afin de les séparer. Deux échantillons de concentré de fer ont été utilisés dans cette étude : l'un venant directement du gisement et passant par une valorisation au laboratoire de Peña Colorada (échantillon 1), et l'autre venant directement de l'usine (échantillon 2). Les travaux de caractérisation ont permis d'identifier les points à étudier suivants :

1. **Les minéraux qui feraient l'objet d'une étude plus approfondie et fondamentale :** la *chamosite*, le *diopside*, l'*épidote*, l'*hématite* et la *magnétite*. Les deux silicates de Fe peuvent être très compliqués à séparer dans un processus comme la flottation, car leurs propriétés de surface peuvent avoir le même comportement qu'un oxyde de fer. Le diopside fait l'objet d'une étude approfondie car il reste présent dans le concentré magétitique. La magnétite en tant que principal oxyde de fer identifié, et l'hématite en tant que référence importante pour la flottation cationique inverse des silicates, ont également été choisies.

2. **La fraction granulométrique optimale pour l'alimentation de la flottation.** La

fraction granulométrique où plus de 80% des particules sont libérées est de 53 µm (Figure 1). Pour étudier l'influence des particules mixtes dans la flottation, un échantillon a été soumis à un tamisage à 53 µm avant la réalisation des essais de flottation. Le broyage de la fraction supérieure à 53 µm a été également étudié pour l'échantillon tamisé.

3. **L'évaluation de réactifs de flottation inhabituels.** La composition minéralogique identifiée a guidé l'étude dans la recherche d'une suite de réactifs plus sélective pour la flottation cationique inverse des minerais de fer en présence de minéraux complexes. Les dépresseurs alternatifs (dextrine, carboxyméthylcellulose, acide humique) ont été étudiés en particulier car le manque de sélectivité de l'amidon de maïs (très utilisé dans l'industrie) a déjà été démontré en présence de minéraux de gangue complexes (Filippov et al., 2013).

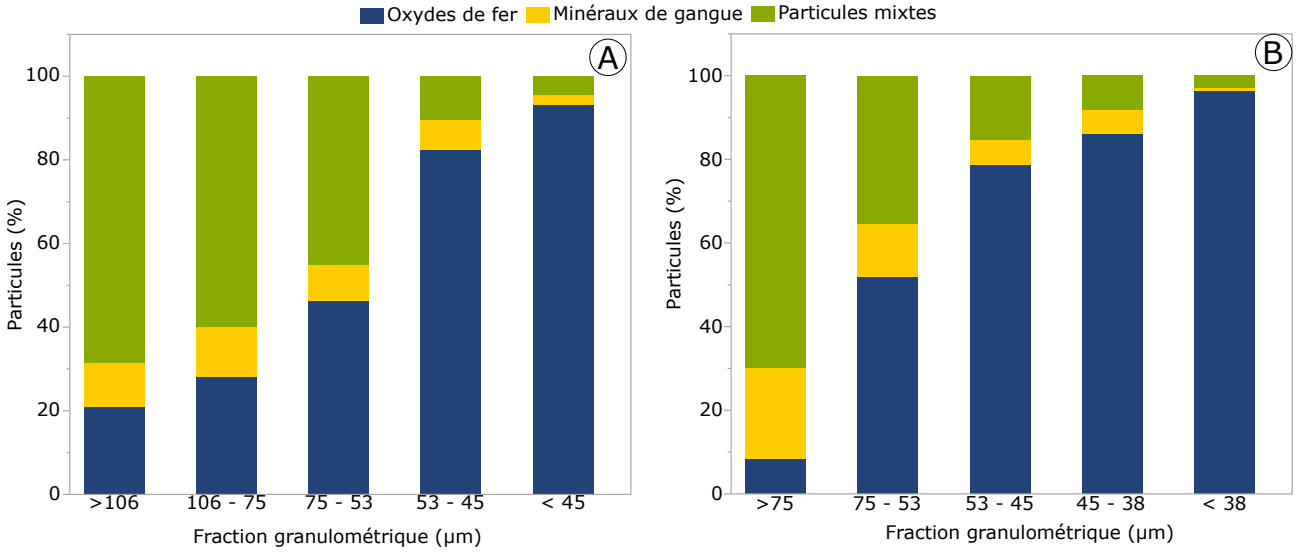

Fig. 1 – Etude quantitative de libération réalisée sur les échantillons 1 (A) et 2 (B).

Etude expérimentale sur l'interaction minéral-déprimant

Les mesures du potentiel zêta indiquent que les silicates — chamosite, diopside et épidote — ont une charge similaire sur leurs surfaces pour toute la plage de pH étudiée. L'hématite et la magnétite présentent des valeurs IEP plus élevées, ce qui peut expliquer la différence de mécanisme d'adsorption entre ces minéraux. Une augmentation du pH de l'amidon de maïs et de sa dérivée, la dextrine, est suivie d'une diminution constante des valeurs du potentiel zêta pour tous les minéraux. La complexation chimique proposée par Weisseborn et al. (1995) et Laskowski et al. (2007) (Figure 2) commencent à se produire pour compenser l'augmentation de la répulsion électrostatique jusqu'à l'obtention d'un pH d'environ 10, où les valeurs du potentiel zêta commencent à se stabiliser Les résultats des expériences d'adsorption confirment la théorie de Filippov et de ses collaborateurs (Filippov et al., 2013; Severov et al., 2016), selon laquelle l'amidon de maïs n'est pas un déprimant sélectif lorsque le minerai de fer est composé de silicates de fer. Liu et al. (2000) a formulé la proposition d'une interaction acide-base entre

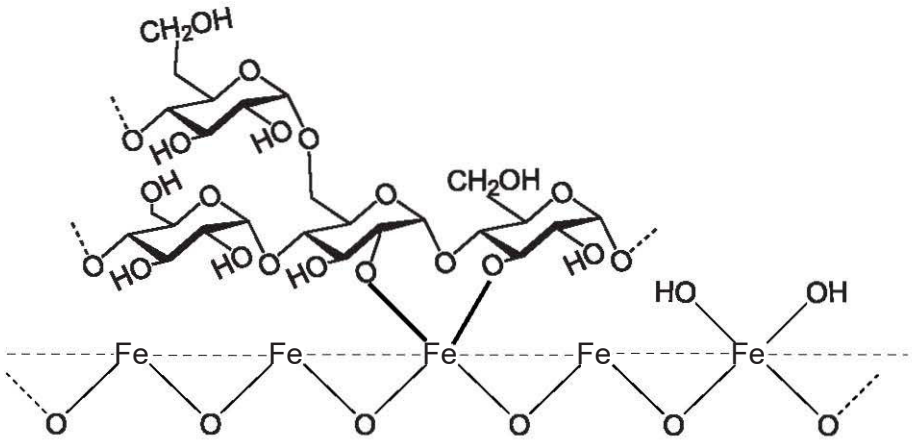

Fig. 2 – Adsorption par complexation chimique entre des groupes hydroxyle et des atomes de fer provenant d'hématite, adapté de Weisseborn et al. (1995).

polysaccharides et minéraux, dans laquelle la détermination du mécanisme d'adsorption en tant que liaison d'hydrogène ou complexation chimique dépend de la basicité de la surface des minéraux. Le comportement observé pour les mesures de potentiel zêta avec l'amidon de maïs confirme cette affirmation.

La carboxyméthylcellulose n'a pas d'adsorption significative sur les minéraux silicatés, mais une affinité plus élevée avec les oxydes de fer a été observée. Cette préférence pour la surface de l'hématite et de la magnétite est encore très controversée, mais la plupart des études ont indiqué que la répulsion électrostatique plus faible et une meilleure affinité pour les sites disponibles à la surface de ces minéraux expliqueraient cette préférence d'adsorption (Liu et al., 2000; Backfolk et al., 2002).

Contrairement à l'amidon de maïs, le mécanisme d'adsorption de l'acide humique semble être lié à une interaction ionique entre les minéraux et le réactif, présentant un caractère d'interaction hydrophobe. (Ramos-Tejada et al., 2003) ont ont déclaré que l'adsorption d'acide humique augmentait l'hydrophobicité de l'hématite. Ce fait lié à l'adsorption inférieure d'acide humique sur les surfaces des silicates pouvait constituer une bonne indication pour un dépresseur sélectif.

Flottation de minéraux purs et de concentré de minerai de fer

Les expériences de micro-flottation ont permis de confirmer que la sélectivité entre les silicates contenant du fer et les oxydes de fer était plus élevée à pH acide (Figure 3) pour les deux collecteurs testés (dodécylamine - DDA et étheramine - ETA). La chamosite a besoin de concentrations de collecteur plus élevées pour atteindre une flottabilité stable par rapport à les autres minéraux. Cela peut s'expliquer par sa grande surface spécifique et ses structures en feuillets, qui nécessitent des concentrations plus élevées pour former la première couche de collecteur.

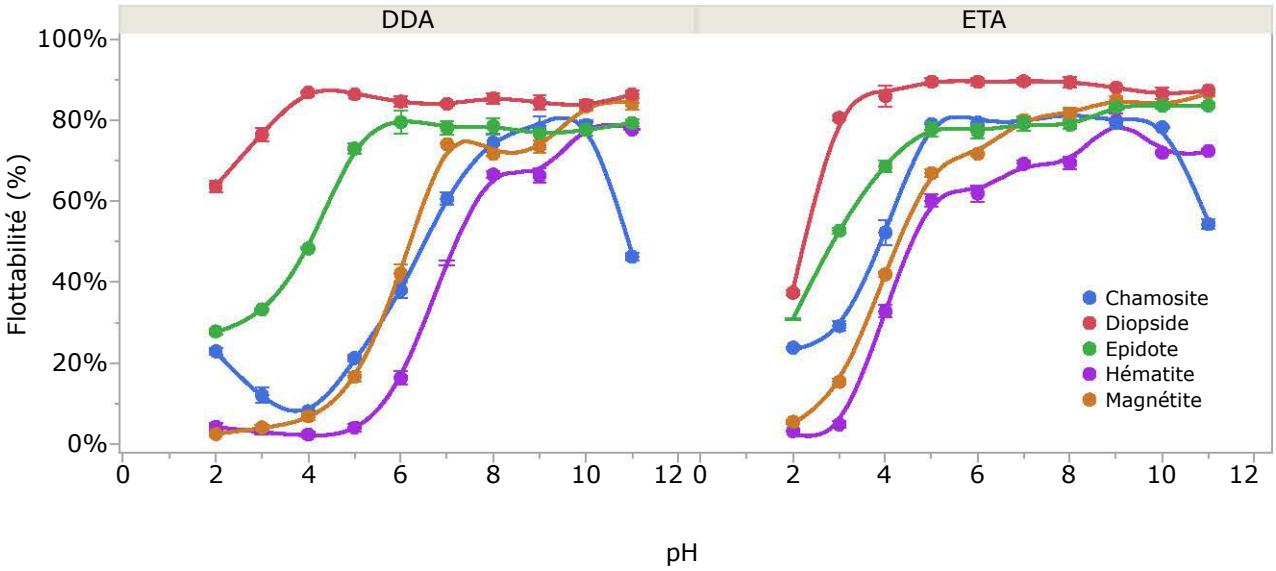

Fig. 3 – Flottabilité des minéraux purs avec DDA et ETA à plusieurs valeurs de pH. L'erreur a été calculée à partir de la différence entre les expériences en double (barres d'erreur).

Les expériences avec des déprimants ont montré que l'amidon de maïs déprimait tous les minéraux et que l'acide humique était plus sélectif. La chamosite est déprimée pour l'amidon de maïs et aussi pour l'acide humique. Ce minéral présente une meilleure flottabilité lorsque l'acide humique et l'ETA sont utilisés dans un rapport égal de 1 par 1. À partir des expériences avec un mélange de minéraux, il est possible de confirmer que l'ETA a une sélectivité inférieure à celle de la DDA. Le diopside et l'épidote sont plus faciles à séparer des oxydes de fer que la chamosite. Les meilleurs résultats ont été observés à pH 4 où les minéraux ont des charges de surface différentes et une fenêtre de séparation peut être observée.

Pour les essais de flottation en échelle laboratoire avec du concentré magnétique de Peña Colorada, l'acide humique apparaît comme le meilleur déprimant présentant la plus faible teneur en silice dans le concentré final. Le tamisage à 53 µm était important pour obtenir des bons résultats, car les particules inférieures à cette fraction granulométrique sont plus libérées. L'influence de l'eau de traitement provenant de l'usine du Mexique a été évaluée et elle n'a pas compromis les résultats de la flottation, au contraire elle a permis d'améliorer la récupération du fer. L'acide humique et le Flotigam EDA ont donné d'excellents résultats en termes de teneur en silice. Cependant, un nouveau polysaccharide industriel appelé Deprapol N05 a donné de meilleurs résultats en termes de récupération du fer sans perdre la qualité obtenue. La présence de charges négatives de haute intensité dans ce polysaccharide peut expliquer son bon résultat, car les dépresseurs anioniques tels que l'acide humique sont plus sélectifs entre les oxydes de fer et les silicates contenant du fer.

Approche industrielle

L'objectif de cette partie de l'étude est d'appliquer les connaissances acquises lors de l'étude

des minéraux et des réactifs dans une approche industrielle par le biais de tests continus. Des essais en cycle fermé («locked cycle test») et des essais pilotes ont été réalisés en utilisant du Flotigam EDA comme collecteur de silicate et du Deprapol N05 en tant que dépresseur. Ce dépresseur a été choisi car il peut être fourni à l'échelle industrielle et donne également des bons résultats en termes de récupération de fer. La Figure 4 illustre la mousse de l'essai pilote de flottation.

Cette approche prouve la capacité de la technique de flottation à améliorer le produit de Peña Colorada. Des concentrés finaux avec une teneur en silice d'environ 2,6% et une récupération de fer de plus de 98% en masse sont obtenus pour un test continu avec des étapes de dégrossissage, épuisage et lavage. L'ajout d'un tamisage fin (à 53 µm) préalable était essentiel pour obtenir un si bon résultat. L'ajout d'une étape de flottation de sulfures avant la flottation de silicates n'a pas eu d'influence sur la réduction de la teneur en silice dans le concentré final. Et puisque la teneur initiale en soufre ($\approx 0.25\%$) est considérée comme étant dans la qualité attendue, cette étape a été supprimée.

Une étude économique a été réalisée en estimant le rendement d'une opération de flottation à l'échelle industrielle à partir des essais continus, afin d'évaluer la valeur potentielle créée par l'ajout d'un tamis fin suivi d'une flottation. Les résultats montrent que le projet est rentable. La valeur actuelle nette (VAN) calculée pour ce projet est de 36 millions de dollars et le taux de rentabilité interne (TRI) de 63%. Un bénéfice de près de 12 millions de dollars par an est attendu, principalement en raison de la réduction des coûts liés à la diminution de la teneur en silice. Outre les bénéfices, le projet est très important car il permet de maintenir la qualité requise du produit final et de maintenir la mine compétitive.

Fig. 4 – Mousse de l'étape de dégrossissage de l'essai de flottation pilote.

Modélisation moléculaire de la surface de la chamosite

La modélisation moléculaire a été utilisée pour essayer d'expliquer le comportement particulier de la chamosite — qui ne flotte pas comme les autres silicates. Bien que d'autres minéraux argileux du groupe chlorite aient fait l'objet de certaines études en modélisation moléculaire (Yin et al., 2012), la chamosite n'a jamais été étudiée auparavant. Le clivage de

la chamosite est bien connu sous le plan (h = 0, k = 0, l = 1) (Anthony et al., 2019).On peut envisager deux possibilités différentes d'exposition en surface pour la chamosite, qui ont été appelées comme :

1. *Small-slab* : où les composants tri-octaédriques de Al et Fe sont exposés;
2. *Big-slab* : où les composants tétraédriques de Si sont exposés.

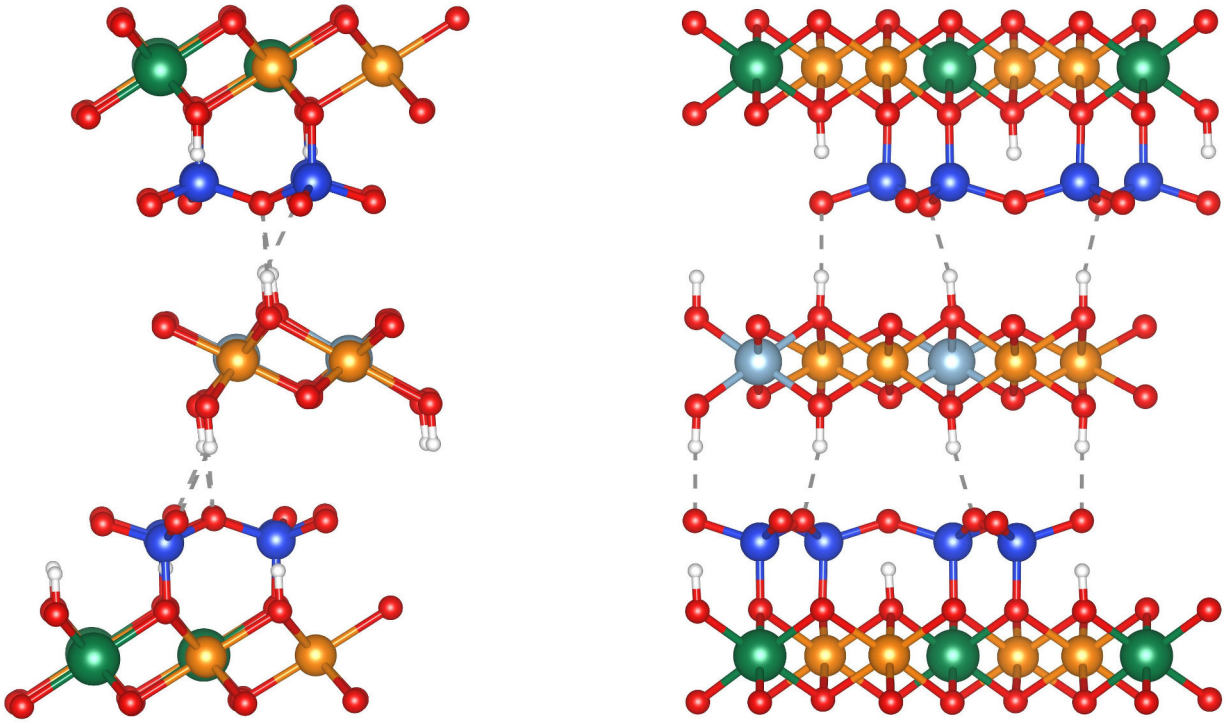

Fig. 5 – Structure cristalline de la chamosite, vue latérale (gauche) et vue frontale (droite), à partir de Walker and Bish (1992). Al = sphères bleu clair; Fe = sphères orange; Mg = sphères vertes; O = sphères rouges; Si = sphères bleu foncé; lignes pointillées = limite de cellules dans la direction *c*.

À partir de la structure proposée par Walker and Bish (1992) (Figure 5),), les deux surfaces possibles ont été transformées en supercellules suivant le plan (0 0 1) et ensuite relaxées. Dans le but d'éviter toute interaction inattendue due à la périodicité de la cellule, un vide supplémentaire de 15 Å a été ajouté entre la surface et le haut de la supercellule. Pendant la relaxation de ces deux supercellules, les atomes ont été autorisés à se déplacer dans les trois directions x, y et z.

Il ressort de cette étude que la chamosite a une surface exposée ou non (selon le clivage) beaucoup moins hydrophile que l'autre. Ces résultats sont corroborés par les recherches de Yin et al. (2012), qui mettent en évidence un état hydrophobe pour certaines surfaces tétraédriques de silice. Dans l'ensemble, cette étude démontre qu'une connaissance approfondie de l'état de

surface des minéraux est une condition préalable à l'optimisation du traitement de la flottation. La modélisation atomique fournit ici des informations très utiles sur le caractère hydrophobique de la chamosite, un archétype du minéral silicaté. Comme ce minéral présente deux surfaces très différentes, de nouvelles stratégies doivent être trouvées pour concevoir une combinaison de réactifs de flottation permettant de le traiter correctement au cours du processus.

Contents

List of Figures

List of Tables

Chapter 1

Introduction

1.1 Importance of iron ore

Iron is the most used metal in our lives, some of its properties as resistance and facility to be shaped makes its replacement very difficult. The iron-bearing minerals most commonly found in nature and economically exploited are magnetite [Fe_3O_4], hematite [Fe_2O_3], goethite [FeO(OH)] and siderite [$FeCO_3$] (Filippov et al., 2014). These minerals are commonly associated with other minerals – most of the time not economically exploited, forming the so-called iron ore. Iron ore is the source of primary iron for the world's iron and steel industries. It has been traditionally the second largest commodity market after crude oil and, despite the currently weaker demand, an increase is expected in the long-term demand especially due to the intense urbanisation that has been taking place in many countries around the world. 98% of the iron mined around the world is processed into steel, which turns into many of the products that we use every single day (US Geological Survey, 2018; Veloso et al., 2018). Australia, Brazil and China are responsible for 70% of the world's iron ore production and holders of approximately 60% of the world's reserves. Figure 1.1 presents the most important countries in terms of iron ore production.

Iron ores consumed in steel industry require a certain level of quality regarding iron content. According to the iron content, it can be used directly as direct-shipping ore (DSO) or converted into briquettes, concentrates, direct reduction iron (DRI), iron nuggets, pellets or sinter. The first one can supply directly blast furnaces without much effort needing a minimum physical processing and no beneficiation. However, the same does not apply to the others, that need to be systematically processed to achieve the desired quality. Iron ore head grades continue to decline as higher quality and easier to mine resources are exhausted, leading to increasing the development of problematic ore types, often requiring beneficiation.

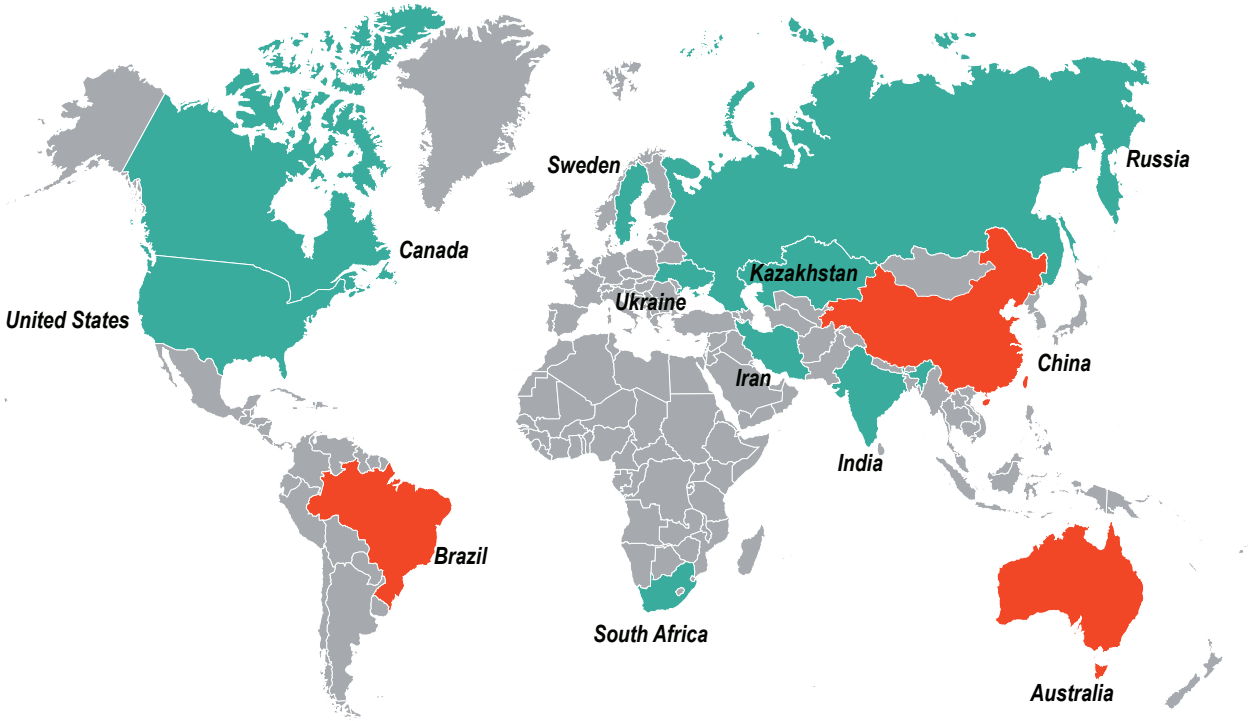

Fig. 1.1 – Map of the world's largest iron ore producing countries (data from US Geological Survey, 2018). Standing out the three largest in orange: Australia, China and Brazil.

1.2 Peña Colorada project

ArcelorMittal is the largest steel producer in the world and consequently one of the largest consumers of iron ore as well. Part of its consumption comes from domestic production obtained from several captive mines located all over the world. Like most iron ore producers, ArcelorMittal is facing problems with the decline in the quality of its ores and the appearance of ores with complex mineralogical assemblages. This project deals specifically with an important asset of the company located in western Mexico, the Peña Colorada mine. The silica content in their final product is expected to average 2.5%, however, in the last few years, this grade has increased to up to 3.5%, sometimes even more, depending on the ore body exploited. The hypothesis of this study is that the degradation of the quality of this ore is directly linked to the mineralogy. The process plant underwent an expansion that started operation in 2017 to maintain production levels due to the lower head-grade of the Run-of-Mine (ROM). However, the current magnetic separation process is not able to generate concentrates with the required qualities to feed the downstream pelletising process.

1.2.1 Geological background

The Peña Colorada iron skarn is one of the most important iron deposits in Mexico, located in the state of Colima in the western part of the country. It is composed by several ore-bodies extending over an area of approximately 5 km^2. The deposit has been classified in three different mineralized bodies (Tritlla et al., 2003):

(i) Massive magnetite;

(ii) Disseminated magnetite;

(iii) Polymictic breccia.

The original resources of this deposit may have been comparable to other iron skarn occurrences around the world. Current values assume that the deposit has approximately 150 Mt with a magnetite content of 36% (Zürcher et al., 2001).

1.2.1.1 Regional geologic setting

A location and geologic setting of Peña Colorada iron skarn is presented in Figure 1.2. The oldest rocks found in the sector are from the Aptian age (125 - 113 Ma) and are mainly composed of volcano sedimentary units of reef limestone, sandstone, shales and rhyolites and are called the Tecalitlàn Formation. A discordant volcano sedimentary unit of Albian-Cenomanian age (113 - 93.9 Ma) is found above the Tecalitlàn Formation and named the Tepalcatepec Formation. Mainly composed of limestone, sandstone and conglomerates, this unit is the host formation of the Peña Colorada ore body (Alva-Valdivia et al., 1996). These terrains are intruded by a calc-alkaline granite of Pacific subduction origin with no clear mineralizing event. Above these terrains, there are andesitic flows, rhyolites and pyroclastic material from the Upper Cretaceous age (93.9-72.1 Ma) in direct continuity. The whole sedimentary package has been confirmed to be the result of a marginal basin behind an island arc with proofs found in the limestones. This 500 m limestones unit, linked to the Morelos Formation, showed cyclic bed disruption through volcanic tectonic activity. The REE pattern of volcanic media showed a tholeiitic origin linked to a primitive arc formation. The end of the sedimentation in the basin is marked by thin layers of conglomerates supposedly deposed in shallow sea and represent the end of the Tepalcatepec Formation. The area reached the surface around the Cenomanian-Turonian age (100.5 - 89.3 Ma) indicated by reddish conglomerates implying continental sedimentation. This conglomeratic unit is called the Cerro de la Vieja Formation. Around the same period, a batholith (Tomaltan batholith) intruded the volcano-sedimentary sequences with calc-alkaline material. The main mineralization event happened during the early to middle Cenozoic age

(magmatic events dated at 63.9 Ma with the K/Ar method on andesite by Alva-Valdivia et al. (1996) when a third dioritic intrusive body induced contact metamorphism in the volcano-sedimentary unit and especially on limestones. This event results in metasomatism with the formation of calcic-sodic skarns and the intrusion of iron-rich solutions producing magnetite and epidote as primary minerals and chlorite as a secondary mineral. At the late tertiary, a final dyke composed mainly by andesitic and quartz-dioritic, intrudes most of the rocks including the ore-body. These dykes are mostly vertical and sometimes can act has a hydrothermal breccia remobilizing the skarn layers.

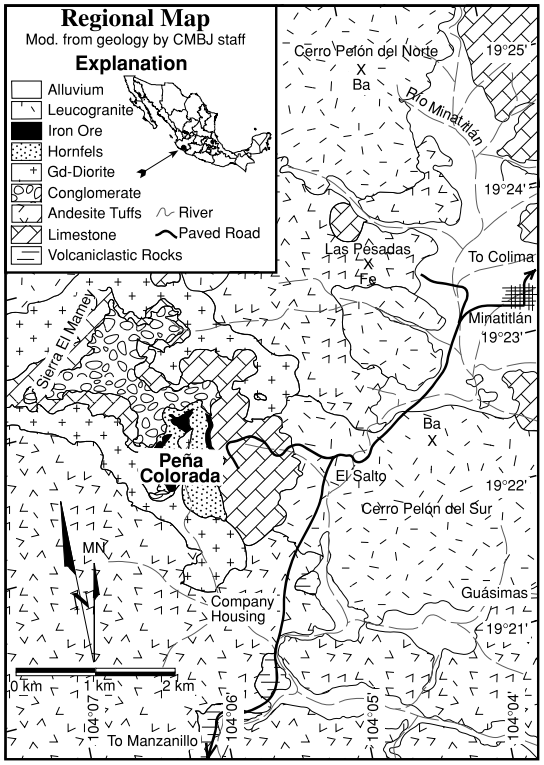

Fig. 1.2 – Regional location and geologic setting of the Peña Colorada iron skarn by Zürcher et al. (2001).

1.2.1.2 Deposit geology

Encased in the volcano-sedimentary Tepalcatepec Formation, the deposit of Peña Colorada is approximately 750 m thick. This deposit has been the subject of several studies along the past years (Alva-Valdivia et al. (1996); Marmolejo-Rodríguez et al. (2007); Corona-Esquivel et al. (2009); Rivas-Sanchez et al. (2006); Tritlla et al. (2003); Zürcher et al. (2001), and despite some controversy, the deposit is commonly classified as a calcic iron skarn. The sector is composed of three different zones of interest: as previous mentioned: *massive magnetite*, *disseminated magnetite* and *polymictic breccia*. Figure 1.3 presents a geology map and the main points of alteration and mineralization in the scale of the mine.

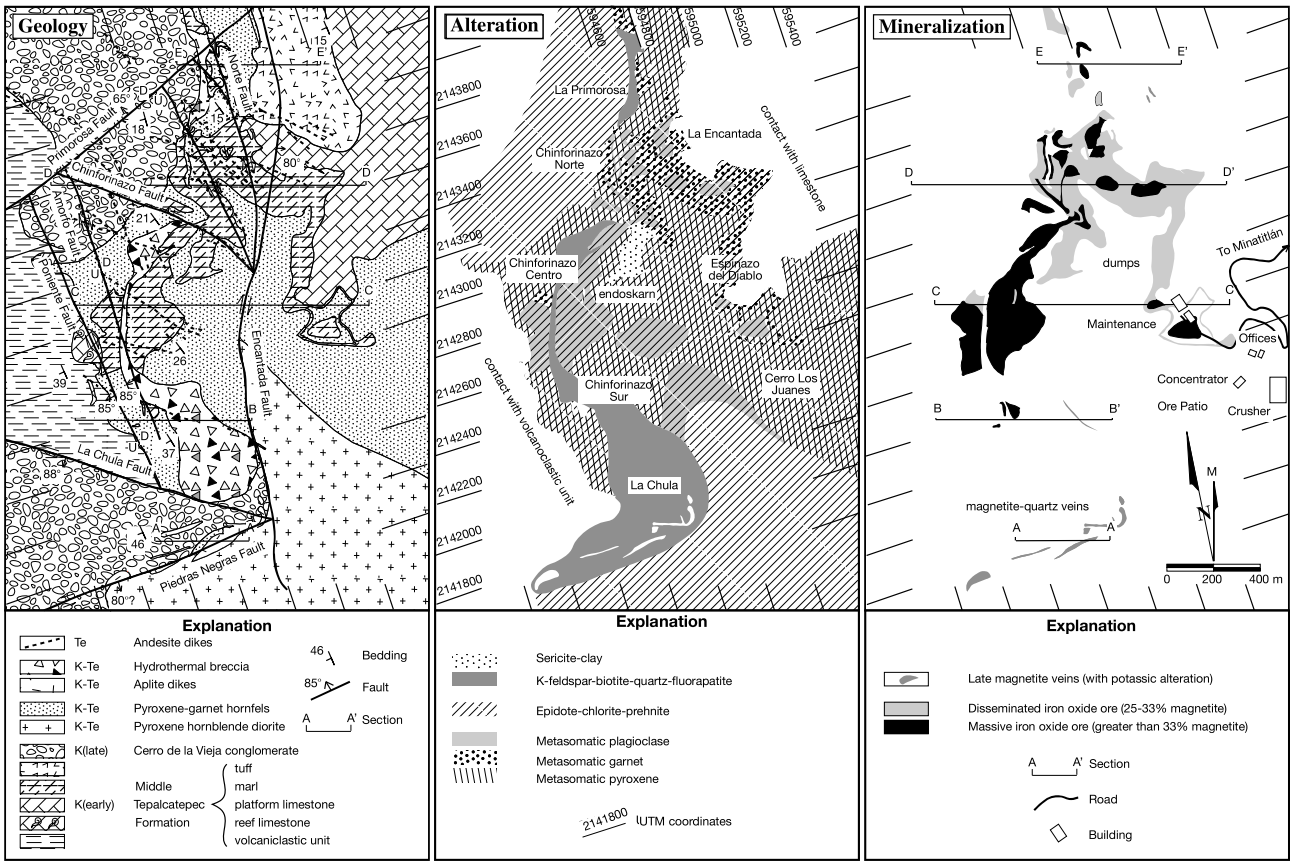

Fig. 1.3 – Peña Colorada mine geology map, alteration and mineralization points. Adapted from Zürcher et al. (2001)

The massive body is composed mainly by magnetite, but also hematite, pyroxene, chlorite, pyrite, apatite and carbonates. The ore-body was 20 m thick by 1 km long and partially in agreement with the rock stratification. The disseminated body is located about 40 m below the main body and has a maximum of 150 m in thickness and the same extension of the massive body. It is composed by several phase minerals: magnetite, pyrite, pyroxene, K-feldspar, epidote, calcite, plagioclase, kaolinite. The third ore-body (polymictic breccia) is the last mineralization occurred in the deposit once it intrudes the two previous ore-bodies. It is composed of andesite rock blocks with a magnetite matrix and is vertical with approximately 5 m thick (Tritlla et al., 2003). Figure 1.4 proposed by Zürcher et al. (2001) presents a stratigraphic column for Peña Colorada.

1.2.1.3 Mineralization and alteration

The main events of mineralization and alteration of Peña Colorada are detailed here below.

Early contact metamorphism

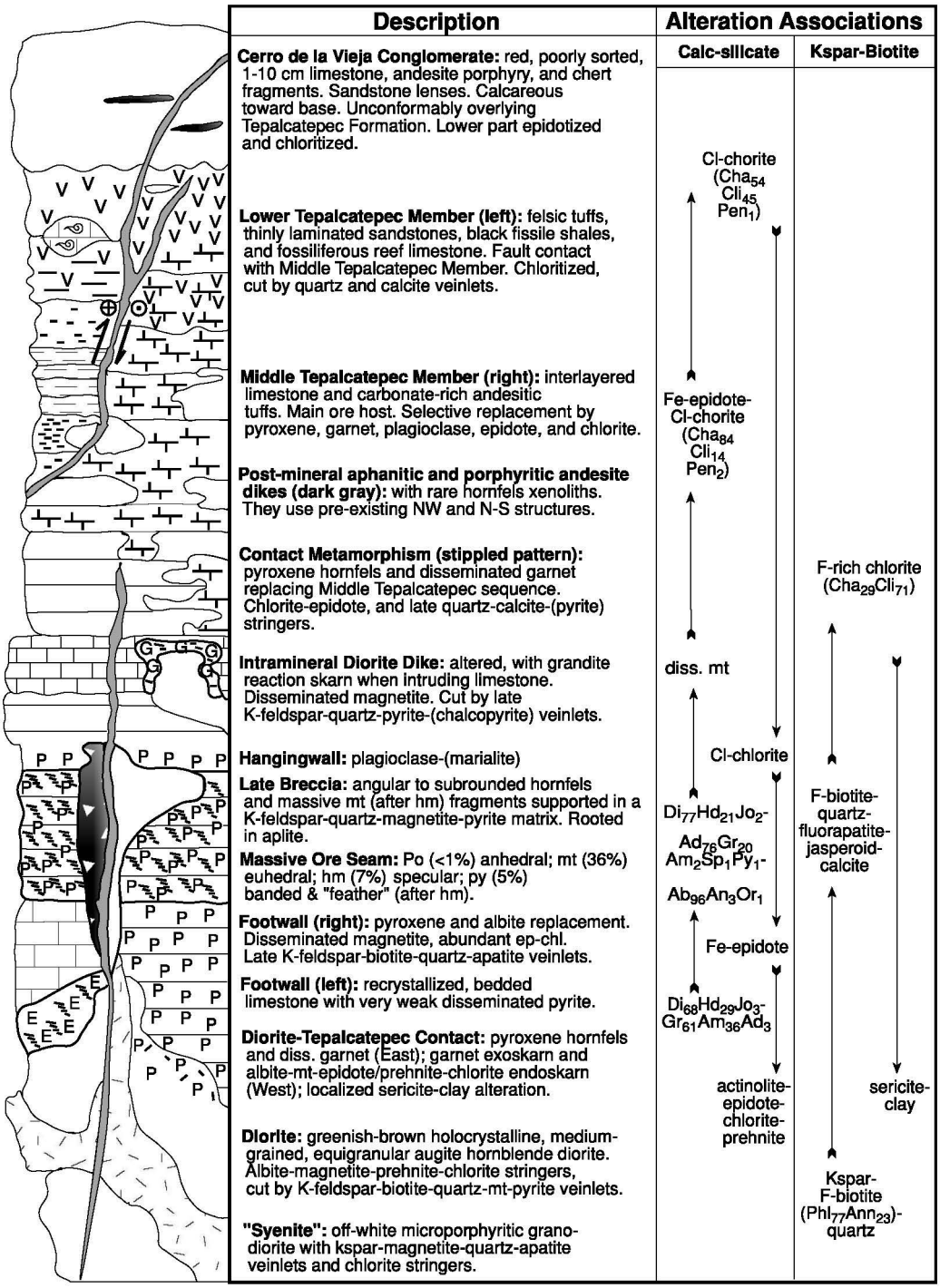

Fig. 1.4 – Peña Colorada stratigraphic column proposed by Zürcher et al. (2001). Vertical scale approximately 700 m. E = endoskarn, G = reaction skarn, P = albite. Minerals abbreviation: Ab = albite, Am = almandine, Ad = andradite, Ann = Annite, Cha = chamosite, Cli = clinochlore, Di = diopside, Gr = grossular, Hd = hedenbergite, hm = hematite, Jo = johannsenite, mt = magnetite, Or = orthoclase, Pen = Phlogopite, Py = pyrope, Sp = spessartine.

Bands of pyroxene and disseminated garnets are found in a 200 m radius around the diorite intrusion. Pyroxene was mainly formed in shales environment and the garnets in tuffs. These minerals will be mobilised in the next skarn events.

Prograde mineralization and alteration

Mostly metasomatic alterations are found in form of pyroxene, garnet and plagioclase formed inside shales and tuffs within or below the marl layer. Pyroxene horizons are sub-horizontal and garnet reaction front follow major faults and contain relic pyroxene in their lattice. These new phases erase the early contacts. The marl layer hosting most of the iron is composed of mainly limestone beds that were replaced by iron oxide and to a lesser extent garnet, pyroxene and plagioclase bands. The massive ore is mainly composed of euhedral magnetite (36% wt) and bladed hematite (7% wt). Sulphides are present with interstitial calcite, dolomite and chlorite. The main replacement texture is magnetite over calc-silicates. Pyrite has also been observed to replace hematite. In between the massive layers of magnetite, disseminated magnetite is observed in small quantities and more secondary minerals such as chlorite group minerals are present (Zürcher et al., 2001).

Regrade mineralization and alteration

The alterations associated with the retrograde progression of the skarn are represented by Cl-Fe rich chlorite (84% chamosite, 14% Clinochlore, 2 % Pennantite) and Fe-epidote veins. At Chinforinazo Centro, an endoskarn inside the diorite is visible. Most of the hornblende was transformed into actinolite and cut by small chlorite veins. This endoskarn bears mineralization such as coarse grains of euhedral magnetite disseminations and iron oxide filled stockworks.

Breccia mineralization and alteration

The fragments of almost all the breccia are cemented by an association of potassic feldspars, quartz and biotite. Around the breccia, an alteration halo of about 200 m is visible and is fluorine rich. When the breccia hits empty layers the mineralization is barren. However well-preserved fragments are found if the breccia pipes go through the massive magnetite.

1.2.2 Peña Colorada plant operation

The current beneficiation plant of Peña Colorada is composed by autogenous grinding of the crushed Run-Of-Mine (ROM) followed by a series of low magnetic separators. The stock piles that feed the plant are composed by a material that goes through a primary crushing stage and a dry low intensity magnetic separation with a magnetic field of 1000 G. This material is fed by conveyor into a Full Autogenous Grinding (FAG) mill to achieve a P_{80} of 500 µm. Subsequently, the material is sieved under 2 mm aperture. The particles above this size pass through a magnetic pulley that directs the magnetic portion to a second cone crusher that returns the material to the FAG. The non-magnetic portion is stockpiled in tailings piles. The particles below 2 mm goes through two Wet Low Intensity Magnetic Separation (WLIMS)

lines, composed of 7 magnetic separators with 3 drums each one. The tailings are transported to the tailings thickener and finally to the tailings dam. The magnetic separation concentrate is fed in a hydrocyclone circuit. The underflow of the circuit is redirected to a ball mill and the overflow is sent to the rougher magnetic concentration stage which consists in 28 magnetic separators with 3 drums each one. Thereafter, the magnetic concentrate passes through a fine screening phase composed of 48 vibrating screens, 24 per line. The coarse portion of the fine screening phase is sent to a fine wet grinding and the fine portion of the screening is addressed to the finisher magnetic concentration which consists in 10 double drums magnetic separators per line. The tailings from the rougher and finisher stages are also sent to the tailings thickener and finally to the tailings dam. A finisher concentration aiming to reduce the silica content in the final product is then applied in the magnetic concentrate that is fed in an equipment called "Magnefloc". It applies a low-intensity magnetic field to aggregate magnetite particles and increase their sedimentation rate, while an upward flow of water removes impurities by the underflow. There are 12 "Magnefloc" in operation at Peña Colorada's plant. Finally, the concentrate is sent to a thickener that prepares the slurry for transportation via a pipeline. There are two 45 km pipelines connecting the beneficiation plant and the pelletizing plant, located in Manzanillo. Since there is an altitude difference of approximately 1000 m between the two plants, the need for pumping is reduced. Figure 1.5 shows a simplified flow-sheet of Peña Colorada plant.

1.2.3 Project objectives

Peña Colorada mine is confronted with the constant decline in the quality of its iron ore and the difficulty of processing it properly. The objective of the company is to have again the product quality practiced in the past, with concentrates having silica content of around 2.5%, with the maximum possible iron recovery. This thesis falls within the scope of this project by performing a flotation approach as an attempt to respond to the technological demand of the industry.

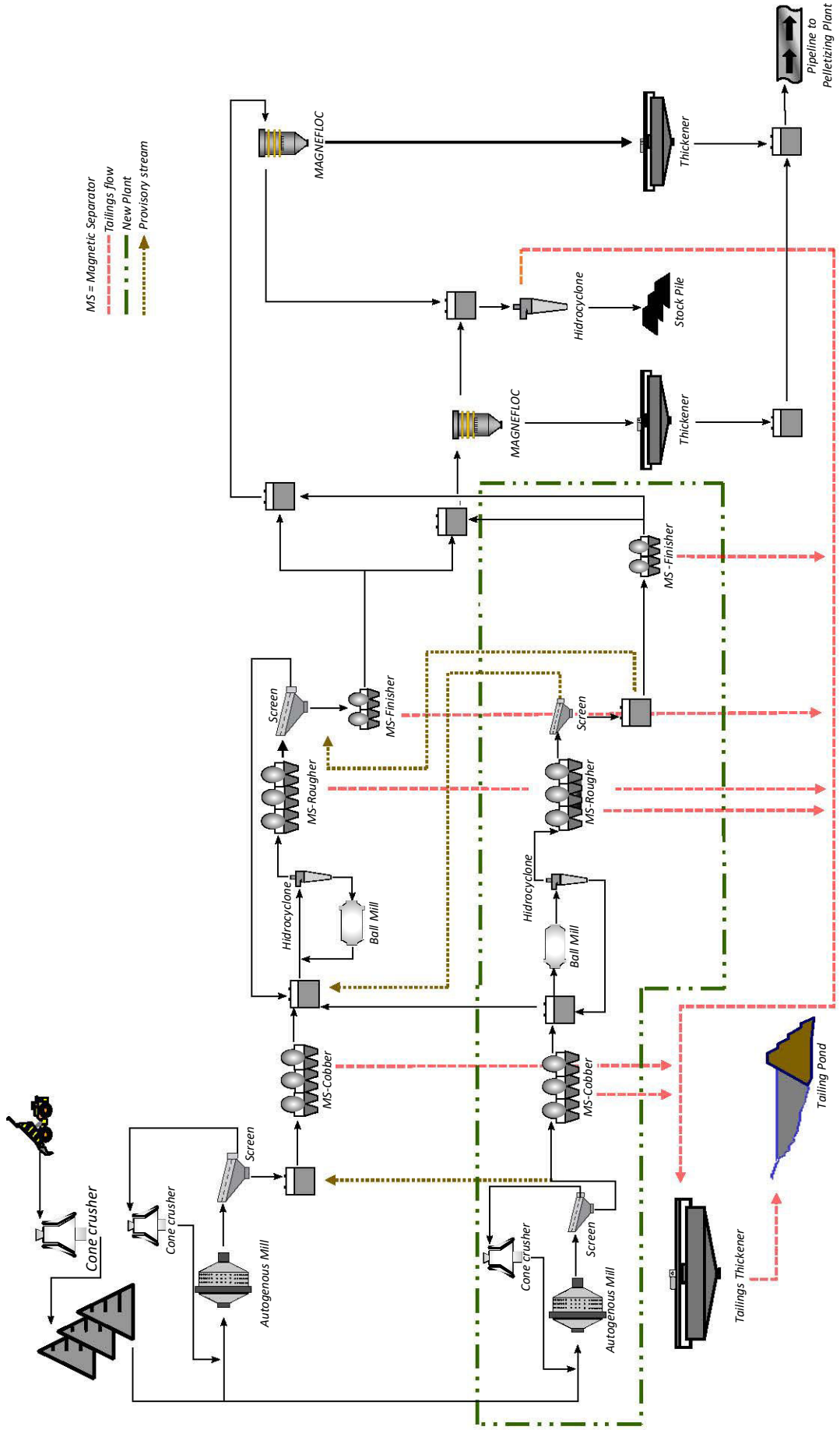

Fig. 1.5 – Simplified flow-sheet of Peña Colorada beneficiation plant.

Chapter 2

Literature Review

When a natural rock occurrence contains enough minerals with economically important elements, such metals, it is called ore. Mineral processing is the separation process of these minerals from others. There are two important steps to achieve such separation, the first is the liberation of the valuable minerals from the so-called gangue minerals and then the process of concentration of these minerals. This chapter will review the properties of the main minerals found in iron ores that affect their separation from other minerals and also the most commonly applied concentration process for iron ore processing.

2.1 The role of mineral properties on iron ore processing

2.1.1 Iron-bearing minerals

Table 2.1 – Major iron-bearing minerals found in iron ores, from Cornell and Schwertmann (1996).

Mineral class	Mineral name	Chemical formula	Fe content (%)	Commonly name
Oxides	Magnetite	Fe_3O_4	72.36	Ferrous-ferric oxide
Oxides	Hematite	α-Fe_2O_3	69.94	Ferric oxide
Oxides	Maghemite	γ-Fe_2O_3	69.94	Ferric oxide
Hydroxides	Goethite	FeO(OH)	62.86	Iron hydroxide
Carbonates	Siderite	$FeCO_3$	48.21	Iron carbonate
Sulphides	Pyrite	FeS_2	46.55	Iron sulphide
Sulphides	Pyrrhotite	$Fe_{(1-x)}S$, (x = 0 to 0.2)	58.22 - 63.52	Iron sulphide

There are several iron-bearing minerals in nature, however not all of them are economically exploited. Based on the new Dana classification for minerals (Gaines et al., 1997), they can be

divided as shown in Table 2.1. Among those minerals, the oxides and hydroxides are the more important in terms of iron ore exploitation, mainly to the high iron content of their composition. Two of them will be further discussed: *hematite* and *magnetite*.

2.1.1.1 Hematite

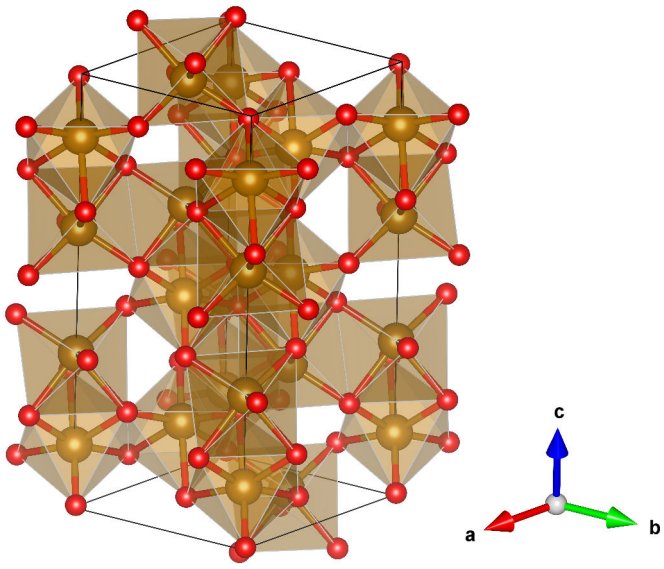

Fig. 2.1 – Hematite crystalline structure from Blake and Hessevick (1966). Fe = orange spheres; O = red spheres; shaded are = octahedral molecular geometry.

Hematite, γ-Fe_2O_3, is the most important ore-mineral of iron due to its wide occurrence in many mineral deposits. It is composed by 69.94% of iron and 30.06% of oxygen. Hematite is a mineral from the group of hematite, found as a primary mineral and as an alteration product in igneous, metamorphic, and sedimentary rocks (Klein, 2007; Deer et al., 2010). The most important hematite deposits formed in sedimentary environments. It is a reddish-black mineral with a hardness between 5.5-6.5 in the Mohs scale and specific gravity of 5.26 g/cm^3. Hematite crystallises in the rhombohedral lattice system (see Figure 2.1), with same crystal structure as ilmenite and corundum (Anthony et al., 2019). Varieties of crystal formations include massive hematite, kidney ore, iron rose, specularite and martite. This last one being the most relevant to the main iron ore deposits in the world. Martite consists in hematite pseudo-morphed after magnetite, formed under conditions of increasing oxygen fugacity (Gaines et al., 1997). Hematite appearance may variate. Its lustre can range from metallic or sub-metallic to dull, but it always produces a reddish streak. Hematite is "antiferromagnetic" below the temperature called the "Morin transition", which is 250 K (-23.2 °C). The term antiferromagnetic refers to the way in which individual molecules align their magnetic poles. At these low temperatures, the molecules of hematite align themselves so that neighbouring molecules magnetic poles are pointed in opposite directions. This causes the magnetic fields to essentially cancel each other

out (Morrish, 1995). Above the Morin transition temperature of 250 K, hematite is weakly "ferromagnetic," which is also referred to as being a "canted antiferromagnetic". For example, more of the individual molecular magnetic poles of the mineral are pointed in one direction than the other, so there is a net magnetic field, but it is not as strong as if all the poles pointed in the same direction. The strength of this ferromagnetic field varies depending on the impurities of any given sample of hematite (Morrish, 1995). Hematite's magnetic properties change again above 948 K, which is referred to as its "Néel temperature." Above this temperature, which can also be expressed as 674.9 °C, hematite is "paramagnetic". In this state, the thermal energy of the mineral is so high that it disrupts any arrangement of molecular orientations that would normally produce magnetism. Paramagnetic materials are attracted to other magnetic fields, but once the external field is removed, they no longer retain any magnetism (Morrish, 1995).

Considering the presented properties of hematite, especially its high specific gravity and weak magnetism, its separation process involves the combination of techniques including gravity separation, high field magnetic separation and reverse flotation.

2.1.1.2 Magnetite

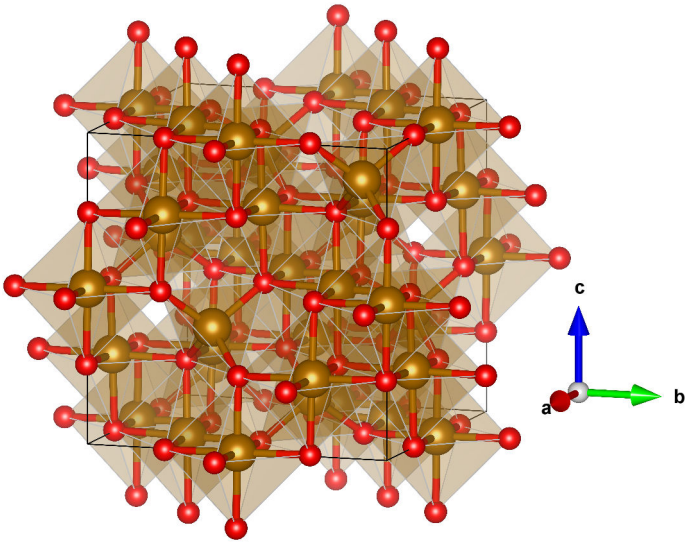

Fig. 2.2 – Magnetite crystalline structure from Wechsler et al. (1984). Fe = orange spheres; O = red spheres; shaded are = octahedral molecular geometry.

Magnetite, $Fe_2^{3+}Fe^{2+}O_4$, is a mineral from spinel group and a primary source of iron. It is composed by 72.36% of iron and 27.64% of oxygen, in a ratio of 31.03% of FeO and 68.97% of Fe_2O_3. It is strongly magnetic and one of the few minerals to be attracted to a common magnet. Magnetite is black, opaque with lustre ranging from metallic to sub-metallic. Its hardness range between 5.5-6.5 in the Mohs scale and it has a specific gravity of 5.20 g/cm^3.

Magnetite crystallises in the cubic lattice system (see Figure 2.2), and its crystals are usually octahedral (Anthony et al., 2019).

The magnetic property of magnetite is important as it assists mineral processing techniques via magnetic separation where it is easily separated from the other minerals.

2.1.2 Gangue minerals

Gangue minerals are defined as the worthless minerals to which valuable minerals are found associated. Among the gangue minerals associated with iron ores, quartz is the most recurring. Phyllosilicates such as stilpnomelane, minnesotaite and greenalite are also found associated with banded iron formations (BIF), as well as iron-rich chlorites, biotite and iron-bearing amphiboles. Pyroxenes as diopside are also identified in hydrothermal deposits. Kaolinite and gibbsite are the main clay minerals occurring in iron ores, calcite and dolomite the common carbonates, and apatite the main phosphate. Despite being an iron-bearing mineral, pyrite is also considered as a gangue mineral for iron ores mainly due to its deleterious effects on steel properties. The properties of those minerals are very important to generate a contrast between them and the iron oxides to promote their separation. Most gangue minerals associated with iron ores are paramagnetic, with low to moderate magnetic susceptibility or even diamagnetic as quartz for example. However, iron-bearing silicates have properties often like iron oxides, such as higher magnetic susceptibility, mainly due to the presence of iron in their structure and thus separation is more complicated. To match the objective of the study, the focus will now be on iron-bearing silicates and the pyroxene which can be problematic for the iron ore processing.

2.1.2.1 Chamosite

Chamosite, $(Fe^{2+}, Mg, Fe^{3+})_5Al(Si_3Al)O_{10}(OH, O)_8$, is a phyllosilicate mineral member of the chlorite group (Anthony et al., 2019). It forms a series with clinochlore, in which the first is the iron-rich member and the other the magnesium-rich member. Chlorite minerals are found in rocks altered during deep burial, plate collisions, hydrothermal activity, or contact metamorphism. They are also found as retrograde minerals in igneous and metamorphic rocks that have been weathered (Hey, 1954). Chamosite is green, has a foliated appearance and perfect cleavage at the plan {0 0 1}. Its hardness range between 2-3 in the Mohs scale and it has a specific gravity of $\approx 3.13\ g/cm^3$. Chamosite crystallises in the monoclinic lattice system (see Figure 2.3). It is a weakly magnetic mineral, but with enough susceptibility to jeopardize the contrast necessary between it and the other minerals (Rosenblum and K. Brownfield, 2000).

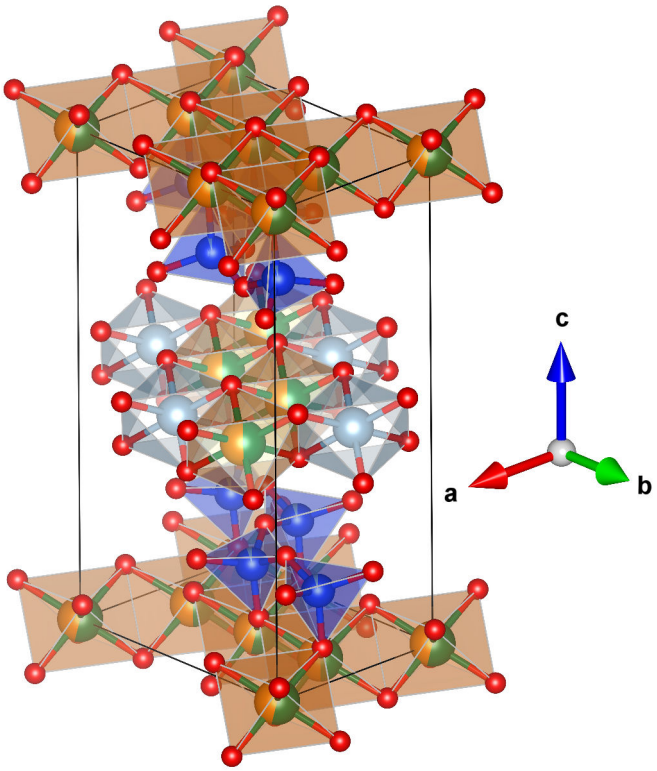

Fig. 2.3 – Chamosite crystalline structure from Walker and Bish (1992). Al = light blue spheres; Fe = orange spheres; Mg = green spheres; O = red spheres; Si = dark blue spheres; shaded area = tetrahedral and octahedral sites.

2.1.2.2 Diopside

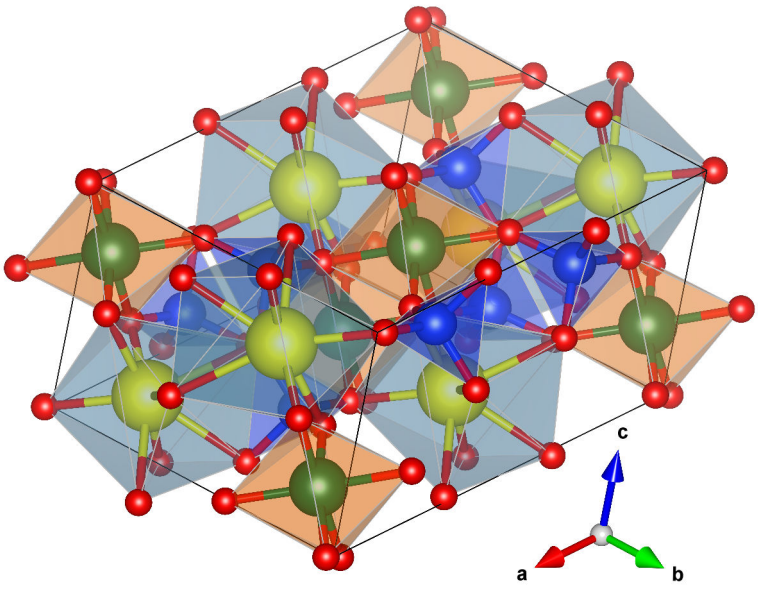

Fig. 2.4 – Diopside crystalline structure from Cameron et al. (1973). Ca = yellow spheres; Mg = green spheres; O = red spheres; Si = dark blue spheres.

Diopside, $CaMgSi_2O_6$, is a silicate member of the pyroxene group. It forms a series with hedenbergite, in which the first is the magnesium-rich member and the other, the iron-rich member. Diopside is commonly found in environments of metamorphosed siliceous Ca, Mg-rich rocks of the pyroxene or epidote-amphiboles groups and is very common in skarns (Anthony et al., 2019). It forms variably coloured but is typically pale to dark green. Diopside has a hardness range between 5.5-6.5 in the Mohs scale and a specific density of $\approx 3.28\ g/cm^3$. It crystallises in the monoclinic lattice system (see Figure 2.4). Diopside is not a magnetic mineral, but its series mineral hedenbergite can presented intrachain ferromagnetic interaction (Baum et al., 1997), and since these minerals are often in the middle of the series transition, a possible influence of hedenbergite properties is not discarded.

2.1.2.3 Epidote

Epidote is the name of a group of silicate minerals that share similar structural and composition characteristics, but also the name of the most common mineral in this group. The

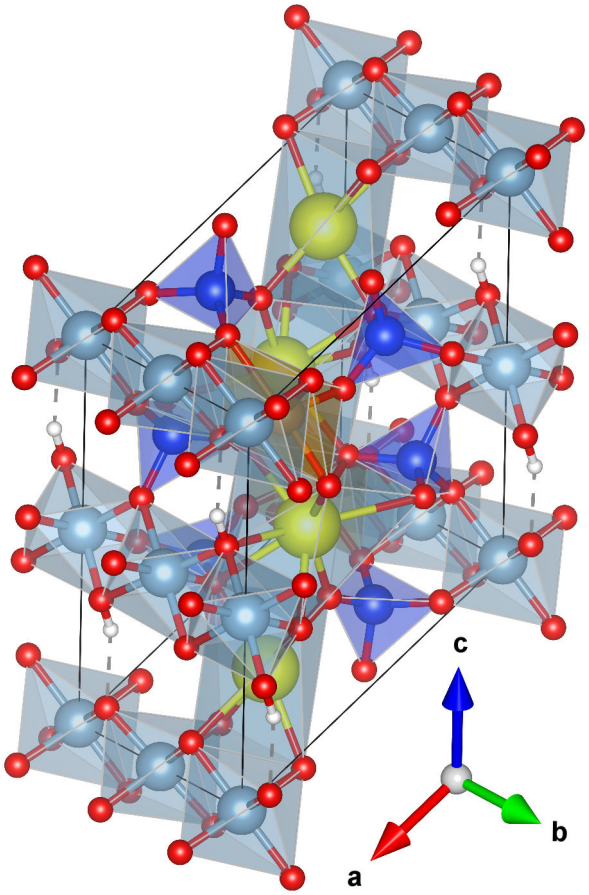

Fig. 2.5 – Epidote crystalline structure from Gabe et al. (1973). Al = light blue spheres; Ca = yellow spheres; Fe = orange spheres; H = white spheres; O = red spheres; Si = dark blue spheres.

mineral epidote, $Ca_2Al_2(Fe^{3+}, Al)(SiO_4)(Si_2O_7)O(OH)$, has a pistachio-green to pale green colour and perfect cleave at the plan {0 0 1} (Anthony et al., 2019). It forms a series with clinozoisite, in which the iron of epidote is gradually replaced by aluminium to the end member clinozoisite. It is commonly found in regionally metamorphosed rocks of low to moderate grade. In these rocks, epidote is often associated with amphiboles, feldspars, quartz, and chlorite. It occurs as replacements of mineral grains that have been altered by metamorphism (Deer et al., 2010). Diopside crystallises in the monoclinic lattice system (see Figure 2.5. It has a hardness range between 6-7 in the Mohs scale and a specific density of $\approx 3.46\ g/cm^3$. It has a weak magnetic susceptibility (Rosenblum and K. Brownfield, 2000).

2.2 Iron ore physical concentration methods

To achieve the first requirement for iron ore processing: *liberation*, it is necessary to introduce operations as comminution and size separation. Only after that, the concentration methods are applied. An important portion of the iron ore produced in the world is still processed only by crushing and screening operations, the so-called Direct Shipping Ores (DSO). However, with the depletion of high-grade iron ores and the emergence of ores with complex mineralogy, concentration processes are becoming increasingly important (Flint et al., 1992). Based on the main characteristics presented for the iron ore constituent minerals, three important concentration methods are widely used: *gravity separation, magnetic separation and flotation.*

2.2.1 Comminution and size separation

Crushing is an operation that is used in all iron ore beneficiation plants. It is accomplished by the compression of the ore against rigid surfaces, it is usually a dry process and can be performed in several stages. In the iron ore processing, gyratory crushers are the most common found equipment for the primary crushing stage, where the ore is crushed as it comes from the mine (run-of-mine). When more stages of crushing are required (secondary or tertiary), the most common crusher employed are cone crushers in jaw, roll and impact models. After crushing, the material goes through another stage of comminution called grinding. Iron ore grinding operations use several techniques as:

- High pressure grinding rolls (HPGR), that utilises compression breakage of a particle bed, in which energy efficient inter-particle breakage occurs (Schönert, 1988);
- Autogenous mills (AG), consisting in a tumbling mill that uses the ore itself as grinding

media;

- Semi-autogenous mills (SAG), like the AG mills but with an addition of steel balls as grinding media;
- Rod mills, that can be considered as fine crushers or coarse grinding machines;
- Ball mills, consisting of a hollow cylindrical shell rotating about its axis with steel balls as grinding media.

Once having their particles reduced in size, iron ores typically proceed to a size separation step. Different types of vibrating screens are employed in a dry or wet basis. Dry screening is generally limited to particles above 5 mm in size and if the ore is not very wet. Wet screening, on the other hand, can go down to sieving very fine fractions at 45 µm for example with the new high-frequency screens. Screw classifier are also employed for size cut around 0.1 mm, proving high unit capacity and less bypass when compared to hydrocyclones. Hydrocyclones are classifiers that utilises centrifugal force to accelerate the settling rate of particles and it has an important utilisation in iron ore processing. It is commonly used in closed-circuit grinding operations but has other important uses as de-sliming for example (Napier-Munn et al., 1996).

2.2.2 Gravity separation

Due to the high difference in the specific density between iron oxides and gangue minerals, gravity separation is a method that works quite well for the separation of such minerals. This technique have proved efficient for concentration of minerals with particle size up to 50 µm (Holland-Batt, 1998). The principle behind gravity separation is quite simple. It separates minerals of different specific gravity by their relative movement in response to gravity and it is very important to have a marked contrast between the minerals. The principal techniques used for gravity separation of iron ores are jigging and spirals.

Jigging is a hydraulic separation process consisting of the expansion and contraction of a bed of particles by the pulsating movement of water. It is normally used to concentrate relatively coarse material and when the specific gravity difference is large finer particles can also be separated. Three main types of jig are used to iron ore processing: pneumatic jigs, mechanical jigs and the diaphragm type.

Spirals are devices composed of a helical conduit of modified semi-circular cross-section. They are typically used in iron ore processing in a very variable particle size range from 2 mm to 75 µm. The iron ore is fed at the top of the spirals and follows the downward flow. The particles are separated due to centrifugal force combined with the differential settling rates and

the wash water that through the flowing particle bed. This last one is an important parameter for a good recovery in spirals' operation.

Other techniques for gravity separation are applied to iron ores as heavy media drum for lump concentration and hydraulic classifiers used for cleaning stages. But among all these techniques, spirals are by far the most used one. In the case of the iron-bearing silicates, their density are higher than regular silicates which can complicate a possible separation by gravity from the iron oxides. The size range is another aggravating factor, if this separation were applied to coarser particles it could have a good effect due the slight difference between the densities of these minerals. However, with the studied iron concentrate having a top size of 38 µm, it is almost impossible to apply gravity as separation method.

2.2.3 Magnetic separation

An important characteristic of iron oxides is the positive response to magnetic fields. The same feature is not observed in the major part of the gangue minerals identified in iron ores. Because this characteristic is well marked between these minerals, this technique is the most applied for iron ore processing. Magnetic separators can be classified into low-intensity from 500 to 2000 G, medium-intensity from 2000 to 7000 G and high-intensity above 7000 G. They can also be divided into dry-feed and wet-feed separator. Dry magnetic separation is confined mainly to the separation of coarse sizes, as a pre-concentration stage (*cobbing*) for iron ores, often employing drum separators. For particles below 0.5 cm, wet magnetic separation replaces the dry method. Drums separators (Figure 2.6) are also used as *rougher*, *cleaner* and *scavenger*

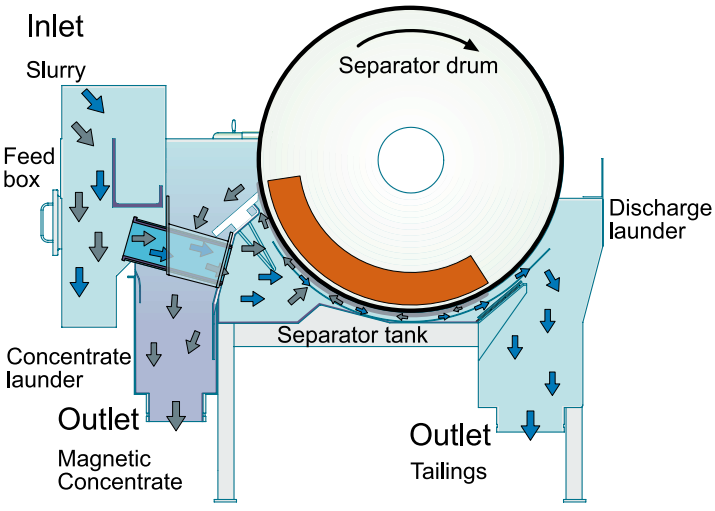

Fig. 2.6 – Counter-rotation drum magnetic separator from Metso®.

steps, depending on the plant configuration. The low-intensity magnetic separators can be installed as single, double or triple drums. The medium-intensity drums separators are very

similar to the low-intensity ones, but they use rare-earth permanent magnets and are typically configured in a single drum. The rare-earth permanent magnets are capable to retain their intensity for a very long period (Norrgran and Marin, 1994). High-intensity magnetic separators are often used in the iron ore processing, since they are able to generate fields up to 1.4 Tesla and then recover hematite and goethite, for example (Svoboda, 1994). Undoubtedly the best known and most used equipment is the *Jones separator*. It consists of boxes containing highly magnetic grooved plates, so-called matrices, arranged in a circular structure (Figure 2.7). The magnetic field is constant, and the circular structure rotates placing the material under the effect of the magnetic field from time to time in continuous cycles. The magnetic particles are held by the plates and the non-magnetic passes through the plate with the help of wash water as well, to avoid entrainment. When the plate boxes reach the point of zero magnetic field, the magnetic particles are washed and collected.

Fig. 2.7 – Circular structure of a high-intensity magnetic separator type Jones from MBE®.

There are also other types of high-intensity magnetic separators as the vertical pulsating magnetic separator called SLon®, which has the same principle as Jones type, but works on the vertical axis and had included a diaphragm to provide pulsation in the separation zone to keep particles in a loose state avoiding entrapment.

The separation of iron oxides and iron-bearing silicates is once again confronted with the technical limitation of the method, as many of the iron-bearing silicates are also attracted by magnetic separators. Rosenblum and K. Brownfield (2000) performed several measurements of magnetic susceptibility with over 300 minerals varying the field strength of the magnet. They found that magnetite has a best extraction range at 0.01 A once it is strongly attracted by a

magnetic field. For hematite this value is between 0.1 and 0.3 A. Chamosite has a value very close to hematite, at 0.3 A, while epidote best extraction range is between 0.4 and 0.7 A.

2.3 Iron ore physical-chemistry concentration method

When the difference in the physical properties of the minerals are not marked enough to make their physical concentration possible, their surface characteristics are modulated and controlled in a technique called *flotation*.

2.3.1 Introduction to flotation

Flotation is a physical-chemistry process that utilises the difference in surface properties of the ore minerals and the gangue minerals to promote their separation. It was originally patented in 1906 and it is an important technique that have allowed the exploitation of many previously considered uneconomic deposits (Wills and Napier-Munn, 2005a). Research on the potential use of flotation in the concentration of iron ores dates from 1931 (Crabtree and Vincent, 1962) and the first industrial application debuted in 1954 (Frommer, 1967). The maximum feed size for flotation can be set depending on the liberation size of the minerals. However, in many cases this size is limited at 300 µm due to the force of adhesion between particle and bubble (Leja, 1982). What means that the upward flow of bubbles is not capable to overflow large particles. The lower limit of the particle size range is set according to the size at which deleterious effects to the system begin to occur, such as the coating of larger particles by sludge or excessive consumption of reagents due to the high specific surface area of the smaller particles (Leja, 1982), but it is typically limited to 10 µm. The main property of the minerals explored in this process is the *wettability*. If a mineral surface is characterised by relatively weak molecular bonds (van der Waals forces) it is considered non-polar and classified as *hydrophobic*. On the other hand, if a mineral has strong covalent or ionic surface bonding it is considered as polar and classified as *hydrophilic*. To adhere to the bubble and thus float, the mineral must present hydrophobic behaviour. However, only few minerals are naturally non-polar (i.e., talc, graphite, molybdenite), and in this case the addition of reagents to render them hydrophobic is necessary (Araujo et al., 2005). Those reagents are classified into anionic, cationic or non-ionic, according to its specific type of the polar group (Leja, 1982). In iron ore flotation, the choice of which reagents to use is closely linked to the chosen route. The main routes in iron ore flotation are: *direct anionic flotation*, *reverse anionic flotation (after calcium activation)* and *reverse cationic flotation* (Ma, 2012). These routes and the reagents used on each of them are detailed below, but first a review of the surface charges of the minerals is necessary due to its link with the

reagents adsorption.

2.3.1.1 Surface charge of minerals

The generation of new surfaces by fragmentation processes causes the appearance of charges on the surface of the minerals by breaking covalent or ionic bonds (Leja, 1982). When in aqueous solution, oxide minerals become charged. This charge is defined by the relative concentrations of the potential determining ions H^+ and OH^- in solution by the following equations(Ma, 2012):

$$\mathrm{MOH} + \mathrm{H}^+ \rightleftharpoons \mathrm{MOH_2}^+ \tag{2.1}$$

$$\mathrm{MOH} + \mathrm{OH}^- \rightleftharpoons \mathrm{MO}^- + \mathrm{H_2O} \tag{2.2}$$

where M represents the metal oxides. It is possible to notice that $\{MO^-\}$ groups are responsible for the negative charge of the surfaces, while $\{MOH_2^+\}$ groups for the positive charge. Therefore, acidic conditions favour the protonation of the surface and lead to a positive surface charge (Equation 2.1). While alkaline conditions favour the deprotonation of the surface leading to a negative surface charge (Equation 2.2). The point where the charge density of each group is equal is defined as the Point of Zero Charge (PZC) (Leja, 1982). The ions H^+ and OH^- are those who set the charges on the surface. It also happens that the so-called counter-ions are adsorbed into the surface by weak bonds. When only the potential determining ions adsorb at the surface, the PZC is the same as the isoelectric point (IEP).

2.3.1.2 Electrical double layer

When an interface is formed the rearrangement of species occurs, resulting in the establishment of a layer of charges that has attracted a layer of counter-charges. The first model for the distribution of these excess charges was proposed by Helmholtz (1879) and Perrin (1904) and they considered the formation of a charged parallel plate condenser along the surface. Based on this first approach, Gouy (1910) and Chapman (1913) proposed that the charges form a diffuse layer of continuum ions. Finally, Stern (1924) combined the condenser model with the diffuse model to propose the so-called Stern model, consisting of two layers in series, the electrical double layer (EDL). In the first layer, the surface charge (either positive or negative), consists of ions adsorbed onto the object due to chemical interactions (compact layer or Stern layer). The second layer is composed of ions attracted to the surface charge via the Coulomb force (diffuse layer). Understand the behaviour of the EDL of the minerals is very important to

the study of reagents adsorption onto these minerals surfaces. A possible form of characterise the electric double layer is the zeta potential measurements, which basically consists of the electrical potential between these two layers (Leja, 1982).

2.3.2 Iron ore flotation routes

2.3.2.1 Direct anionic flotation

Direct anionic flotation was the first technique applied to the flotation of iron ores, back in the 1950's (Ma, 2012). In this technique, anionic collectors are used to float iron oxides. The pulp pH is normally controlled at lower than 9, in which these minerals have positive surface charges and the gangue minerals (typically silicates) have negative surface charges. To avoid the possible electrostatic attraction between metal cations and the anionic collectors, a depressant is normally added to improve the selectivity of this process. Based on the IEP (6.7) for hematite reported by Iwasaki (1990), Fuerstenau and Palmer (1976) have stated that the flotation of hematite at pH $>$ 6.7 was probably due to the formation of hemicelle instead of electrostatic attraction, but the IEP of hematite has been reported to variate in a broad range from pH 4.8 to 9.4. Thus, the surfaces of hematite could remain positively charged and the electrostatic interactions may still contribute to its flotation. Fatty acids are typically the anionic collectors used in this process, although the use of amphoteric collectors such as sarcosinates and sulphosuccinamates have shown satisfactory yields (Araujo et al., 2005). Sodium silicate is the traditional depressant for the direct anionic flotation of iron oxides. However, the efficiency of its selectivity has been questioned by several authors (Araujo et al., 2005) and hydroxamates may be an alternative that has not been explored.

2.3.2.2 Reverse anionic flotation

In the reverse anionic flotation of iron ores, the gangue minerals are floated by anionic collectors. The pH of the pulp is adjusted between 11 and 12 in which the silicates and oxides have negative surface charges. Consequently, the attraction between the anionic collector and the silicates surface would not be possible. To promote this attraction, hydrolysable metal cations are added to activate the silicates surfaces (Ma, 2012). Many metal cations can be used as silicate activators. Iwasaki et al. (1960) demonstrated that calcium is an efficient activator for quartz with a better efficiency in the pH range of 11 to 12, due to the large charge differences. The pH range for the reverse anionic flotation of iron ores is mostly determined because of the optimum activation requirements. The depression of iron oxides particles (charged negatively at this pH range) is usually made with the use of corn starch and the collectors used are fatty

acids. Although the reverse anionic flotation of iron ores have been reported to have a lot of advantages to the reverse cationic flotation (Cooke et al., 1960; Houot, 1983), experiments conducted by Ma et al. (2011) trying to compare the reverse anionic flotation with the reverse cationic flotation, have shown that reverse anionic flotation has slower kinetics than the reverse cationic and desliming was found to be essential for both processes.

2.3.2.3 Reverse cationic flotation

The reverse cationic flotation of iron ores involves the removal of silicates by the use of cationic collectors without the need for activation with calcium ions as for the anionic flotation. The collectors used in the reverse cationic flotation of iron ores belong to the amine group (Leja, 1982). This group has a characteristic property of producing water-repulsion by the cation where the polar group is based (Wills and Napier-Munn, 2005a). Primary fatty amines such as dodecylamine were initially used as quartz collector, but these amines have low solubility in pulp and were replaced by more soluble ether amines (Scott and Smith, 1991), what involves the use of ether monoamines [$R{-}O(CH_2)_3{-}NH_2$], or a combination with ether diamines [$R{-}O(CH_2)_3{-}NH{-}(CH_2)_3{-}NH_2$] (Ma, 2012). Amines are partially neutralized with acetic acid and sometimes partially replaced with emulsified fuel oil (Araujo et al., 2005). In solution, amines protonate as represented in Equation 2.3 (Leja, 1982). The pKa of primary amines from decylamine to octadecylamine varis from 10.64 to 10.60.

$$RNH_{2(aq)} + H_2O \rightleftharpoons RNH_3{}^+ + OH^- \tag{2.3}$$

The fact that the reverse cationic flotation uses pH in the range of 9 to 12 (Iwasaki et al., 1960) is mainly related to the dissociation of amines. At pH $\approx$ 10.5, amines are half in cationic state and half in molecular state, acting as collector and frother, respectively. At this pH value, the froth is very stable and there is no need of adding frothers to the pulp. The adsorption of amines into the surface of minerals is related to specific electrostatic attraction between the negative surface of the minerals with the ether aminium cation and also the van der Waals forces between the carbon chains of the ether aminium ions and the molecular ether aminium (Lima, 1997). Prior to the collecting of silicates, iron oxides need to be depressed to increase selectivity of flotation, since both iron oxides and silicates have negative surface at alkaline pH values, thus prevent iron oxides to float is important. Iron oxides are commonly depressed by corn starch or some other polymer of the same family (Araujo et al., 2005). The reverse cationic flotation is thus made as follows:

- Adjust of pH value to $\approx$ 10.5;

- Depression of iron oxides by polymers;
- Collection of silicates by cationic collectors.

Several chemicals were reported to act as depressants to iron oxides, including starches, dextrin, quebracho, cellulose, lignin sulphonate, humic acid and guar gum (Balajee and Iwasaki, 1969; Khosla and Biswas, 1984; Liu and Laskowski, 1989; Pinto et al., 1992; Peres and Correa, 1996; Turrer and Peres, 2010; Santos and Oliveira, 2007; Filippov et al., 2013; Veloso et al., 2018; Shrimali et al., 2018).

In general, depressants are used only for hematite ores because of their high floatability when in presence of amines. Magnetite, on the other hand, should not float in presence of amines and the separation of magnetite and silicates may be realized at natural pH using only collectors (Ma, 2012). However, the lack of selectivity is an important problem for the reverse cationic flotation of magnetite ores. Starches and their derivatives, commonly employed on the flotation of hematite ores, were tested on magnetite ores without success (Iwasaki, 1990; Filippov et al., 2013). The search for a selective depressant for magnetite ores in the reverse cationic flotation is therefore a key point for the success of the process.

2.3.3 Depressants in the reverse cationic flotation of iron ores

2.3.3.1 Corn starch

Starches are the main depressant used in the reverse cationic flotation of iron ores (Araujo et al., 2005). Starch of chemical formula $(C_6H_{10}O_5)_n$ is one of the most important polysaccharides that can be found in several plants, where n represent the number of glucose monomers that form the macromolecule (Liu et al., 2000; Leja, 1982). Its main source is corn, although some variations are found as potato starch and tapioca starch (Pugh, 1989). Starches are composed of two main components: *amylopectin* and *amylose* (Figure 2.8). Normally it contains 80% of a branched fraction amylopectin and 20% of the linear fraction amylose (Araujo, 1988).

The chain length and molecular weight of the starch depend upon its source, but in general amylose and amylopectin have molecular weight ranging from 40,000 to 65,000 Da and from 10,000 to 100,000 Da, respectively (Pearse, 2005). Starch can be modified by thermal degradation under acidic conditions into a product consisting of smaller and more branched molecules called dextrin (Valdivieso et al., 2004), which is also used in mineral processing and will be further discussed. The hydrophilic character of the starch molecule is conferred by the presence of a large number of OH^- radicals in α-D(+) glucose units (Peres and Correa, 1996). Starches are considered non-ionic compounds, however Balajee and Iwasaki (1969) concluded that corn

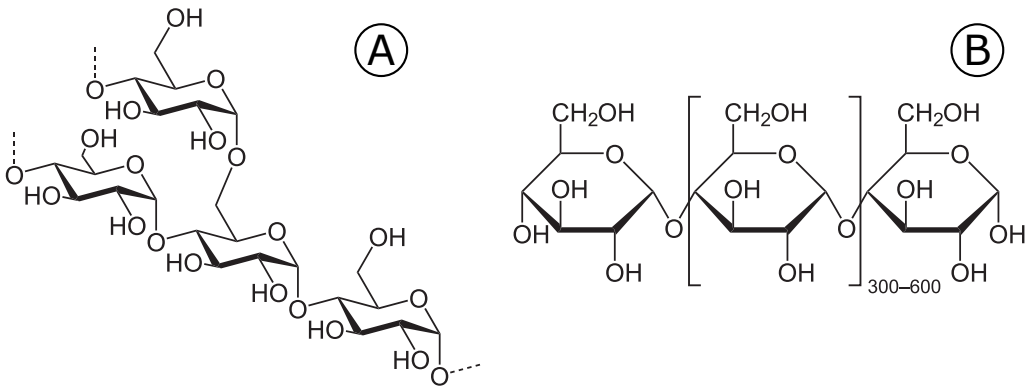

Fig. 2.8 – Schematic structure of amylopectin (A) and amylose (B)

starch molecule has a negative charge that increases with pH, reaching a maximum at pH values between 9 and 10. According to the authors, this charges result from the oxidation and hydrolysis of the macromolecules. To solubilize starch, it is necessary to submit it to a process of breaking the intragranular bonds called gelatinization. This process can be accomplished by a thermal or an alkali process. In the thermal gelatinization, the temperature raises up to 70 °C, causing the break of hydrogen bonds through vibration of the molecules (Bertuzzi et al., 2007). As grain swells continue, starch molecules are completely hydrated and separated due to fragmentation in the micellar interlacing. The alkali gelatinization occurs with the addition of sodium hydroxide. When in presence of an alkaline solution, the protons of the −OH groups are dissociated leading to a negative charge on starch molecules, which results in an expansion of the amylose coil (Jane, 1994; Bertuzzi et al., 2007).

The mechanism of starch adsorption in mineral particles has been a constant object of studies over the years. Initially it was proposed that the main responsible for the attraction between the starch molecule and a certain mineral surface would be hydrogen bonding. With the emergence of new analytical techniques, a chemical complexation between these two components were suggested (Figure 2.9). Electrostatic interactions are less important in the adsorption of starches, however the interaction between the slightly anionic starch molecule with the mineral surface can change the adsorption densities of starches on minerals surfaces. The adsorption behaviour of long chain polymers is very complex and not well understood (Liu et al., 2000). The main propositions for the adsorption of starches are:

1. **Hydrogen bonding**, proposed by Balajee and Iwasaki (1969); Hanna (1974); Afenya (1982); Ma et al. (2011);

2. **Hydrophobic bonding**, proposed by (Wie and Fuerstenau, 1974; Miller et al., 1983, 1984);

3. **Chemical complexation**, proposed by Somasundaran (1969); Khosla and Biswas (1984);

Weisseborn et al. (1995); Filippov et al. (2013);

4. **Electrostatic force**, proposed by Balajee and Iwasaki (1969); Ma (2010); Ma and Bruckard (2010);

5. **Acid/base concept**, proposed by Liu et al. (2000); Laskowski et al. (2007);

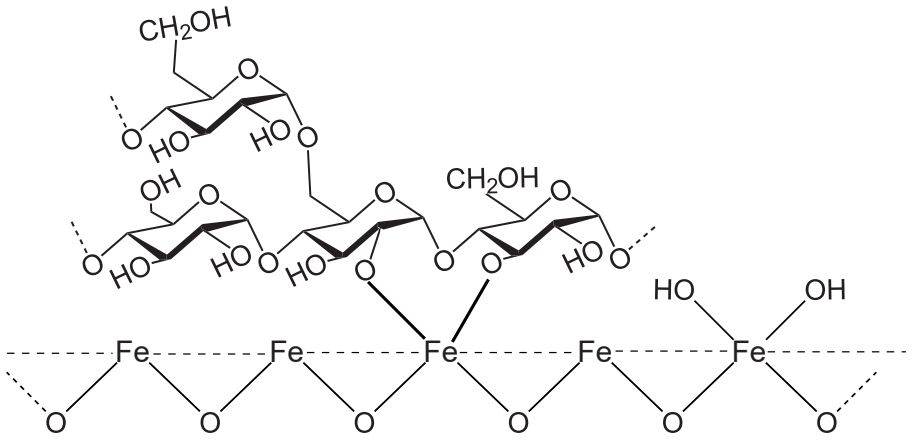

Fig. 2.9 – Adsorption by chemical complexation between hydroxyl groups and iron atoms from hematite, adapted from Weisseborn et al. (1995).

The depressing effect of corn starch can be achieved by three different mechanisms. Corn starch molecules cover the minerals surface inhibiting the adsorption of collectors, or it co-adsorb with collectors but keeps the hydrophilic character of the mineral due to its long carbon chains (Ma, 2012). Also, the space inside the helicoidal structure formed by starch macromolecules can provide a parking space for surfactants (a hydrophobic space) in which these surface-active reagents become occluded and cannot impart hydrophobicity onto the mineral surfaces. This is observed when iodine is displaced by oleate and amine, changing the UV-VISIBLE spectra of solubilized starches (Araujo, 1988).

2.3.3.2 Carboxymethyl cellulose

Cellulose is the most abundant polymer in the world, is non-toxic, biodegradable and, therefore, its derivatives have a wide application (Hoogendam et al., 1998b). The main sources are wood and cotton (Pearse, 2005). It is a natural polymer formed during photosynthesis. In the cellulose chain, glycosidic units are rings of six atoms. They are linked by oxygen atoms between the C1 and C4 carbons to glucose rings forming a linear compound. Glucose units are commonly called anhydroglucose. Carboxymethylcellulose, $(C_8H_{16}NaO_8)_n$, commonly called CMC and illustrated in Figure 2.10, is obtained by replacing hydroxyl radicals of cellulose with carboxymethyl groups. These groups distributed along the cellulose chain make the polymer significantly anionic. The degree of substitution (DS) is the average number of carboxymethyl

groups per anhydroglucose unit with a maximum of three, but in commercially samples this number ranges from 0.5 to 1.5 (Khraisheh et al., 2005). The CMC molecule is 25% and 50% dissociated at pH 3 and 4, respectively (Hoogendam et al., 1998a). The soluble form of CMC can be obtained by the reaction with a chelating agent resin (Porsch and Wittgren, 2005). Sodium carboxymethyl cellulose is prepared by the action of sodium hydroxide and mono-chloracetic acid on cellulose (Pearse, 2005). CMC is widely used in the pharmaceutical, cosmetics and food industries. It has also been used as an alternative binder in the pelletising process. CMC is used in the flotation of other some minerals. However, its application in iron ore processing is somehow limited and has been discussed in recent years.

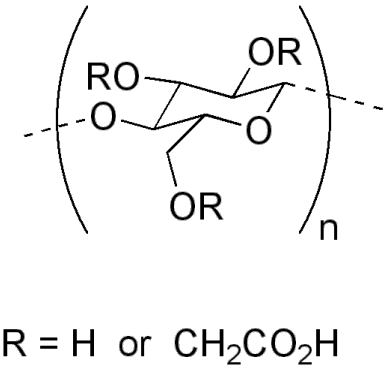

Fig. 2.10 – Schematic structure of carboxymethyl cellulose.

Three main factors impact the performance of a sodium carboxymehtyl cellulose (Pearse, 2005):

- Purity;
- Molecular weight;
- Degree of substitution.

These factors are so important that they may lead to different conclusions about the action of this molecule. In studies using CMC as a talc depressant, Shortridge et al. (2000) found that CMC was inefficient to depress talc and a decrease in talc depression as observed with the increase of CMC concentration. However, Khraisheh et al. (2005) demonstrated that an increase in the molecular weight of CMC leads to an increase in talc depression. Also, low dosages were required for the necessary coverage of the talc surface (Shortridge et al., 1999). The use of CMC was also reported for the depression of secondary copper minerals (Bulatovic et al., 2001) and a higher yield was observed with the depression of galena. Some other reported studies of successful use of CMC as a depressant are: clay depression in potassium flotation (Pearse, 2005); low grade nickel ore (Pugh, 1989); dolomite depressant (Zheng and Smith, 1997); pyrite depression (Bicak et al., 2007); chromite depression in PGE group flotation (Ekmekçi et al.,

2003); huntite in the concentration of carbonates (Kangal et al., 2005); calcite depression in cassiterite flotation Tian et al. (2017).

Castro and Ribeiro (2005) compared the performance of CMC and starch as depressant in iron ore flotation. They found good results for dosages above 500 g/t. Araujo et al. (2005) have performed several flotation tests on different types of iron ore varying degrees of substitution and molecular weight. They have observed a better silica removal when CMC is used as depressant instead of starch, however, a slightly high iron loss to the tailings was also observed. According to the same authors, in terms of operational costs, the replacement of starch by CMC would only be competitive if the CMC dosage is 5 times lower than starch. As for starch adsorption on mineral surfaces, CMC adsorption was initially attributed to hydrogen bonding between the minerals and this reagent (Steenberg and Harris, 1984). Liu et al. (2000) suggest, however, that the breaking of hydrogen bonds formed between the polymer and water would be fundamental for the adsorption by hydrogen bonding of CMC on the mineral surface. However, this breaking seems to be not favorable. Liu and Laskowski (1999) studied the role of hydroxyl and carboxyl groups in the adsorption of carboxymethyl cellulose on mineral surfaces. They observed that CMC does not adsorb strongly in natural or hydrophobized quartz, however, the situation is reversed in the presence of metal ions. According to their findings, the authors stated that three fundamental reactions govern the adsorption between this polymer and minerals in aqueous solution. The reaction between carboxyl groups with metal cations, the reaction of hydroxy complexes with metal cations and the reaction of hydroxyl groups only with metal cations. This is due to the difference in pKa between these groups. Hydroxyl groups have pKa close to 12. What means that in the typically pH for flotation process, they will not be completely dissociated. On the other hand, carboxyl groups have pKa of 4.4. From this pH value, the molecule will become negatively charged with the charge density being a function of its degree of substitution. Bicak et al. (2007) however, stated based on measurements of adsorption, zeta potential and floatability that both electrostatic adsorption by hydrogen bridge and chemistry by acid-base mechanisms are part of the CMC adsorption process. Studies were also conducted with CMC in the presence of amines. Fujimoto and Petri (2001) performed experimental investigations on surfaces coated by amines. They found that the CMC adsorption kinetics on this surface can be divided into 3 stages. In the first, the polymer spreads over the exposed surface in a rapid process. After this stage, the few adsorbed chains must obtain a conformation that enables the adsorption of new chains, a slow process, in which the first electrostatic barrier must be overcome. The rearrangement of the polymer is then especially slow in a medium with high ionic strength and acid pH. Then, steric repulsion between loops of uncharged segments of the CMC must be overcome until complete surface coverage. Hoogendam et al. (1998b) observed that the amount of adsorbed CMC decreases with pH and does not change with the degree of substitution, indicating electrostatic contribution to adsorption. According to Backfolk et al.

(2002), the adsorption of CMC into calcium carbonate took place by the formation of an endothermic acid/base reaction, which originated from the attraction of the carboxylic groups to the hydrated calcium carbonate surface sites. Khraisheh et al. (2005) concluded in their study on talc depression that CMC adsorption occurs by electrostatic and multilayer interactions and, therefore, the adsorption occurs preferentially in the talc planes.

2.3.3.3 Dextrin

The term dextrin is applied for several products obtained from the "dextrinization" of starches. It has the same monomer as starches, $(C_6H_{10}O_5)_n$, but it is a smaller macromolecule, with more branched structures (Liu, 1988). Dextrin keeps the same ratio of amylopectin and amylose from its original source, having a change in the numbers of n glucose units (Peres and Correa, 1996). Its molecular weight is also around 10 times smaller than regular starches, ranging from few thousands to 79,000 (Liu, 1988). Dextrins are white, yellow, or brown powder that are partially or fully water-soluble, yielding optically active solutions of low viscosity. The process of dextrinization occurs basically by the acidification of starches with a simultaneous heating, when the hydrolysis of starch takes place. Dextrins are mixtures of polymers of D-glucose units linked by $\alpha-(1\rightarrow 4)$ or $\alpha-(1\rightarrow 6)$ glycosidic bonds (Haas, 1913), as presented in Figure 2.11.

The quality of a dextrin depends on the base starch used in the dextrinization process. The product of the dextrinization is still hydrophilic, but its structure may be not long enough to establish bonds between surface and polymer (Peres and Correa, 1996). This difference in the structure between starches and dextrin is the reason that induce researches on the use of this polymer as depressant in flotation for example. Small molecule polymers are known to have affinity for some minerals and to be able to access certain areas of the mineral surface that large molecules cannot (Liu, 1988).

The first application of dextrin in flotation dates from 1957, in the depression of pentlandite in a differential flotation of Cu−Pb (Valdivieso et al., 2004). Studies were also conducted using dextrin in the flotation of sulphides (Laskowski et al., 1991), molybdenite (Wie and Fuerstenau, 1974; Braga et al., 2014), talc (Mierczynska-Vasilev et al., 2008), pyrite and/or spharelite (Kydros et al., 1994; Rath and Subramanian, 1999; Valdivieso et al., 2004; Beaussart et al., 2011), coal (Miller et al., 1983), chalcopyrite and/or galena (Rath and Subramanian, 1999; Liu et al., 2000; Valdivieso et al., 2007). It is possible to realize that the use of dextrin as depressant was widely used for hydrophobic minerals as talc and molybdenite.

The use of dextrin in iron ore flotation is not very much explored. Probably because its source is already been widely used and has a better economic benefit than a treated product

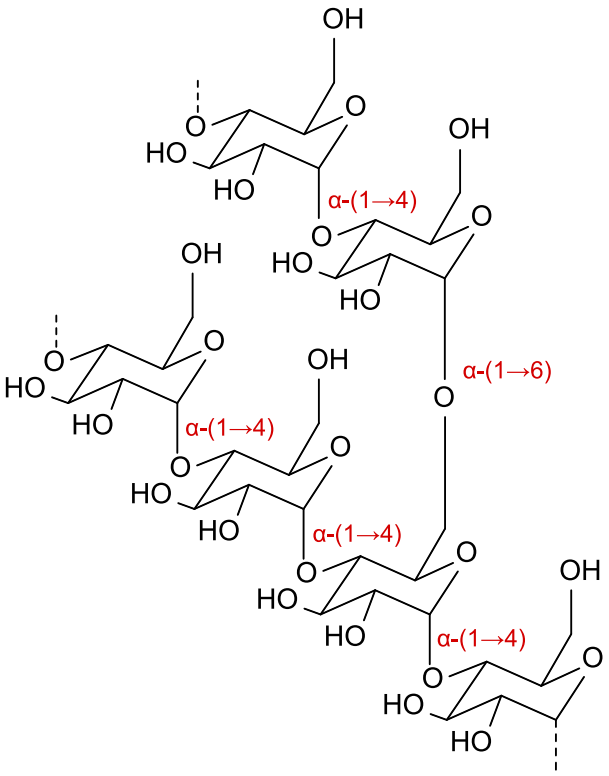

Fig. 2.11 – Schematic structure of $\alpha-(1\rightarrow4)$ or $\alpha-(1\rightarrow6)$ dextrin adapted from (Miller et al., 1983).

such as dextrin. Beattie et al. (2006) compared the performance of starch and dextrin as depressants in a mineral mixture composed of talc and sulphides (chalcopyrite and pentanditla). Micro-flotation tests showed that the starches with higher molecular weight were better talc depressant, while dextrin with smaller structures exhibited better selectivity, thanks to less dextrin adsorption on the sulphide surface. The adsorption mechanisms proposed for the adsorption of dextrin are mainly the same discussed for starches, based on the same structure. (Liu et al., 2000) found that dextrin adsorption is pH dependent, although other studies have shown that polysaccharide adsorption does not depend on pH (Rath and Subramanian, 1999)

2.3.3.4 Humic acid

Humic substances are possibly the most abundant natural organic macromolecules in the earth's crust. It is responsible for 60-70% of natural organic matter in soils and 30-50% of aquatic organic matter (Santos and Oliveira, 2007). These substances are the product of incomplete decomposition of organic matter and when in natural waters they behave as anionic ligands and are subdivided into humine, fulvic acid and humic acid (Brum and Oliveira, 2005). Humic acid (HA), $(C_9H_8Na_2O_4)_n$, consists of a mixture of various organic compounds with molecules of different sizes and major chemical differences. Its molecular weight can variate

from from a few thousand to 1,000,000 or more. The smaller size fractions are composed of molecules with a larger number of aromatic and acidic clusters than the larger fraction (Illés and Tombácz, 2003). Humic acid structure is very complex and have not been perfectly established. However, it can be described as an association of covalent bonds, consisting of aliphatic and aromatic chains, containing several functional groups, of which we can highlight the phenolic and carboxylic groups (Jones and Bryan, 1998; Santos and Oliveira, 2007). Figure 2.12 presents an humic acid structure proposed by (Stevenson, 1994).

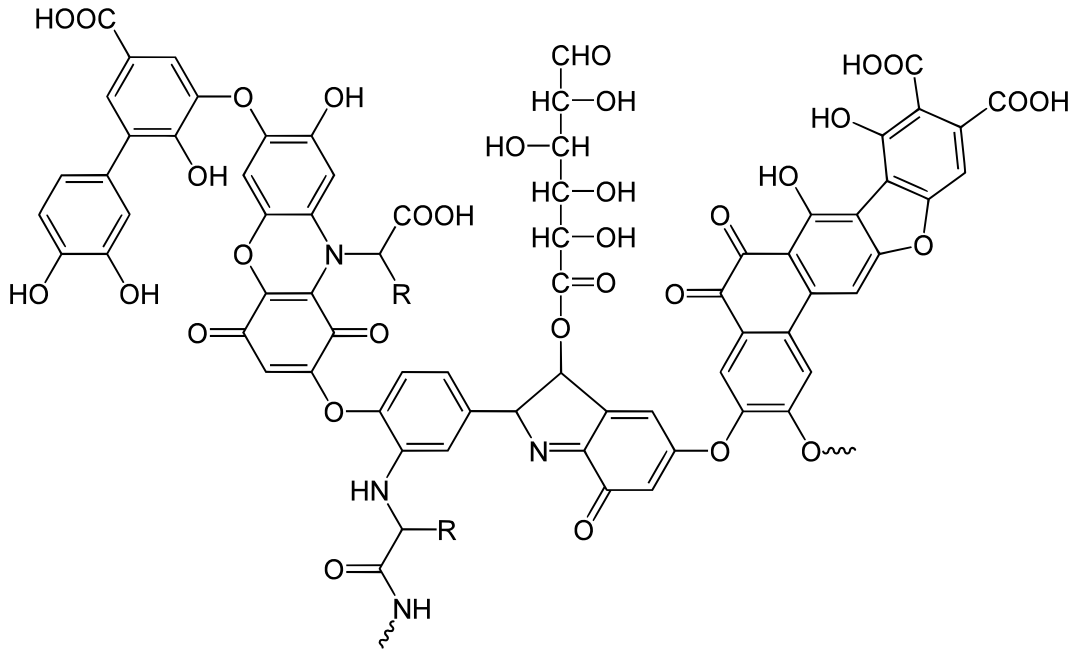

Fig. 2.12 – Schematic structure of a typical humic acid, having a variety of components including quinone, phenol, catechol, and sugar moieties, adapted from (Stevenson, 1994).

The dissociation of carboxylic groups and hydroxyl phenols in water leads to the appearance of negative charges attached to the carbonic chain of the macromolecule. Increasing pH and ionic strength leads to increased dissociation and, consequently, increased negative charge of the molecule (Illés and Tombácz, 2003). It may occur in salt form, but HCl treatment converts to the widely marketed acid form. Humic acid has high solubility at pH $>$ 2 and the colour of its solution varies from dark yellow to black depending on its concentration. Despite the complexity of the structure of HA, with its high content of aromatic, aliphatic and many carboxylic groups, it is not a toxic substance (Brum and Oliveira, 2005). Avena et al. (1999) used 8 different samples of humic acid to define the PZC as being close to pH 3. They studied the influence of humic acid concentration, pH and ionic strength of the solution. The electrostatic repulsion among negative charged groups tend to expand the humic acid molecule. Studies using humic and fulvic acids were reported by several authors in some mineral processing systems: kaolinite (Hur and Schlautman, 2003); vermiculite (Abate and Masini, 2003).

Although no industrial application is known in iron ore processing for humic acid, its use in flotation of iron oxides has been studied for sometime. Santos and Oliveira (2007) indicated that humic acid proved to be an excellent hematite depressant, being possible to affirm that its results were better than those of corn starch. Edwards et al. (1996) studied the influence of carboxylic groups and phenols on the adsorption of natural organic matter rich in humic acid onto iron oxide surface. The authors concluded that adsorption is mainly governed by the carboxylic groups. Vermeer et al. (1998) studied the adsorption of acidic humic acid in hematite and concluded that charge compensation favours adsorption, whereas electrostatic repulsion inhibits it. According to the same authors, at acidic pH, an important part of the adsorbed molecules are not in direct contact with the surface, which results in a high adsorbed amount and an enlargement of the EDL. Ramos-Tejada et al. (2003) however, explained the higher adsorption at acidic pH on hematite surfaces, based on the formation of complexes between humic acid and the available mineral sites of Fe^{3+} or $Fe-OH$. This is also supported by Tombácz et al. (2004) who also studied the adsorption of humic acid on the magnetite surface and stated that adsorption occurs by complexation at points $Fe-OH$. According to Illés and Tombácz (2003), the electrostatic component has an important role in humic acid adsorption only at acidic pH values and complexation dominate the adsorption mechanisms at alkaline pH values. Nayak et al. (1990) highlighted the importance of the electrostatic component that caused an increase of the acid character of the polymer and consequently a greater electrostatic repulsion on the hematite adsorption. Illés and Tombácz (2003) show that there is competition between the larger and smaller molecules of humic acid for the available magnetite sites. They also observed that smaller molecules (more aromatic) have higher affinity for the mineral surface than larger molecules (more aliphatic). Hur and Schlautman (2003) have also stated that small molecules of humic acid have more affinity to hematite surface and the adsorption was attributed to hydrophobic interactions. The adsorption rate of humic acid into iron oxides is very high up to 5 minutes. After that, a little adsorption occurs due to the rearrangement of the molecules (Petteys and Schimpf, 1998).

2.4 Molecular modelling applied to flotation

The better understanding of the molecular mechanisms involved in flotation reagent adsorption such as depressants, activators, and collectors is very important to help in the search for better process selectivity or recovery. The determination of adsorption energies and structural configurations allows to adapt the reagents used during flotation to the ore mineralogical association. Moreover, it brings clarity in the comprehension of the synergistic effects that are commonly exhibited when reagents are used in combination.

The energy of systems describing the adsorption processes can be calculated using highly accurate methods based on quantum mechanical descriptions such as Hartree-Fock, post-Hartree-Fock, and density functional theory (DFT) (Sholl and Steckel, 2009; Evans et al., 2017). Besides, energies and structures can be determined using classical potentials-based simulations that require accurate force fields and are not able to fully describe quantum mechanisms such as chemical bond cleavage or formation (Evans et al., 2017). DFT is the most common applied methodology for this approach. DFT calculations are used to determine the structure and energy of a system in its ground-state and, hence, do not describe atoms movements and the thermal motion.

Three important steps are linked with the study of flotation reagents adsorption.

Surface exposure

Every mineral processing technique needs a comminution step prior to the concentration process. When a mineral is crushed or ground, existing bonds between their molecules are broken. The mineral cleavage happens in the surface with the lowest surface energy (Whittaker, 1982; Gao et al., 2014). The most exposed surface of a mineral need to be investigated, since all the adsorption processes will occur onto those surfaces (Gao et al., 2012; Hu et al., 2012; Gao et al., 2017, 2019). The surface behaviour determination should constitute the first task to be performed in a molecular modelling approach. For example, *ab-initio* studies confirmed successfully that the (104) surface is the most exposed for calcite (Gao et al., 2012, 2017), the (001) and (112) for scheelite (Cooper and de Leeuw, 2003; Gao et al., 2013), and the (001) and (210) for barite (Bittarello et al., 2018).

Hydration

Once the mineral surface is well defined and investigated, hydration is the next step in its molecular modelling investigation. Since flotation occurs in aqueous medium, it is supposed that the minerals surfaces are fully hydrated. Different possibilities for the adsorption of water (molecular, dissociated) should be considered until its completely coverage. The hydration mechanisms of some mineral surfaces have been investigated over the past years by atomistic simulations. Sulphides were studied by DFT simulations (Badawi et al., 2011; Chen et al., 2014; Haider et al., 2014; Long et al., 2016b; Li et al., 2019) to bring clarity in the hydration mechanisms, mostly accompanied by oxidation phenomena. In addition, oxide minerals were deeply investigated since they represent an important source for non-base metals and mineral commodities. The hydration mechanisms of calcium/magnesium carbonates were described by DFT calculations (de Leeuw and Parker, 1997, 1998; Escamilla-Roa et al., 2013; Lopez-Berganza et al., 2015; Goverapet Srinivasan et al., 2017). Other sparingly soluble salts were also deeply investigated with atomistic simulations to consider hydrated surfaces for the flotation

reagents adsorption, such as scheelite (Cooper and de Leeuw, 2003; de Leeuw and Cooper, 2003), fluorite (de Leeuw et al., 2000; Khatib et al., 2016; Foucaud et al., 2018a), apatite (Zahn and Hochrein, 2003; Pareek et al., 2008, 2009; Ulian et al., 2018), and rare-earth-elements-bearing minerals (Srinivasan et al., 2016; Goverapet Srinivasan et al., 2017; Stack et al., 2018). Metallic oxides/hydroxides such as rutile (Heydari et al., 2019), manganite (Xia et al., 2007), corundum (Janeček et al., 2014), pyrochlore (Bjørheim et al., 2012), goethite (Aquino et al., 2007; de Leeuw and Cooper, 2007; Chen et al., 2017), and hematite (de Leeuw and Cooper, 2007; Souvi et al., 2013) were also studied since they are known to form hydroxylated species at their surfaces in the presence of water molecules. The hydration mechanisms of many silicates, such as olivine (Kerisit et al., 2013; Prigiobbe et al., 2013; Liu et al., 2019) or phyllosilicates (Wang et al., 2005; Wungu et al., 2012; Peng et al., 2016), have been investigated with however a high number of studies focusing on quartz (Rignanese et al., 2004; Du and de Leeuw, 2006; Skelton et al., 2011; Wang et al., 2018).

Reagent adsorption

When the surface of the mineral is fully hydrated it is ready for start the reagent adsorption modelling. Several researches have been reported in the study of reagent adsorption onto minerals. The adsorption of the most widely used collectors for sulphides (xanthates, thiophosphate, carbamate) have been investigated by DFT for pyrite (Hung et al., 2003, 2004), galena (Chen et al., 2014; Long et al., 2016b), chalcopyrite (Jiao et al., 2015; Zhao et al., 2016; Ma et al., 2017; Sarvaramini and Larachi, 2017), and sphalerite (Liu et al., 2013a, 2014; Jiao et al., 2015; Long et al., 2016a; Sarvaramini et al., 2016b; Liu et al., 2018). Few studies exist which focus on the adsorption of flotation reagents onto silicates. The adsorption of amines onto such minerals was investigated by DFT calculations on muscovite (Xu et al., 2013; Wang et al., 2014) and kaolinite (Xia et al., 2009). Moreover, the adsorption of anionic collectors, mostly fatty acids, was investigated by molecular modelling for quartz (Li et al., 2017), but mostly for other valuable silicates that have a significant affinity for fatty acids such as feldspars (Xu et al., 2017a,b) or spodumene (Yu et al., 2014; He et al., 2014; Yu et al., 2015; Xu et al., 2017a; Zhu et al., 2018). Researches on adsorption mechanisms of anionic collectors, mostly carboxylate and hydroxamate, by DFT onto rare-earth minerals (Sarvaramini et al., 2016a; Espiritu et al., 2018, 2019), onto scheelite (Cooper and de Leeuw, 2004; Zhao et al., 2013; Yin et al., 2014), cassiterite (Gong et al., 2017; Liu et al., 2017; Tian et al., 2018), apatite (Mkhonto et al., 2006; Xie et al., 2018)), hematite (Chernyshova et al., 2011; Rath et al., 2014), and fluorite (de Leeuw and Cooper, 2002; Foucaud et al., 2018b) have also been reported.

Once these three steps are completed, a lot of information about the mineral surface and the adsorption mechanisms involved in the mineral-reagents interactions is generated. This information can be useful for enhancing selectivity or recovery with the current used reagent

or even for the formulation of new reagents. The studies presented above outlined the use of molecular modelling in the flotation of several mineral systems. A significant increase in the number of this type of studies has been reported over the years. Molecular modelling is a powerful tool that allows an in-depth study of the molecular interactions between minerals and reagents that are often difficult to be observed in experimental investigations and represents a breakthrough in the study of mineral processing by flotation. A detailed review of the DFT method employed in this study is presented in chapter 8.

2.5 Study purpose and strategy

The studies presented above highlighted the main issues related to the processing of complex iron ores, especially when iron-bearing silicates are present as gangue minerals. Each mineral plays an important role in iron ore process, as its intrinsic characteristics are used in the separation processes. Gravity concentration might be a possibility to the separation of iron oxides from these complex silicates, since their specific densities are relatively different. However, the size range of the material used in this study does not allow the use of this technique. Magnetic concentration, a widely used technique in the concentration of magnetite iron ores, have already shown to be inefficient at the processing plant in Mexico. This is expected, since the magnetic susceptibility of iron-bearing silicates are high enough to make them be picked-up for a magnetic field.

From the techniques used for iron ore processing, flotation is the most appropriate for promoting this separation, because if no contrast is observed between minerals, the addition of reagents can create such contrast in order to render one mineral hydrophobic or hydrophillic. Among the routes for iron ore flotation, the reverse cationic flotation is the most applied considering the facility of floating simple silicates, like quartz. During the reverse cationic flotation of magnetite iron ores, depressants are normally not used, due to the low floatability of magnetite when in presence of cationic collectors. However, there is a lack of selectivity in this process, even though with the use of depressants.

The main question this study faces is whether **it is possible to beneficiate a highly complex iron ore by flotation?** From this question others arise and are important for the research: *Is it possible to separate assemblages of iron-bearing silicates mainly from iron oxides? What are the physical-chemistry conditions governing the selective adsorption of polymers onto minerals surface leading to a separation contrast? Is there a link between crystal chemistry and surface hydration of iron-bearing silicates defining differential flotation behaviour?*

Trying to answer these questions, fundamental research leading with the interaction of the

studied silicates and iron oxides with reagents was performed through surface charge characterisation; adsorption equilibrium studies with depressants; single and multi-mineral microflotation with collectors and depressants; and molecular modelling of the most problematic iron-bearing silicate studied, chamosite.

Applied research on the reverse cationic flotation of an iron concentrate, containing the minerals studied in the fundamental research, were also conducted. This flotation route has high potential for the separation of magnetite from complex assemblages of gangue minerals. The use of depressants is considered important for the study, because of the high concentration of magnetite in the material (already a concentrate) and the need to have the most selective flotation possible, considering the proximity between the properties of iron oxides and iron-bearing silicates. The search for a selective depressant is a problematic addressed in this thesis, through a complete study of alternative depressants for the flotation of magnetite iron ores.

Chapter 3

Materials and Methods

3.1 Pure mineral samples

Natural mineral samples were used in the present study. Chamosite sample comes from the original deposit at Chamoson in Switzerland, diopside samples comes from Brazil, epidote sample comes from Madagascar, hematite and magnetite samples also come from Brazil. These pure minerals samples were prepared according to the scheme shown in Figure 3.1. The samples were first crushed using laboratory crushers. After crushing to D_{95} of about 2 mm, they were further ground in a tungsten carbide ring mill to avoid contaminations from conventional mills. The grinding operation was performed in stages of 3 minutes, to avoid the generation of fines, followed by wet screening on sieves with apertures of 106 µm and 38 µm. The oversize was

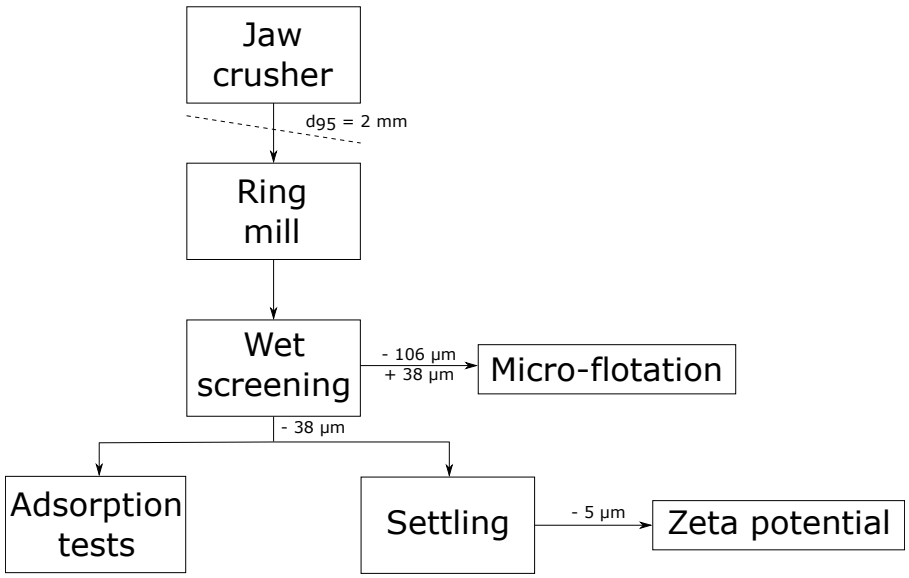

Fig. 3.1 – Sample preparation protocol for chamosite, diopside, epidote, hematite and magnetite.

Table 3.1 – Chemical analyses of pure mineral samples by XRF.

Mineral	Elemental analyses (% of oxides)						
	FeO	Fe_2O_3	SiO_2	Al_2O_3	CaO	MgO	LOI
Chamosite (106-38 µm)	31.40	17.83	21.20	11.65	1.14	1.89	9.41
Chamosite (< 38 µm)	30.60	17.00	21.40	11.60	1.15	1.95	10.25
Diopside (106-38 µm)	3.95	0.60	55.90	0.63	20.40	15.75	0.53
Diopside (< 38 µm)	4.03	0.82	55.20	0.70	20.30	15.95	1.90
Epidote (106-38 µm)	0.25	13.74	37.60	22.50	22.70	0.08	2.06
Epidote (< 38 µm)	0.35	13.77	37.80	22.40	22.50	0.14	1.09
Hematite (106-38 µm)	0.52	99.08	0.27	0.03	0.03	0.05	0.28
Hematite (< 38 µm)	0.43	98.79	0.28	0.10	0.12	0.08	0.28
Magnetite (106-38 µm)	29.50	63.39	3.11	2.29	0.23	0.13	-2.80
Magnetite (< 38µm)	29.90	68.92	0.75	0.59	0.02	0.04	-3.24

added to fresh feed material and another stage was initiated. The fraction below 106 µm and above 38 µm was used to perform the micro-flotation tests. The fraction below 38 µm was used for all the adsorption experiments. Part of the fraction below 38 µm was also used to perform the electrophoresis measurements after passing by a beaker decantation to yield a size fraction below 5 µm.

Sample characterisation

Table 3.1 presents the results for the chemical analyses performed on the five mineral samples by size, showing the purity of each size fraction used in the different experiments. Chamosite has a good purity, MgO is lower than the reported in literature, however this may indicate that the specimen is located on the pole iron of the solid-solution series that this mineral form with clinochlore. Diopside has the same SiO_2 content reported in literature, with a little bit less CaO and MgO, but still a good purity is observed. Epidote is of high purity, presenting a small deviation from the original deposit in Bourg, France (Armbruster et al., 2006). Hematite is extremely pure, with around 99% of Fe_2O_3. Magnetite has also very high purity with almost 30% of FeO and some small impurities specially in the coarser sample.The XRD diffractograms of each sample are also presented in Appendix A.

3.2 Iron concentrate samples

Two different samples of iron concentrate coming from Peña Colorada mine in Mexico were used in this study to evaluate the reverse cationinc flotation of silicates:

(i) ***Sample 1:*** drill core sample processed at Peña Colorada laboratory in Mexico;

(ii) ***Sample 2:*** output stream of the plant (magnetite concentrate).

Sample description

Sample 1 was collected during a drilling campaign conducted along the deposit and it was processed by a series of laboratory scale tests. Figure 3.2 shows the procedure adopted for preparing the sample. The entire sample of the drill holes (approximately 2 t) was crushed and sieved to ensure that the particles were below 2 mm prior to the concentration stages. Then, a first step of dry magnetic separation was performed and repeated 5 times under a magnetic field of 550 G. The magnetic portion was ground in a ball mill to reach a P_{80} of 38 µm, and finally, the material goes through a wet magnetic separation for 3 times with a magnetic field of 550 G.

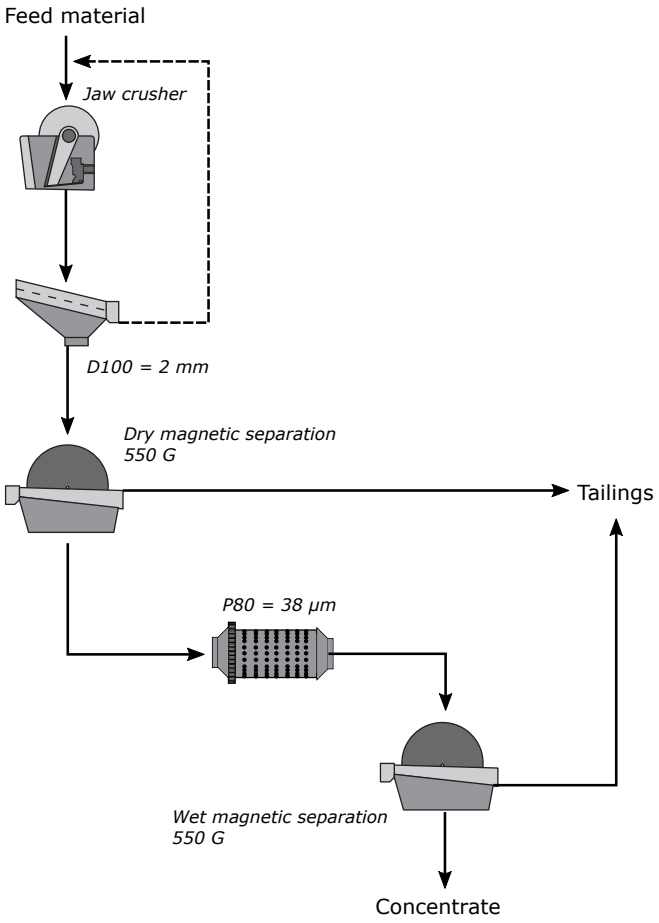

Fig. 3.2 – Sample preparation protocol for drill core samples used in Mexican laboratory.

Sample 2 was collected during a sampling campaign conducted in the plant in the beginning of 2018. Approximately 3.2 t of the final concentrate coming from the underflow of the Magnefloc (see Figure 1.5 in chapter 1) has been continuously recovered aiming to obtain a representative material of the final product of the plant.

Sample preparation

When received from the mine, both samples 1 and 2 were completely homogenised forming

piles with the help of a shovel. Sample 1 was split into 25 kg buckets which were later used for the bench-scale experiments. Sample 2 was first split into a large sample (around 2.5 t) that was used in the pilot flotation tests and the rest of the sample was also split into 25 kg buckets, used for the bench-scale experiments. The complete characterisation of both samples 1 and 2 are presented in the next chapter.

3.3 Chemicals

The chemicals used in this study are presented here below. They were divided in three groups: *depressants*, *collectors* and *others* and they are all reagents of high purity.

3.3.1 Depressants

The following depressants, supplied by Sigma-Aldrich, were used to perform several flotation tests:

- *Corn starch*, with a number-average molecular weight of 500,000;
- *Carboxymethyl cellulose sodium salt*, with a number-average molecular weight of 700,000 and a substitution degree of 0.9;
- *Dextrin from maize starch*, with a number-average molecular weight of 20,000;
- *Humic acid sodium salt*, with a number-average molecular weight of 500,000.

In addition, other alternative depressants supplied by Piestch Chemicals were tested:

- *Deprapol HMT*, is a mixture of humic and fulvic acids with altered anionic character, presented in its salt form;
- *Deprapol VF*, is a short-chain derivative of humic acid, presented in its acid form;
- *Deprapol N05*, is a pre-gelatinized natural polysaccharide with different proportions of amylose.

A stock solution of each depressant was prepared daily to avoid degradation of the compounds as discussed by Balajee and Iwasaki (1969). Corn starch was the unique depressant that was gelatinized by adding 1 g of caustic soda per 5 g of corn starch and the other depressants were solubilized with deionised water.

3.3.2 Collectors

The silicate collectors used in this study are:

- *Flotigam EDA*, supplied by Clariant. It is an alkyl ether amine partially neutralized with acetic acid, of molecular weight of 233 $g.mol^{-1}$ and derived from fatty amines;
- *42L/21*, supplied by Piestch Chemicals. It is a di-amine with prevalence of aliphatic radicals. Its neutralization is made with strong organic acid and it has a molecular weight of 390 $g.mol^{-1}$;
- *ODLL123*, supplied by Piestch Chemicals. It is a di-amine with strong cationic character, neutralized with strong organic acid and a molecular weight of 378 $g.mol^{-1}$;
- *7-15*, supplied by Piestch Chemical. It is a di-amine with prevalence of branched aliphatic radical mixtures and it has a molecular weight of 348 $g.mol^{-1}$;
- *Dodecylamine hydrochloride (DDA)*, supplied by Acros Organics with 99% purity. It is a primary amine with 221.81 $g.mol^{-1}$ of molecular weight;
- *Dodecyloxypropylamine (ETA)*, supplied by Sigma-Aldrich as a pure sample not neutralised with a molecular weight of 243.42 $g.mol^{-1}$;
- *Potassium Amyl Xanthante (PAX)*, supplied by Clariant, is an organosulfur compound with a molecular weight of 202.37 $g.mol^{1}$. It is used for the flotation of sulphides;
- *Hostaflot-LIB*, supplied by Clariant. It is a sodium dialkyldithiophosphate, generally replacing xanthates.

The preparation of the collectors was performed only by diluting the reagents in deionized water to the desired concentration. The only reagent that had to undergo pre-treatment was ether amine. It was necessary to neutralise it before, following the procedure:

1. Three grams of the ether amine were added drop by drop in 20 mL of high grade ethanol with moderate agitation to prevent foaming;
2. Four mL of 37% HCl were added dropwise;
3. The mixture temperature was set to 60 °C to evaporate the ethanol, water and remaining HCl;
4. After proper evaporation, the paste was scraped and put to dry in petri dish for 24h;

5. The dry powder was then gently grounded and put in a glass bottle for future use.

An ATR-IR spectrum of the ether amine after 100% neutralization is presented in Appendix B and is being compared to two theoretical IR spectra of ether-amine, simulated by the software Orca, proving the purity of the neutralized reagent.

3.3.3 Others

Besides depressants and collectors, the following chemicals were used during the study:

- *Flotanol H53*, supplied by Clariant was used as frother during sulphide flotation. It is an alcohol (4-methyl-2-pentanol) of 102.17 $g.mol^{-1}$ molecular weight;
- *Potassium chloride*, from VWR was used as supporting electrolyte for electrophoresis measurements;
- *Sodium hydroxide*, from VWR was used as pH modifier and for gelatinization of starch;
- *Potassium hydroxide*, from VWR was used as pH modifier for the electrophoresis experiments;
- *Hydrochloric acid*, from VWR was used as pH modifier for flotation and electrophoresis experiments;
- *Ethanol*, from VWR was used for ether amine preparation and for cleaning.

3.4 Experimental methods

3.4.1 Material characterisation

3.4.1.1 Particle size analysis

Screening

Coarser particles (> 38 µm) were sized by wet screening using a single screen vibrator with standards 8" screens. The sieves were periodically cleaned in an ultrasonic bath. The material used in the pilot flotation tests was screened using an industrial screen DF200 from Derrick.

Cyclosizer

The Cyclosizer consists basically of a console cabinet on which five hydrocyclones are mounted together with a sample container assembly, rotameter, pressure gauge, thermometer and electrical control panel. To determine the size distribution of a sample, a known weight is slurried with water and transferred to the sample container. The initial distribution of the sample is an approximate size separation with each cyclone and apex chamber containing an excess of under size material. The effective separating sizes of the five cyclones are calculated from the specific limiting sizes and the correction factors for the actual levels of the operating variables.

Decantation

Conventional beaker decantation was used for the recovery of samples smaller than 5 µm from the fraction below 38 µm, which was used for electrophoresis measurement. In all cases, Stokes law behaviour was assumed.

Laser diffraction analysis

Alternatively, particle size analyse has been performed using a Helium-Neon Laser Optical System Malvern 2000 supplied by Malvern Instruments, now MalvernPanalytical coupled with a Hydro Extended Volume sample dispersion unit. The equipment uses the principles of static light scattering and Mie theory to calculate the size of particles in a sample. The basic principle is that small particles will scatter light at large angles and large particles will scatter light at small angles. The scattering pattern produced by the sample is recorded and by applying Mie scattering theory the distribution of particle size can be calculated. For the acquisition, samples were introduced in the equipment until an obscuration level of 15% is reached. Malvern 2000 operates in a size range of 0.02 to 2000 µm.

3.4.1.2 Optical microscopy

An optical microscope creates a magnified image of an object specimen with an objective lens and magnifies the image further more with an eyepiece to allow the user to observe it by the naked eye. To do that is necessary to obtain a clear and sharp image and to change its magnification. The illumination optical system should supply and collect light and adjust its intensity to generate the necessary contrast to have a good observation.

The microscope used in this study is a Leica DM4500 P equipped with a camera allowing the acquisition of images in a fast and accurate way. It uses transmitted and incident light as illumination techniques and its composed by four objectives lens aggrouped in an objective turret and it has a usable field of view of 25 mm.

3.4.1.3 Chemical analysis by X-ray fluorescence

Chemical assays were carried out using an Axios FAST, model PW4600 (Panalytical). Axios FAST is equipped with a rhodium anode SST-mAX tube. Beam attenuators are installed enabling all channels to measure concentrations from ppm levels up to 100%, while maintaining a high tube power setting. A prepared sample (0.66 g) is fused with a 12:22 lithium tetraborate – lithium metaborate flux which also includes an oxidizing agent (Lithium Nitrate), and then poured into a platinum mould. The resultant disk is in turn analysed by XRF spectrometry. The XRF analysis is determined in conjunction with a loss-on-ignition at 1000°C. The resulting data from both determinations are combined to produce a "total".

3.4.1.4 Chemical analysis by wet method

The determination of ferrous iron was performed by acid decomposition and titration with potassium dichromate. Potassium dichromate is used for oxidising Fe^{2+} to Fe^{3+} in acidic conditions. It can hence be used to determine the amount of Fe^{2+} in a sample. A prepared sample (0.25 – 1 g) is digested with sulphuric and hydrofluoric acids. The sample solution containing ferrous iron is then titrated in a beaker containing diluted sulphuric acid, orthophosphoric acid and boric acid with potassium dichromate solution.

3.4.1.5 Sulphur analysis

For samples with sulphur content above 5% weight, XRF is not the most appropriate technique because of its sensibility. Instead, the analysis of sulphur content through an induction and/or resistance furnace is most indicate. Sulphur in the sample forms gaseous molecules like SO_2 during combustion. The released amounts of SO_2 are measured in up to 4 element-selective infrared cells. Usually, two infrared cells are used for measuring one gas to ensure that both very low and very high concentrations are analysed precise and correctly.

ELTRA's ELEMENTRAC CS-d analyser was used for the sulphur measurements in samples with more than 5% of sulphur content. It is equipped with both an induction and a resistance furnace, allowing the analysis of organic and inorganic compounds.

3.4.1.6 Magnetic susceptibility

Measuring the total magnetic moment of a sample in a saturating magnetic field is a quick accurate and reliable method of measuring the magnetic material content of a sample. The principle behind the Satmagan is to measure the force acting on the sample in a magnetic

field with a spatial gradient. Its operation is based on measurement of the magnetic moment after the magnetic component in the sample has been magnetized for saturation. The magnetic moment is determined by measuring the force acting on the sample in a non-homogeneous magnetic field and comparing it with the gravitational force acting on the sample. Measuring the ratio of the magnetic to the gravitational force and multiplying this by a coefficient gives the percentage of the magnetic component in the sample.

The saturation magnetization analyser used for the measurements is a Satmagan model 135 operating in a range of measurement from 0 to 100% by magnetite weight. Samples were inserted into an acrylic container of approximately 4 g capacity in the case of the samples analysed. Calibration of the equipment have been done in a monthly basis with a set of standards made by mixing pure magnetite and silicon.

3.4.1.7 Mineralogical analysis by X-ray diffraction

XRD spectra were acquired on a Bruker D2 PHASER, operating with a cobalt $K_{\alpha 1}$ ray (WL = 1.7926 Å), a tension of 30 kV and an intensity of 10 mA. The obtained diffractograms were interpreted by EVA software to identify qualitatively the phases present in each sample. Reference diffractograms of pure species from the Crystallography Open Database (COD) and Power Diffraction File (PDF) were used to identify the peaks and compare the mineral phases of the samples. The quantitative analysis of the phases was performed by the Rietveld method using TOPAS software and data from chemical analysis. This method, known as modal analysis, is an interactive method that uses the estimated mineral phases distribution obtained by XRD and the chemical composition of these minerals trying to compare with the chemical analysis of the sample in a back-calculating methodology.

3.4.1.8 Scanning electron microscopy

The equipment used for the textural observations is a high performance Schottky field emission SEM (FEG-SEM) supplied by Zeiss model LEO 1550, capable of resolution in 2-5 nm size ranges and equipped with an Oxford INCA Energy E2H X-ray Energy Dispersive Spectrometer (EDS) system. The accelerating voltage was 20 kV for all the analyses and AzTEC and INCA software packages were used for chemical analyses. Sample mounts were coated with carbon by vacuum evaporation to ensure the superficial conduction of electrons and to prevent the accumulation of electrostatic charge at the surface.

3.4.1.9 Infrared spectroscopy

The equipment used is a benchtop FT-IR spectrometer supplied by Bruker model ALPHA, capable of collecting spectra from 7,500 cm^{-1} to 375 cm^{-1}. This is equivalent to a wavelength range of 1333 nm to 26.6 µm. When necessary, sample was mixed with KBr ensuring that its dilution was not affecting the absorbance bands in the linear region of Lambert-Beer's law. The preparation of KBr pellets relied on a standardized procedure with constant sample/KBr weight ratio, pressure and pellet weight to enhance reproducibility.

3.4.2 Surface characterisation

3.4.2.1 Surface area determination

The specific surface area (area per unit mass or volume) of the samples was measured by a multi-point BET method with N_2 adsorption. This method consists of modelling the portion of the isotherm that corresponds to the end of the adsorption of the first layer of gas ($0.05 < P/Po < 0.2$) by a theoretical isotherm of multilayer adsorption proposed by (Brunauer et al., 1938). In the linearized form the BET equation reads:

$$\frac{p}{v\ (p_0 - p)} = \frac{1}{v_m.c} + \frac{(c-1)}{v_m.c} \times \frac{p}{p_0} \tag{3.1}$$

where p/p_0 is the relative vapor pressure of the adsorbate, v the volume of gas adsorbed, v_m the volume of gas adsorbed in a monolayer and c is a constant related to the energy of adsorption. A linear regression of the left side of the equation and p/p_0 yields a slope of intercept from which c and v_m are obtained. The specific surface area is then calculated from v_m and the area occupied by one molecule of the adsorbate – 0.162 nm^2 / molecule for N_2.

The measurements were carried out on a Belsorp-mini II automatic volumetric adsorption measurement instrument of BELJAPAN, Inc. It is equipped with a turbomolecular pumping unit which ensures a limit vacuum of 0.01 Pa. The cells containing the samples to be analysed are equipped with a sensor providing pressure measurement in the range of 0 - 133 kPa. The nitrogen used during the measurement is supplied by Alphagaz and purity of 99.995%.

3.4.2.2 Zeta Potential measurements

The development of a net charge at the particle surface affects the distribution of ions in the surrounding interfacial region, resulting in an increased concentration of counter-ions (ions

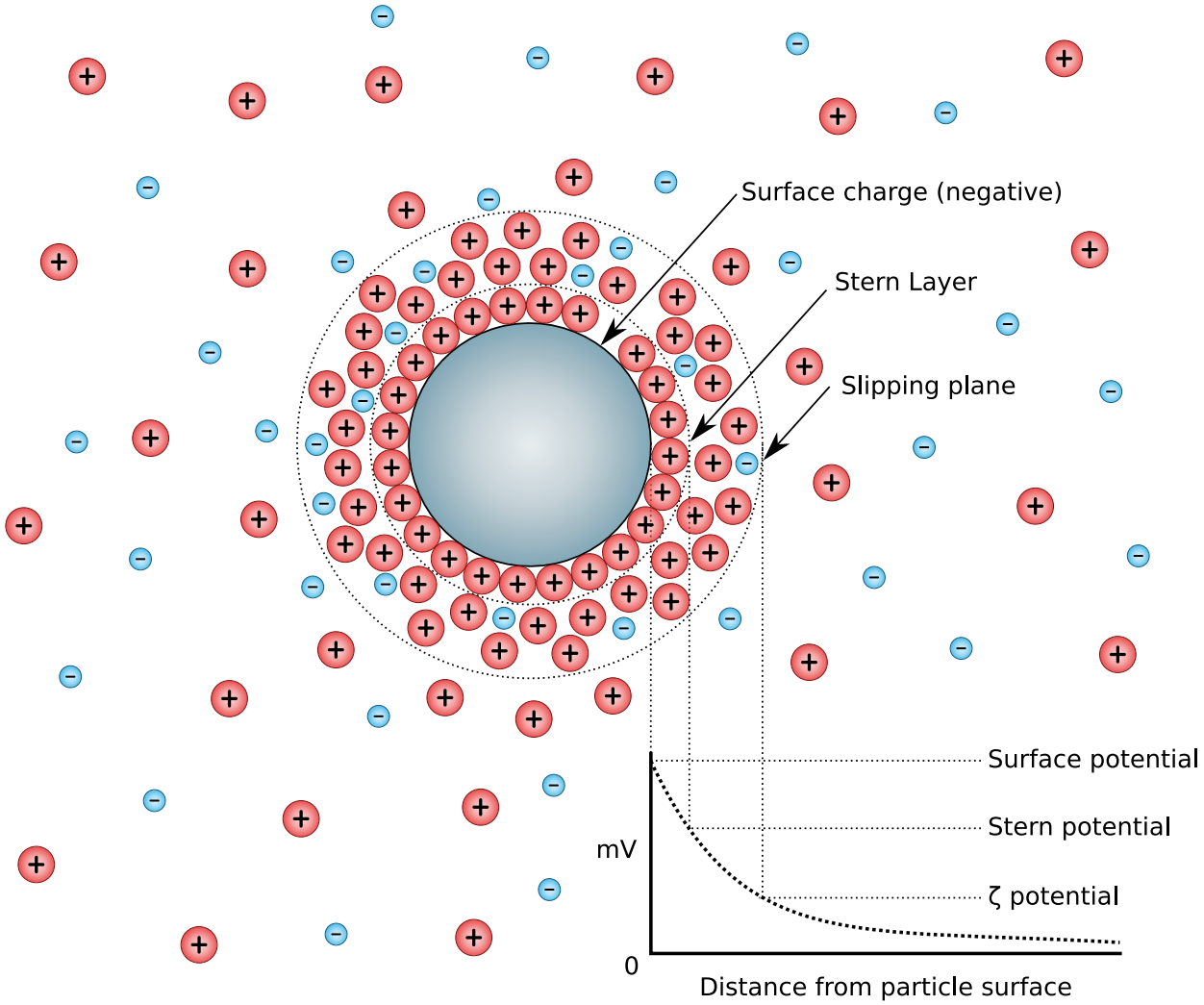

Fig. 3.3 – Diagram presenting the ionic concentration and potential difference as a function of distance from the charged surface of a particle suspended in a dispersion medium,

of opposite charge to that of the particle) close to the surface. Thus, an electrical double layer exists around each particle. The liquid layer surrounding the particle exists as two parts; an inner region, called the Stern layer, where the ions are strongly bound and an outer, diffuse region where they are less firmly attached. Within the diffuse layer there is a notional boundary inside which the ions and particles form a stable entity. When a particle moves (e.g. due to gravity), ions within the boundary move with it, but any ions beyond the boundary do not travel with the particle. This boundary is called the surface of hydrodynamic shear or slipping plane. The potential that exists at this boundary is known as the Zeta potential (Figure 3.3). When an electric field is applied across an electrolyte, charged particles suspended in the electrolyte are attracted towards the electrode of opposite charge. Viscous forces acting on the particles tend to oppose this movement. When equilibrium is reached between these two opposing forces, the particles move with constant velocity. The velocity of a particle in an electric field is commonly referred to as its electrophoretic mobility.

The electrophoretic mobility of particles in suspension was measured at room temperature as a function of pH for three ionic strength using a Zetaphoremetre IV (CAD Instrumentations). Electrophoretic mobility evaluation consisted in following the displacements of particles in a quartz Suprasil® rectangular capillary when subjected to a constant direct-current electric field (around 800 V/m) via tracking the reflection by particles of a laser beam at a 90° angle by means of a Charge-Coupled Device camera. The magnitude and sign of the colloid charge were determined by observing the speed and direction of the particle movement under the influence of the applied field. Trajectories were recorded in real time and were processed with an image analysis software to derive (Gaussian-like) mobility distribution from which mean value was extracted. As for hard particles the measured speed is directly proportional to the magnitude of the particle charge, the zeta potential distribution and mean value was obtained using Helmholtz-Smoluchowski equation.

For the measurements of the minerals in presence of depressants, a ZM3-D-G meter, Zeta Meter system 3.0+, with direct video imaging from Zeta Meter, Inc, USA, was used. Before each test, the completely opened Zeta Meter cell was washed intensively with tap water and then with distilled water. Before each measurement the platinum and the molybdenum electrodes were washed with distilled water. The voltage used in the test was always the highest possible voltage that did not generate vortex due to the heating of the suspension during the measurements.

3.4.3 Adsorption

3.4.3.1 Total organic carbon analysis

Total Organic Carbon (TOC) is a rapid method that determines the amount of total carbon (TC) present in a sample aliquot. Total carbon consists of inorganic and organic carbon. The sample pass through a combustion furnace which is supplied with purified air. The combustion of the sample up to 680° starts with a platinum catalyst. It decomposes and is converted to carbon dioxide which is, once cooled, detected by a non-dispersive infrared (NDIR) detector, giving the amount of total carbon present in the sample. Furthermore, by subjecting the oxidised sample to a sparging process with acid, the inorganic carbon (IC) in the sample is converted to carbon dioxide and its concentration is obtained by again with the use of a non-dispersive infrared detector. Finally, TOC value be determined by subtracting IC value from TC value.

The TOC analyser used in this study is a Shimadzu TOC-VCSH which has a measurement range of 0-25,000 mg.L^{-1} and 0-30,000 mg.L^{-1} for TC and IC respectively. Samples are automatic injected by a syringe pump and a volume between 5 and 7 mL is required per

measurement.

3.4.3.2 Depressant adsorption test work

The amount of depressant adsorbed onto the surfaces of the mineral samples was measured with the help of TOC analyses. The following experimental procedure was used:

(i) One g of mineral powder was transferred to a 100 mL flask;

(ii) 50 mL of the depressant solution to be tested, at the pre-chosen concentration and pH was also added to the flask;

(iii) Agitation was set at 200 rpm in an orbital shaker for 60 minutes;

(iv) The solution was centrifuged at 12,000 G for 15 minutes and the liquid phase was used for the TOC analysis;

(v) A calibration curve was stablished correlating organic carbon and depressant concentration;

(vi) The amount of depressant adsorbed was calculated by difference between the initial concentration and the residual one.

Before performing the adsorption isotherms for each depressant, an investigation of the optimum adsorption pH was performed, having been tested the following pH values: 5, 7, 9 and 11, the initial concentration for this part of the study was set at 100 ppm for all the depressants. Once the pH value of higher adsorption established, the adsorption isotherms were performed at several initial concentrations: 25, 50, 100, 150, 200, 250 and 300 ppm.

3.4.4 Laboratory scale flotation

3.4.4.1 Micro-flotation test work

Investigations of the effects of collectors and depressants on the flotation of the studied minerals were carried out by micro-flotation in two different cells: a modified Hallimond tube (Hallimond, 1944), where magnetic stirring is used and the volume of solution was fixed in 180 mL and a modified Smith-Partridge tube (Partridge and Smith, 1971) to allow the introduction of a stirring rod eliminating the use of magnetic stirring and which had its volume fixed in 240 mL. Figure 3.4 shows a schematic drawing of the two tubes, it is important to note that the

lower part of the tubes is exactly the same to avoid hydrodynamic influences in the different performed experiments. Airflow rate was set to 100 mL/min for all tests. The magnetic stirrer was always set to the same speed and the stirring rod was set to 700 rpm to ensure a mechanical entrainment below 5%. Reagents conditioning time and froth collecting time were investigated before and the results were the basis for the following tests. Single mineral micro-flotation of diopside and epidote were performed in the modified Hallimond tube while chamosite, hematite and magnetite were floated in the other tube. The other experiments involving mixtures of minerals and the use of depressants were all performed in the modified Smith-Partridge. Each test used approximately 1 gram of mineral in the size fraction between 106 µm and 38 µm.

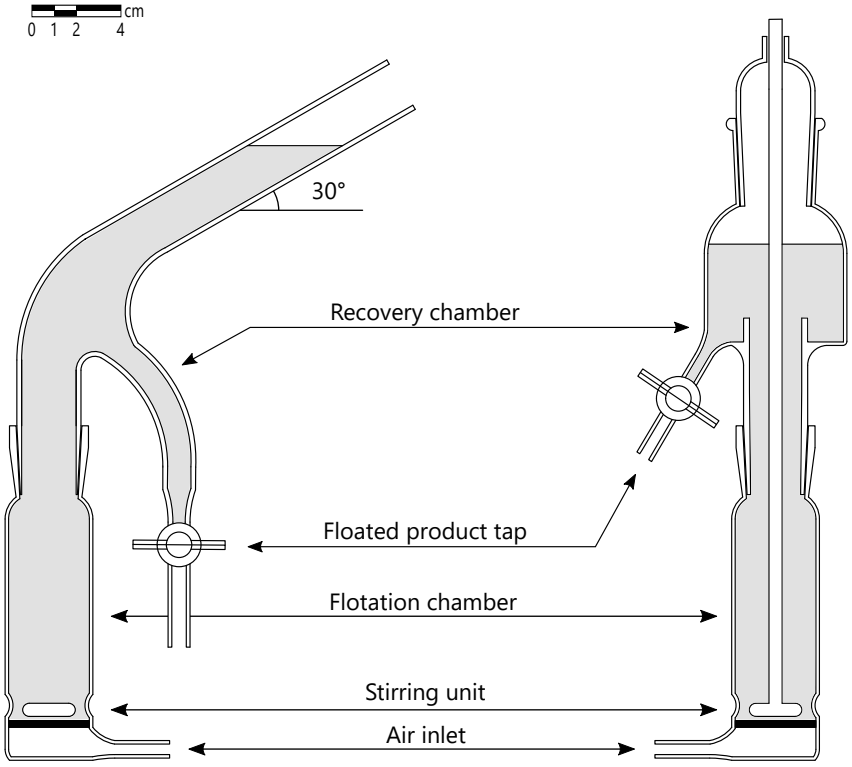

Fig. 3.4 – Schematic drawing of a modified Hallimond tube (*left*) and a modified Smith-Partridge tube (*right*) developed for the flotation of magnetic minerals.

3.4.4.2 Bench scale flotation test work

During this study, several bench flotation tests were performed with different configurations and objectives. This section presents the equipment and parameters that were constant in all tests. If any modifications were made during a test, they will be mentioned when discussing their results.

Figure 3.5 presents the equipment used for all the bench flotation tests, a Denver type flotation machine, Metso D-12. This machine is composed of an impeller surrounded by a

Fig. 3.5 – Denver type flotation machine, Metso D-12.

stator consisting of several blades arranged in a concentric circle with gaps between the blades to facilitate the movement of slurry in the cell. Air is introduced through the hollow shaft to the impeller region. 1.2 L cell was used for almost all tests. The airflow rate was 4 L/min and the impeller speed 900 rpm.

Flotation tests

For all the individual bench scale tests, 500 g of iron concentrate in the size fraction below 53 µm was used as feed material. Once the sulphur content in the feed material was initially considered high for the purposes of the final product (direct reduction iron process), a sulphide flotation step was added prior to the silicates flotation, except in some cases mentioned later. The main steps before and during the flotation tests were: grinding, desliming, sulphide flotation and silicate flotation. Grinding was performed prior flotation for one minute aiming to activate by friction the oxidized surface of sulphide minerals from the transit time of the concentrate till the flotation test itself. Desliming was performed by differential settling. The slurry containing approximately 10% solids was placed into the flotation cell under agitation. After a certain time, the agitation was turned off allowing the coarse particles to settle for 1 minute, then the supernatant water containing slimes was siphoned. Conditioning with reagents has been performed directly in the flotation cell, with pulp density at 60% solids by weight and flotation at 40% solids by weight. Reagents dosages variate according to objective of each test and will be presented before discussing the results. The pH value was followed during all flotation steps and adjusted when necessary by adding NaOH or HCl. The following procedure was used for

the bench scale tests:

(i) Pyrite surface reactivation by grinding for 1 minute;

(ii) Pulp transfer to the flotation cell;

(iii) Desliming by differential settling;

(iv) Conditioning of sulphide collectors and frother (3 minutes);

(v) Air injection and collecting of sulphides tailings;

(vi) Conditioning of depressant (5 minutes) and silicate collector (2 minutes);

(vii) Air injection and collecting of silicates tailings;

(viii) Oven drying and weighing of sunk and floated products.

For the tests without sulphide flotation stage, the items i, iv and v were disregarded.

3.4.4.3 Locked cycle flotation test work

A locked cycle (LC) test consists of repeating several bench scale tests in which the middlings generated in one cycle are recirculated to the subsequent cycle. This kind of test has been used to experimentally simulate a continuous process (Taggart, 1948; Nishimura et al., 1989). The main difficult in performing this test is to achieve steady state in the recirculated flows. This state is verified by the stability of the recirculated solid mass. The effectiveness of LC tests was evaluated in this study and the results compared with the pilot flotation tests.

Once one stage of rougher flotation has shown good results in terms of silica reduction, the main goal of the LC tests was to improve the iron recovery in the final product. Two different tests were performed in this study. Both LC tests implemented a separate rougher flotation stage prior to the continuous LC circuit, that was performed using 3 kg of sample in a 5.5 L flotation cell. This configuration was chosen because a very low silica content could be achieved with only the rougher stage and to obtain enough feed material (rougher tailings) to run the continuous circuit. LC 1 consisted of a separate rougher stage followed by scavenger and cleaner stages. The tailings from the cleaner stage were recirculated back to the scavenger stage. The flow-sheet (Figure 3.6) and reagents dosages (Table 3.2) for LC 1 are presented below.

For the second LC test several changes were made to the flow-sheet. The main changes were the addition of sulphide flotation prior to the rougher stage and a re-cleaner stage following the cleaner. The objective of these changes was to further reduce the final silica content, even

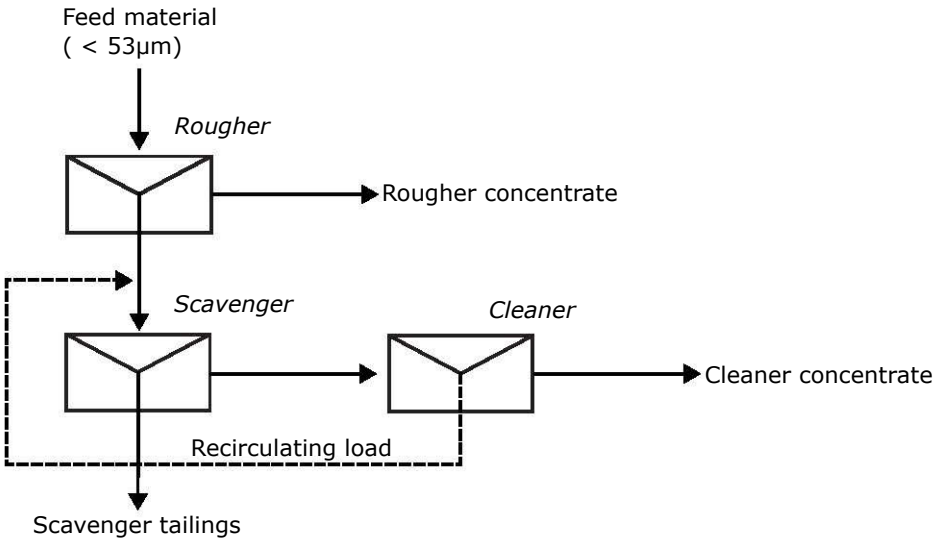

Fig. 3.6 – Flow-sheet of the flotation experiments applied to the locked cycle 1.

Table 3.2 – Dosages of depressant and collectors used during locked cycle test 1.

Reagent	Dosages (g/t) per stage		
	Rougher	Scavenger	Cleaner
Deprapol N05	300	300	300
Flotigam EDA	110	130	90

if that meant decreasing the final recovery. The flow-sheet (Figure 3.7) and reagents dosages (Table 3.3) for LC 2 are presented below.

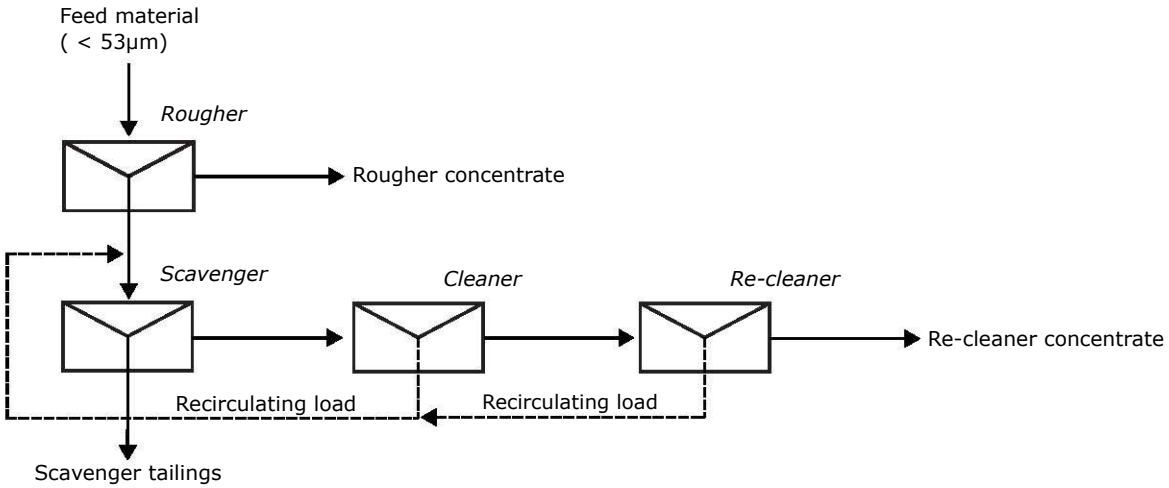

Fig. 3.7 – Flow-sheet of the flotation experiments applied to the locked cycle 2.

Table 3.3 – Dosages of depressant and collectors used during locked cycle test 2.

Reagent	Dosages (g/t) per stage			
	Rougher	Scavenger	Cleaner	Re-cleaner
Flotanol H53	2 drops*	-	-	-
Hostaflot LIB	20	-	-	-
Deprapol N05	300	300	300	350
Flotigam EDA	110	130	90	60

* Frother added to help on froth stability

3.4.5 Pilot scale flotation

3.4.5.1 Mechanical flotation test work

The pilot flotation test was performed using Minemet mechanical cells. Each flotation bank is composed of two open flow cells of 25 L and have a mechanical impeller close to the bottom of the cell. The energy consumption of each flotation bank is 1.5 kW/h. The test was performed in two stages: rougher and scavenger. The solid material was fed at a rate of 60 kg/h into

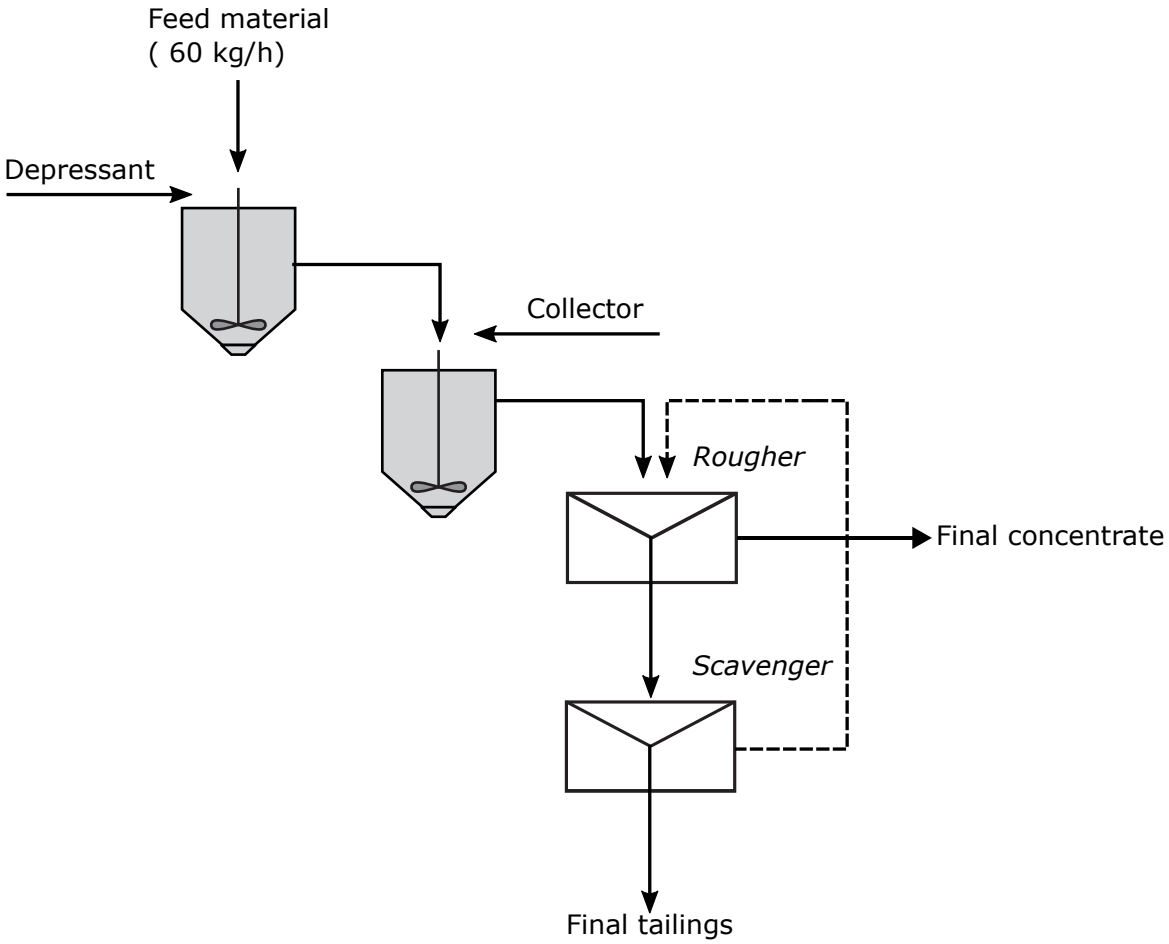

Fig. 3.8 – Flow-sheet of the pilot flotation experiments carried out at Steval laboratory.

a 6 L conditioner tank with water to generate a pulp with 60% solids. The pulp was then conditioned with depressant inside this first tank with a residence time of 5 minutes and then transferred to a second conditioner tank, maintaining the same percentage of solids, where the collector was added and conditioned for two minutes. After the conditioning, the pulp fed the first bank of flotation cells, rougher stage. The percentage of solids was adjusted to 40% and the air was opened. The concentrate from this stage was considered as final concentrate and the tailings was feeding the next scavenger stage where reagents were added directly inside the cells. The tailings from this second stage was sent to the final tailings and the concentrate was recirculated into the rougher stage. A flow-sheet of the pilot test is presented in Figure 3.8. Once the process reached stability, all the streams were sampled three times for 20 seconds and a one-minute interval between each aliquot was respected. After this first sampling aiming to determine the flow rate of the pulp in each stage, a representative sample of the final tailings and concentrate was collected for one hour to perform the mass balance.

3.4.5.2 Column flotation test work

The column flotation used for this pilot tests is a home-made column of the Steval (Station Expérimentale de Valorisation des matières premières et des substances résiduraires) laboratory, located in Nancy, France (Filippov et al., 2000). The column is automated with level control and pressure pickups spaced every meter. The possibility of read the pressure in real time helps with the estimation of the gas hold-up (volume fraction of the dispersed gas phase) and allows to determinethe average bubble diameter (Filippov et al., 2018). The column has 6 meters in height and a diameter of 75 mm (3") and the froth was kept within 50 cm height. The superficial velocities of pulp and gas phases are also controlled and depend respectively of the feed rate and gas rates. The bubbles were generated at the bottom of the column using Flotair sparger. The conditioning with reagents was also performed using two conditioner tanks of 6 L. The solid material fed the first one at a rate of 60 kg/h and it was mixed with water to form a 40% solids pulp. Then, the depressant was added and conditioned for 5 minutes. The pulp was sent to the second tank where the collector was added and conditioned for two minutes. Airflow rate was kept in 3 L/min during all the test. Deprapol N05 was used as depressant in a dosage of 350 g/t and Flotigam EDA as collector with 130 g/t of dosage. Once stability was reached in the column flotation, tailings and concentrate were sampled for 15 minutes.

Chapter 4

Definition of the experimental approach based on the characterisation study

The aim of this chapter is to present the characterisation results performed on the two iron concentrate samples used in this study and explain how this part of the study was the basis for several decisions taken and how it has guided this study several times.

4.1 Size-by-size analysis

The particle size distribution (PSD) of a given material is an essential parameter for any beneficiation route. Coarse particles are usually not fully liberated. This situation prevents mineral phases from separation and from being effectively concentrated. Contrarily, fine particles, because of low inertia and high specific area may impact the physical separation efficiency and/or increase the reagents consumption in concentration methods such as flotation and badly affect filtration and thickening operations. In addition, size distribution analysis is also important for accessing sieving efficiency, classifiers partition curves and for controlling specifications of final products (Lima and Luz, 2001). Therefore, knowing the size range of the material is important for anticipating these circumstances. A complete PSD study is presented here below for each sample, including a chemical analysis by size.

Sample 1

Figure 4.1 presents the PSD of sample 1. The complete chemical composition size-by-size is found in Table 4.1. The results show that the fine particles below 45 µm compose most of the sample (around 85%). It is worth to mention that there is a considerable amount of silica in all fractions, particularly above 53 µm. Another aspect that should be highlighted is that,

as particle size decreases, the silica content also decreases. However, there is a peak of silica content on the finest fraction, below 7 µm. This indicates the presence of very fine silicate minerals in the material. In addition, the highest iron content and the lowest silica content are in the size range comprehended between 45 µm and 27 µm. The D_{80} of this material is around 38 µm, meaning that 80% of the sample is smaller than 38 µm.

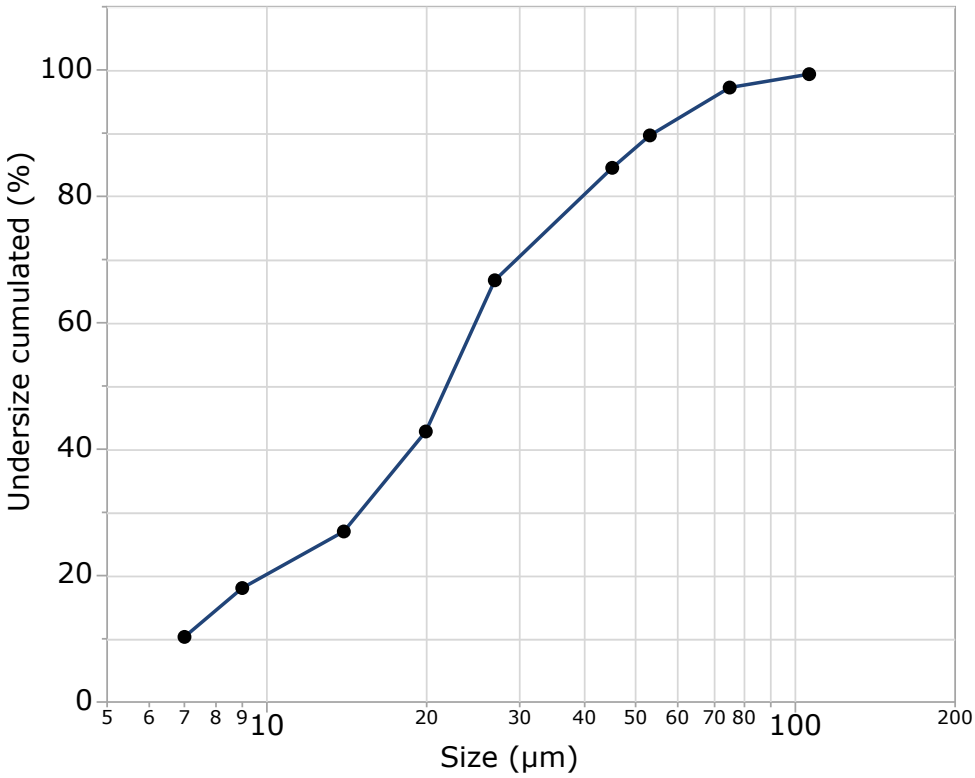

Fig. 4.1 – Particle size distribution of iron concentrate sample 1. D_{80} around 38 µm representing a very fine material.

Table 4.1 – Chemical assays results size-by-size on iron concentrate sample 1.

Size fraction (µm)	Elemental analyses (% of oxides)										
	% weight	Fe (t)	FeO	SiO_2	Al_2O_3	S	P	CaO	MgO	Na_2O	LOI
> 106	**0.67**	45.80	16.40	18.50	4.35	1.10	0.048	4.98	1.72	0.816	2.38
106 - 75	**2.13**	52.29	19.40	13.60	3.93	0.68	0.033	3.83	1.49	0.619	0.40
75 - 53	**7.57**	58.27	23.00	8.56	2.64	0.40	0.022	2.47	1.15	0.361	-1.48
53 - 45	**5.13**	66.57	25.20	3.70	1.10	0.12	0.011	1.12	0.62	0.134	-2.18
45 -27	**17.79**	68.71	25.90	2.27	0.68	0.14	0.008	0.68	0.50	0.043	-2.23
27 - 20	**23.92**	65.26	25.30	4.58	1.35	0.15	0.014	1.40	0.71	0.140	-2.11
20 - 14	**15.82**	64.21	25.40	4.55	1.33	0.09	0.013	1.42	0.67	0.164	-2.15
14 - 9	**8.95**	66.63	25.30	3.80	1.08	0.06	0.010	1.02	0.57	0.133	-2.11
9 - 7	**7.73**	67.68	25.90	3.13	0.90	0.04	0.007	0.85	0.46	0.104	-2.24
< 7	**10.30**	58.96	21.60	13.90	0.77	0.07	0.017	1.06	0.33	0.151	-0.93
Head sample		64.93	25.10	4.56	1.38	0.18	0.010	1.30	0.72	0.160	-2.03

Sample 2

The size fractions used for the PSD analysis of sample 2 were 75 µm, 53 µm, 45 µm, 38 µm and the under 38 µm that has passed through the cyclosizer analysis. The difference in the

PSD size range between sample 1 and sample 2 reflects the fact that sample 2 was submitted to an industrial process where all the particles are supposed to be below 75 µm and sample 1 was submitted to a laboratory protocol test to generate the same parameters as the plant, but this protocol cannot replicate the same behaviour of the plant. Figure 4.2 presents the PSD of sample 2 and Table 4.2 the chemical analysis by size. It is important to notice here that the fraction above 75 µm is responsible for a high degree of impurities. The silica and alumina contents are extremely high and even though in terms of % weight this fraction does not represent a big amount of material, the presence of such grains can disrupt the beneficiation process, especially flotation.

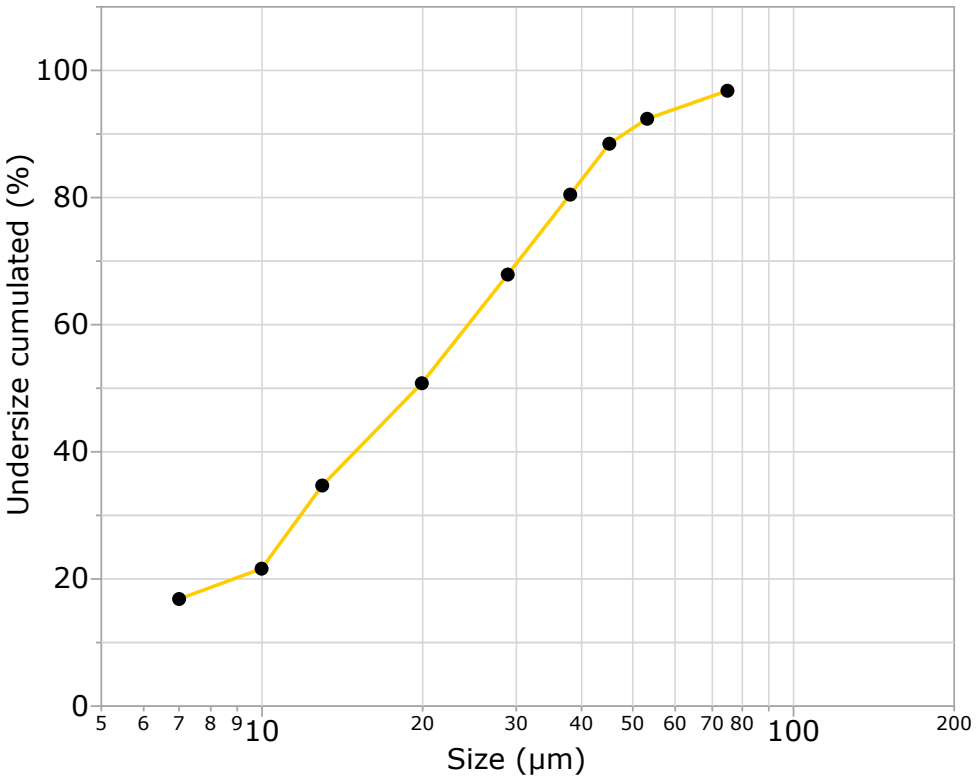

Fig. 4.2 – Particle size distribution of iron concentrate sample 2. Same trend of particle size distribution observed for this sample.

Table 4.2 – Chemical assays results size-by-size on iron concentrate sample 2.

Size fraction (µm)	Elemental analyses (% of oxides)										
	% weight	Fe (t)	FeO	SiO_2	Al_2O_3	S	P	CaO	MgO	Na_2O	LOI
> 75	**3.20**	23.12	10.30	40.00	11.80	0.49	0.134	4.85	1.95	3.630	0.62
75 - 53	**4.41**	51.88	20.80	14.85	4.69	0.70	0.086	2.95	1.19	1.110	-1.22
53 - 45	**3.93**	62.99	24.70	6.26	2.11	0.55	0.050	1.64	0.68	0.411	-2.14
45 -38	**8.01**	64.92	25.80	4.84	1.63	0.40	0.038	1.22	0.57	0.289	-2.30
38 - 29	**12.57**	69.22	29.00	1.40	0.61	0.20	0.016	0.64	0.27	0.066	-2.78
29 - 20	**17.10**	67.49	28.30	2.71	1.02	0.26	0.027	0.92	0.39	0.156	-2.64
20 - 13	**16.09**	67.45	28.30	2.85	1.06	0.21	0.024	0.88	0.40	0.186	-2.71
13 - 10	**13.07**	68.81	28.80	1.70	0.70	0.25	0.017	0.69	0.29	0.090	-2.85
10 - 7	**4.78**	69.06	28.20	2.01	0.77	0.05	0.011	0.88	0.33	0.147	-2.63
< 7	**16.85**	68.61	27.60	1.84	0.65	0.05	0.011	0.66	0.27	0.095	-2.46
Head sample		65.86	26.90	4.09	1.40	0.29	0.028	0.92	0.48	0.270	-2.47

4.2 Liberation study

According to Wills and Napier-Munn (2005b), the liberation degree is defined as the percentage of the valuable mineral occurring as free particles in the ore in relation to the total content. This parameter is essential for determining the beneficiation routes. For instance, if a material is poorly liberated at the beginning of its mineral processing, this may increase the number of fragmentation stages necessary to have a complete liberation. Consequently, the cost with comminution arises in the operation. For the liberation study presented here below in the two iron concentrate samples, the particles were counted and identify as *free iron oxides minerals*, *free gangue minerals* and *mixed particles*.

Sample 1

The liberation study was performed by analysing polished sections through an optical microscope. The size range for each section is comprehended between (+106 µm), (-106 µm +75 µm), (-75 µm +53 µm), (-53 µm +45 µm) and (-45 µm). The results of the quantitative liberation analysis presented in Figure 4.3 A, reveal that a good liberation degree (around 90%) is achieved below 53 µm. In total, more than 2000 particles were counted to perform sample A analysis and magnetite was the most common mineral identified among the free particles. Figure 4.4 is presenting a image of part of the counted particles by size fraction in order to provide a comparative analysis regarding the liberation degree. From the figure, it is noticeable the reduction on the number of red circles as the particle size decreases. This situation is expected since higher liberation is achieved in finer particles, having the sample less mixed particles.

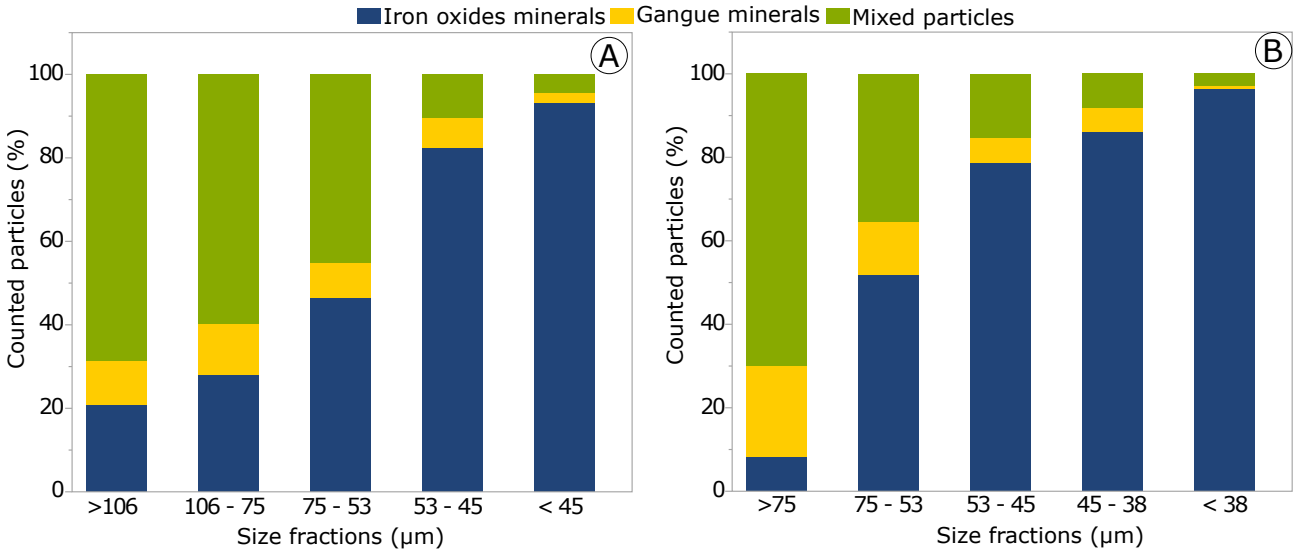

Fig. 4.3 – Quantitative liberation study performed on sample 1 (*A*) and 2 (*B*).

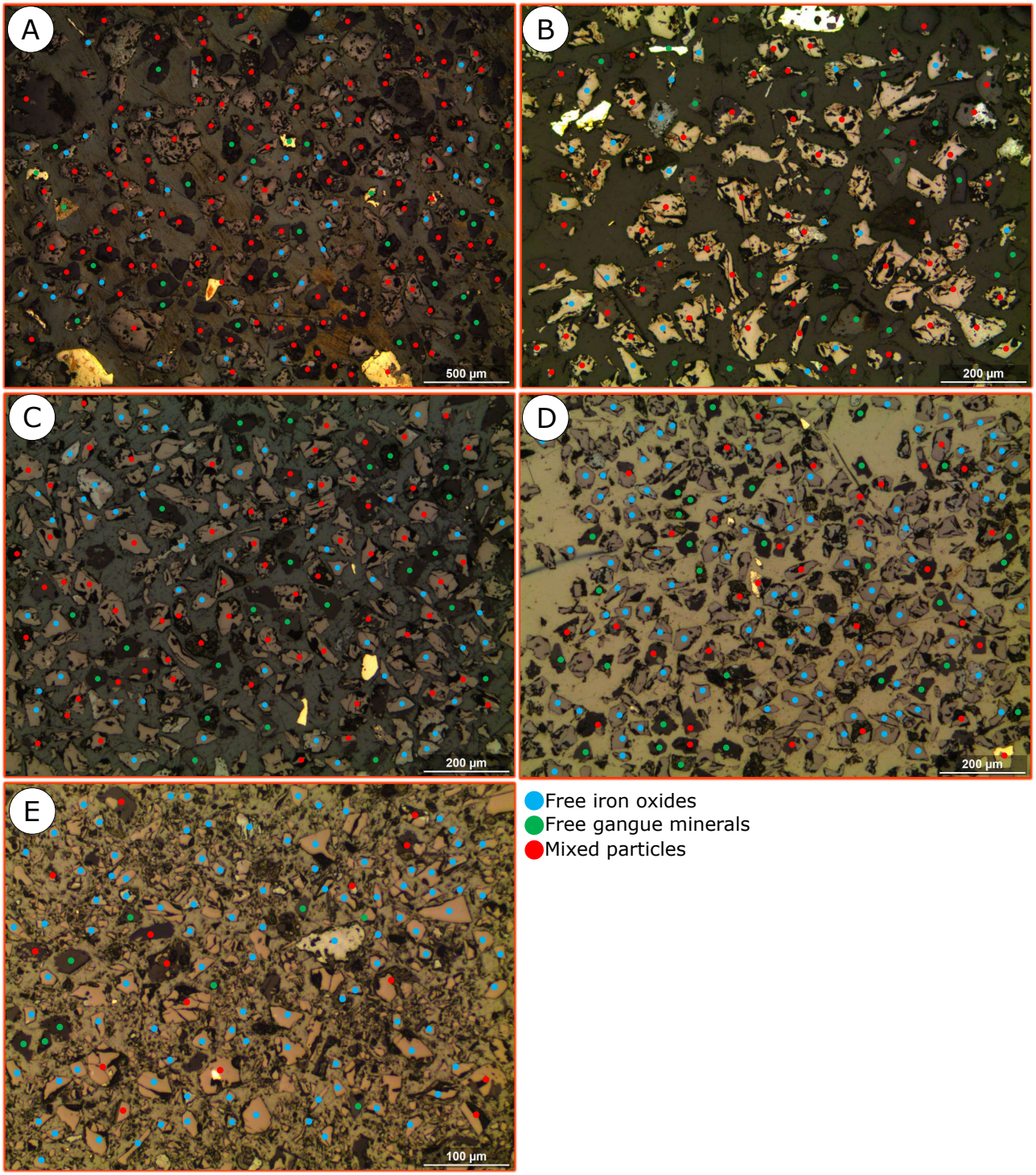

Fig. 4.4 – Optical microscopy images size-by-size on sample 1. A: (+106 µm); B: (-106 µm +75 µm); C: (-75 µm +53 µm); D: (-53 µm +45 µm); E: (-45 µm).

Sample 2

The liberation study on sample 2 was also performed by analysing polished section through an optical microscope. However, the size fractions studied were different for the same reasons mentioned in section 4.1. Figure 4.5 is presenting images that were used for the liberation

study on sample 2. The following particle size fractions were analysed, (+75 µm), (-75 µm +53 µm), (-53 µm +45 µm), (-45 µm +38 µm) and (-38 µm). The quantitative analysis of sample 2 is presented in Figure 4.3 B. The presence of mixed particles drops sharply from 53 µm, as observed in sample 1, showing that at this fraction a good compromise between liberation is achieved. It is also important to highlight that the fraction above 75 µm has a low amount of iron oxides, showing that the plant process has being effective in separating those minerals at coarser size fractions. For the second sample around 1500 particles have been counted and identified.

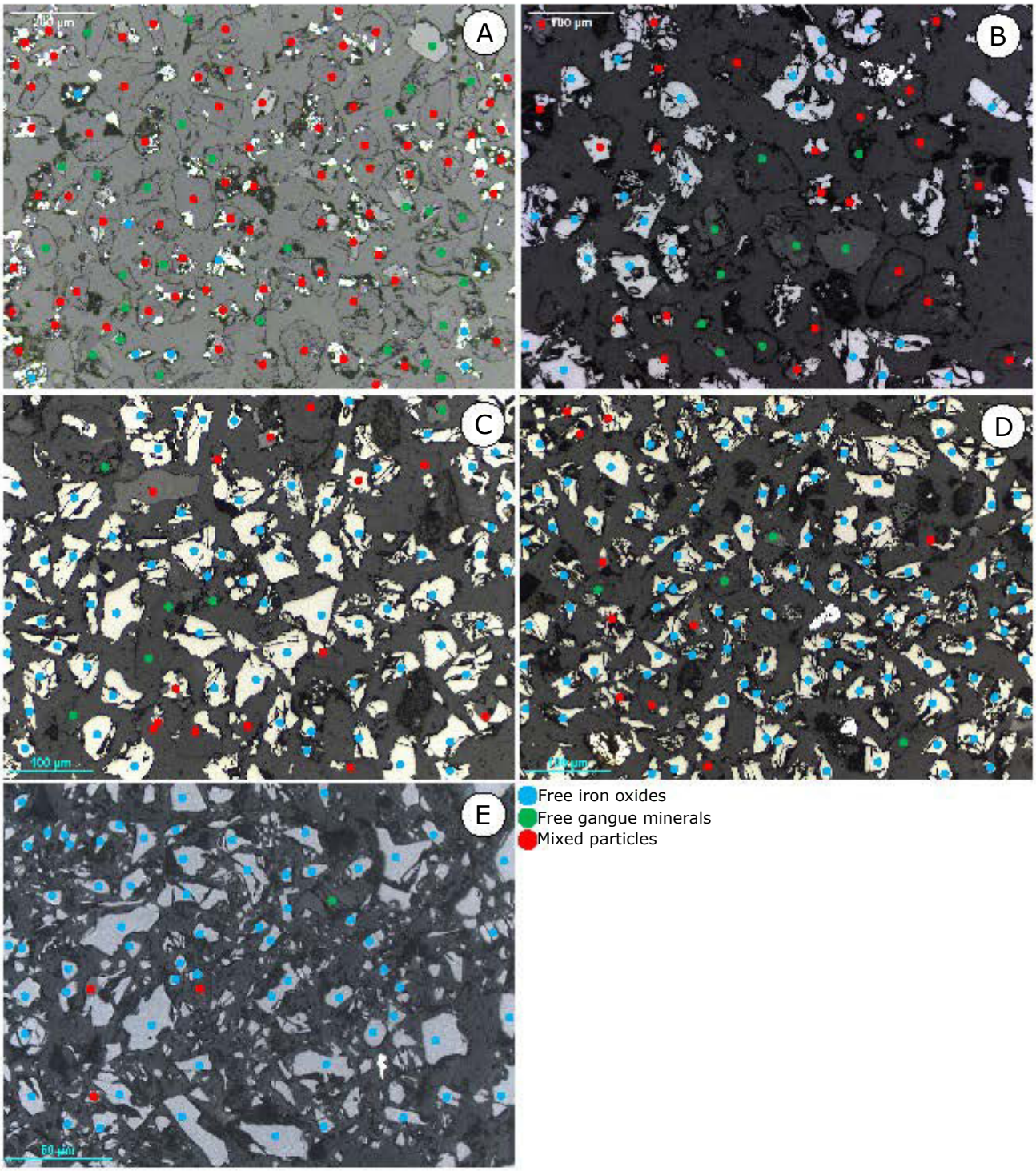

Fig. 4.5 – Optical microscopy images size-by-size on sample 2. A: (+75 µm); B: (-75 µm +53 µm); C: (-53 µm +45 µm); D: (-45 µm +38 µm); E: (-38 µm).

4.3 Mineralogical study

A quantitative study of mineralogical composition was performed on both samples 1 and 2. The modal analysis was done considering data acquired by a first qualitative XRD analysis. The X-ray diffractograms of both samples 1 and 2 are presented in Appendix C. They were used to determine the list of the main minerals present in both samples. Then, using also chemical assays results (XRF and wet method), magnetite content analysis and stoichiometric chemical compositions of mineralogical phases available on handbooks of mineralogy it was possible to determine the contribution of each mineral on the samples.

Sample 1

From the results of various methods mentioned before, it was possible to estimate the amount of each mineral present in the sample. Figure 4.6 presents its quantitative mineralogical analysis and it can be highlighted the major role of iron oxides in the composition of the sample. Magnetite and hematite correspond to almost 90% of the material content, demonstrating that it is already a rich concentrate. Furthermore, the modal analysis confirms the presence of 2.8% of epidote, 2.2% of diopside, 2.1% of chamosite, 1.5% of albite and 2.4% of another gangue minerals. The presence of such minerals, especially the Fe-bearing silicates (chamosite and epidote) can badly affect the contrast needed between minerals to promote a separation. Trying to identify better the minerals present in sample, SEM analyses were performed on the polished sections used for the liberation study.

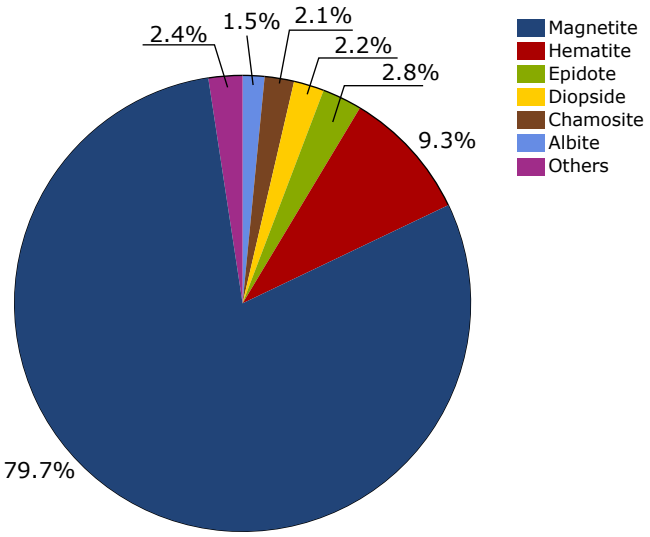

Fig. 4.6 – Quantitative mineralogical composition of sample 1 by modal analysis, normalized to 100%.

A complete analysis in the scanning electron microscope (SEM) enabled the visual identification of minerals hitherto identified only by chemical and crystallographic analysis. Figure 4.7 presents the images of analysis performed on sample 1. The presence of disseminated iron oxides as shown in Figure 4.7 B, highlights the level of complexity of the mineral grains that composed this sample. The presence of complexes assemblages of minerals is still observed in the finest size fraction image (Figure 4.7 F), where grains of magnetite and silicates are presented. The mineral phases identified through the SEM observations were: albite, apatite, calcite, chamosite, diopside, epidote, orthoclase, pyrite, quartz, titanite, magnetite, hematite

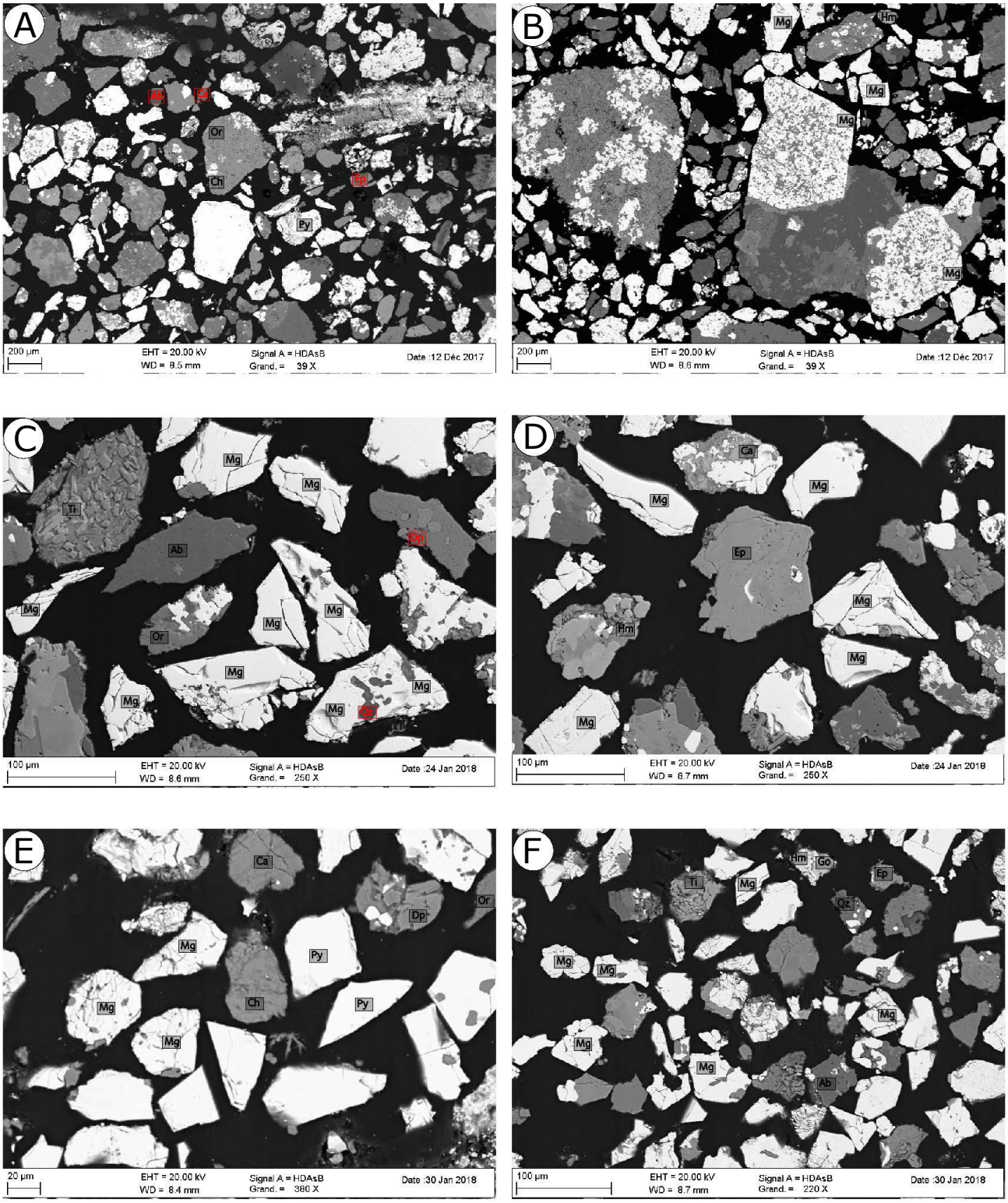

Fig. 4.7 – Scanning electron microscope observations of sample 1. A: $+106m$, B: $+106m$, C: $-106m+75m$, D: $-106m+75m$, E: $-53m+45m$, F: $-53m+45m$. Ab = albite. Ca = calcite. Ch = chamosite. Dp = diopside. Ep = epidote. Go = goethite. Hm = hematite. Mg = magnetite. Or = orthoclase. Py = pyrite. Qz = quartz. Ti = titanite.

and goethite. Magnetite and epidote are the iron oxide and silicate with more occurrence in the sample.

Sample 2

The mineralogical study performed on sample 2 confirmed also its complexity in terms of mineralogical composition, see Figure 4.8. Almost 90% of the sample is composed by iron oxides. However, the amount of magnetite is bigger than sample 1. More than 87% of the sample is composed by magnetite. Chamosite is the main silicate found in this sample, with 3.2%. Followed by albite with 2.3% and epidote with 1.0%. Calcite appears with 1.3%, and the amount of diopside in this sample is smaller than sample 1, placing it in the category "others". The iron-bearing silicates that may complicate the separation processes of ore minerals from gangue minerals were again identified.

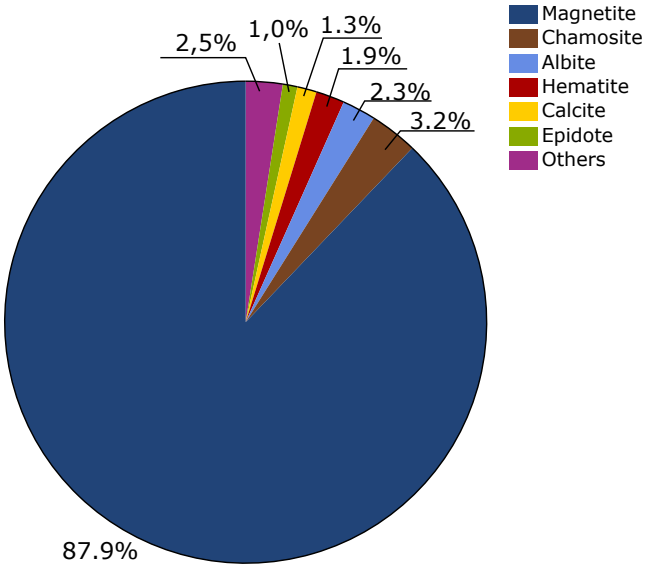

Fig. 4.8 – Quantitative mineralogical composition of sample 2 by modal analysis, normalized to 100%.

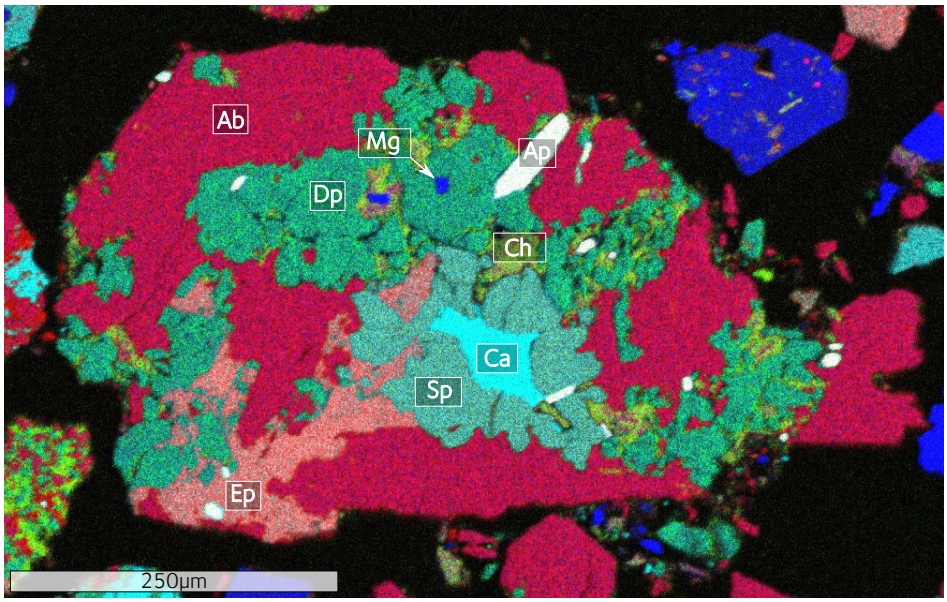

Fig. 4.9 – Scanning electron microscope observations of a mixed grain of gangue minerals of the size fraction + 106 µm of sample 2. Ab = albite. Ap = apatite. Ca = calcite. Ch = chamosite. Dp = diopside. Ep = epidote. Mg = magnetite. Sp = spinel.

An SEM campaign was also performed on sample 2. The mineral phases identified through the SEM observations were: albite, andradite, apatite, calcite, chamosite, diopside, epidote, K-feldspar, hematite, magnetite, pyrite, quartz and titanite. Figure 4.9 presents the image of a mixed grain composed by several gangue minerals. The grain of around 500 µm is composed by albite, apatite, calcite, chamosite, diopside, epidote, magnetite and spinel. It must pass through a comminution step to promote liberation of these minerals. However, it illustrates the complexity of the minerals assemblage present in this sample. Grains composed by many minerals are almost never fractured in a way that generates complete separation, causing difficulties in the concentration processes.

4.4 Concluding remarks

The characterisation presented in the sections above generates a lot of information about how the minerals were distributed in size ranges, if their particles were liberated or not and it was also possible to combine different techniques to confirm the mineral phases present in each sample.

4.4.1 General observations

Particle size distribution

From the particle size analyses, it is possible to affirm that despite the different way of sampling, the overall size ranges are the same for both samples 1 and 2. The D_{80} of both samples are quite the same and the presence of fines is high ($\approx$ 50% below 20 µm). Two points should be highlighted here:

- The big difference in SiO_2 content between the two samples. This is explained by the absence of a last cleaning stage of magnetic separation on the sample 1 that have been treated in the laboratory. In fact, the Magnefloc equipment is responsible for overflowing all the light particles in fine size range, especially. This information is showing that Magnefloc was properly working during the sampling of sample 2 at the beneficiation plant;
- The % weight of the fraction (+75 µm) is not high but is responsible for carrying a lot of impurities to the final concentrate. Since the plant is operating screens with 75 µm panels, this size fraction should not be present in this sample. Of course, a screen is never 100% efficient, but a better size separation process should be investigated for the plant.

Liberation study

The geometrical form of minerals needs to be understood, because it is always very irregular (King, 1994). From the quantitative analysis performed on both samples it is possible to identify that most of the mixed particles come from the coarser fractions. From Figure 4.4 and Figure 4.5 it is possible to see that the mixed particles are composed of small inclusions or small grains and their fully liberation is complicated to achieve it. At 53 µm more than 80% of both samples are composed of free iron oxides. This particle size seems to be most suitable to achieve good separation results of these minerals. Other important point is the presence of less free iron oxides particles in the coarser sizes of sample 2. This is an indicator that the comminution process of the plant is also operating correctly, enabling these particles to be likely separated by the magnetic separation process.

Mineralogical study

The minerals identified during this study are totally in agreement with the geological studies carried out in the deposit, as reviewed in chapter 1. The list of the main minerals constituting samples 1 and 2 was established from this study. As expected the amount of magnetite is high since both samples are already magnetic concentrates. The main difference between the samples is in the amount of hematite. This can be explained by the fact that samples 1 and 2 did not come from the same localisation in the mine or may also be related to the laboratory protocol test that sample 1 has passed through. The gangue minerals identified are almost the same. Although diopside is not shown in the modal graph, it was also identified in sample 2, but in smaller quantities. Diopside is not an iron-bearing silicate and its magnetic susceptibility is lower when compared to chamosite and epidote (Rosenblum and K. Brownfield, 2000). This means that diopside may be more easily separated from iron oxides by magnetic separation than chamosite and epidote.

4.4.2 Guidelines for the study

Characterisation of an ore sample is essential for providing information that will be useful in making decisions between methodologies and approaches for a fundamental and thorough research on how to generate the necessary contrast between minerals to separate them. Some important decisions that were made based on this study are:

1. The minerals that would undergo a deeper and more fundamental study: *chamosite*, *diopside*, *epidote*, *hematite* and *magnetite*.
   Between the silicates, the two Fe-bearing minerals may be very complicate to separate in a process like flotation, because its surface proprieties, essential for separation in this

process, may have the same behaviour as an iron oxide. Diopside was also included because even after magnetic separation, it remained in the concentrate. Magnetite as the main iron oxide identified and hematite as an important reference for the reverse cationic flotation of silicates were also chosen.

2. The optimum size fraction for the flotation feed.
   The size fraction where more than 80% of the particles are liberated was determined to be 53 µm. To investigate the influence of the mixed particles in flotation, sample 1 was floated as received and sample 2 was submitted to a sieving at 53 µm before performing the flotation tests. Re-grinding of the oversize was also investigated for the sieved sample.

3. The evaluation of unusual flotation reagents.
   The identified mineralogical composition guided the study in the search for a more selective reagent suite for the reverse cationic flotation of iron ores in the presence of complex minerals. Depressants in particular were focused since the lack of selectivity of the widely used corn starch has already been demonstrated when in the presence of complex gangue minerals (Filippov et al., 2013).

Chapter 5

Experimental study on the mineral-depressant interaction

5.1 Zeta potential

The electrophoretic mobility of each mineral was measured in an indifferent electrolyte solution of KCl of concentration 1.0×10^{-2} M at pH from 2 to 12. The pH value was adjusted through the addition of analytical grade HCl or KOH. The zeta potential of each point was determined from at least 100 particles measurement and then calculated by Smoluchowski equation (Hunter, 1989). The experiments were repeated twice, and the results were averaged. The standard deviation was calculated using the average all those values. For the measurements with depressants, distilled water was used to prepare the solutions. The minerals were conditioned with the depressants for 12 hours at a concentration of 300 $mg.L^{-1}$.

The zeta potential of chamosite, diopside, epidote, hematite and magnetite pure samples as a function of pH are presented in Figure 5.1 to Figure 5.5, as well as the zeta potential of these minerals after interaction with the depressants *corn starch*, *carboxymehtyl cellulose (CMC)*, *dextrin* and *humic acid*.

The isoelectric points (IEPs) of the chamosite, diopside and epidote were achieved at pH values of 3.1, 2.8 and 2.9, respectively. Despite a certain deviation, the zeta potential results are quite well aligned with the expected values according to previously published studies (Table 5.1). For instance, the IEPs values are in agreement with Deju and Bhappu (1966) study which states that the higher the O:Si ratio of the silicates, the more alkaline the pH of the IEP, because silicate minerals with higher O:Si ratio would have higher H^+ surface adsorption. Classifying the studied minerals in increasing order of the ratio O:Si, one should have: diopside, epidote

Table 5.1 – IEPs of iron oxides, iron-bearing silicates and pyroxene reported by several authors.

Mineral	pH_{IEP}
Chamosite/Clinochlore	< 3.0[a], 4.8[b], 5.0[c], 5.5[d]
Diopside	2.8[e], 3.0[f], 3.4[f], 4.5[g]
Epidote	4.0[h],4.0[f], 6.1[i]
Hematite	4.8[j], 5.4[k], 5.7[k], 6.0[l], 6.2-6.5[m], 6.6[k], 6.7[n], 7.6[o], 8.0[p], 8.4[q], 8.8[r], 9.4[s]
Magnetite	4.4[t], 4.8[u], 5.0[v], 6.0[u], 6.5[k], 7.0[x], 8.0[z]

a) Tan et al. (2012); b) Oelkers et al. (2009); c) Sondi et al. (1996); d) Fornasiero and Ralston (2005); e) Fuerstenau et al. (1977); f) Kosmulski (2011); g) Alvarez-Silva et al. (2010); h) Jordens et al. (2014); i) Kursun et al. (2019); j) Rohem Peçanha et al. (2019); k) Parks (1965); l) Montes et al. (2007); m) Henriques et al. (2009); n) Iwasaki et al. (1960); o) Zhang et al. (1985); p) Ramos-Tejada et al. (2003); q) Atkinson et al. (1967); r) Ma (2008); s) Penners and Koopal (1987); t) Henriques (2012); u) Kolarik et al. (1980); v) Erdemoğlu and Sarikaya (2006); x) Raju et al. (1997); z) Illés and Tombácz (2006).

and chamosite, the same order observed for the pH values of the IEPs. It should also be noted that the trend observed by Tartaj et al. (2000) for the phyllosilicate serpentine, in which the lack of Mg sites in particle surface layers leads to a lower IEP was observed in the case of the phyllosilicates from chlorite group. Chamosite has a smaller amount of Mg in its composition when compared to clinochlore used by Oelkers et al. (2009), and indeed its IEP was lower than that of clinochlore.

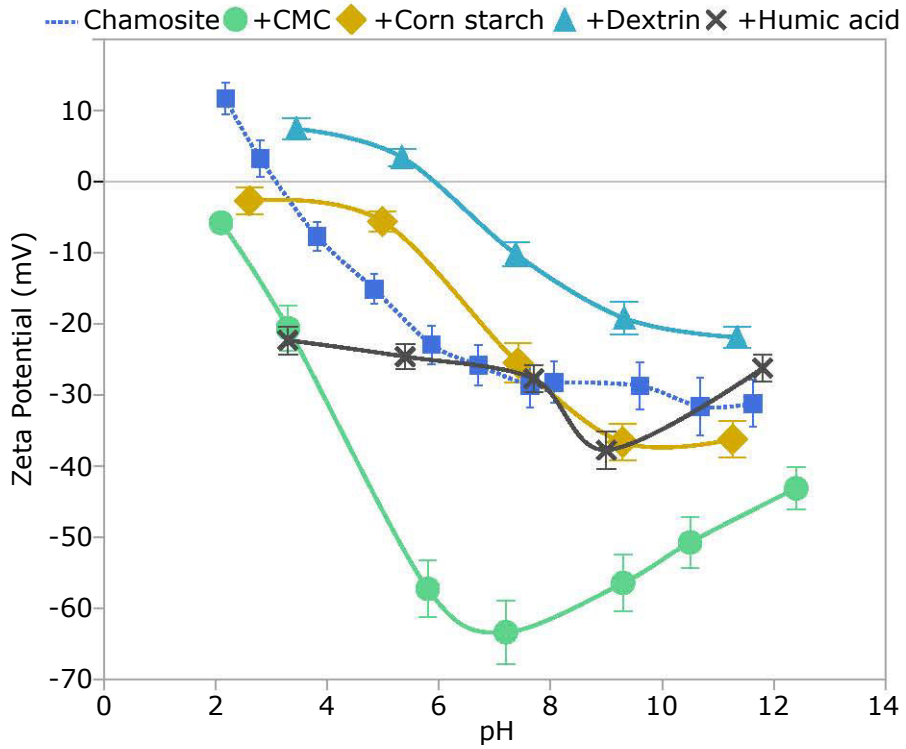

Fig. 5.1 – Zeta potential of pure chamosite in KCl solution and after interaction with corn starch, carboxymethyl cellulose, dextrin and humic acid.

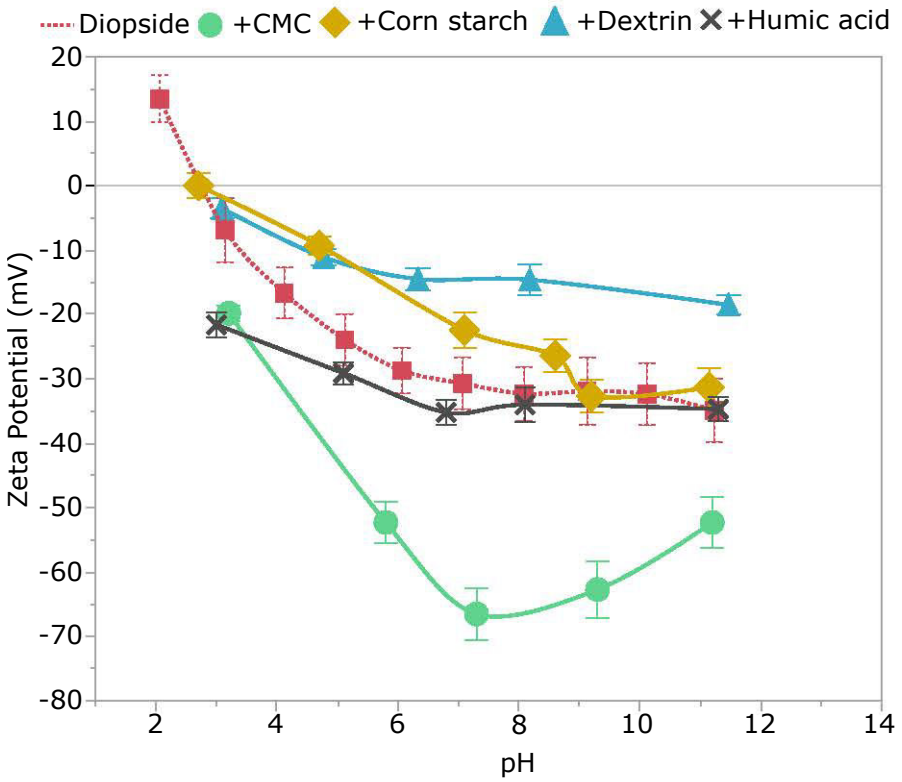

Fig. 5.2 – Zeta potential of pure diopside in KCl solution and after interaction with corn starch, carboxymethyl cellulose, dextrin and humic acid.

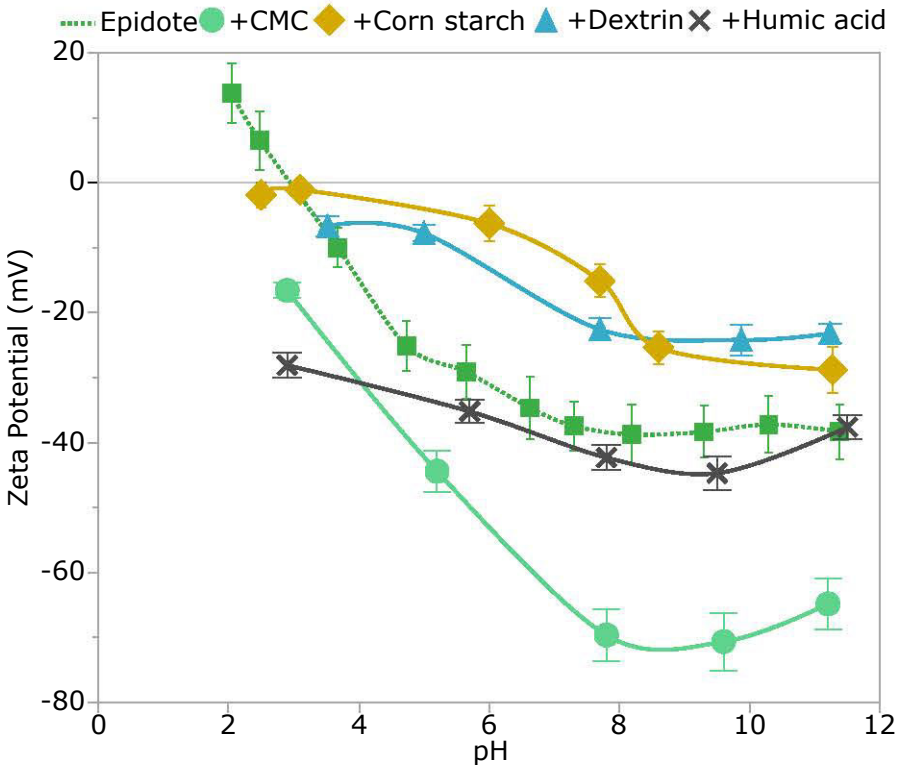

Fig. 5.3 – Zeta potential of pure epidote in KCl solution and after interaction with corn starch, carboxymethyl cellulose, dextrin and humic acid.

Thomas et al. (1999) and Fuerstenau and Pradip (2005) have also stated that layer-silicate minerals negative surface charges is related to substitutions of Al^{3+} for Si^{4+} in tetrahedrons and Mg^{2+} for Al^{3+} in octahedrons, and it is independent of solution conditions. Severov et al. (2016) have also observed that the IEP of an amphibole was displaced to higher values because of surface Mg sites. Diopside IEP of 2.8 is close to the value reported by Fuerstenau et al. (1977), however the values found in the literature vary up to 4.5. The reported IEP values for epidote are different from the found value of 2.9. However, it is noteworthy that epidote is a group of minerals and the reported values may represent minerals of different compositions.

From Figure 5.4 and Figure 5.5, the IEP of hematite and magnetite were achieved at pH values of 6.2 and 5.4, respectively. Both values are aligned with the values reported in the literature presented in Table 5.1. The values variation is most of the time related to the natural variation in the crystal structure or even with the methods of sample preparation and measurements, as well as differences in supporting electrolytes. Also, the use of natural and synthetic minerals has been reported as an important factor that justifies the different values achieved. The zeta potential values obtained are in total agreement with the theory of pH dependence, since an important variation of these values with the pH is observed. In aqueous medium, iron oxides are hydroxylated and the addition of acids (H^+) will lead to a positive value of zeta potential while the addition of bases (OH^-) will lead to a negative value of zeta potential.

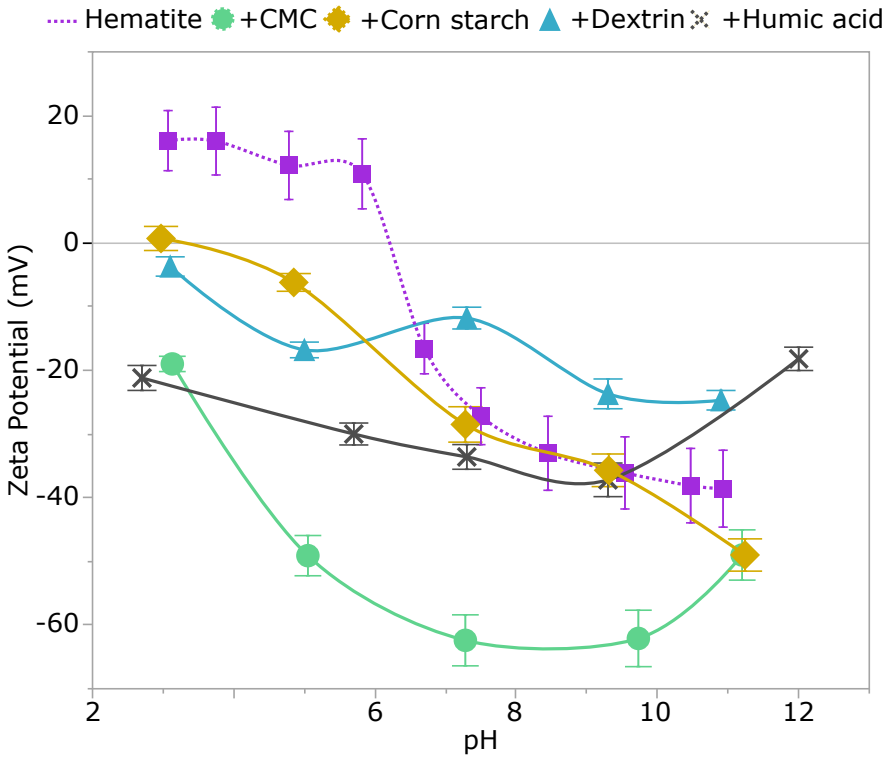

Fig. 5.4 – Zeta potential of pure hematite in KCl solution and after interaction with corn starch, carboxymethyl cellulose, dextrin and humic acid.

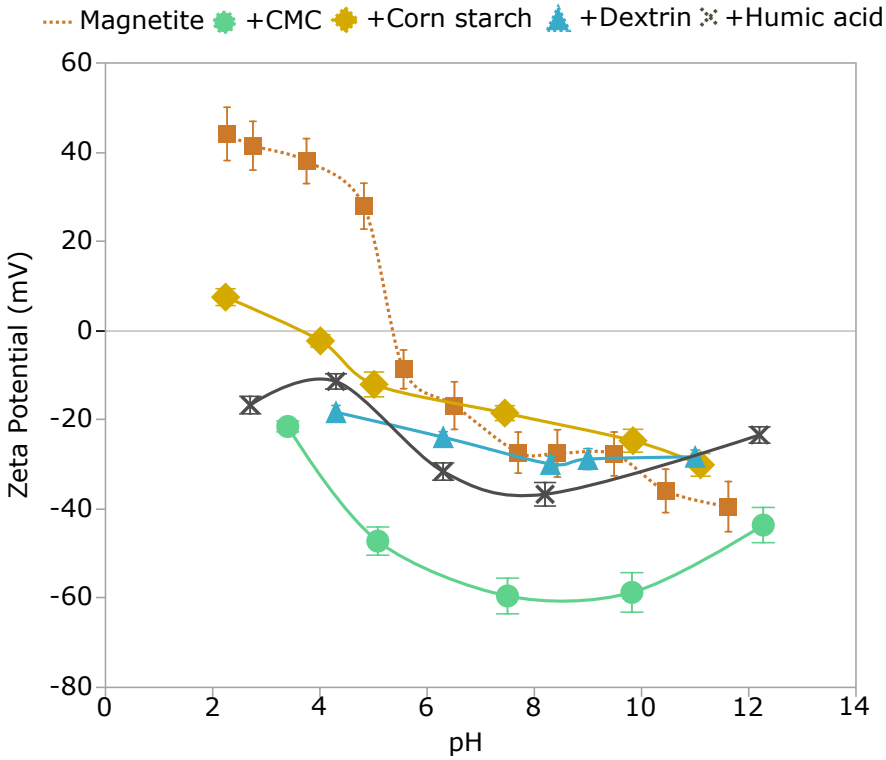

Fig. 5.5 – Zeta potential of pure magnetite in KCl solution and after interaction with corn starch, carboxymethyl cellulose, dextrin and humic acid.

Corn starch was the least depressant in reducing the zeta potential of all minerals. The silicates had slightly displaced IEP, but less evident than iron oxides. An increase in pH for corn starch and its derived dextrin, is followed by a constant decrease in zeta potential values for all minerals. The chemical complexation proposed by Weisseborn et al. (1995) and Laskowski et al. (2007) start to occur to compensate for the increasing electrostatic repulsion until a pH value around 10 where the zeta potential values begin to stabilize. Dextrin followed the trend of corn starch, except for chamosite where the IEP has been shifted to more basic pH values, when in the presence of this polymer.

CMC behaviour should be highlighted. The zeta potential values of all minerals dropped sharply when in the presence of this polymer, with a minimum value reached close to the natural pH. With an increase in pH, there is also an increase in negative charges on the mineral surfaces and this may explain the rise in CMC curves, after reaching its minimum values. There are, however, two other possible explanations for this effect of CMC. The first one is that CMC macromolecules parked inside the double layer and masked the surface charge measurements of the minerals and the second one is the compression of the double layer, causing this decrease in the potential zeta value. This same trend is observed for the other anionic depressant, humic acid. However, the intensity of the zeta potential values is quite lower when compared to CMC and its minimum values are achieved at more basic pH values. The surface charge of the minerals was more strongly modified by humic acid than by corn starch, especially in the iron

oxides. Several authors have attributed humic acid adsorption to iron oxides to electrostatic interactions at acid pH values, and to chemical interactions (complex formation and hydrogen bonding) at basic pH values (Nayak et al., 1990; Vermeer et al., 1998; Hur and Schlautman, 2003; Ramos-Tejada et al., 2003; Illés and Tombácz, 2003; Tombácz et al., 2004).

5.2 Adsorption equilibrium study of polymers on silicates and iron oxides

The specific surface area (area per unit mass or volume) of each mineral is presented in Table 5.2 and was used for the determination of their adsorption density. Chamosite is a layer-silicate and its specific surface area is 20 times bigger than the other silicates due to the sheet-structure observed in this mineral.

Table 5.2 – Specific surface area of pure minerals by BET method.

Mineral	BET surface area ($m^2.g^{-1}$)
Chamosite	21.4 ± 0.5
Diopside	1.2 ± 0.2
Epidote	0.8 ± 0.1
Hematite	0.9 ± 0.2
Magnetite	1.4 ± 0.2

5.2.1 Maximum pH adsorption determination

Before determining the adsorption isotherms of the minerals in the presence of the studied polymers, some experiments were carried out under different pH values to set the value of highest adsorption. These tests were conducted with an initial concentration of the depressants of 100 mg/L. The pH of maximum adsorption was then used in the following tests to establish the adsorption isotherms. The amount adsorbed on chamosite, diopside and epidote for the four depressants tested is presented in Figure 5.6 and in Figure 5.7 for hematite and magnetite. No significant adsorption of CMC and dextrin at any pH value for the initial concentration used during the tests were observed. This may be related to the low initial concentration used for determining the maximum pH value of adsorption. Corn starch presented high adsorption in all the pH ranges and the highest adsorption was also observed at pH 7. Humic acid presented a different behaviour from the other depressants its highest adsorption was observed at pH 5. Based on this first exploratory adsorption experiments and in the zeta potential measurements,

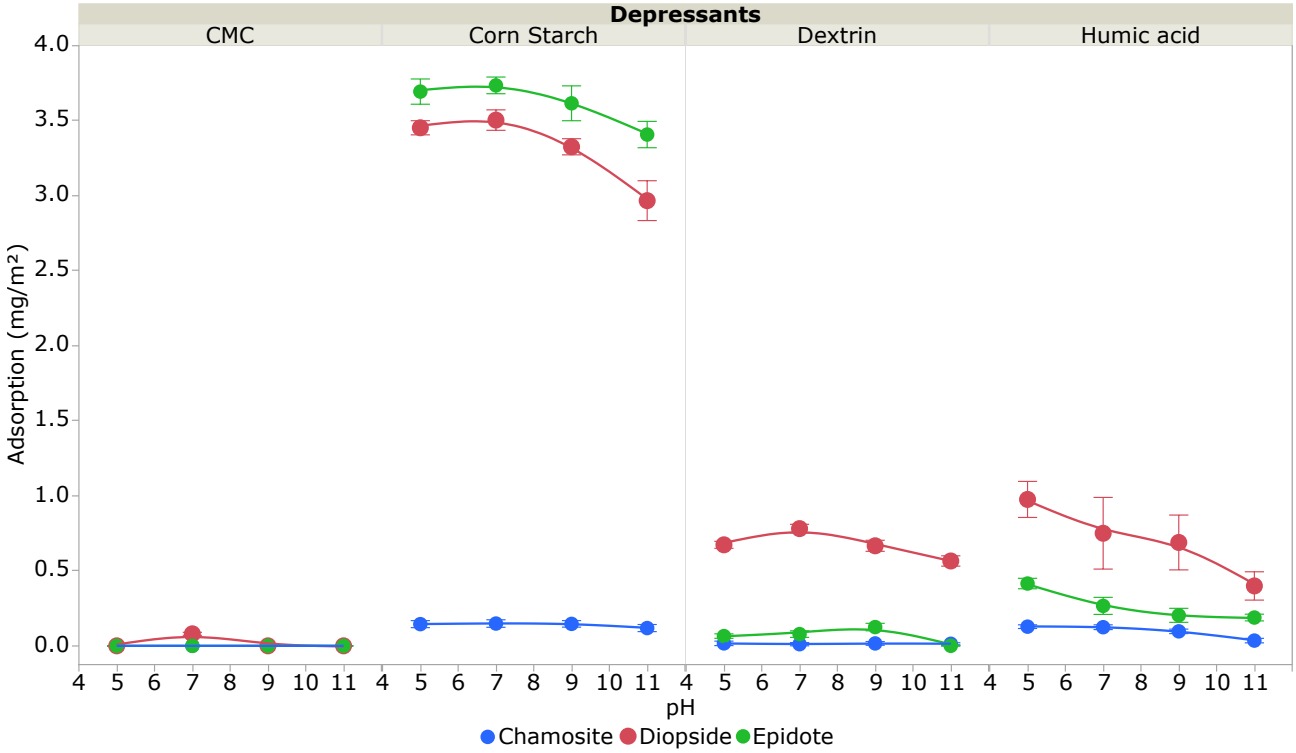

Fig. 5.6 – Amount adsorbed of corn starch, CMC, dextrin and humic acid as function of pH for chamosite, diopside and epidote.

the adsorption isotherms of chamosite, diopside and epidote were determined at pH 7 for corn starch, CMC and dextrin and at pH 5 for humic acid.

Figure 5.7 presents the results of the adsorption tests into hematite and magnetite for pH range between 5 and 11. Almost no adsorption was observed for CMC into hematite and magnetite surfaces. Humic acid and dextrin showed better affinity for these minerals, but corn starch is by far the best performer. According to the electrophoretic measurements (Figure 5.4 and Figure 5.5) at pH 7 both iron oxides present negative surface charge and positive at pH 5. Since humic acid and CMC are anionic polymers and at lower pH values, the carboxylic acidic groups become protonated and less negatively charged (Arnason and Keil, 2000), a higher adsorption was expected at a pH value below their IEP. This behaviour was slightly observed for humic acid, however CMC showed almost no adsorption with the initial concentration used for the pH tests. Based on the pH value that showed the highest adsorption for each polymer, the equilibrium adsorption isotherms presented later were determined at pH 7 for all the adsorbates except for humic acid which was obtained at pH 5, this is the same behaviour observed for the silicates minerals.

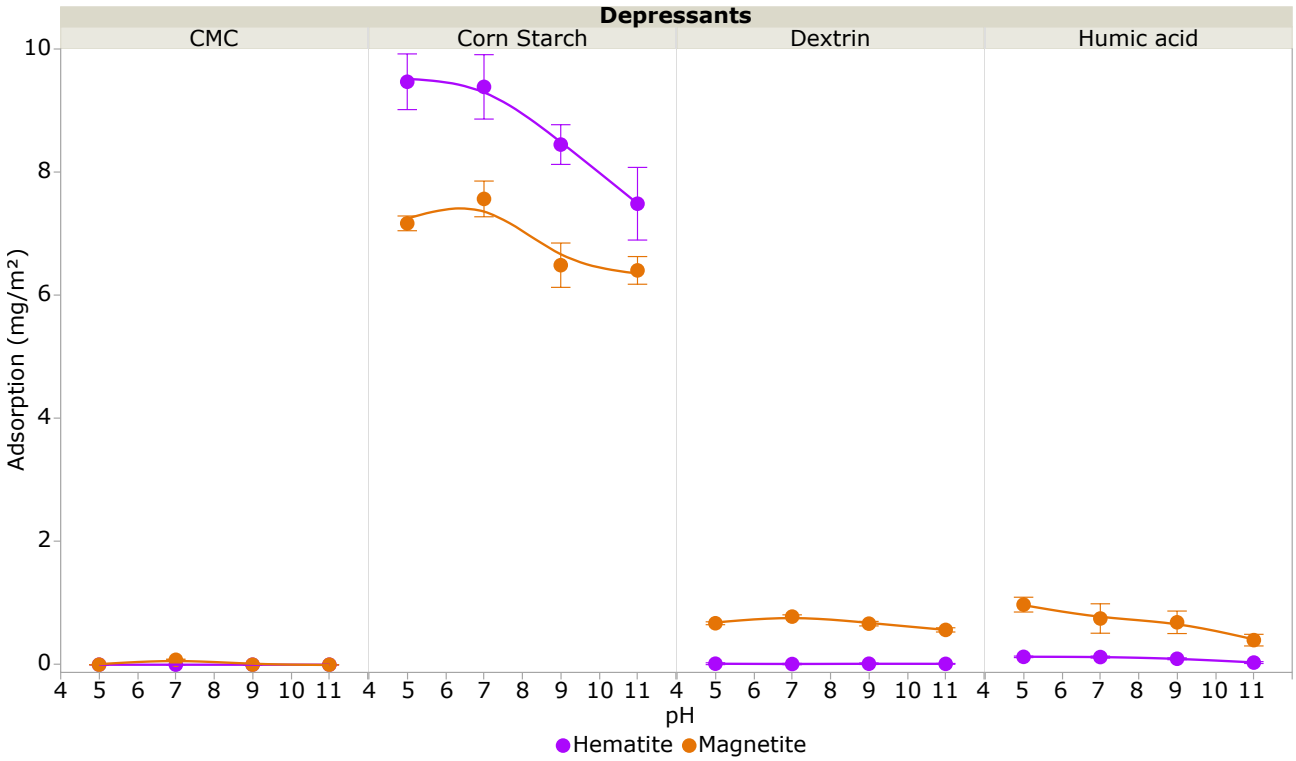

Fig. 5.7 – Amount adsorbed of corn starch, CMC, dextrin and humic acid as function of pH for hematite and magnetite.

5.2.2 Equilibrium adsorption isotherms

The equilibrium adsorption isotherms of corn starch, CMC, dextrin and humic acid onto chamosite, diopside, epidote, hematite and magnetite surfaces are presented in Figure 5.8 to Figure 5.11.

Corn starch adsorption on silicate surfaces is considerable when compared to the other polymers (Figure 5.8). This polymer is also the one the presents the highest adsorption densities for hematite. The higher ability of corn starch to form hydrogen bonds with iron oxides have been reported (Peres and Correa, 1996) and is confirmed in this study. Pavlovic and Brandao (2003) and Lima (1997) concluded in adsorption studies of corn starch and amines onto hematite and quartz, that starch adsorption on the surface of hematite is much more intense than on quartz. The higher adsorption of corn starch on diopside surface when compare to epidote can be explained by the greater amount of Ca sites available in its structure, which was proposed by Somasundaran (1969) as a chemical complexation existing between starch rings and calcium ions and confirmed by the studies of Khosla and Biswas (1984) and Araujo (1988).

CMC had no relevant adsorption densities on the surface of the studied silicate minerals. This result was unexpected because previous studies with different minerals (Burdukova et al., 2008; Wang and Somasundaran, 2005) have shown that this reagent is well adsorbed on the

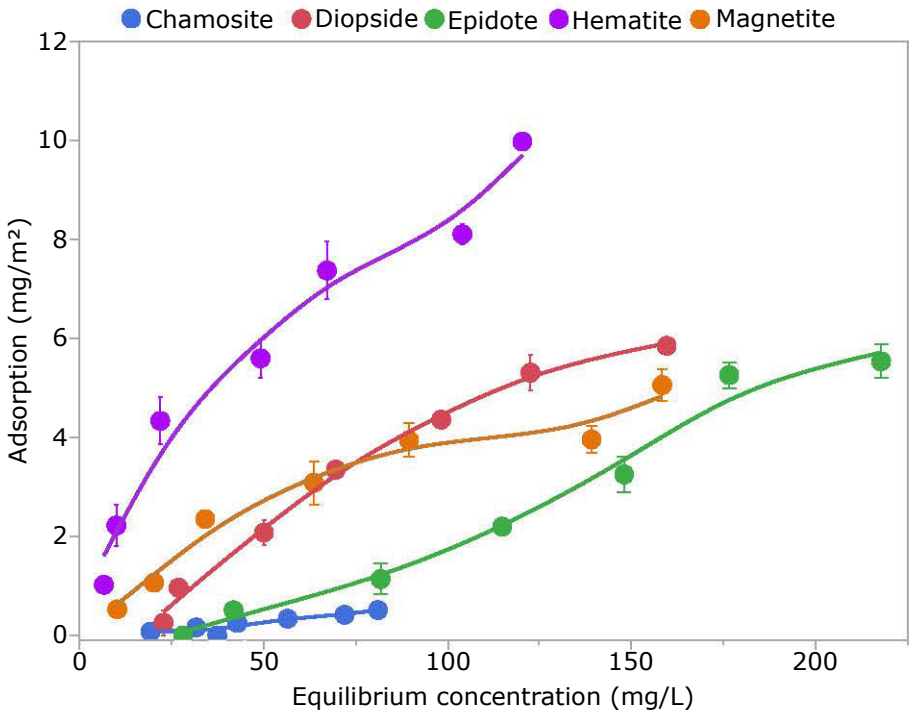

Fig. 5.8 – Adsorption isotherm of chamosite, diopside, epidote, hematite and magnetite as a function of its equilibrium concentration for corn starch at pH 7.

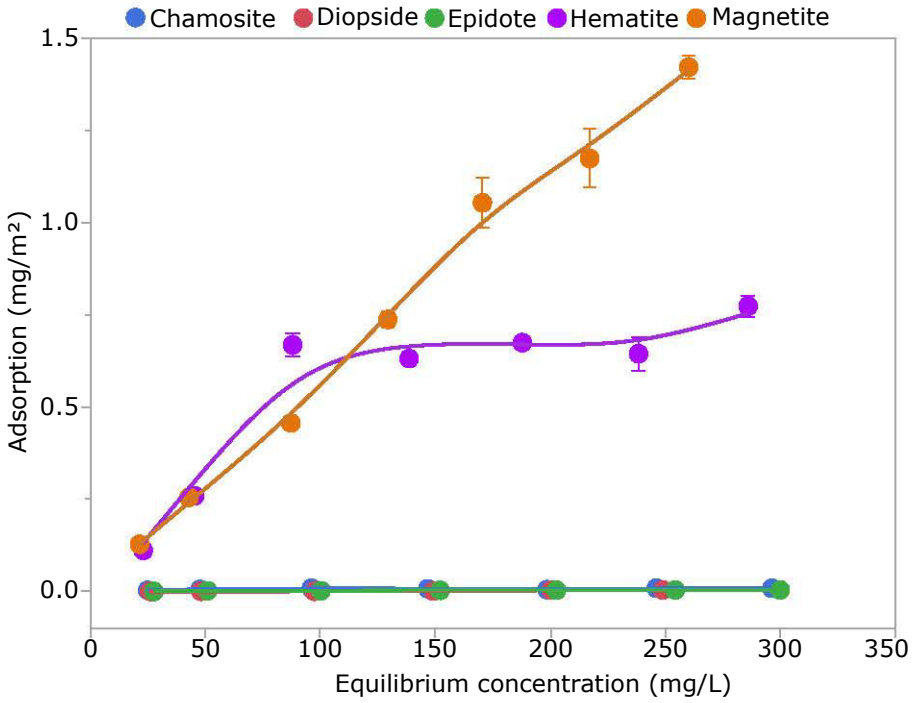

Fig. 5.9 – Adsorption isotherm of chamosite, diopside, epidote, hematite and magnetite as a function of its equilibrium concentration for CMC at pH 7.

silicates and presents a pH-dependence. The adsorption density of CMC onto hematite and magnetite is much bigger than onto silicates. These results are in accordance with the proposed by Liu and Laskowski (1999) that CMC adsorption is enhanced by the presence of metal cations.

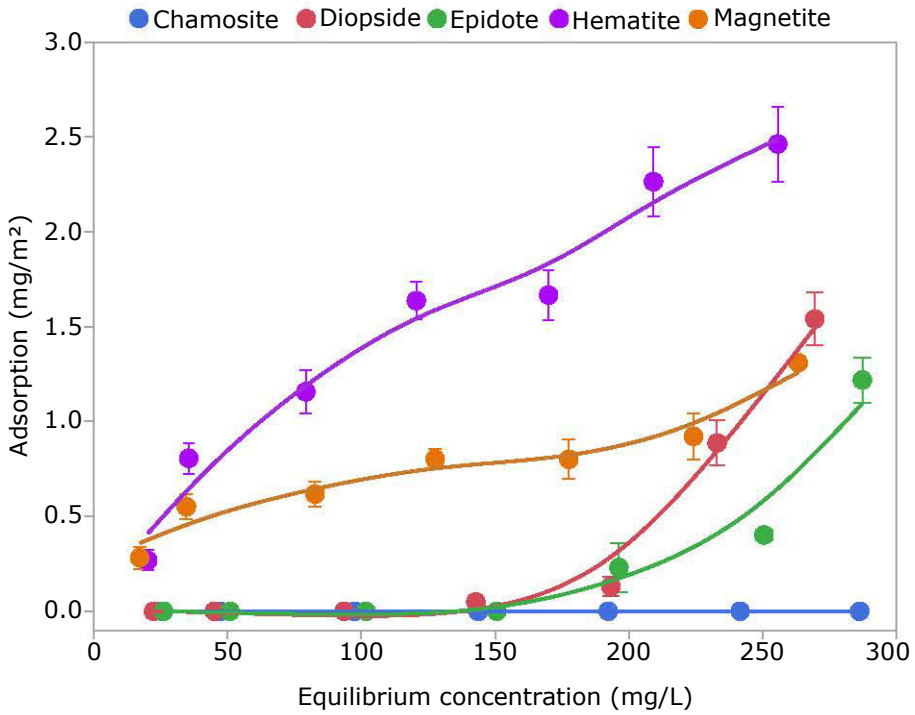

Fig. 5.10 – Adsorption isotherm of chamosite, diopside, epidote, hematite and magnetite as a function of its equilibrium concentration for dextrin at pH 7.

Dextrin has smaller molecules than corn starch and its isotherms show higher adsorption values for adsorbate concentrations from 150 mg/L for the silicates and more affinity with the iron oxides, where the adsorption densities goes up to 2.5 mg/m^2 (Figure 5.10). At high concentrations the free energy of adsorption contributes more to the system and favours the adsorption of the low molecular weight depressants, this explains the significant increase for diopside and epidote. The interaction and adsorption between chamosite and dextrin were not observed. As in corn starch case, there is not a strong variation in the adsorbed amounts varying the pH. This can prove that the adsorption of dextrin is not dependent of pH and comes in accordance with the proposed by Wie and Fuerstenau (1974).

The observed decrease on humic acid adsorption (Figure 5.6 and Figure 5.7) on the minerals surface as the pH becomes more basic is expected since this depressant is an anionic reagent and the minerals are negatively charged in the same pH range. Opposed to corn starch, the adsorption mechanism of humic acid seems to be related to an ionic interaction between minerals and reagent, having a hydrophobic interaction character. Ramos-Tejada et al. (2003) stated that the adsorption of humic acid increases hematite hydrophilicity and this fact related to the lower humic acid adsorption on silicates surfaces may be a good indication for a selective depressant. Humic acid showed a slightly difference in the amount adsorbed when pH is variated. The same behaviour was reported by several studies leading with humic substances (Parfit et al., 1977; Tipping, 1981; Davis, 1982; Murphy et al., 1992; Gu et al., 1995; Jardine et al., 2010). The increase or decrease in the amount adsorbed related to the pH value is consistent with

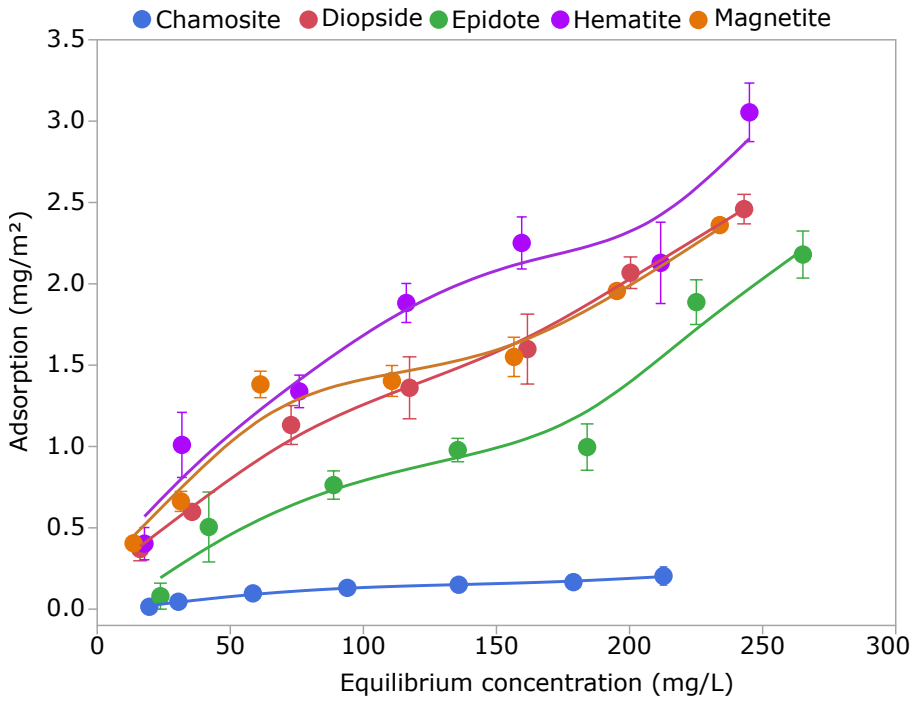

Fig. 5.11 – Adsorption isotherm of chamosite, diopside, epidote, hematite and magnetite as a function of its equilibrium concentration for humic acid at pH 5.

the proposition of a complexation-ligand exchange mechanism for humic substances (Gu et al., 1995) and also with the possibility of a protonation of surface hydroxyls to form complexes (Davis, 1982). In general, an anion adsorption at oxides surfaces involves ligand exchange with surface $Fe{-}OH_2^+$ and $Fe{-}OH$ groups, whereby the carboxylate groups displace surface hydroxyl and H_2O.

It is important to highlight the influence of the large specific surface area of chamosite in the equilibrium adsorption isotherms interpretation. Since this mineral has almost 20 times more specific surface area than the other minerals, its adsorption has been masked by the low values of adsorption densities presented in mg/m^2. Figure 5.12 presents a comparison between chamosite and magnetite adsorption in mg/g. This unit allows the interpretation of how much depressant has been adsorbed onto 1 gram of each mineral.

CMC and dextrin did not adsorb well on chamosite surface and only slightly better on magnetite surface. Chamosite presented high affinity for corn starch, much more than magnetite, indeed. Humic acid was also stronger adsorbed into chamosite surface than into magnetite surface. These results can lead to the conclusion that corn starch and humic acid would inhibit the adsorption of collectors rendering chamosite hydrophilic. However, the high specific surface area of chamosite is now an ally, because it allows enough parking place for the collector to adsorb. During a flotation process, both depressant and collector adsorb into minerals surfaces. What determines whether a mineral float is the coverage ratio between these two reagents on

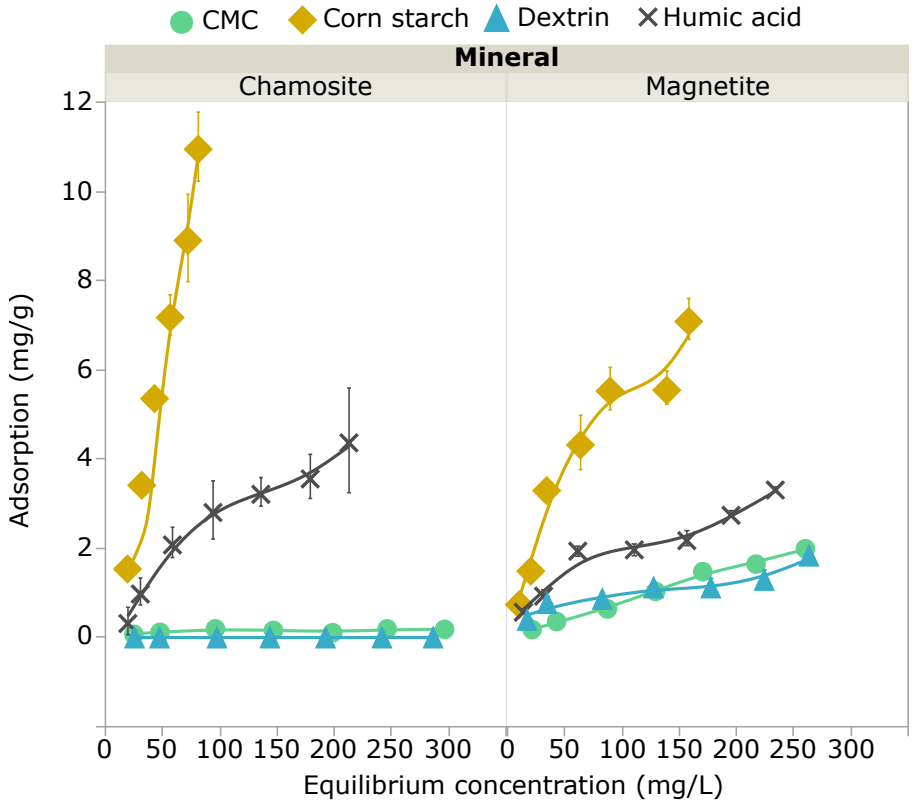

Fig. 5.12 – Adsorption isotherm of chamosite and magnetite in *mg/g* as a function of its equilibrium concentration for corn starch, CMC, dextrin and humic acid.

the mineral surface.

5.3 Concluding remarks

The zeta potential measurements indicate that the silicates – chamosite, diopside and epidote – have similar charge on their surfaces for the entire pH range studied. The relationship between the presence of available site of Mg and the IEP was observed in the case of chamosite when compared to the mineral in its series, clinochlore. Hematite and magnetite present higher IEP values than the silicates what can explain the difference in adsorption mechanism between those minerals.

The adsorption experiments results confirm the theory of Filippov and co-workers (Filippov et al., 2013; Severov et al., 2016), that corn starch is not a selective depressant when the iron ore is composed by iron-bearing silicates as the ones studied here. Corn starch adsorbed in all minerals, including the silicates. Nakatani et al. (1990) found that glucose adsorbed much more strongly on a basic alumina surface than on an acid one, this fact associated with other researchers findings of Liu et al. (2000), made possible the proposition of an acid-base interaction between polysaccharides and minerals, in which the determination of the adsorption

mechanism as hydrogen bonding or chemical complexation depends on the basicity of the minerals surface. This behaviour was observed in the zeta potential measurements at basic pH values, where chemical complexation begins to occur to compensate the increasing electrostatic repulsion. Dextrin had the same trend in adsorption as corn starch, except for chamosite where no adsorption was observed. The adsorption densities of dextrin are not high, and this polymer seems to be not efficient in the depression of iron oxides.

CMC had no significant adsorption on silicate minerals, indicating a better affinity with iron oxides minerals. This preference for hematite and magnetite surface is still very controversial, but most studies stated that the lower electrostatic repulsion and a better affinity for the available sites in these minerals surface would explain this preference in the adsorption (Liu et al., 2000; Fujimoto and Petri, 2001; Backfolk et al., 2002).

Humic acid adsorption occurs most effectively by the formation of complexes between this anionic depressant and the surface of the minerals. This depressant should be effective in the separation of iron oxides and silicates, since it does not adsorb quite well onto silicates and it promotes a hydrophobic interaction character in iron oxides.

Chapter 6

Flotation study of pure minerals and iron ore concentrate

6.1 Micro-flotation of pure minerals

Before starting the micro-flotation tests, it is important to determine the best conditions for the tests, i.e., stirring, collectors conditioning and flotation time.

Entrainment

Entrainment can be described here as the unwanted raise of the mineral inside the tube due mainly to turbulence caused by the bubbles and the excessive stirring, which give an artificial floatability to hydrophilic minerals. The entrainment could then be controlled by adjusting the size of the bubbles or the speed of the stirring. The first one is a parameter that cannot be adjusted in this case, since it depends on the porosity of the glass frit located in the bottom of each tube. Thus, the optimum stirring for the two tubes presented in Figure 3.4 were determined trying to avoid the natural mechanical entrainment of the mineral particles. It should also be considered that the stirring needs to be enough to ensure that no settling will occur during the tests. Diopside and epidote single mineral micro-flotation tests were carried out in a modified Hallimond tube with magnetic stirring, and for the other three minerals (chamosite, hematite and magnetite) the modified Smith-Partridge tube was employed with mechanical stirring. For the modified Hallimond tube the stirring was adjusted to a speed of approximately 450 rpm and for the modified Smith-Partridge tube a digital overhead stirrer was set at 700 rpm for chamosite and 900 rpm for hematite and magnetite.

Figure 6.1 shows that the entrainment for all the minerals were below 5% according to the stirring speed settings. All the following tests were performed under these stirring conditions.

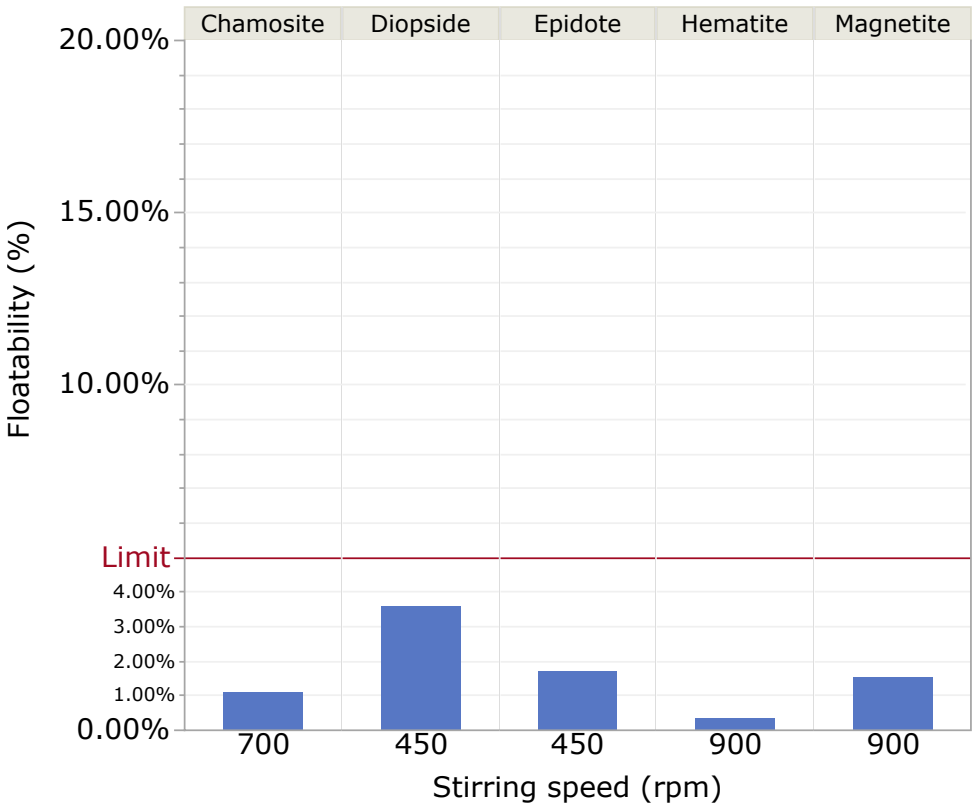

Fig. 6.1 – Mechanical entrainment of micro-flotation tests on modified Hallimond tube and on modified Smith-Partridge tube.

Collectors conditioning and flotation time

For the micro-flotation tests two collectors were tested (DDA and ETA). These experiments aimed to establish optimum collector conditioning and flotation time for all the five minerals. To do that, two other parameters were fixed: *pH* and *collector concentration*. The pH value chosen was 10 in which all the minerals have negative surface, as demonstrated in section 5.1 of chapter 5, and because amines have half anionic and half molecular forms at this pH value, acting also as a frother in this case. The concentration was set at 1.0×10^{-4} M, based in many other studies conducted in silicates flotation (Scott and Smith, 1991, 1993; Ari, 2001; Irannajad et al., 2009). This concentration leads to the monolayer adsorption allowing a total flotation of the pure minerals as reported by Scott and Smith (1991) for quartz and by Filippov et al. (2012) for tecto and phylosilicates with primary and ether-amines.

Figure 6.2 presents the conditioning and flotation time study of DDA in the five minerals. It is possible to notice an increase in the overall floatability with time, reaching a stabilization after 2 minutes of flotation. The influence of the conditioning time for most minerals is small and most curves are closely packed. The mineral that had the most difficult in floating was chamosite. Collector conditioning time did not have much influence on floatability. Two minutes collector conditioning time and two minutes flotation time was assumed as safe since they were all around 80% floatability.

The same tests were performed using ETA as collector. Globally, the same trend observed

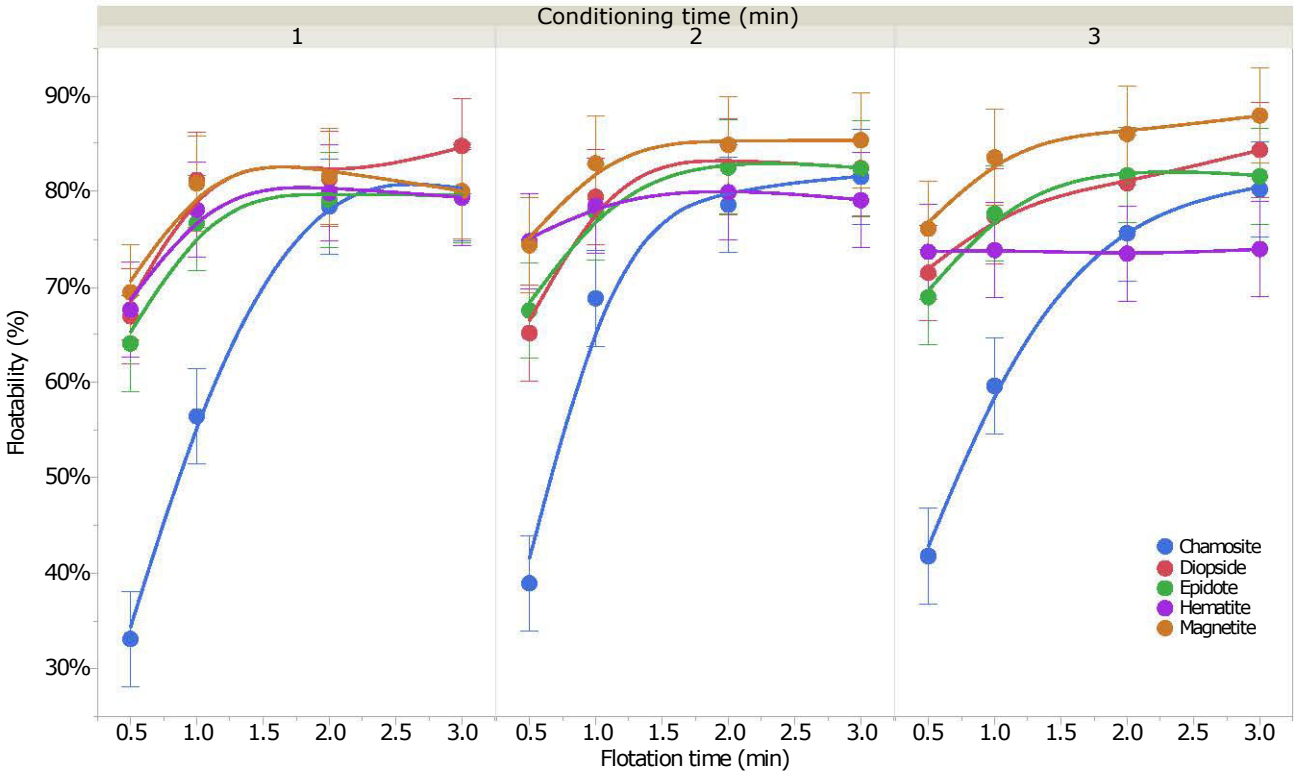

Fig. 6.2 – DDA conditioning and flotation time on pure mineral samples.

with DDA applies to ETA. The conditioning time here is insignificant and increases the floata-

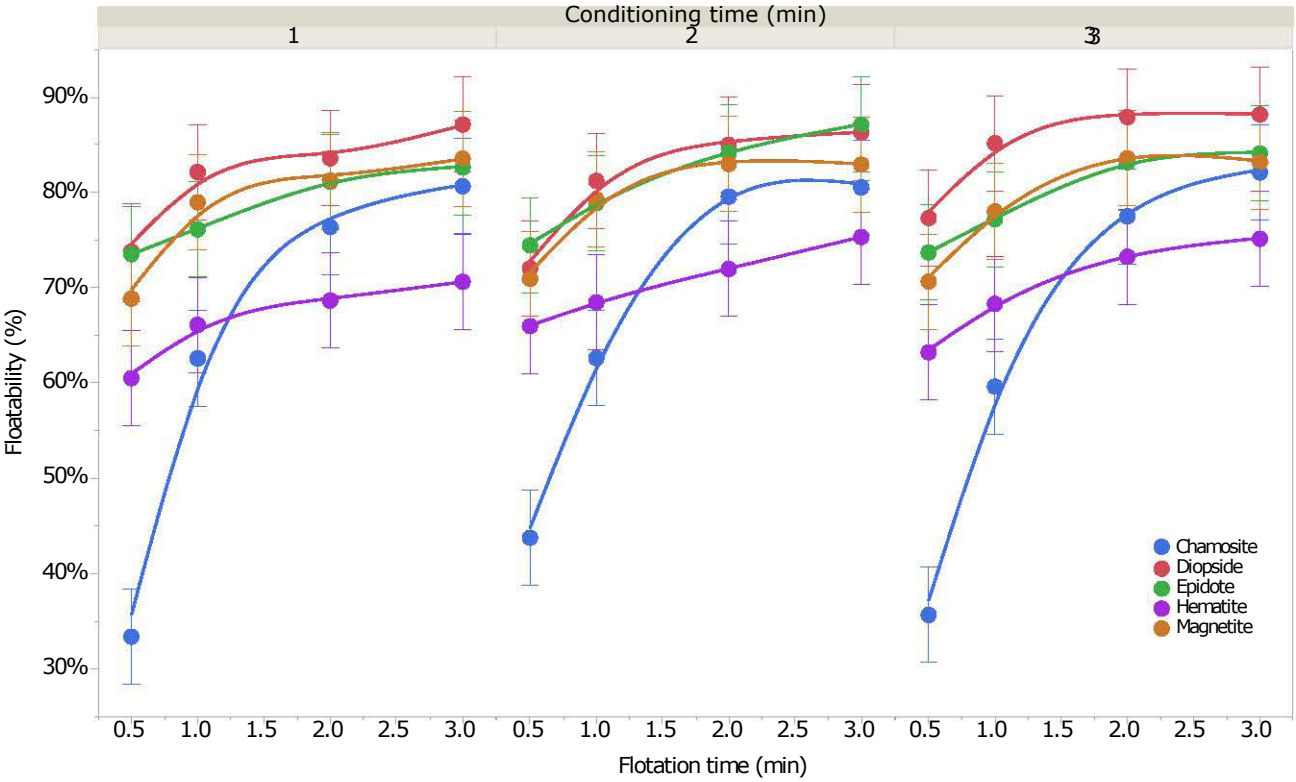

Fig. 6.3 – ETA conditioning and flotation time on pure mineral samples.

bility of the minerals by only 1 to 2% and no negative effects is observed on chamosite and hematite meaning that any conditioning time is acceptable for ETA. Again, after two minutes of flotation, the minerals reached the plateau of floatability (see Figure 6.3). All the following tests, with DDA and ETA were performed considering 2 minutes of conditioning and 2 minutes of flotation time.

6.1.1 Single mineral micro-flotation

pH study

After the parameters of stirring speed, conditioning and flotation time have been well explored, a study on the influence of pH on each mineral was started. The pH value of the collector was variate from 2 to 12 for DDA and ETA, and the collectors were prepared at 1.0×10^{-4} M. All tests were performed in duplicate. The curves for both DDA and ETA are presented in Figure 6.4 and it is possible to observe a trend in all curves to be like logistic curves ("S" shape) with maximum floatability in the higher pH values and minimum floatability in low pH values range. The silicates, except for chamosite, seem to only start lose floatability below pH 5. On the other hand, a reduction in floatability is observed for iron oxides at pH below 8. This decrease agrees with zeta potential theory and it is especially visible for the iron oxides since they have high and distinctive IEPs. It is possible to see that diopside and epidote are reaching a plateau in their floatability almost after pH 7. Chamosite is also following this trend when floated with ETA but not when DDA is employed. Chamosite is presenting a strange behaviour when floated at pH 11 with both collectors, a huge drop in floatability, that may be explained by an instability of the adsorption layer on phyllosilicates. The maximum and minimum values of floatability was achieved with DDA, respectively:

- *Chamosite*: 78.6% (pH = 10); 8.1% (pH = 4);
- *Diopside*: 87.3% (pH = 4); 62.3% (pH = 2);
- *Epidote*: 82.1% (pH = 6); 27.1% (pH = 2);
- *Hematite*: 79.4% (pH = 10); 1.6% (pH = 4);
- *Magnetite*: 85.5% (pH = 11); 2.4% (pH = 2).

For ETA, the experiments show:

- *Chamosite*: 81.4% (pH = 8); 23.8% (pH = 2);
- *Diopside*: 90.5% (pH = 6); 36.7% (pH = 2);

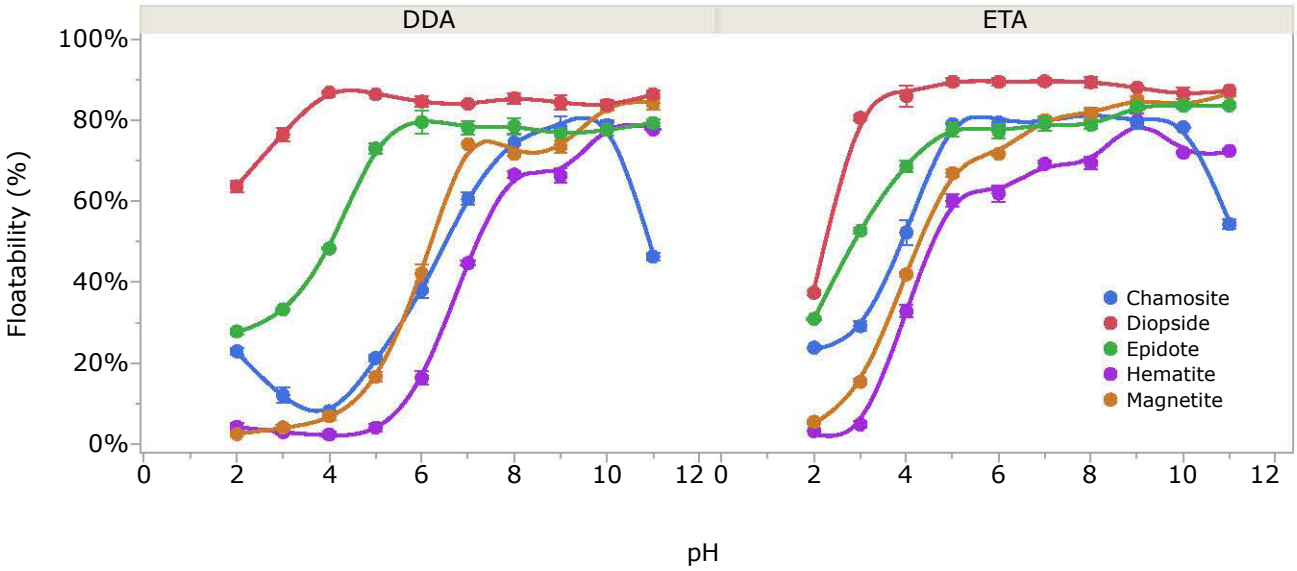

Fig. 6.4 – Floatability of pure minerals with DDA and ETA at several pH values. The error was calculated from the difference between the duplicate experiments (error bars).

- *Epidote*: 84.2% (pH = 5); 30.6% (pH = 2);
- *Hematite*: 81.4% (pH = 9); 3.0% (pH = 2);
- *Magnetite*: 87.4% (pH = 11); 5.0% (pH = 2).

ETA is a more competent collector in terms of floatability, but all the minerals float with this collector and no clear separation window is visible. On the other hand, DDA has good floatability for all minerals, and offers a possible separation window between iron oxides and silicates at pH value around 4. In fact, at this pH, the iron oxides are only floating in the 5% range while diopside and epidote are near 50% and 80% respectively, a separation factor of about 10 times. However, chamosite, the most complicated of the three silicates, does not follow the trend of other silicates and has low floatability at pH 4. This result does not necessarily imply that the DDA is the best collector for the reverse cationic flotation of iron ores because the role of the depressants may change the trend in the floatability of the silicates and iron oxides.

Concentration study

Figure 6.5 is presenting the curves for the micro-flotation experiments with chamosite, diopside, epidote, hematite and magnetite using DDA and ETA as collectors with concentration from 1.0×10^{-6} M to 5.0×10^{-4} M at pH 10. For both collectors, no flotation is observed between concentration 1.0×10^{-6} M and 5.0×10^{-6} M, where a small floatability is observed for all minerals. From concentration of 5.0×10^{-5} M the plateau of floatability is observed for almost all minerals, expect chamosite. At this concentration, ETA presents a better capability

of collection when compared to DDA, meaning that the plateau for ETA is reached before DDA. Chamosite is presenting a behaviour very different from all the other minerals. It is in fact starting to reach a plateau in concentration of 1.0×10^{-4}, where the adsorption layer is close to the monolayer. This concentration is already a zone of over dosage for all the other minerals, where the formation of a second layer begins due to the interaction between the hydrocarbon chains, and no improvement in floatability is observed after this value. At this same zone, DDA starts to have hydrophobic aggregation. This effect is especially visible for diopside which loses 15% in floatability. The usability of DDA at this concentration is also difficult since at pH 10, the dissociation of the amine is high and molecular amine starts to precipitate on the walls of the tubes.

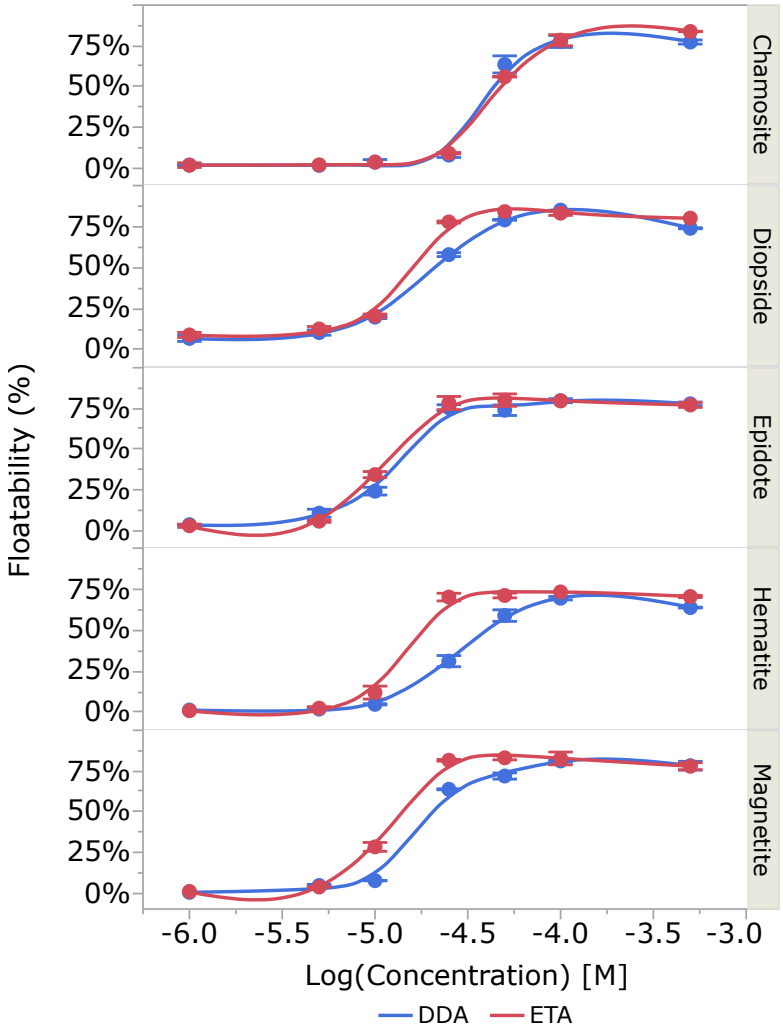

Fig. 6.5 – Floatability of pure minerals with DDA and ETA at several concentration values at pH 10. The error was calculated from the difference between the duplicate experiments (error bars).

Depressants study

Aiming to better understand how competition occurs between depressant and collector during flotation and which minerals are those with the lowest selectivity, a study using depressants

and collectors was performed. For these experiments, the same collectors DDA and ETA were used, and two depressants were introduced here: *corn starch* as a reference and the most used depressant for the reverse cationic flotation of silicates (Araujo et al., 2005) and *humic acid* which demonstrated potential to promote better selectivity. For this study, only the modified Smith-Partridge tube was used, stirring speed was kept for the minerals that had already been floated in this tube and adjusted at the same level for diopside and epidote. The procedure was modified a little bit with the introduction of the depressants. First the depressant was conditioned inside the tube for 5 minutes, then the collector was added and conditioned for 2 minutes. The solution level was adjusted to the tube volume with pre-regulated pH water. The flotation time was also 2 minutes. Four different ratios between depressant and collector were tested: 1, 5, 7.5 and 10. This ratio represents the concentration of depressant in relation to the collector. For example, DDA in a concentration of 1.0×10^{-4} M has 167.94 mg per litre of solution, in a ratio 1 the depressant was prepared at the same concentration, in a ratio of 5 it was prepared at 5 times that concentration and successively. The pH was set at 10 for all tests.

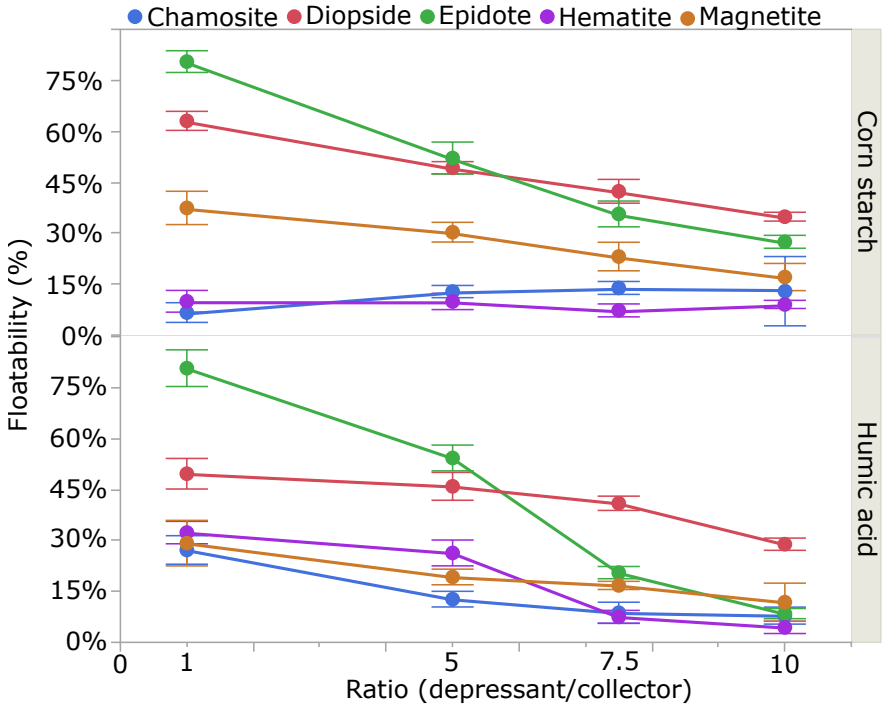

Fig. 6.6 – Floatability of pure minerals with corn starch and humic acid as depressants and DDA as collector at pH 10.

Corn starch is more powerful in depressing iron oxides. It is possible to notice from Figure 6.6 and Figure 6.7 that the floatability of hematite and magnetite in presence of this depressant is quite low. For corn starch at ratio 1, magnetite is still floating while hematite and chamosite are being depressed. When the amount of corn starch in solution increases, it begins to depress silicates as well, due to the inhibition of the collector adsorption and to the formation of a clathrate structure that masks the amine effect (Shrimali et al., 2017). The adsorption of corn

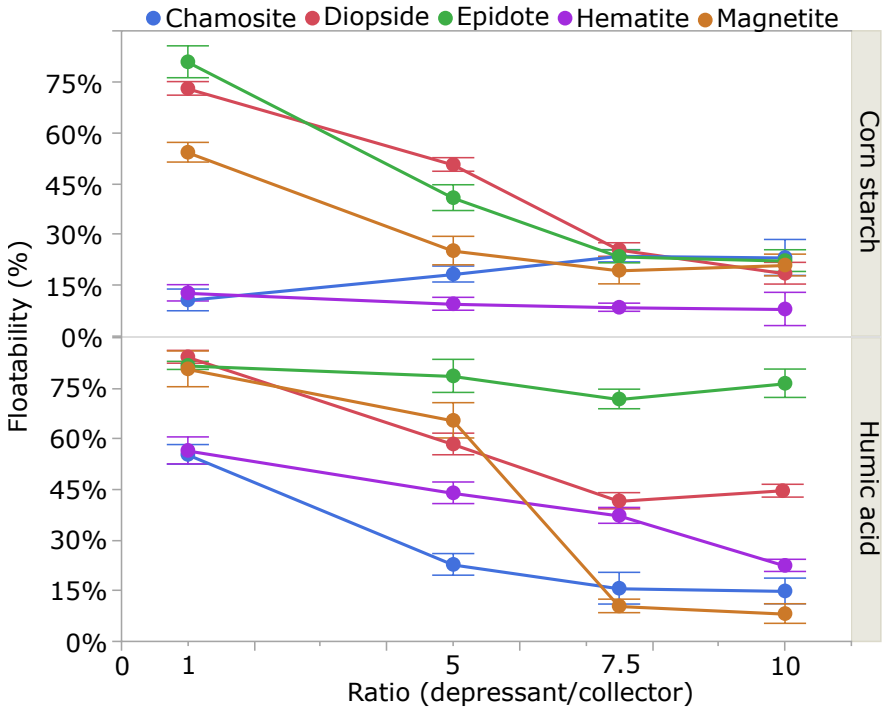

Fig. 6.7 – Floatability of pure minerals with corn starch and humic acid as depressants and ETA as collector at pH 10.

starch is high in all these minerals. Chamosite has a different behaviour when compared to the other minerals. The more corn starch, the more it floats. Humic acid seems to be more selective than corn starch. When DDA is used together with humic acid, the floatability behaviour is quite like corn starch, meaning that the more depressant, the less floating minerals. Diopside and epidote were the minerals less sensible to humic acid adsorption. However, when ETA is used as collector together with humic acid, the behaviour is quite different. Epidote suffered no interference and continued to float normally. At ratio 10, both iron oxides are being quite well depressed, while diopside and epidote are floating well. As always, chamosite is the problematic mineral having a behaviour quite close to the iron oxides and being mostly depressed in these tests. Only in the experiment with humic acid and ETA at ratio 1 was possible to observe chamosite flotation.

6.1.2 Multi-mineral micro-flotation

After the study on the single minerals, it was necessary to understand how the minerals behave when in presence of other one. For the following experiments, the study was divided in two groups of minerals assemblage:

1. *Hematite and silicates (chamosite, diopside and epidote)*;

2. *Magnetite and silicates (chamosite, diopside and epidote).*

For each test, 0.5 g of iron oxide was mixed with 0.5 g of silicate in order to form 1 g of sample to perform the micro-flotation tests. The collector concentration used for this test was 1.0×10^{-4} M, where the plateau of floatability was reached for all minerals. Two pH values were tested, pH 10 that was observed to be the optimum value for floatability and pH 4 in which a separation window was observed and need to be investigated in more details. All the experiments were performed in duplicate. Figure 6.8 and Figure 6.9 present the results for the experiments with hematite and silicates and magnetite and silicates, respectively. The point where 100% of the silicates floated and 100% of the iron oxides did not float, is indicated in the figures as the ideal separation point. When the points are close to the coordinates (100,0), silicates have shown good floatability, but also the iron oxides and thus, no separation is observed.

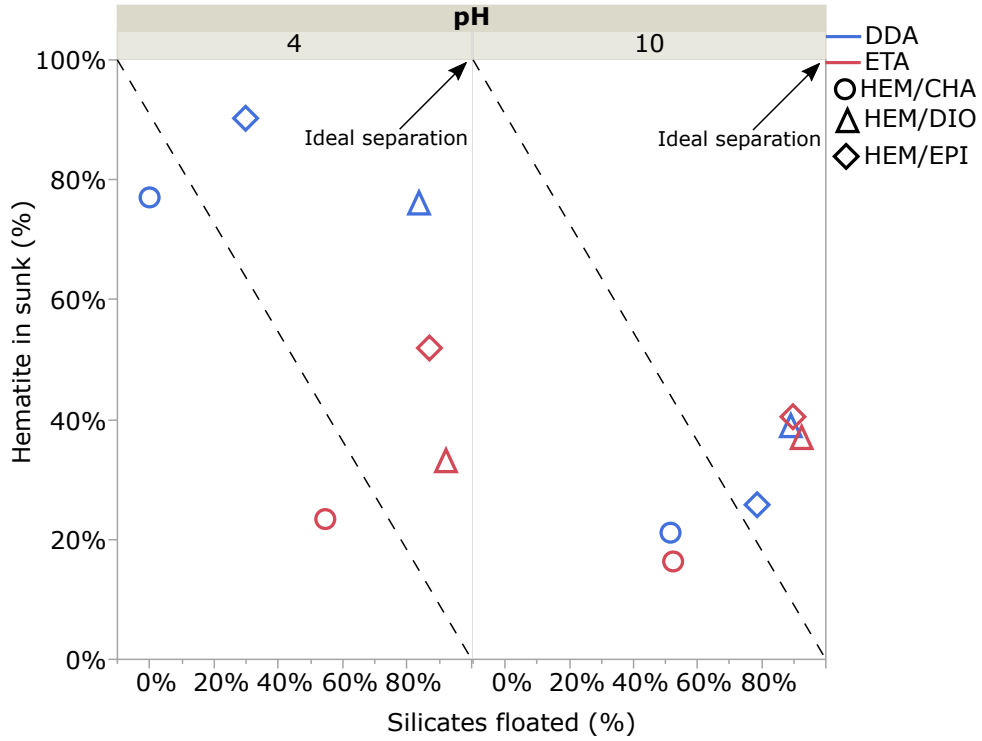

Fig. 6.8 – Recovery of hematite and silicates with DDA and ETA micro-flotation at pH 4 and 10.

DDA showed better selectivity than ETA. The presence of an extra hydrophilic group from the ether function improves floatability by increasing the solubility of the ETA and facilitating its access to the interfaces (Araujo et al., 2005), and this can lead to a low selectivity, with ETA floating all minerals. The window separation at pH 4 was confirmed. At this pH value it is possible to observe the best separation between iron oxides and silicates. Overall, the best results were achieved with mixtures of diopside and epidote with iron oxides. Chamosite is not being separate; at pH 4 almost no flotation is observed with DDA. At the same pH 4,

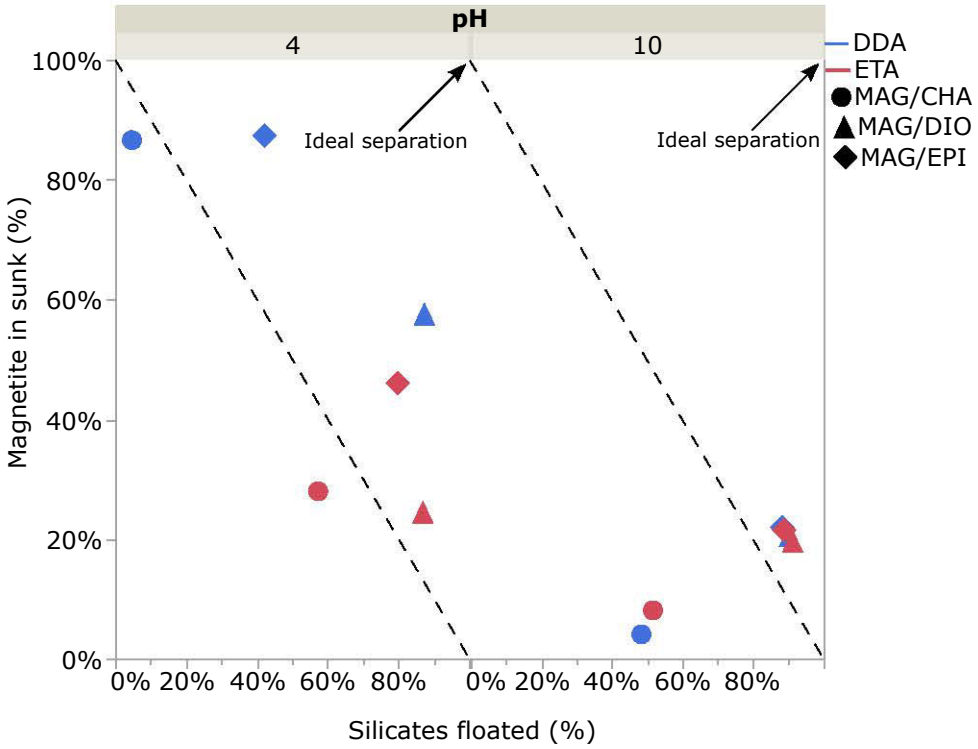

Fig. 6.9 – Recovery of magnetite and silicates with DDA and ETA micro-flotation at pH 4 and 10.

chamosite is being floated with ETA, but so are the iron oxides. When the pH increases to 10, the floatability increases as well, but almost all minerals are floating, evidenced by the points being close to the coordinates (100,0). Although the chamosite IEP is close to that of other silicates, its behaviour is very similar to iron oxides in terms of surface properties. Overall, for the ETA results hematite was more resistant to float than magnetite and the window separation at pH 4 is less evident. In summary, when all the minerals have negative surface charge (pH = 10), the separation efficiency is low. However, when the pH decreases to 4, it is noticeable the preference in collector adsorption at the silicates surfaces.

6.2 Batch flotation of iron concentrate

This section is dedicated to the study of the iron concentrate used in this study, in which all the pure minerals studied in the last section are present. This study was divided in two parts:

- *Exploratory tests*, aiming to identify the main factors that impact the flotation results and define optimum points;
- *Structured tests*, that were dedicated to test other parameters that have influence on the flotation, as water source for example.

For all tests, the objectives were: minimize the silica content in the final product keeping the maximum iron recovery possible. The flotation protocol used for all the following tests can be found in section 3.4.4 of chapter 3.

6.2.1 Exploratory tests

The investigation begins trying to evaluate the influence of important factors for the reverse cationic flotation of iron ores such as reagents type, their dosages and the pH of flotation. A commonly used approach for performing experiments is the one-factor-at-a-time. This method consists of selecting a starting point for each factor and then variate one factor at a time holding all the other factors constant. The main problem with this method is that it does not consider interactions between the factors (Montgomery, 2012). In flotation, for example, it is obvious that pH has influence in the adsorption of reagents. In this case, the best approach to be used is to conduct a factorial experiment, in which the factors are varied together, and those interactions can be considered.

6.2.1.1 Design of experiments

To perform the investigation under several factors, the Surface Response Methodology (SRM) was employed. This methodology is useful when a problem has a response influenced by several factors and the objective is to maximize or minimize it (Montgomery, 2012). To fit the response surface, the Box-Behnken (1960) design was used. The design does not contain any points at the highest levels of the factors and this is advantageous in our case, because high dosages of reagents are prohibitively expensive for the industry. The generation of the experimental designs (runs) and data analysis were performed by the software JMP® (SAS). Three factors were investigated: depressant dosage, collector dosage and pH, and iron recovery and silica content in the final product were the responses analysed. Table 6.1 presents the factors and their levels used for the design of experiments. The focus here was also to investigate the depression effect of non-usual depressants for iron oxides. For that, four experimental designs were made, one for each of the following depressants: *corn starch*, *carboxymethyl cellulose*, *dextrin* and *humic acid*. The silica collector tested was Flotigam EDA, an ether amine. Prior sulphide flotation was conducted using Potassium Amyl Xanthate (PAX) and Hostaflot LIB as sulphide collectors in a ratio of 1:1 and 40 g/t of total dosage and Flotanol H53 as frother in a dosage of 20 g/t. The iron concentrate sample 1 was used for this study (see section 3.2 in chapter 3). The levels for depressant dosage, silicate collector dosage and pH were chosen based on preliminary tests with the same material and the reported in the literature. Table 6.1 presents the factors and levels used for the DOE analysis.

Table 6.1 – Factors and corresponding levels used for the design of experiments.

Factors	Levels		
	Low	Centre	High
Depressant dosage (g/t)	300	450	600
Collector dosage (g/t)	90	110	130
pH	7	9	11

6.2.1.2 Results

The method of Box-Behnken proposed a series of 15 experiments that was repeat four times, one for each depressant. The experimental results for iron recovery and silica content in the final product are separately presented for each depressant tested.

Corn starch

Table 6.2 presents all the levels used for each factor for the 15 runs using corn starch as depressant.

Table 6.2 – Three-variable Box-Behken design used for the tests, iron recovery and silica content results for corn starch.

Run	Factors			Responses	
	Depressant dosage (g/t)	Collector dosage (g/t)	pH	Fe recovery (%)	SiO_2 content (%)
1	450	110	9	73.96	3.56
2	450	110	9	71.86	3.56
3	600	130	9	70.25	3.57
4	450	110	9	71.86	3.56
5	450	90	7	73.43	3.42
6	300	110	11	73.93	3.89
7	300	90	9	72.96	3.71
8	600	110	7	72.41	3.61
9	450	90	11	70.71	3.65
10	450	130	7	63.44	3.25
11	600	110	11	71.70	3.88
12	600	90	9	75.98	3.59
13	300	110	7	63.23	3.46
14	450	130	11	65.49	3.52
15	300	130	9	69.70	3.51

The best result regarding silica content reached in test 10, with 3.25% of SiO_2 and 63.44%

of iron recovery. Surprisingly the best results were observed close to neutral pH, around 7 and 9. This outcome was not expected since reverse cationic flotation of silicates normally has better response when performed in alkaline pH (Peres and Correa, 1996). However, as shown in Figure 6.4, at this range of pH the silicates studied have already a good floatability, whereas iron oxides floatability is less important.

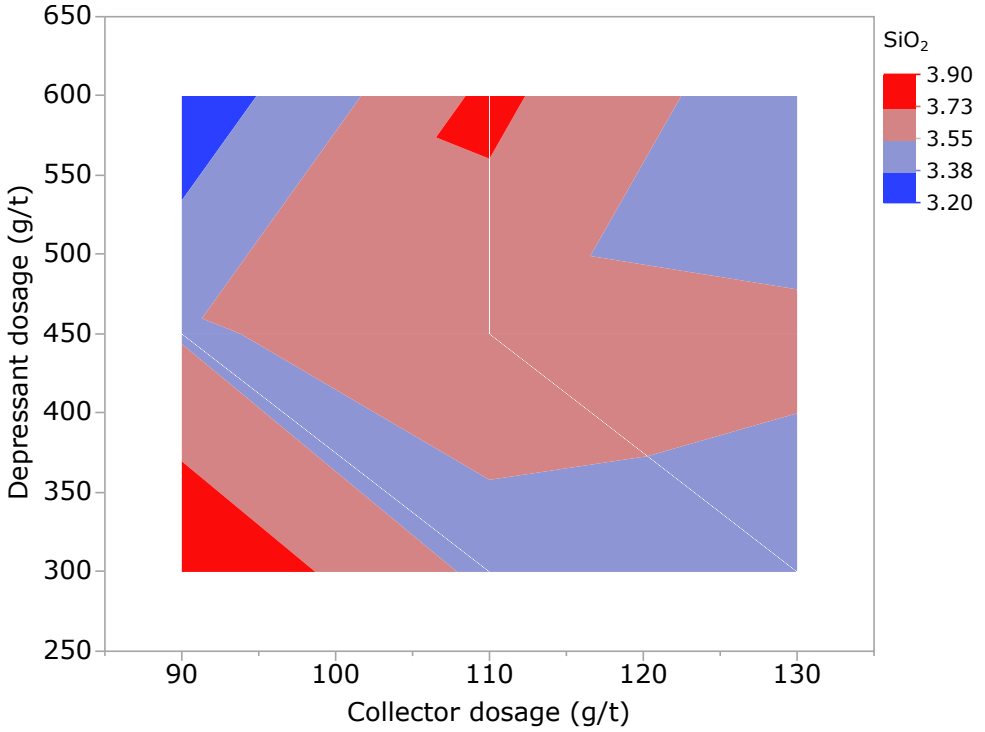

Fig. 6.10 – Corn starch and Flotigam EDA dosages variation related to SiO_2 content in final product.

From Figure 6.10 is possible to see that the zone where silica has the lowest value is the zone where corn starch dosage is the highest possible. Also, the minimum silica content achieved when corn starch is used was 3.20% . The increase in silica content may be related to the depression of iron-bearing silicates or mixed particles containing also silicate particles. The inefficiency of corn starch as depressant in the reverse cationic flotation of complex iron ores has been discussed herein before and these results only prove this statement.

Carboxymethyl cellulose

Table 6.3 presents all the levels used for each factor for the 15 runs using carboxymethyl cellulose as depressant.

The best result when carboxymethyl cellulose is used as depressant was achieved in test number 6, where the iron recovery was 61.21% and the silica content in the final concentrate 3.76%. The values for iron recovery are quite low. This is an indication that carboxymethyl cellulose was not acting as a depressant. The presence of carboxyl group is an indication that

Table 6.3 – Three-variable Box-Behken design used for the tests, iron recovery and silica content results for carboxymethyl cellulose.

Run	Factors			Responses	
	Depressant dosage (g/t)	Collector dosage (g/t)	pH	Fe recovery (%)	SiO_2 content (%)
1	450	110	9	37.89	4.06
2	450	110	9	40.16	3.95
3	600	130	9	28.2	4.05
4	450	110	9	39.2	3.99
5	450	90	7	26.03	4.1
6	300	110	11	61.21	3.76
7	300	90	9	46.14	3.87
8	600	110	7	21.16	3.8
9	450	90	11	66.15	3.85
10	450	130	7	59.01	4.09
11	600	110	11	57.01	3.83
12	600	90	9	34.69	4.38
13	300	110	7	36.45	4.05
14	450	130	11	24.07	4.25
15	300	130	9	43.69	3.98

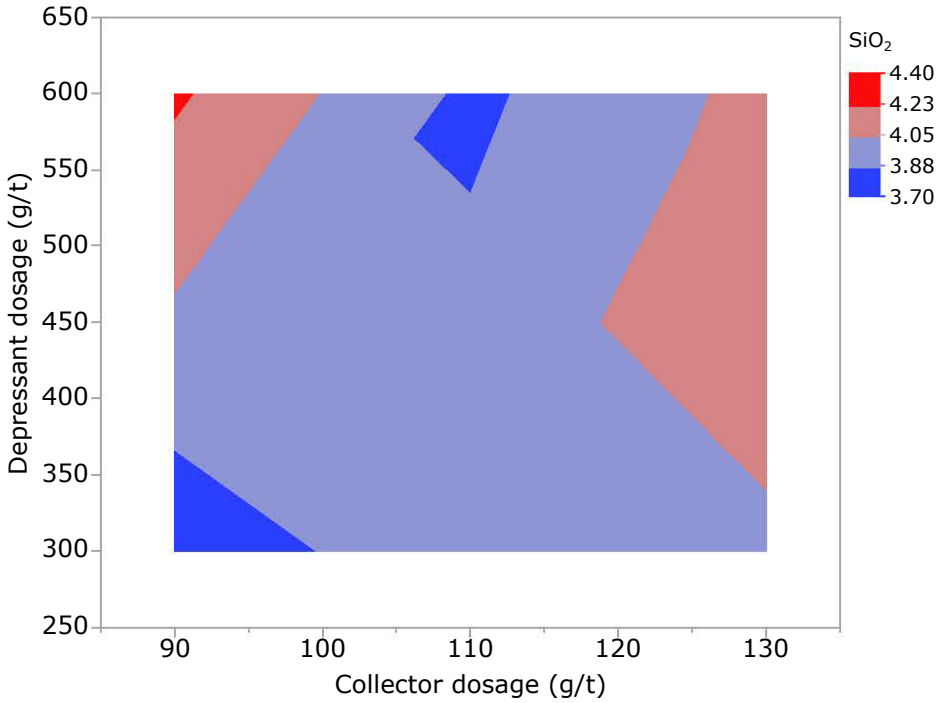

Fig. 6.11 – Carboxymethyl cellulose and Flotigam EDA dosages variation related to SiO_2 content in final product.

depression would be favoured, but other factors such as the degree of substitution, degree of polymerization and its structure could affect the carboxymethyl cellulose depressant character (Pugh, 1989).

From Figure 6.11 is possible to see that the zone where silica has the lowest value is in the range of 300 - 350 g/t of carboxymethyl cellulose and in a small area between 550 - 600 g/t. No trends can be observed for the behaviour of this depressant. To further investigate carboxymethyl cellulose as depressant in the reverse cationic flotation of iron ores, it will worth to test different substitution degrees and molecular weight. This depressant was the worst in terms of silica reduction and iron recovery.

Dextrin

Table 6.4 presents all the levels used for each factor for the 15 runs using dextrin as depressant.

Table 6.4 – Three-variable Box-Behken design used for the tests, iron recovery and silica content results for dextrin.

Run	Factors			Responses	
	Depressant dosage (g/t)	Collector dosage (g/t)	pH	Fe recovery (%)	SiO_2 content (%)
1	450	110	9	79.84	3.35
2	450	110	9	79.69	3.28
3	600	130	9	80.30	3.27
4	450	110	9	79.69	3.28
5	450	90	7	85.11	3.70
6	300	110	11	89.92	3.69
7	300	90	9	83.77	3.36
8	600	110	7	85.55	3.70
9	450	90	11	81.53	3.29
10	450	130	7	83.09	3.57
11	600	110	11	88.92	3.69
12	600	90	9	81.62	3.22
13	300	110	7	82.81	3.76
14	450	130	11	87.00	3.57
15	300	130	9	78.50	3.24

The best results in terms of silica content was achieved in the test number 12. At this test, the use of dextrin leads to an iron recovery of 81.62% with a silica content in the final concentrate of 3.22%. In terms of silica reduction, the result is comparable to corn starch, but a higher iron recovery is observed for dextrin. It is important to highlight that an increase in dextrin dosage

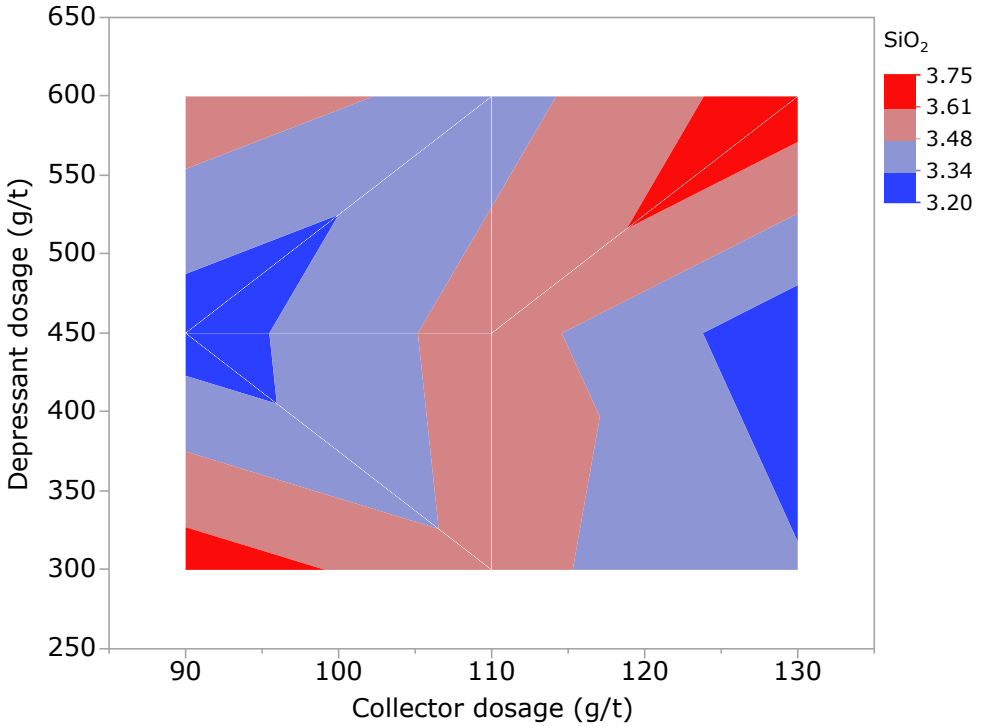

Fig. 6.12 – Dextrin and Flotigam EDA dosages variation related to SiO_2 content in final product.

does not imply in a better or worse depression effect, this is mainly due to the fact the it has a high branched rigid structure that remains unchanged with the increase of the adsorption density (Pugh, 1989). In fact, it seems that 300 g/t is already a reasonable concentration to generate the adsorption density necessary to depress the iron oxides. Figure 6.12 presents a correlation graph between collector and depressant dosages. No trend is observed for the case of dextrin, the silica content is varying a lot and there is no zone where it is constant.

Humic acid

Table 6.5 presents all the levels used for each factor for the 15 runs using humic acid as depressant. Humic acid has stand out as the best depressant for this iron concentrate. From the 15 runs, it is possible to see that a very low silica content was achieved (2.78%) with 83.38% of iron recovery (Table 6.5), in test 13. Figure 6.13 confirms that high concentrations of humic acid are not required to achieve good results in silica content. Instead, the best results are achieved in lower dosage zones. Humic acid has been shown to be more strongly adsorbed into the surface of iron oxides than to silicates and the addition of collectors does not change the hydrophilic character given by humic acid (see Figure 6.6 and Figure 6.7). It had already been reported that humic acid was a potential alternative depressant to the reverse cationic flotation of hematite iron ores (Santos and Oliveira, 2007). This result makes it possible to extend this statement also to magnetite iron ores. The excellent effect of humic acid depression at pH 7 can be explained by the intensification of the existent adsorption via coordinative interactions between Fe^{3+} or Fe−OH by the electrostatic interaction between the iron oxides surfaces (close

Table 6.5 – Three-variable Box-Behken design used for the tests, iron recovery and silica content results for humic acid.

Run	Factors			Responses	
	Depressant dosage (g/t)	Collector dosage (g/t)	pH	Fe recovery (%)	SiO_2 content (%)
1	450	110	9	70.09	3.11
2	450	110	9	75.42	3.21
3	600	130	9	71.84	3.06
4	450	110	9	74.71	3.19
5	450	90	7	79.2	3.28
6	300	110	11	77.92	3.25
7	300	90	9	83.38	3.40
8	600	110	7	71.85	3.09
9	450	90	11	82.69	3.38
10	450	130	7	73.33	3.04
11	600	110	11	79.83	3.16
12	600	90	9	73.06	3.10
13	300	110	7	83.72	2.78
14	450	130	11	69.73	3.03
15	300	130	9	74.05	3.10

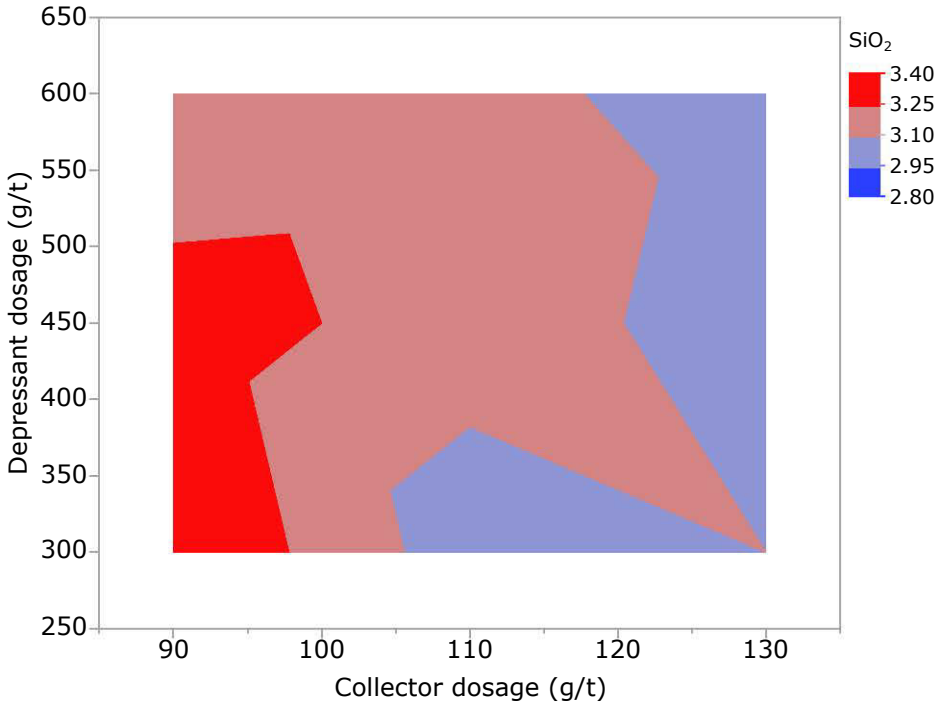

Fig. 6.13 – Humic acid and Flotigam EDA dosages variation related to SiO_2 content in final product.

to IEP) and the anionic humic acid molecule (Ochs et al., 1994; Ramos-Tejada et al., 2003).

Due to the very good result achieved with humic acid, the optimisation of its results through the design of experiments were performed. From the model analysed by the 15 runs carried out with humic acid, it is possible to construct a prediction profile (Figure 6.14) for different responses according to the changes in the factors. The data analysis was performed by the software JMP® using the desirability function. This approach is one of the most widely used methods for the optimisation of multiple response processes. In this case, the desirability function was set to minimize the silica content and to maximize the iron recovery in the final product. Desirability value of 1 means that both criteria were 100% met, while value equal to 0 means that there was no optimisation. From Figure 6.14 is possible to see that the desirability value for this model is ≈ 0.84. At this optimum point, the iron recovery would be of 84% with a silica content in the final concentrate of 2.89%. Levels for the factors of 300 g/t of depressant, ≈ 110 g/t of collector at pH 7 would be able to produce that result. Coincidentally, these parameters were tested on run number 13, randomly generated by the software. The predicted silica content and iron recovery from the prediction profiler were very close to the experimental values, validating the model for the prediction of humic acid results.

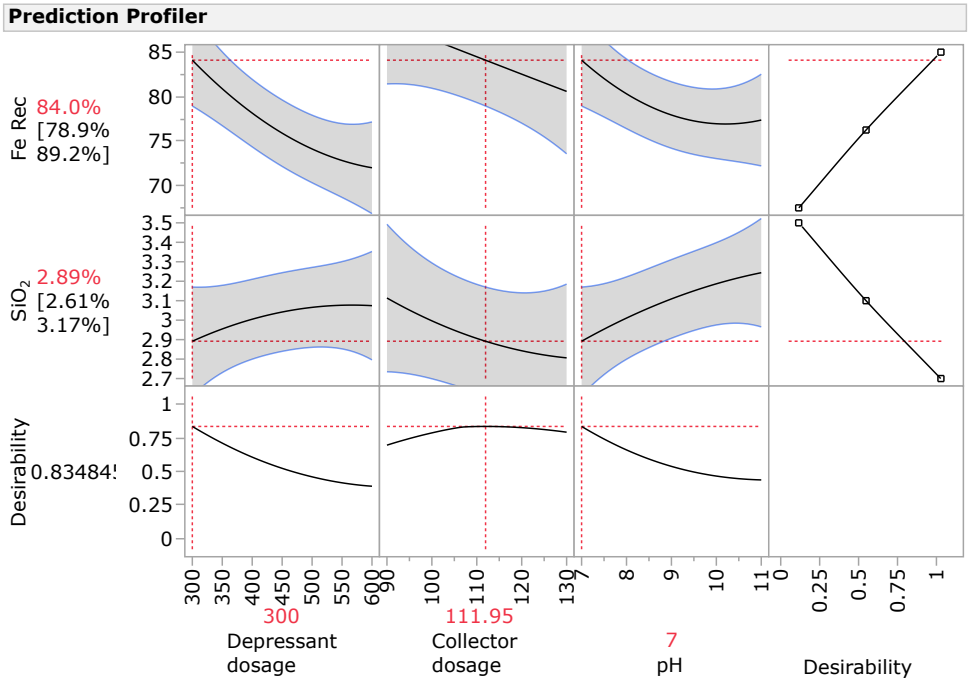

Fig. 6.14 – Optimisation of humic acid design of experiments results through the desirability function. Shaded area corresponds to the 95% confidence limit for the model.

6.2.2 Structured tests

From the exploratory tests it was possible to identify that humic acid is more effective as depressant than the other depressants tested. It was also found the optimal points for depressant and collector dosages, as well as the optimum flotation pH. Based on that, the next step was to test other parameters that have influence in the flotation process. The test work was divided in three programs:

1. Investigation on fine screening prior flotation;
2. Investigation of the influence of process water;
3. Investigation on another reagent suite.

Sample 2 (see section 3.2 in chapter 3) was used for these tests. Basically, the same conditions of the previous tests were kept. Sulphide flotation was also performed prior silicate flotation. From the exploratory tests, humic acid was used as depressant with a dosage of 300 g/t, Flotigam EDA as collector with a dosage of 110 g/t, for the first and second programs. The collectors tested for the third program will be further listed.

Fine screening prior flotation

As mentioned in chapter 4, sample 2 was received from the process plant and its complete characterisation was performed and leaded to the conclusion that the liberation degree was not reached in particles above 53 µm. For this reason, the sample gave origin to three different feed material for the flotation tests, as follows:

(A) *Global sample*, as received from the process plant, without any sieving;

(B) *Re-ground sample*, which was sieved at 53 µm and had the oversize re-ground until 100% of the material was passing at 53 µm;

(C) *53 µm exclusive sample*, which was sieved at 53 µm and the oversize was discarded.

Samples A and B have the chemical composition as described in the chapter 4. However, the chemical composition of sample C was modified, since some of the gangue minerals were removed when the almost 10% above 53 µm was discarded. The new chemical head composition for this sample is presented in Table 6.6.

Table 6.7 shows the best results in terms of silica content in the final product for each sub-sample A, B and C. A prior screening at 53 µm and a re-grinding of the material above

Table 6.6 – Chemical composition recalculated for size fractions of sample 2 above and below 53 µm.

Size fraction (µm)	Recalculeted from size-by-size analyses (% of oxides)										
	% weight	Fe (t)	FeO	SiO_2	Al_2O_3	S	P	CaO	MgO	Na_2O	LOI
> 53	**7.61**	30.81	12.39	9.89	3.10	0.42	0.054	1.87	0.75	0.760	-0.69
< 53	**92.39**	67.64	26.46	2.72	1.01	0.27	0.022	0.76	0.39	0.163	-2.64

53 µm (≈ 10%) leads to a decrease in silica from 3.58% in the sample A to 2.13% in sample B (Table 6.7), after flotation. In fact, it has been demonstrated that particles above 53 µm are not fully liberated. Although the re-grinding process does not completely liberate the particles, especially those that contain encrusted grains, it increases the chance of having more silicates floating. The introduced CS term is the coefficient of separation and it was calculated by the following formula:

$$CS(\%) = \frac{Fe_{\ (rec)} + SiO_{2\ (dist)}}{Fe_{\ (total)} + SiO_{2\ (total)}} \times 100 \tag{6.1}$$

where $Fe_{\ (rec)}$ is the amount of iron that goes to the concentrate (iron recovery); $SiO_{2\ (dist)}$ is the amount of silica that goes to the tailings and $Fe_{\ (total)}$ and $SiO_{2\ (total)}$ are the total amount of iron and silica, in this case 100% for both.

From Table 6.7 it is possible to see that this coefficient is increasing when the sample A are passing through a grinding to increase liberation of the particles or when the size fraction above 53 µm are being discarded. The best result in terms of silica content was achieved with sample C, using only the material below 53 µm. Since this is the target of the study, this sample was used for the next test programs, number 2 and 3.

Table 6.7 – Flotation results on sub-samples A, B and C.

Sample ID	Distribution		Grades		
	Fe recovery (%)	SiO_2 in tailings (%)	$Fe_{(t)}$ (%)	SiO_2 (%)	CS (%)
Global	65.38	35.70	66.77	3.58	50.5
Re-ground	65.93	53.32	68.48	2.13	59.6
53 µm exclusive	59.70	58.63	68.95	1.82	59.2

Process water influence

Water source is a factor that has a lot of influence in flotation. The presence of ions in the water can disturb the adsorption of reagents and jeopardize the flotation results. This topic has been the subject of several researches (Ozdemir et al., 2007; Santos et al., 2012; Liu et al., 2013b; Ikumapayi et al., 2012; Luukkanen et al., 2003) and since it is known that Mexico plant water is a carbonate water due basically to the region's carbonate geological formation, some

plant water sample were used to perform these tests and to compare it with the laboratory water used on the previous tests. The chemical composition of both process and laboratory water is presented in Table 6.8.

Table 6.8 – Process plant and laboratory water analyses.

Water source	Elemental analysis ($mg.L^{-1}$)				
	SO_4	Ca	Mg	Na	S
Process plant	1260.00	377.00	75.300	82.700	421.00
Laboratory	< 5.00	0.20	< 0.003	0.131	< 0.06

The tests performed with process water show an increase in iron recovery compared to the tests where laboratory water was used (Table 6.9). In terms of silica content, there is no difference between the two water sources. The increase in iron recovery is probably due to the presence of ions Ca in the water that are acting as a bridge between the minerals surface and the negatively charged carboxyl groups of humic acid (Evans and Russel, 1959; Jucker and Clark, 1994), enhancing in this way the power of depression of this substance. This mechanism is similar to that one observed for natural polysaccharides and reported by several authors (Schulz and Cooke, 1953; Hanna, 1974; Liu et al., 2000).

Table 6.9 – Flotation results on sub-samples C with process plant and laboratory water.

Water source	Distribution		Grades		
	Fe recovery (%)	SiO_2 in tailings (%)	$Fe_{(t)}$ (%)	SiO_2 (%)	CS (%)
Process - pH 7	65.88	53.64	68.92	1.83	59.7
Laboratory - pH 7	59.70	58.63	68.95	1.82	59.2
Process - natural pH	67.15	48.43	68.10	1.89	57.8

A test with the natural pH of the process water was conducted. This test was conducted because the pH value of the process water is close to the neutral pH (≈ 7.8) and if there is no need of pH modifiers, the process will be cheaper and easier to control. The silica content and iron recovery were almost the same. In possession of these information, program 3 tests were conducted with sample C, using process water and at natural pH.

Best reagent suite

The humic acid used until right now is a sample provided by Sigma-Aldrich and has a technical grade that may not be possible to be supplied in an industrial scale. For this reason, some tests were performed with two different humic acids: *Deprapol HMT and Deprapol VF* and a natural polysaccharide *Deprapol N05*, all suplied by Piestch Chemicals. Other silicate collectors were also tested: *42L/21*, ODLL-123 and *7-15*, also supplied by Piestch Chemicals.

The reagents are described in the chapter 3, and the protocol for tests as well as the reagents dosages were the same that previous programs 1 and 2.

The results presented in Table 6.10 show a significant increase in iron recovery when the combination of *Deprapol N05* and *7-15* are used. The silica content off the three tests are quite similar, what means that *Deprapol N05* is more selective in terms of depression and it is preventing iron oxides to be floated. The amine *7-15* is also playing a very important role by properly floating the silicates. High iron recovery was also reached for this test in one single flotation step.

Table 6.10 – Flotation results on reagent suite tests.

		Distribution		Grades		
Depressant	**Collector**	**Fe recovery (%)**	**SiO_2 in tailings (%)**	**$Fe_{(t)}$ (%)**	**SiO_2 (%)**	**CS (%)**
Humic acid	**Flotigam EDA**	67.15	48.43	68.10	1.89	57.8
Deprapol N05	**Flotigam EDA**	78.10	38.36	68.86	1.83	58.2
Deprapol N05	**7-15**	84.30	40.62	69.21	1.82	62.5

Unfortunately, the supplier did not give a lot of information on the composition or formulation of the reagents tested, because they are in phase of development to the market. But, this result proves that flotation of a material in this size fraction and composed by several complex gangue minerals is possible, with excellent grades and good recoveries.

6.3 Concluding remarks

Micro-flotation

From the micro-flotation experiments, it was possible to confirm that the selectivity between iron-bearing silicates and iron oxides is higher at acidic pH for two collectors tested. Chamosite needs higher collector concentrations to achieve stable floatability compared to the other minerals. This may be explained by its large specific surface area and its sheet-like structures, which require higher concentrations to form the first collector layer.

The experiments with depressants showed that corn starch depressed all minerals and humic acid is more selective. Chamosite is being depressed for both corn starch and humic acid. The point where chamosite presents better floatability is when humic acid and ETA are used in a ratio 1. From the experiments with mix of minerals, is possible to confirm that ETA has a lower selectivity when compared to DDA. Diopside and epidote are easier to separate from iron oxides, than chamosite. The best results were observed at pH 4 where the minerals have

different surface charges.

Batch flotation

The bad selective of corn starch has also been proved by batch flotation tests. Humic acid stands out as the best depressant showing the lowest silica content in the final concentrate. Sieving at 53 µm was important to achieve good results as particles below this size are much more liberated. The process water of the plant, did not jeopardize the flotation results, instead it helps to improve the iron recovery. Probably due to the presence of calcium ions that enhance the adsorption of humic acid.

Humic acid and Flotigam EDA presented excellent results in terms of silica content, a concentrate with 1.89% of silica content and 67.15% of iron recovery was obtained. However, a new industrial polysaccharide called *Deprapol N05* gave excellent results in terms of iron recovery (up to 84%) without losing the quality achieved. The presence of high-intensity negative charges in this polysaccharide may explain its good result, since anionic depressants such as humic acid are more selective between iron oxides and iron-bearing silicates.

Chapter 7

Industrial approach: testing continuous flotation flow-sheet

The objective of this chapter is to apply the knowledge generated with the study of the minerals and reagents in an industrial approach through continuous testing to enable a first approach on the new installation design (Mular, 1980). Locked cycle tests (Nishimura et al., 1989), and pilot tests were performed using Flotigam EDA as silicate collector and Deprapol N05 as depressant. This depressant was chosen because it can be supplied in an industrial scale and it gave excellent results in terms of iron recovery as demonstrated in the previous chapter.

7.1 Locked cycle tests

Two different locked cycle tests were performed as described in Figure 3.6 and Figure 3.7 of chapter 3. The main difference between the two tests were the addition of a sulphide flotation step and a re-cleaner stage in the second locked cycle test. The reagents and dosages used are presented in Table 3.2 and Table 3.3. Both feed material of locked cycle tests 1 and 2 were sieved at 53 µm. However, locked cycle 1 feed was sieved in laboratory sieves and locked cycle 2 in an industrial sieve, what explain the difference in their chemical composition.

Locked cycle test 1

As it was necessary to generate mass for the cleaner and scavenger stage, it was not possible to simply alternate between these stages. This created an irregular pattern of scavenger and cleaner cycles, presented in Figure D.1 of Appendix D. Figure 7.1 is recapping the already exposed flow-sheet of locked cycle test 1, but now with the numbered flows that will be important for data analysis.

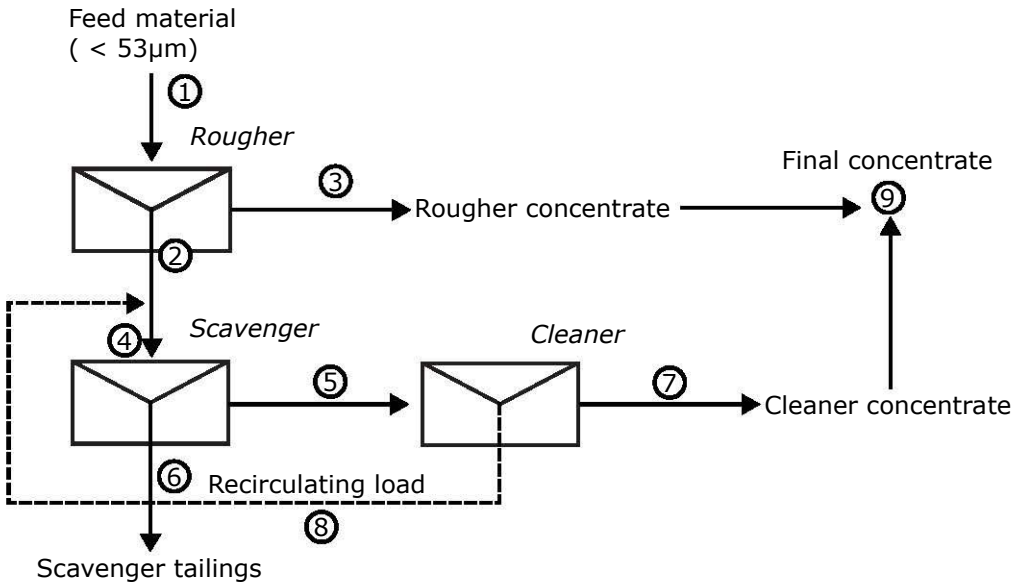

Fig. 7.1 – Locked cycle test 1 flow-sheet with the corresponding numbered flows.

The stabilization for locked cycle test 1 was achieved after seven cycles. Thirteen scavenger and 10 cleaner stages were completed (see Figure D.2 in Appendix D). Overall, the test has a circulating load of approximately 12% showing real stabilization in the three last cycles. The stabilization of the recirculated load was used as parameter to stop the test, as previously mentioned. The mass and metallurgical balance was recalculated by the software Bilco from

Table 7.1 – Locked cycle 1 reconciled data by BILCO.

Description	Distribution		Grades		
	Mass recovery (%)	Fe recovery (%)	$Fe_{(t)}$ (%)	SiO_2 (%)	S (%)
Feed	100.00	100.00	67.14	2.87	0.25
Rougher tailings	6.99	6.20	59.54	8.14	0.44
Rougher concentrate	93.01	93.80	67.71	2.48	0.23
Scavenger feed	7.04	6.24	59.51	8.16	0.43
Scavenger concentrate	5.40	5.07	62.93	6.06	0.41
Scavenger tailings	1.64	1.17	48.20	15.10	0.53
Cleaner concentrate	5.35	5.03	63.00	6.02	0.41
Cleaner tailings	0.05	0.04	55.58	10.84	0.37
Final concentrate	98.36	98.83	67.45	2.67	0.24

CASPEO (Table 7.1) and shows a total iron recovery of 98.83% and a final concentrate with 2.67% of silica content. This result is very important to prove that continuous mode separation can achieve satisfactory results for the desired quality. Also, this result is very close to the ones achieved in the previous studies of optimisation and selection of reagents. Cleaner stage was not efficient since it was fed with almost the same contents of the concentrate. The flow

number 5 could be re-circulated in the rougher stage instead of the cleaner. However, since the rougher stage was performed separately, to create a continuous flow of material, it could be difficult to do it. The flow number 8 is being recirculated in scavenger stage and its contents are close to the feed material of these stage, not causing sudden variations.

Locked cycle test 2

Locked cycle test 2 was performed at the same conditions of locked cycle test 1, but with the addition of a prior sulphide flotation and a re-cleaner stage (Figure 7.2). In total, for locked cycle test 2, 21 scavenger, 10 cleaner, and 5 re-cleaner tests were carried out as shown in Figure D.3 of Appendix D. Due to the addition of another stage, it took longer for the test to stabilize. The recirculated mass from the cleaner stage stabilized after 5 cycles (see Figure D.4 in Appendix D), but the re-cleaner never fully stabilized (see Figure D.5 in Appendix D). The decision to stop the test was taken after almost 5 cleaner tests under stabilized conditions. The re-cleaner was still varying, but whitin the same range, due to the constant changes in the feed material of this cycle. The mass and metallurgical balance was again recalculated by the software Bilco from CASPEO. The results are presented in Table 7.2 and the calculations are showing only the silicate flotation. The final concentrate (flow 11) has an iron recovery of 85.09% with a silica content of 2.78%. A large difference between the rougher tailings of locked cycle 1 and 2 can be noticed. This is probably due to the presence of a frother from the prior sulphide flotation that is generating entrainment of iron oxides particles to the tailings, proven by the highest iron content in locked cycle 2 rougher tailings. Almost all the flows were richer in iron than those of locked cycle test 1. Because of being richer, the re-cleaner stage was useless, since the feed of this stage (flow 7) has 1.22% of silica. Even though this result was worse in terms of silica content and iron recovery, it is very close to the results found in batch tests and confirm the ability of flotation to generate high-level quality products.

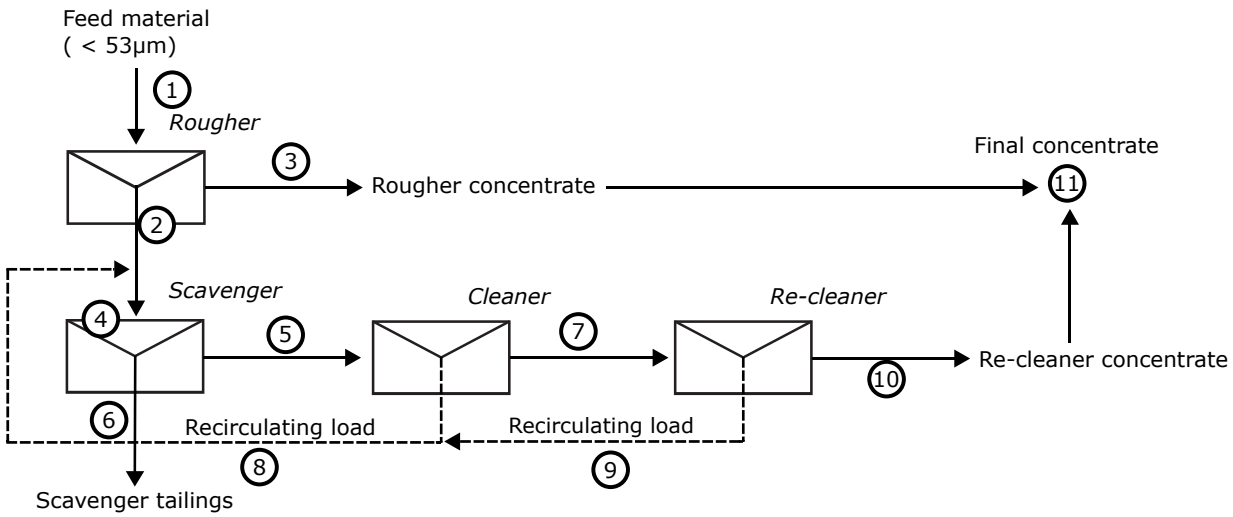

Fig. 7.2 – Locked cycle test 2 flow-sheet with the corresponding numbered flows.

Table 7.2 – Locked cycle 2 reconciled data by BILCO.

Flow	Description	Distribution		Grades		
		Mass recovery (%)	Fe recovery (%)	$Fe_{(t)}$ (%)	SiO_2 (%)	S (%)
1	Feed	100.00	100.00	66.36	3.46	0.28
2	Rougher tailings	18.86	17.69	62.24	6.19	0.29
3	Rougher concentrate	81.14	82.31	67.32	2.83	0.28
4	Scavenger feed	25.72	24.75	63.85	5.04	0.26
5	Scavenger concentrate	9.48	9.84	68.90	1.72	0.19
6	Scavenger tailings	16.24	14.91	60.91	6.98	0.30
7	Cleaner concentrate	5.13	5.43	70.29	1.22	0.15
8	Cleaner tailings	4.35	4.41	67.26	2.30	0.24
9	Re-cleaner tailings	2.51	2.65	70.08	1.10	0.11
10	Re-cleaner concentrate	2.62	2.78	70.48	1.33	0.19
11	Final concentrate	83.76	85.09	67.42	2.78	0.27

7.2 Pilot tests

The feed material used in both mechanical cell flotation and column flotation tests was previously sieved in an industrial high-frequency screen at 53 µm to guarantee the required liberation.

Mechanical cell flotation

The pilot flotation test was performed in two stages *rougher* and *scavenger* as described in section 3.4.5 of chapter 3. Figure 7.3 illustrate the froth of the rougher stage and Figure 7.4 is presenting the flow-sheet of the pilot test with the corresponding flow numbers. Deprapol N05 was used as depressant at a dosage of 350 g/t for rougher stage and 180 g/t for scavenger stage. Flotigam EDA was employed at dosages of 130 g/t and 40 g/t for rougher and scavenger, respectively. Flotation was carried out at natural pH, around 8. The circuit was running for 8 hours until stabilization was reached. Once the flows stabilized, a sampling of the final concentrate and final tailings was performed for one hour. During this time, all flows were sampled for flow rate determination.

Fig. 7.3 – Froth of the rougher stage of the pilot flotation test.

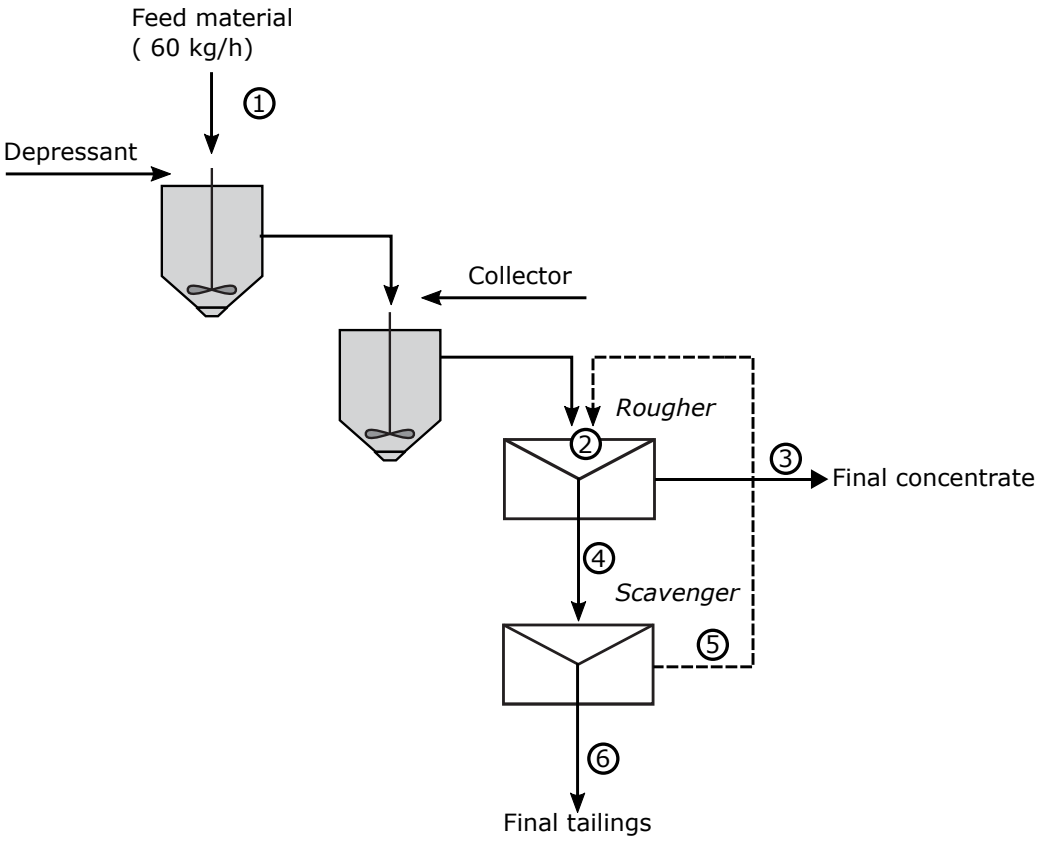

Fig. 7.4 – Pilot flotation test flow-sheet with the corresponding numbered flows.

The mass and metallurgical balance was recalculated by the software Bilco from CASPEO. The results are presented in Table 7.3.

Table 7.3 – Pilot flotation reconciled data by BILCO.

		Distribution		Grades		
Flow	**Description**	**Mass recovery (%)**	**Fe recovery (%)**	**$Fe_{(t)}$ (%)**	**SiO_2 (%)**	**S (%)**
1	**Feed**	100.00	100.00	67.01	3.30	0.29
2	**Rougher feed**	105.63	105.69	67.05	3.27	0.29
3	**Rougher concentrate**	62.70	64.02	68.43	2.06	0.25
4	**Rougher tailings**	42.93	41.67	65.04	5.02	0.33
5	**Scavenger concentrate**	5.63	5.69	67.77	2.69	0.31
6	**Scavenger tailings**	37.30	35.98	64.64	5.38	0.33

A concentrate with 2.06% of silica content was achieved in this pilot test. Despite the good result for silica content, the iron recovery of 64.02% is very low compared to the values achieved in the locked cycle tests and in the bench scale flotation tests. In fact, the scavenger stage was not operating properly. A lot of iron (35.98%) was sent to the final tailings (flow 6). This is mainly related to the low efficiency of scavenger stage in recovering iron. From the 41.67% of iron feeding the scavenger stage, only 5.69% is being recovered to the concentrate. A better iron

recovery for the scavenger stage needs to be achieved in order to not lose too much material. An increase in depressant dosage or the use of a different equipment may increase the efficiency of this stage.

Column flotation

The column flotation test was performed as described in section 3.4.5.2 of chapter 3. Deprapol N05 and Flotigam EDA were used at dosages of 350 g/t and 130 g/t, respectively. Flotation takes place at natural pH, around 7.8. The column has 6 meters in height and a diameter of 75 mm (3") and the froth was kept within 50 cm height, Figure 7.5 shows a top and a lateral view of the column during the test. A sampling was performed for 15 minutes once steady state was reached.

Fig. 7.5 – Column flotation froth view on top *(left)* and lateral *(right)*.

The software BILCO was employed to recalculate the mass and metallurgical data from this column test and the results are presented in Table 7.4. In this test, only three flows were analysed, since no re-circulation was employed. Flow number 1 corresponds to the feed material used for this test, and is the same material used for the pilot flotation with the mechanical cells. Flow number 2 corresponds to the concentrate of the column that was sampled on the bottom of the column, and finally flow number 3 corresponds to the froth sampled on the top of the column. The silica content in the tailings is high (10.90%) indicating that flotation is happening. The iron recovery of 96.20% in the concentrate is an excellent number. However, the silica content reduction was very small, from 3.32% of silica content in the feed to 2.96% of silica content in the concentrate. Despite this lean result, the column flotation proved to be very

efficient in maintaining a high metallurgical recovery in a single flotation stage. This equipment could be used for the scavenger stage, once it was demonstrated that the iron recovery in the mechanical cells was not good. Parameters as bubble size and wash water may be adjusted to achieve better silica content results.

Table 7.4 – Column flotation reconciled data by BILCO.

Flow	Description	Distribution		Grades		
		Mass recovery (%)	Fe recovery (%)	$Fe_{(t)}$ (%)	SiO_2 (%)	S (%)
1	Feed	100.00	100.00	67.30	3.32	0.25
2	Concentrate	95.50	96.20	67.78	2.96	0.25
3	Tailings	4.50	3.80	57.03	10.90	0.22

7.3 Value creation study

Based on the results of locked cycle test 1, the yield of an industrial flotation operation was estimated, and a study of the potential value created by the addition of this process was performed on a conceptual approach. Table 7.5 presents the assumptions used in this economic evaluation.

Table 7.5 – Economic evaluation project assumptions.

Assumptions			
Item	Description	Value	Unity
1	Total production (pellets)	4,000,000	ton/year
2	Working days per year	365	day
3	Working hours	24	hour
4	Plant utilisation	80.5	%
5	Total working hours	7,048	hour
6	Plant feed	568	ton/hour
7	Lost on screening	2	%
8	Project factor	1.2	-
9	Scale-up factor	0.9	-
10	Contingency	25	%
11	Silicate colector price	7	USD/kg
12	Depressant price	500	USD/t
13	Energy cost	0.1	USD/kWh
14	Product price FOB (pellets)	100	USD/t
15	Cost reduction with upgrade	7.1	USD/%SiO_2/t
16	SiO_2 reduction	1.5	%
17	Taxes (on profit)	27	%
18	Discount rate	15	%
19	Cashflow period	10	year

Item 1 is based on the budget production of Peña Colorada for 2019, 4,000,000 tons of pellets. The plant utilization (item 4) was estimated from an average of the data from the plant and it leads to a feed of 568 tons/hour of material. The additional of fine screening prior flotation was also considered, thorough the replacement of the existent screens of the plant for 18 stack-sizers from Derrick corporation. An undersize at 53 µm with a loss of 2% of the feed material in screening stage was considered. Item 8 present a project factor of 1.2 that is related to the equipment design and item 9 a scale-up factor of 0.9 related to the change of scale from bench to industrial. A contingency of 25% on the CAPEX was considered for unexpected costs. Reagents costs (item 11 and 12) were estimated based on information from suppliers. Energy cost was estimated based on Mexican prices. The price of iron pellets FOB (free-on-board) (item 14) consider an average of market prices. Item 15 lies on the cost reduction, in the upstream processes (DRI), associated with the decrease of 1% of silica content in the final product, and a reduction of 1.5% was estimated for this project composed by fine screening and flotation. Taxes and discount rate were based on internal ArcelorMittal information.

The capital expenditures (CAPEX) for this project are presented in Table 7.6. Item 1 consider the installation of 18 high-frequency screens, flotation cells for rougher, scavenger and cleaner stages, as well as the conditioning tanks, reagent preparation plant and slurry pumps. From the equipment value, the other values were estimated based on adjusted factors presented by Mular (1980). The factors used are as follow:

Table 7.6 – Capital expenditures for implementation of the project.

CAPEX			
Item	**Description**	**Cost (USD)**	**% of total cost**
1	Equipment	6,680,000	41.8
2	Construction work	4,542,400	28.5
3	Electrical work	1,269,200	8.8
4	Equipment assemblage	1,402,800	7.9
5	Piping	1,068,800	6.7
6	Site improvements	334,000	2.1
7	Project and engineering	668,000	4.2
8	Total CAPEX	15,965,200	100.0
9	Contingency (25% total CAPEX)	3,991,300	-
10	Total cost	19,956,500	-

2. Construction work - 68% of equipment costs;
3. Electrical work - 19% of equipment costs;
4. Equipment assemblage - 21% of equipment costs;
5. Piping - 16% of equipment costs;

6. Site improvements - 5% of equipment costs;

7. Project and engineering - 10% of equipment costs;

A total cost of USD 19,956,500 including 25% of contingency is necessary to implement this project.

Table 7.7 presents the operational expenditure (OPEX) for this new installation.

Table 7.7 – Operational expenditures for implementation of the project.

OPEX				
Item	**Description**	**USD/year**	**USD/t**	**% of OPEX**
1	Maintenance and spare parts	375,300	0.10	6.6
2	Power	745,004	0.19	13.0
3	Personnel	525,600	0.14	9.2
4	Reagents	4,061,888	1.05	71.2
5	Total	5,707,792	1.48	100.0

Items 2 and 4 from Table 7.7 were calculated considering the price of energy and reagents of the assumptions. Item 1 used an average of 5% of equipment CAPEX and item 3 considered 3 shifts of 8 hours with 6 new employees at a cost of USD 10 per hour. In total, an operating expenditure of USD 5,707,792 is expected to perform the upgrade in this concentrate.

Table 7.8 presents the final economic results for the value creation. Item 1 is presenting the pellets production, considering the yield of combined fine screening with flotation ($\approx 95\%$). Based on this production and in the improvement of the product quality, earnings of USD 37,185,794 per year is achieved. The total operating expenditures for the project are of USD 1.48 per tonne produced.

Table 7.8 – Final economic results for project implementation.

Economic results			
Item	**Description**	**Value**	**Unity**
1	Pellets production	3,857,600	dry ton/year
2	Earnings with silica reduction	37,185,794	USD/year
3	Lost in production	-14,240,000	USD/year
4	CAPEX	19,956,500	USD
5	OPEX	5,707,792	USD/year
6	OPEX/ton	1.48	USD
7	Profit	12,949,872	USD/year
8	Payback	19	month
9	NPV	36,242,842	USD
10	IRR	62.38	%

This economic study is a first approach to the feasibility of the project and has shown that

indeed the project is highly feasible, with a profit of USD 12,949,872 per year. The complete cash flow for the implementation and operation are presented in Figure E.1 of Appendix E. A payback period of 19 months is necessary to recover the investment cost of the project. However, payback ignores the time value of money and for that reason, NPV (Net Present Value) and IRR (Internal Rate of Return) are presented in items 8 and 9.

NPV is the difference between the present value of cash inflows and the present value of cash outflows over a period, considering a certain discount rate. The basic concept of NPV dictates that an investment with positive NPV will be profitable, and an investment with a negative NPV will result in a net loss. The positive NPV calculated for this project is $\approx$ 36 million dollars (item 8).

IRR is the internal rate of return that a project is expected to generate. It is calculated by the condition that the discount rate is set such that the NPV = 0 for the project. The higher a project's IRR, the more desirable it is to undertake. In this project the IRR is of 62%, meaning that the project adds value.

7.4 Concluding remarks

Locked cycle tests produced a final concentrate with 2.67% of silica and 98.83% of iron recovery in the first configuration with rougher, scavenger and cleaner stages. The addition of sulphide flotation and re-cleaner stages did not improved the silica content in the final concentrate in locked cycle 2 (2.78%), and it decreases the iron recovery to 85%. Prior fine screening at 53 µm was important to achieve the liberation required to perform the flotation of such fine particles, eliminating the mixed particles that may jeopardize the flotation selectivity.

Pilot flotation test with rougher and scavenger stages produced a final concentrate with 2.06% of silica content and 64% of iron recovery. The inefficiency of scavenger stage was an important factor for the low iron recovery value found, since only 13% of the iron that was fed at this stage was recovered in the concentrate.

Column flotation results were not as good as expected. A discrete silica reduction from 3.32% to 2.96% was achieved. However, the iron recovery achieved a very high value of 96.2%. Some parameters as bubble size and wash water may be adjusted to find a better compromise between silica reduction and iron recovery. The use of column flotation as a scavenger stage is envisaged, because this equipment could increase the results achieved in the pilot test with mechanical cells.

The value creation study has shown that the project is feasible. A good value of NPV

(USD 36,242,842) and IRR (62%) was achieved, considering the implementation of fine screening and silicate flotation. A profit of 12 million dollars per year is expected due to the cost reduction in decreasing silica content. In addition to the profit, the project is very important because it allows to maintain the required quality of the final product and in keeping the mine competitive.

Chapter 8

Computer simulation of surfaces and interfaces

8.1 Density Functional Theory

8.1.1 Introduction

The research in quantum chemistry has developed a lot in recent years with the emergence of supercomputers and software, which have allowed the study of the mechanisms of a system at the molecular and atomic levels. Molecules consists of atomic nuclei and atoms and the strength of the chemical bonds between the atoms is ensured by the electrons that give cohesion to the molecule. The treatment of the electronic structure within molecules is based on the Schrödinger equation (Schrödinger, 1926):

$$\hat{H}_T \varphi(\vec{r}) = E\ \varphi(\vec{r}) \tag{8.1}$$

where $\hat{H}_T$ represents the total Hamiltonian operator of the system; $\varphi(\vec{r})$ is the wave function that depends on the nuclear and electronic spatial coordinates and E represents the energy of the system described by the wave function $\varphi(\vec{r})$.
For a system containing N electrons and M atomic nuclei, the function $\varphi(\vec{r})$ is written in the form: $\varphi(\vec{r}) = \varphi(\vec{x_1}, \vec{x_2}, \dots\ \vec{x_N}, \vec{R_1},\ \vec{R_2}, \dots\ \vec{R_M})$, with $\vec{x_i}$ corresponding to the space and spin coordinates of the electron i and $\vec{R_j}$ to the spatial coordinates of the nucleus j.
The Hamiltonian operator associated with this system is the sum of the operator kinetic energy

total $\hat{T}_T$, and the operator describing the set of Coulomb interactions $\hat{V}_T$, therefore:

$$\hat{H}_T = \hat{T}_T + \hat{V}_T \tag{8.2}$$

The total kinetic energy operator is the sum of the kinetic energy operator of the electrons ($\hat{T}_e$) and that of the kernels ($\hat{T}_n$) while $\hat{V}_T$ contains electron-electron repulsion interactions ($\hat{V}_{ee}$), kernel-electron attraction $\hat{V}_{ne}$ and core-core repulsion $\hat{V}_{nn}$. The total Hamiltonian can then be expressed as:

$$\hat{H}_T = \hat{T}_e + \hat{T}_n + \hat{V}_{n-e} + \hat{V}_{e-e} + \hat{V}_{n-n} \tag{8.3}$$

where:

$\hat{T}_e = -\frac{\hbar^2}{2}\sum_i^N \frac{\nabla^2 \vec{x_i}}{m_e}$ is the kinetic energy of N electrons of mass m_e;

$\hat{T}_n = -\frac{\hbar^2}{2}\sum_A^M \frac{\nabla^2 \vec{R_A}}{M_A}$ is the kinetic energy of M nuclei of mass M_A;

$\hat{V}_{n-e} = -\frac{1}{4\pi\varepsilon_0}\sum_i^N \sum_A^M \frac{Z_A e^2}{|\vec{x}_i - \vec{R}_A|}$ is the attractive coulombic interaction between electron i and nuclei A;

$\hat{V}_{e-e} = \frac{1}{2}\sum_i^N \sum_{j\neq i}^N \frac{e^2}{4\pi\varepsilon_0 |\vec{x}_i - \vec{x}_j|}$ is the repulsive coulombic interaction electron-electron;

$\hat{V}_{n-n} = \frac{1}{2}\sum_A^M \sum_{B\neq A}^M \frac{Z_A Z_B e^2}{4\pi\varepsilon_0 |\vec{R}_A - \vec{R}_B|}$ is the repulsive coulombic interaction core-core.

Solving the above Hamiltonian is the major problem of quantum chemistry and condensed matter physics. Indeed, the Coulomb interaction in the last term makes the problem impossible to solve, except for small systems like an atom or a small molecule, where it is possible to obtain the wave function via configuration interaction type methods. Nevertheless, the numerical effort increases rapidly with the size of the system, making the resolution of Equation 8.3 impossible.Different approaches to the problem are therefore essential if realistic systems are target. Among these, we can mention the Hartree approximation (1928) where the Coulomb term is simply replaced by an electrostatic potential resulting from the electron density. This approach has been proved to be too simplistic, and was extended to reflect Pauli's principle, which resulted in the Hartree-Fock method. This approximation provides a fairly reasonable description of atoms and molecules, but neglecting electronic correlations can lead to very high bandgap values for solids. Slater (1930) overcame this limit using the $X\alpha$ method where the exchange potential is simulated by a local potential and the constant α adjusted to simulate the correlations. Although this method remains semi-empirical, it can be considered as a precursor of the density functional theory.

8.1.2 Hohenberg-Kohn theorems

In the 1960's, Pierre Hohenberg and Walter Kohn (1964) proved that the energy of the ground state of an electronic system could depend only on its density. In their first theorem, Hohenberg and Kohn demonstrate that the energy of the ground state E_0 can be expressed as a functional F_{HK}, which depends only on the electronic density of this state ρ, to which it is added the interaction potential between electrons and nuclei $V_{ne}(\vec{r})$:

$$E[\rho\,(\vec{r})] = F_{HK}[\rho\,(\vec{r})] + \int V_{ne}(\vec{r})\rho\,(\vec{r})\,d\vec{r} \tag{8.4}$$

To know the true density of the ground state, Hohenberg and Kohn formulated a second theorem based on the variational principle. This theorem specifies that the optimal electronic density will minimize the energy by approaching the energy of the real system without ever reaching it ($E_0 < E[\rho(\vec{r})]$). The equality between E_0 and $E[\rho\,(\vec{r})]$ is only obtained if $\rho\,(\vec{r})$ is the exact electronic density of the system to the ground state. So far, it has been proven that a solution exists, but it is not known how to calculate it, because the exact form of the universal functional of Hohenberg and Kohn remains unknown and it is the Kohn-Sham formalism that will allow this problem to be circumvented.

8.1.3 Kohn-Sham equations

The Hohenberg-Kohn functional (introduced by Equation 8.4) is equal to the sum of the kinetic energies of the electrons $T[\rho]$ and the electron-electron interaction potential $E_{ee}[\rho]$. This last part is divided into a classical component of the Coulomb repulsive interactions $J[\rho]$, whose expression as a function of density is well known, and a non-classical second part $E_{ncl}[\rho]$ integrating the correlation and exchange effects. The total energy will be given by:

$$E[\rho] = T[\rho] + J[\rho] + E_{ncl}[\rho] + \int V_{ne}(\vec{r})\rho\,(\vec{r})\,d\vec{r} \tag{8.5}$$

The first difficulty lies in the determination of the kinetic energy of the electrons as a function of the electron density. Although this magnitude can be expressed in an easy way for the bosons (integer spin), Pauli's exclusion principle makes things much more complex for fermions (half integer spin, as for the electrons) due to the different states that can be occupied. In this respect, the method of Walter Kohn and Lu Jeu Sham (1965) has introduced an auxiliary system where kinetic energy makes it possible to consider the Pauli principle. In their model, they imagined a fictitious system of N electrons that do not interact with each other, and that move in an effective field of potential V_s. This potential must be chosen so that the calculated

density of this fictitious system is equal to that of the actual interacting electron system. This fictitious system is completely described by a Slater determinant, whose spin-orbitals φ_i, called orbitals of Kohn-Sham can be determined by analogy to the Hartree-Fock method using a self-consistent convergence process, through the equations:

$$h^{KS}\varphi_i = \varepsilon_i \varphi_i \tag{8.6}$$

where h^{KS} corresponds to the monoelectronic Kohn-Sham operator:

$$h^{KS} = \frac{\hbar^2}{2m_e}\nabla^2 + V_s(\vec{r}) \tag{8.7}$$

The kinetic energy of this fictitious system is different from that of the real system, but has the advantage of being able to express itself directly from these Kohn-Sham orbitals, which can be directly related to the density:

$$T = -\frac{\hbar^2}{2m_e}\sum_i^N \langle\varphi_i|\ \nabla^2|\varphi_i\rangle \tag{8.8}$$

These Kohn-Sham orbitals have no physical meaning. However, the sum of their squares makes it possible to reach the electronic density:

$$\rho\,(r) = \sum_i^N\ |\varphi_i|^2 \tag{8.9}$$

The expression of the total energy of the real system (in interaction) thus becomes:

$$\begin{aligned} E[\rho] = &-\frac{\hbar^2}{2m_e}\sum_i^N \langle\varphi_i|\ \nabla^2|\varphi_i\rangle + \frac{1}{2}\sum_i^N\sum_{j\neq i}^N \iint \frac{e^2}{4\pi\varepsilon_0}\,|\varphi_i(\vec{r_1})|^2\frac{1}{r_{12}}\,|\varphi_j(\vec{r_2})|^2\,d\vec{r_1}d\vec{r_2} \\ &+ E_{xc}\,[\rho] - \frac{1}{4\pi\varepsilon_0}\sum_i^N \int \sum_A^M \frac{Z_{Ae}^2}{\left|\vec{R}_A - \vec{r}1\right|}\,|\varphi_i(\vec{r_1})|^2\,d\vec{r_1} \end{aligned} \tag{8.10}$$

Equation 8.10 involves a new term E_{xc} called exchange-correlation energy. This energy contains not only the quantum contributions $E_{ncl}[\rho]$, but also the difference between the kinetic energy of the real system and that of the fictitious system. Such a difference will depend mainly on the electron-electron interactions neglected in the fictitious system considered. The analyt-

ical form of all the terms in Equation 8.10 is known, except that of the exchange-correlation energy E_{xc}. Several approximations were thus used to better describe this term, which gave rise to several types of functional.

8.1.4 Local density approximation

The Local Density Approximation (LDA) is the simplest approximation for the exchange-correlation potential. It is based on the fact that in the case of a homogeneous electron gas, the exact exchanger-correlation energy can be determined using variational quantum Monte-Carlo calculations (Ceperley and Alder, 1980). In this case, the exchange-correlation energy is written in the form:

$$E_{xc}^{LDA}\ [\rho] = \int \rho(r)\varepsilon_{xc}\left[\rho\left(r\right)\right] dr \tag{8.11}$$

where ε_{xc} is the exchange-correlation energy for each particle of a uniform electron gas, parameterized for different values of the electron density. At first glance, this simplistic approximation should give correct results only if the density varies little. However, in practice it often gives satisfactory results, which probably results from a compensation for errors made in the exchange term and in the correlation term. Nevertheless, this success must be moderated, because in some cases LDA does not give a satisfactory result. For example, the equilibrium distances are often underestimated, the cohesion energies of the solids are overestimated, as well as the vibration frequencies for some small systems. In order to find a better approximation for the exchange-correlation potential, it is natural to think of taking into account the variations of the density ρ through its gradient $\nabla_\rho(r)$, which led to the approximations of the gradient type (GGA, Generalized Gradient Approximation). As part of the GGA, the exchange energy can be written as follows:

$$E_{xc}^{GGA}\ [\rho] = \int f(\rho\left(r\right), \nabla(\rho(r))dr \tag{8.12}$$

The most complex remains however the determination of the analytical expressions of each of the components of exchange and correlation. Several forms have been proposed to express the function $f(\nabla(\rho(r))$, like that of Becke (1988). The theoretical treatments to describe the correlation term are much more complex to obtain than those of the exchange term. Among the various possible functionals, one can mention the one developed by Perdew and Yue in 1986, whose purpose was to obtain precisely the correlation energies in the case of atoms, molecules, and possibly metal surfaces. A different functional but also commonly used is

that of Perdew and Wang (1992), which corrects both exchange and correlation. It has been constructed to replicate the properties of the exchange-correlation hole in both low- and high-density boundaries, but also for metals. Finally, it is important to highlight the *PBE* functional proposed by Perdew et al. (1996), which is a reformulation of that of Perdew and Wang, and which is probably the most used GGA functional today.

8.1.5 Periodic system case

The resolution of the Schrödinger's equation for a crystal or any infinite three-dimensional structure supposes the description of an infinite number of electrons, which would correspond in the Kohn-Sham method to the determination of an infinity of monoelectronic wave functions. Of course, such calculation is impossible and to solve this problem it is necessary to rely on Bloch's theorem (Kittel, 2004). A crystal is made up of a periodic arrangement of ions in a three-dimensional space. The effective potential applied to the electrons is therefore periodic as well and the Hamiltonian to which the electrons are subjected is written as:

$$H = T + U(r) \tag{8.13}$$

where T is the kinetic energy and $U(r)$ is an effective potential with the same periodicity as the crystal arrangement. In a periodic solid, Bloch's theorem makes it possible to write each electronic wave function $\varphi_{i,k}(\vec{r})$ as being the product of a plane wave $e^{i\vec{k}.\vec{r}}$ of vector $\vec{k}$ (vector of the first Brillouin zone) and of a periodic function f having the same periodicity as the crystal. This function f is decomposed in the reciprocal lattice by Fourier series which makes it possible to write:

$$\varphi_{i,k}(\vec{r}) = f \times e^{ik.\vec{r}} = \sum_{\vec{G}} C_{i,\vec{k},\,\vec{G}} \times e^{i(\vec{k}+\vec{G}).\vec{r}} \tag{8.14}$$

where the vectors $\vec{G}$ are vectors of the reciprocal lattice which satisfy the relation: $\vec{G}.\vec{r} = 2\pi m$ with $\vec{r}$ being a vector of the direct lattice and m an integer. The problem of calculating an infinite number of monoelectronic wave functions returns by applying Bloch's theorem to calculate a finite number of wave functions by an infinite number of $\vec{k}$ vectors. Bloch also proved that the calculation can be limited to a finite number of $\vec{k}$ vectors represented by the first Brillouin zone. The error associated with the discretization can be systematically evaluated using denser point grids. In practice, the convergence of energy must be verified for the set of points k chosen. According to this formalism, the resolution of the Kohn-Sham equations take place in reciprocal space (vector base $\vec{G}$). The corresponding matrix must be diagonalized at

each point $\vec{k}$ in the chosen basis set. However, the coefficients $C_{i,\vec{k},\ \vec{G}}$ associated with planar waves of high kinetic energy are significantly lower than those associated with plane waves of lower kinetic energy. This justifies the introduction of a cut in the basis set to be used from a certain energy called "cut-off" energy ($E_{cut-off}$). In practice, it is also important to verify the convergence of the system energy with the increase of the cut-off energy.

8.1.6 Pseudo-potentials

For the calculations, the wave functions of the valence electrons must be orthogonal to the wave functions of the core electrons; this causes oscillations in the region near the nucleus. If a plane wave basis is used, the exact description of these oscillations would imply the use of a large basis making calculations almost impossible. A solution for that is replace the effects of the motion of the core electrons (non-valence) of an atom and its nucleus with a pseudo-potential. This is possible because the atomic orbitals of the core are very little modified by their environment. In addition, the properties of solids are generally much more dependent on valence electrons than those of the core. It therefore seems more judicious to represent the electrons of the core by an effective potential called pseudo-potential (Grotendorst, 2000), instead of treating them all explicitly. Pseudo-potentials are characterised by the maximum number of core electrons they replace and the maximum angular momentum they consider. They make it possible, by reducing the number of electrons explicitly treated, to reduce the size of the used basis. As fundamental properties, they must respect the following constraints:

- *hardness*: a hard pseudo-potential is associated with a large base to properly develop the wave function;

- *precision*: the pseudo-charge density must reproduce the density as accurately as possible outside the core radius;

- *transferability*: a pseudopotential corresponds to a given electronic configuration; the transferability corresponds to the precision with which it reproduces the wave functions for other configurations (degree of oxidation, coordination, etc.).

8.2 *Ab-initio* investigation on chamosite

8.2.1 Methodology

8.2.1.1 Chamosite structural model

Although other clay minerals from the chlorite group have been the subject of some studies in DFT, chamosite has never been investigated before. As discussed in chapter 2, chamosite is a phyllosilicate belonging to the group of chlorites. It makes a series with clinochlore, presenting higher amount of Fe atoms than its series counterpart. Chamosite from different deposit sources may have variable chemical composition according to the crystallisation processes it went through. Variations in the amount of aluminium, silicon, iron and magnesium are commonly observed. It is a monoclinic crystal system ($a \neq b \neq c$) structure, composed by regular layers with tetrahedral and tri-octahedral components (Rivas-Sanchez et al., 2006). The bulk

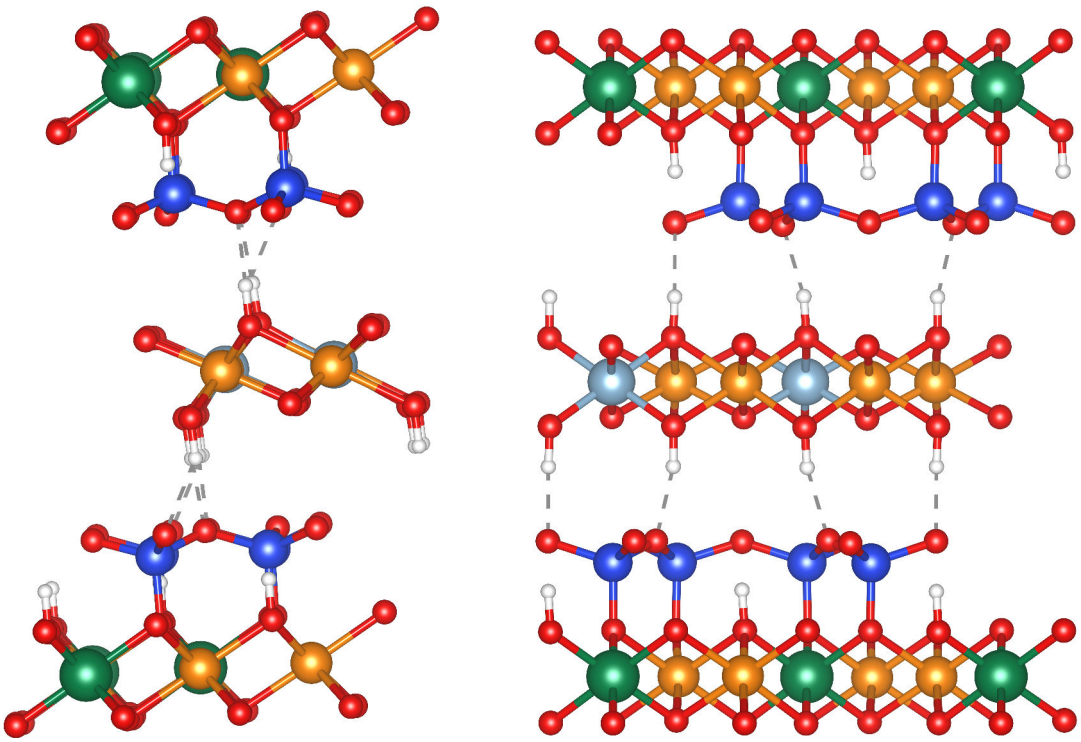

Fig. 8.1 – Chamosite bulk crystalline structure from (Walker and Bish, 1992), lateral view (left) and frontal view (right). Al = light blue spheres; Fe = orange spheres; H = white spheres; Mg = green spheres; O = red spheres; Si = dark blue spheres.

structure used in this study is presented in Figure 8.1, it has a sheet shape and have been optimised with relaxation to obtain lattice parameters $a = 5.369$ Å, $b = 9.303$ Å, $c = 14.261$ Å with angles $\alpha = 90.31°, \beta = 97.23°, \gamma = 90.02°$, in a triclinic symmetry system. The cleavage

of chamosite is well known as ($h = 0$, $k = 0$, $l = 1$) (Anthony et al., 2019). From Figure 8.1 is possible to identify two different possibilities for chamosite surface exposition, which were called:

1. *Small-slab*: where the tri-octahedral components of Al and Fe are exposed;
2. *Big-slab*: where the tetrahedral components of Si are exposed.

From the relaxed bulk structure, the two possible surfaces for chamosite, following the plan (0 0 1) were transformed into two super-cell containing 132 atoms each (4 Mg, 16 Fe, 4 Al, 16 Si, 72 O, 20 H), see Figure 8.2. The neutrality of both slabs in terms of charges was achieved by

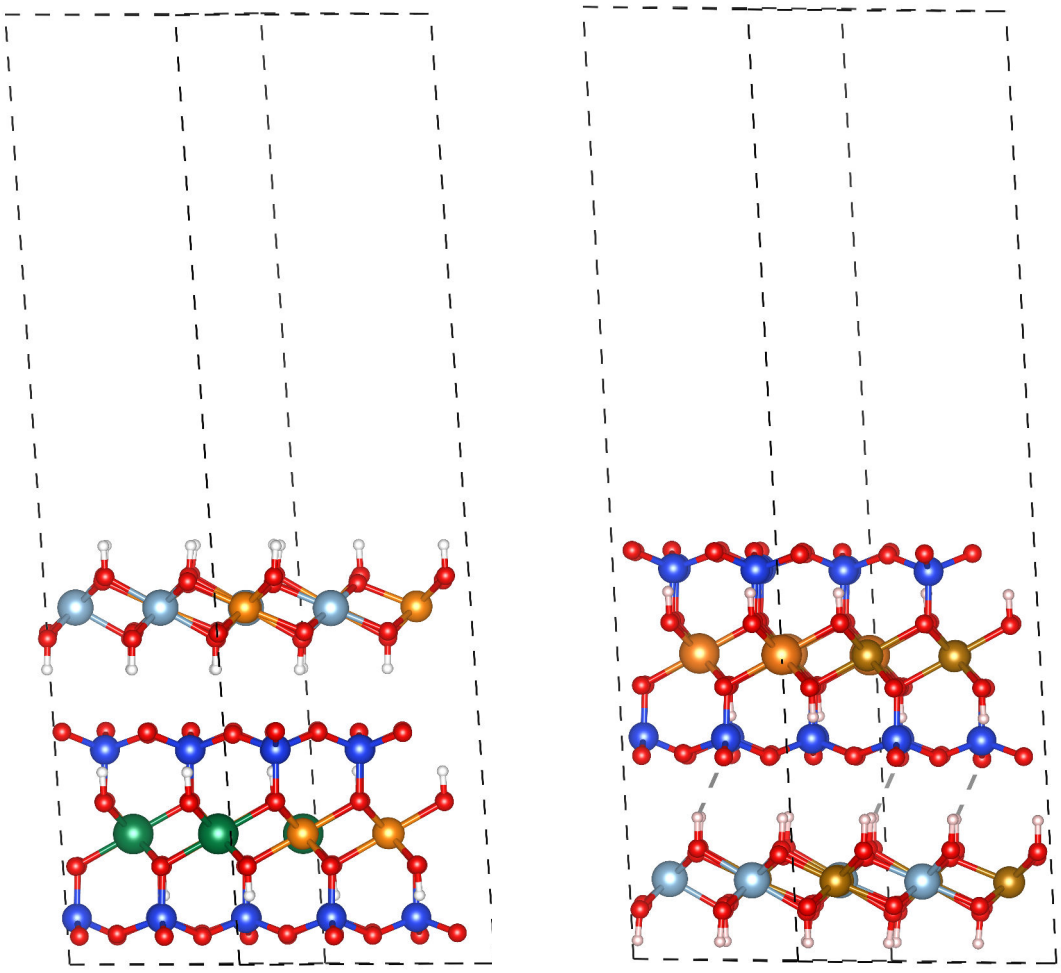

Fig. 8.2 – Frontal view of *small* (left) and *big* (right) slabs of chamosite used for the calculations. Al = light blue spheres; Fe = orange spheres; H = white spheres; Mg = green spheres; O = red spheres; Si = dark blue spheres; dashed lines = super-cell limit, with an extra 15 Å in *c* direction.

the addition of H protons located between the two slabs, which are responsible for the bonding between the slabs, and also on the surface of the big-slab in the middle of the "Si rings". Aiming to avoid any unexpected interaction due to the periodicity of the cell, an extra 15 Å of vacuum

was added between the surface and the top of the super-cell. During the relaxation of these two super-cells, the atoms could move in all three directions x, y and z.

8.2.1.2 Calculation settings

The adsorption energies and the structure of the system were determined using periodic DFT calculations (Quantum Espresso Package). The approximation for the exchange-correlation potential was done by the reformulated generalized gradient approximation *PBE* functional proposed by Perdew-Burke-Ernzerhof (1996). To describe the magnetism of itinerant electrons, the calculations were done with spin-polarized. DFT+U was also employed to correct the self-interaction error of GGA that would lead some electrons of iron to an artefactual delocalisation (Lebègue et al., 2008). Kohn-Sham (1965) equations were used for performing the calculations until the difference in energy between cycles became lower than 10^{-6} eV. The cut-off energy was set to 51.45 Ry. The crystal relaxation calculations were performed until the forces were smaller than 0.02 $eV/$Å. The dispersion interactions (van-der-Waals forces) of the system are very important to understand the interaction between water molecules and chamosite surface. Due to their non-local nature they cannot be described by the DFT method in its standard local density approximations (LDA or GGA). To solve this problem, the DFT+D method was employed. This method consists of preserving the DFT (often in the GGA approximation) for the description of the covalent or ionic interactions but adding a term at the end to include the dispersion effects at the dipole-dipole level. In this study, D2 (Grimme, 2006) Grimme's correction were used.

8.2.1.3 Energy calculation exploitation methodology

Three separate energy calculations are required to determine the adsorption of water into chamosite's surface, as follow:

1. E_{Cha}, which correspond to the total energy of chamosite slab alone;
2. E_X, which correspond to the total energy of the water molecule alone in vacuum;
3. E_{Cha-X}, which correspond to the total energy of chamosite slab in presence of n water molecules.

The adsorption energy at 0 K can thus be determined by:

$$\Delta E_{ads} = E_{Cha-X} - E_{Cha} - E_X \tag{8.15}$$

The calculation of the dispersion energies contribution can be done similarly to the determination of the adsorption energy by:

$$\Delta E_{disp} = E_{disp\ Cha-X} - E_{disp\ Cha} - E_{disp\ X} \tag{8.16}$$

When n water molecules are adsorbed onto chamosite surface, the adsorption and dispersion energies per molecule can be determined by dividing Equation 8.15 and Equation 8.16 per n, respectively.

8.2.2 Results and Discussions

8.2.2.1 Isolated water molecule on chamosite

The investigations on chamosite surface started by exploring the adsorption of an isolated water molecule on both small-slab and big-slab in its molecular state.

Chamosite small-slab

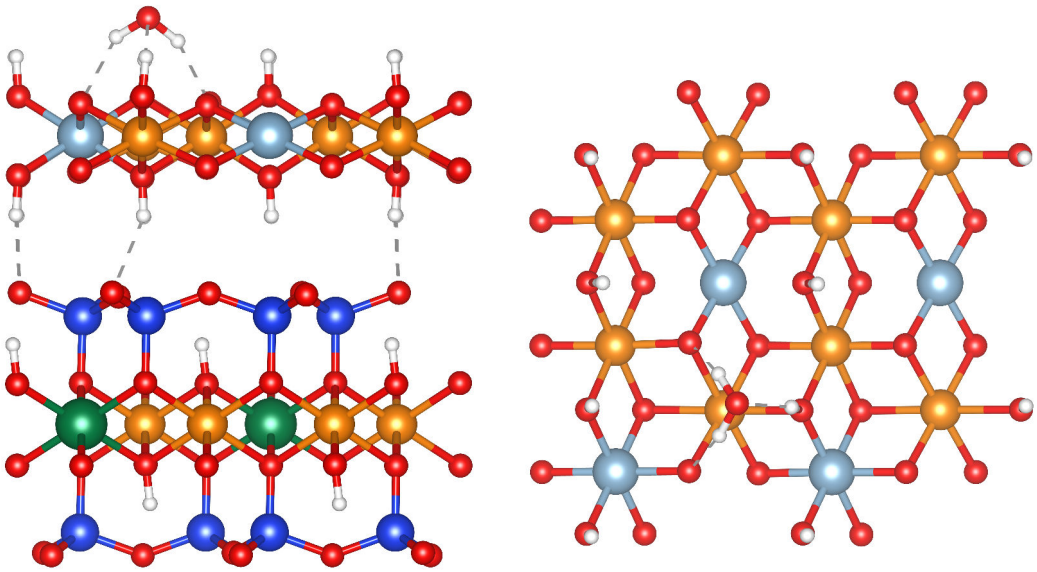

Fig. 8.3 – Adsorption of molecular water onto chamosite *small-slab* surface, after relaxation. Frontal view (*left*) and top view (*right*). Al = light blue spheres; Fe = orange spheres; H = white spheres; Mg = green spheres; O = red spheres; Si = dark blue spheres.

For the investigations on chamosite small-slab, the water molecule was placed above both Fe and Al atoms with different orientations. The oxygen was placed close to the metal ion and the hydrogen atoms were oriented (*up*, *down* and *flat*) in relation to the top of the super-cell.

In total, at least 10 different configurations were tested. The most favourable one is presented in Figure 8.3, with the water molecule above a Fe atom. The initial configuration placed the H of the water molecule in the *flat* direction. In the final configuration, however, the molecule was slightly inclined toward the chamosite surface, with O adsorbed onto chamosite surface through an H atom with a length of 1.80 Å. The two H atoms of the water molecule adsorbed onto the two O atoms of chamosite surface and have lengths of 1.79 Å and 1.92 Å. The calculated adsorption energy for this system is $\Delta E_{ads} = -93.92\ kJ.mol^{-1}$, including $\Delta E_{disp} = -31.97\ kJ.mol^{-1}$, showing a favourable adsorption of water onto chamosite *small-slab* surface.

Chamosite big-slab

For the investigations on chamosite big-slab, the water molecule was place in two different positions: in the middle of the "Si rings", and in the corner of the ring, above two oxygen atoms. More than 5 different configurations were tested. The most favourable one is presented in Figure 8.4, with the water molecule placed in the middle of the "Si ring". In the final configuration the water molecule is slightly adsorbed onto the H atom of the bottom part of the big-slab that is located exactly in the middle of the "Si ring".

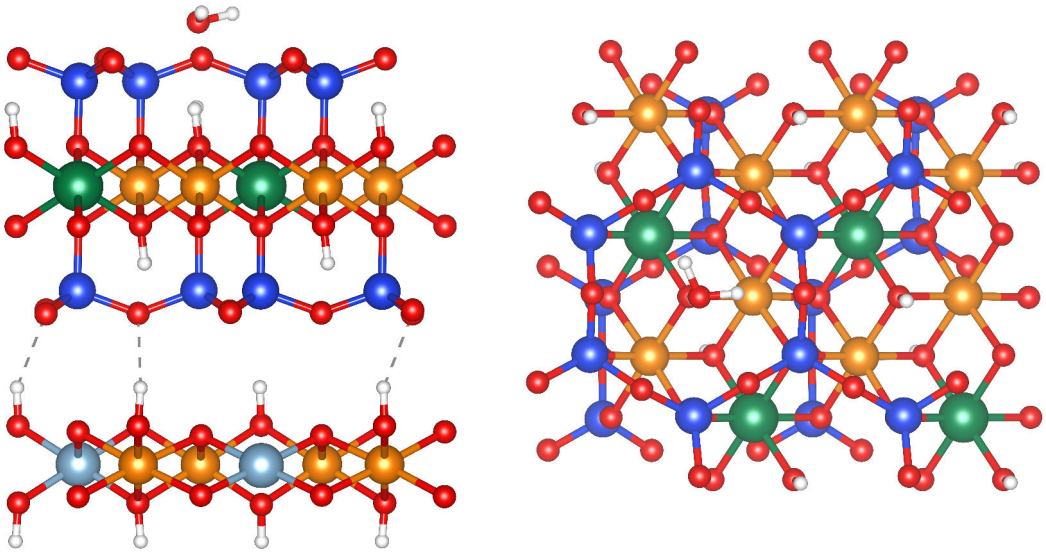

Fig. 8.4 – Adsorption of molecular water onto chamosite *big-slab* surface, after relaxation. Frontal view (*left*) and top view (*right*). Al = light blue spheres; Fe = orange spheres; H = white spheres; Mg = green spheres; O = red spheres; Si = dark blue spheres.

After relaxation, the distance between the oxygen atom of the water molecule and the hydrogen located in the middle of the "Si ring" of chamosite surface is 2.18 Å. The hydrogen atoms of the water molecule are placed in an equal distance of 2.18 Å from the oxygen atoms of the chamosite surface and of 2.95 Å from the silicon atoms of the chamosite surface. The

calculated adsorption energy for this configuration was $\Delta E_{ads} = -30.94\ kJ.mol^{-1}$, including $\Delta E_{disp} = -17.48\ kJ.mol^{-1}$.

8.2.2.2 Towards full hydration of chamosite surfaces

After the determination of the most favourable configuration for each chamosite slab, the progressive hydration of both surfaces was investigated.

Chamosite small-slab

For the hydration investigation of chamosite *small-slab*, 2, 4, 6 and 8 water molecules were placed on the surface. Figure 8.5 presents the configuration of 8 water molecules placed onto this surface. The increase in the number of water molecules present on the surface leads to a decrease in the hydration energy per water molecule (see Figure 8.7). The calculated adsorption energy for this configuration was $\Delta E_{ads} = -633.82\ kJ.mol^{-1}$, including $\Delta E_{disp} = -159.05\ kJ.mol^{-1}$, which represents a value of $\Delta E_{ads} = -79.22\ kJ.mol^{-1}$ per water molecule. At this point, the

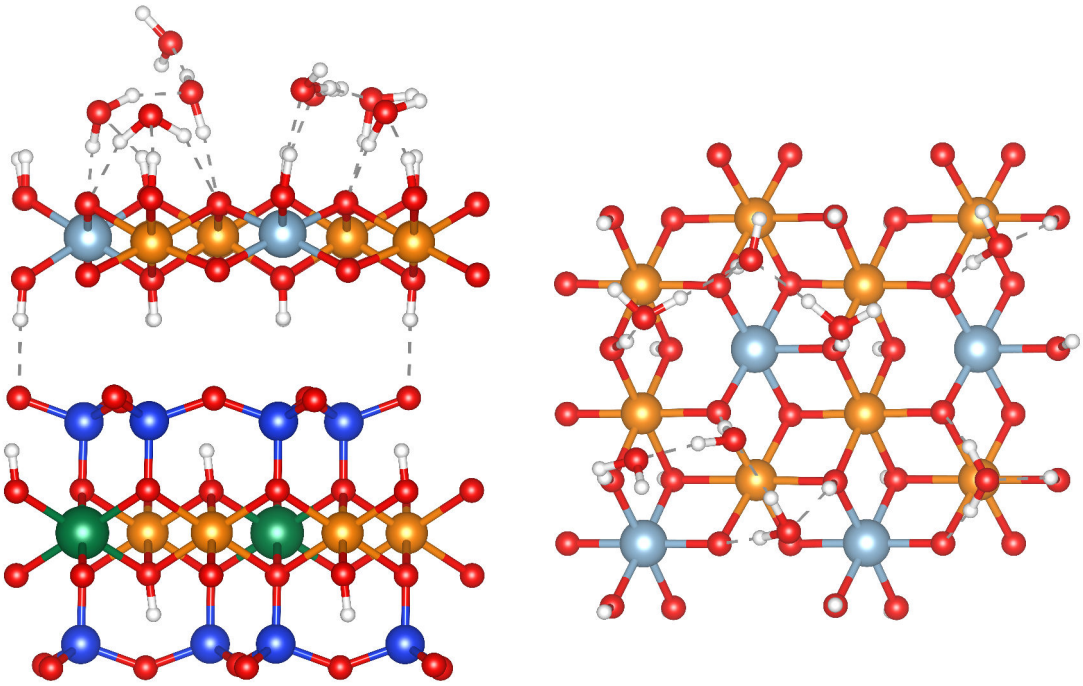

Fig. 8.5 – Adsorption of eight molecular water onto chamosite *small-slab* surface, after relaxation. Frontal view (*left*) and top view (*right*). Al = light blue spheres; Fe = orange spheres; H = white spheres; Mg = green spheres; O = red spheres; Si = dark blue spheres.

formation of the first layer of water is completed and the investigation on the next layers should be conducted.

Chamosite big-slab

Chamosite *big-slab* has less available sites for water adsorption, achieving full hydration with less water molecules on its surface. Then, 2, 4 and 6 water molecules were placed on this surface for the investigation. Figure 8.6 presents the configuration of 6 water molecules placed onto this surface. The increase in the number of water molecules present on the surface also leads to a decrease in the hydration energy per water molecule (Figure 8.7). The calculated adsorption energy for this configuration was $\Delta E_{ads} = -254.35\ kJ.mol^{-1}$, including $\Delta E_{disp} = -92.83\ kJ.mol^{-1}$, which represents a value of $\Delta E_{ads} = -42.39\ kJ.mol^{-1}$ per water molecule. The change observed in the value of the adsorption energy when 6 water molecules are placed on the chamosite *big-slab* surface is related to the stabilizing effect of the monolayer of water by the hydrogen bonds. In the beginning, each water molecule is totally isolated from the others and it is the saturation of the monolayer that allows the interaction between them.

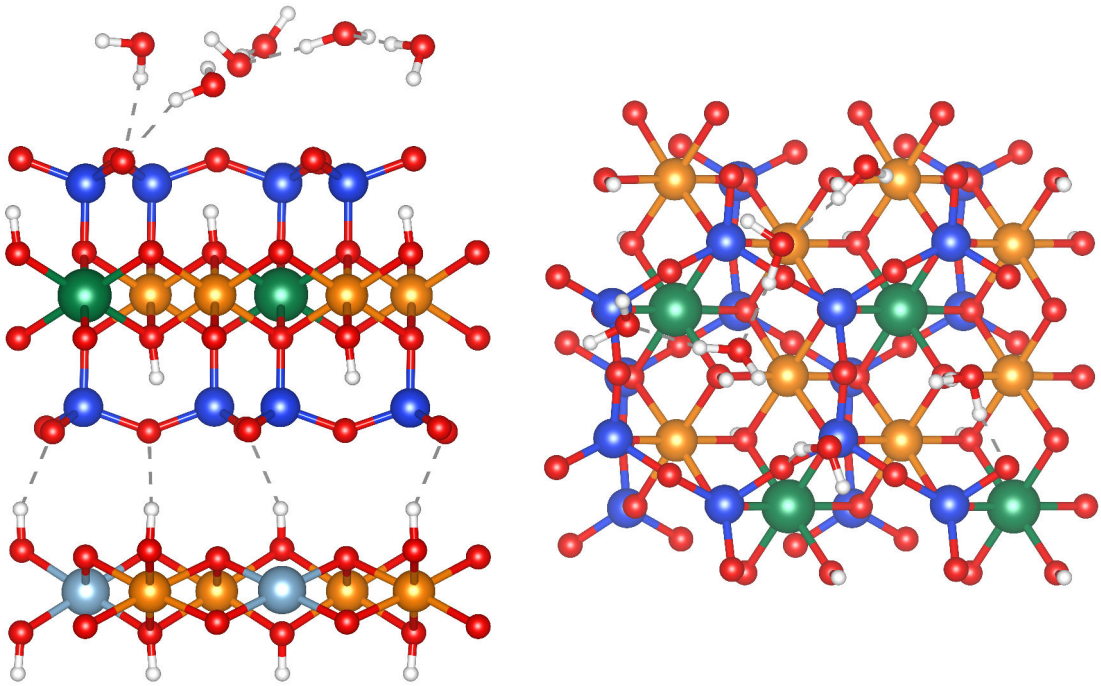

Fig. 8.6 – Adsorption of six molecular water onto chamosite *big-slab* surface, after relaxation. Frontal view (*left*) and top view (*right*). Al = light blue spheres; Fe = orange spheres; H = white spheres; Mg = green spheres; O = red spheres; Si = dark blue spheres.

The energy values presented for the adsorption of molecular water onto chamosite *big-slab* is almost three times lower than the energy values for the adsorption onto chamosite *small-slab*. These low values of adsorption energy coupled with the lower availability of adsorption sites lead to the conclusion that chamosite *big-slab* surface is less hydrophilic than chamosite *small-slab* surface.

The study of the adsorption of the second and third layers of water needs to be performed

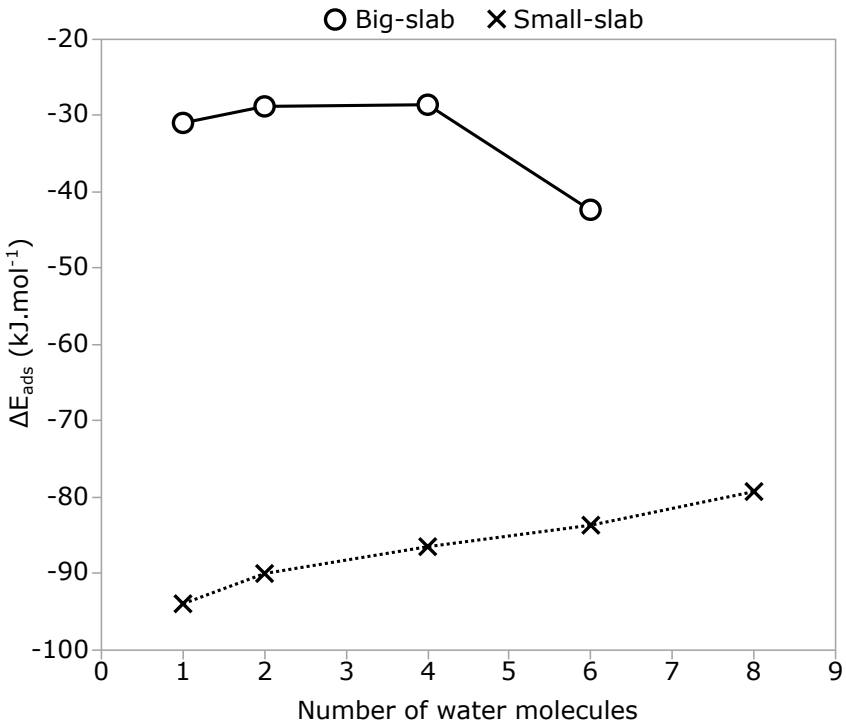

Fig. 8.7 – Adsorption energies per water molecule for the coverage of chamosite *small-slab* and *big-slab* surfaces.

to confirm this tendency on both surfaces to have a decrease in their adsorption energies with increasing amount of water molecules.

8.3 Conclusions

From this *ab-initio* study it was possible to investigate the adsorption of water onto the chamosite surface through differential functional theory. Since the cleavage of chamosite can expose two different faces, both were investigated and named *small-slab* and *big-slab*. Water in its molecular form has been shown to have adsorption affinity with both surfaces. However, the difference between the energy values of the adsorption of one water molecule is quite high. Chamosite *small-slab* and chamosite *big-slab* have respectively $\Delta E_{ads} \approx -94\ kJ.mol^{-1}$ and $\Delta E_{ads} \approx -30\ kJ.mol^{-1}$, a factor of more than three times. Due to this low adsorption energy and to the low availability of adsorption sites, chamosite *big-slab* surface is considered less hydrophilic than chamosite *small-slab* surface. This result is supported by the research of Yin et al. (2012), that found a hydrophobic state for certain silica tetrahedral surfaces. The formation of the first layer of water onto both chamosite surfaces showed a tendency to decrease the adsorption energy by number of water molecules on both surfaces and an investigation on the formation of the second and third layers may help to better understand the adsorption mechanism behind chamosite hydration.

Overall, this investigation demonstrates that a deep knowledge of the surface state of minerals is a pre-requisite for flotation processing optimisation. Atomistic modelling provides here very useful insights regarding the hydrophobic character of chamosite, an archetype of silicate mineral. As this mineral exhibit two very different surfaces, new strategies must be found to design combination of flotation reagents to treat it correctly during the process.

Chapter 9

Conclusions and perspectives

9.1 General conclusions

Reverse cationic flotation has proved to be efficient in promoting separation between complex assemblages of gangue minerals and iron oxides. A high-grade concentrate with 67.45% of iron and 2.67% of silica was obtained after fine screening at 53 µm and silicate flotation in a continuous operation at laboratory scale, with almost 96% of overall iron recovery. Pilot flotation testing showed even better results with respect to the concentrate quality, with 68.43% of iron and 2.06% of silica, but with 64% of iron recovery. Its lower recovery can be increased by replacing the scavenger stage mechanical cell with a column, for example. Column flotation produces a high-grade concentrate of 67.78% of iron and 2.96% of silica, with more than 96% of iron recovery.

Continuous tests allowed the determination of the best route for flotation of this iron magnetic concentrate. Rougher, scavenger and cleaner stages were employed to generate the results mentioned. Sulphide flotation helps on the reduction of silica as well, due mainly to the presence of mixed sulphide-silicate particles. However, the sulphur content is already low and the presence of frother from the sulphide flotation affects the silicate flotation, increasing the entrainment.

Peña Colorada iron concentrate is dominated by magnetite, hematite, chamosite, diopside and epidote and the particles present 80% of liberation at 53 µm. The biggest challenge for successful use of flotation as separation technique is mineralogy, and part of this study was devoted to studying these minerals properties.

The zeta potential measurements indicate an IEP of 3.1, 2.8, 2.9, 6.2 and 5.4 for chamosite, diopside, epidote, hematite and magnetite, respectively. These IEP values indicate a proximity

of surface charge characteristics for the silicates. The presence of polymers used as depressants greatly changes the surface charge of the minerals. CMC was the polymer that most changed the surface charge of the minerals, however it possibly its macromolecules parked inside the double layer and masked the surface charge measurements of the minerals.

Corn starch strongly adsorbed onto chamosite, diopside, epidote, hematite and magnetite surfaces thus presenting no selectivity towards iron oxide depression. Dextrin showed low adsorption onto silicate surfaces, but its short chain did not favour strong adsorption on the iron oxide surface neither. CMC had no significant adsorption on silicate minerals and had a better affinity with iron oxides minerals. Humic acid presented a good adsorption onto iron oxides, however the adsorption onto silicates was also significant.

The mechanism of complexation and acid-base interactions are used to explain the adsorption of starches and dextrin onto mineral surfaces. Despite the low adsorption density of CMC onto silicates, its adsorption onto hematite and magnetite surfaces is explained by the lower electrostatic repulsion that these minerals present when compared to silicates. Humic acid adsorption mechanism is explained by the formation of complexes with the surface of the minerals.

A complete micro-flotation study showed that ether-amine has higher floatability than dodecylamine. This also implies a lower selectivity of ether-amines that floats almost all minerals at high values. The existence of a separation window at pH range between 4 and 5 is proved for dodecylamine. Concentration of 1.0×10^{-4} M was enough to achieve the plateau of floatability for all minerals. While diopside is the most easily separated silicate from hematite and magnetite, chamosite is the more difficult.

The influence of depressant dosage, collector dosage and pH has been investigated by the Design of Experiments (DOE) approach. Corn starch and dextrin required high dosages to achieve good results in terms of silica reduction. On the other hand, CMC did not need high dosages but only limited reduction of silica was achieved (3.70% of silica). Humic acid requires low dosage of depressant (300 g/t) with medium dosage of Flotigam EDA (110 g/t) to achieve the best result among the depressants: a concentrate with 2.78% of silica content and an iron recovery of 83.72%. In terms of slurry pH, the best results were achieved at pH 7 for corn starch and humic acid, at pH 9 for dextrin and at pH 11 for CMC.

Flotation tests with the process water from Peña Colorada mine proved the capacity of this water to slightly increase the iron recovery by helping to depress iron oxides when humic acid is used, due to the presence of calcium ions.

A flotation testing campaign determined the best reagent suite as humic acid at 300 g/t and Flotigam EDA at 110 g/t as depressant and collector, respectively at natural pH (around

8). A concentrate with 1.89% of silica content and 67.15% of iron recovery was obtained during laboratory scale testing. The use of an industrial depressant Deprapol N05 has increased the iron recovery to 78.10% when Flotigam EDA was used as collector and to 84.30% when another industrial amine collector (7-15) was used instead, of Flotigam EDA, maintaining the same level of silica content.

An economic evaluation was carried out and allowed the evaluation of the implementation of a new installation composed by fine screening and reverse cationic flotation of silicates. A CAPEX of almost 20 million US dollars is necessary to implement this new installation. This investment is paid back in 19 months, generating a profit of almost 13 million US dollars per year. An OPEX of 1.48 US dollars per ton produced is expected. Earnings related to silica reduction are around 38 million US dollars per year. The project has a NPV of almost 37 million dollars and an IRR of 62%.

Finally, the *ab-initio* study on molecular modelling of chamosite surface interaction with water allowed to understand the behaviour presented by this mineral when compared to other silicates. Chamosite *small-slab* and chamosite *big-slab* have respectively $\Delta E_{ads} \approx -94\ kJ.mol^{-1}$ and $\Delta E_{ads} \approx -30\ kJ.mol^{-1}$, a factor of more than three times. Chamosite *big-slab* is much less hydrophilic than the chamosite *small-slab*, presenting also less available sites for adsorption to occur. As this mineral shows two very different surfaces, new strategies must be found to design combination of flotation reagents to treat it correctly during the process.

9.2 Suggestions for further work

Some conclusions found in this thesis lead to the need for further research. Some suggestions are to:

1. Investigate the effect of cationic collectors onto the surface of the iron-bearing silicates, through equilibrium adsorption experiments, zeta potential measurements.

2. Investigate the competition between depressant adsorption and collector adsorption through micro-flotation or adsorption tests onto mineral surfaces, when two or more minerals are present at the same time in a pulp. This study would clarify which mineral is less separated within an ore flotation system composed of all these minerals.

3. Investigate the use of modified carboxymethyl cellulose with different substitution degrees. The CMC used in this study was not efficient in depressing iron oxides. However, as it showed little affinity with silicates, a modified CMC may have greater efficiency in the adsorption of iron oxides.

4. Investigate the flocculation effect of the polymers studied and how it influences in the equipment design of plant equipment and in the processing of fine tailings.

5. Investigate the complete water adsorption mechanism onto chamosite surface and possibly other iron-bearing silicates through molecular modelling. This investigation would help to generate a deep knowledge of the surface state of the minerals and consequently helping in the flotation processing optimisation. Then study the adsorption of collectors and/or depressants on these minerals and possibly propose new formulations that may be even more effective in the separation process.

Bibliography

Abate, G. and Masini, J. C. (2003). Influence of pH and ionic strength on removal processes of a sedimentary humic acid in a suspension of vermiculite. *Colloids and Surfaces A: Physicochemical and Engineering Aspects*, 226(1):25 – 34.

Afenya, P. (1982). Adsorption of xanthate and starch on synthetic graphite. *International Journal of Mineral Processing*, 9:303–319.

Alva-Valdivia, L. M., Dunlop, D. J., and Urrutia-Fucugauchi, J. (1996). Rock magnetic properties of iron ores and host rocks from the Peña Colorada mining district, western Mexico. *Journal of Applied Geophysics*, 36:105–122.

Alvarez-Silva, M., Uribe-Salas, A., Mirnezami, M., and Finch, J. A. (2010). The point of zero charge of phyllosilicate minerals using the Mular-Roberts titration technique. *Minerals Engineering*, 23(5):383–389.

Anthony, J. W., Bideaux, R. A., Bladh, K. W., and Nichols, M. C. (2019). *Handbook of Mineralogy*. Mineralogical Society of America, Chantilly, VA 20151-1110, USA.

Aquino, A. J. A., Tunega, D., Haberhauer, G., Gerzabek, M. H., and Lischka, H. (2007). Quantum chemical adsorption studies on the (110) surface of the mineral goethite. *The Journal of Physical Chemistry C*, 111(2):877–885.

Araujo, A. C. (1988). *Starch modification of the flocculation and flotation of apatite*. PhD thesis, The University of British Columbia.

Araujo, A. C., Viana, P. R. M., and Peres, A. E. C. (2005). Reagents in iron ores flotation. *Minerals Engineering*, 18(2):219–224.

Ari, V. (2001). *Flotation of Silicate Minerals : Physico-chemical Studies in the Presence of Alkylamines and Mixed (Cationic/Anionic/Non-ionic) Collectors*. PhD thesis, Luleå University of Technology.

Armbruster, T. H., Vice-chairman, P. A. B., Akasaka, M. A., Bern, U., Bern, C., Pira, V. L., and Firenze, I. (2006). Recommended nomenclature of epidote-group minerals. *European Journal of Mineralogy*, 2:551–567.

Arnason, T. S. and Keil, R. G. (2000). Mechanisms of pore water organic matter adsorption to montmorillonite. *Marine Chemistry*, 71:309–320.

Atkinson, R. J., Posner, A. M., and Quirk, J. P. (1967). Adsorption of potential-determining ions at the ferric oxide-aqueous electrolyte interface. *The Journal of Physical Chemistry*, 71(3):550–558.

Avena, M., Vermeer, A., and Koopal, L. (1999). Volume and structure of humic acids studied by viscometry: pH and electrolyte concentration effects. *Colloids and Surfaces A: Physicochemical and Engineering Aspects*, 151(1):213 – 224.

Backfolk, K., Lagerge, S., Rosenholm, J. B., and Eklund, D. (2002). Aspects on the interaction between sodium carboxymethylcellulose and calcium carbonate and the relationship to specific site adsorption. *Journal of Colloid and Interface Science*, 248(1):5 – 12.

Badawi, M., Paul, J., Cristol, S., Payen, E., Romero, Y., Richard, F., Brunet, S., Lambert, D., Portier, X., Popov, A., Kondratieva, E., Goupil, J., Fallah, J. E., Gilson, J., Mariey, L., Travert, A., and Maugé, F. (2011). Effect of water on the stability of mo and como hydrodeoxygenation catalysts: A combined experimental and dft study. *Journal of Catalysis*, 282(1):155 – 164.

Balajee, S. R. and Iwasaki, I. (1969). Adsorption mechanism of starches in flotation and flocculation of iron ores. *Trans. SME/AIME*, 244(December):401–406.

Baum, E., Treutmann, W., Lottermoser, W., and Amthauer, G. (1997). Magnetic properties of the clinopyroxenes aegirine and hedenbergite: A magnetic susceptibility study on single crystals. *Physics and Chemistry of Minerals*, 24(September):294–300.

Beattie, D. A., Huynh, L., Kaggwa, G. B., and Ralston, J. (2006). The effect of polysaccharides and polyacrylamides on the depression of talc and the flotation of sulphide minerals. *Minerals Engineering*, 19(6):598 – 608. Selected papers from the Centenary of Flotation Symposium, 5–9 June 2005, Brisbane, Australia.

Beaussart, A., Mierczynska-Vasilev, A. M., Harmer, S. L., and Beattie, D. A. (2011). The role of mineral surface chemistry in modified dextrin adsorption. *Journal of Colloid and Interface Science*, 357(2):510–520.

Becke, A. D. (1988). Density-functional exchange-energy approximation with correct asymptotic behavior. *Physical Review A*, 38(6):3098–3100.

Bertuzzi, M., Armada, M., and Gottifredi, J. (2007). Physicochemical characterization of starch based films. *Journal of Food Engineering*, 82(1):17 – 25.

Bicak, O., Ekmekci, Z., Bradshaw, D., and Harris, P. (2007). Adsorption of guar gum and CMC on pyrite. *Minerals Engineering*, 20(10):996 – 1002. Selected papers from Reagents '06, Cape Town, South Africa, November 2006.

Bittarello, E., Bruno, M., and Aquilano, D. (2018). Ab initio calculations of the main crystal surfaces of baryte (baso4). *Crystal Growth & Design*, 18(7):4084–4094.

Bjørheim, T. S., Besikiotis, V., and Haugsrud, R. (2012). Hydration thermodynamics of pyrochlore structured oxides from TG and first principles calculations. *Dalton Transactions*, 41(43):13343.

Blake, R. and Hessevick, R. (1966). Refinement of the hematite structure. *The American Mineralogist*, 51:123–129.

Box, G. E. P. and Behnken, D. W. (1960). Some new three level designs for the study of quantitative variables. *Technometrics*, (2:4):455–475.

Braga, P., Chaves, A., Luz, A., and França, S. (2014). The use of dextrin in purification by flotation of molybdenite concentrates. *International Journal of Mineral Processing*, 127:23 – 27.

Brum, M. C. and Oliveira, J. F. (2005). Interação de ácido húmico com surfatantes catiônicos e sua remoção por flotação [Interaction of humic acid with cationic surfactants and their removal by flotation]. In *Encontro Nacional de Tratamento de Minérios e Metalurgia Extrativa*, pages 357–364, Natal, RN, Brazil.

Brunauer, S., Emmett, P. H., and Teller, E. (1938). Gases in multimolecular layers. *Journal of the American Chemical Society*, 60(1):309–319.

Bulatovic, S., Wysouzil, D., and Bermejo, F. (2001). Development and introduction of a new copper/lead separation method in the Raura plant (Peru). *Minerals Engineering*, 14(11):1483 – 1491.

Burdukova, E., Van Leerdam, G. C., Prins, F. E., Smeink, R. G., Bradshaw, D. J., and Laskowski, J. S. (2008). Effect of calcium ions on the adsorption of CMC onto the basal planes of New York talc - A ToF-SIMS study. *Minerals Engineering*, 21(12-14):1020–1025.

Cameron, M., Sueno, S., Prewitt, C., and Papike, J. (1973). High-temperature crystal chemistry of acmite, diopside, hedenbergite, jadeite, spodumene, and ureyite. *American Mineralogist*, 58:594–618.

Castro, E. B. and Ribeiro, F. S. (2005). Avaliação da aplicação de reagentes CMC na flotação catiônica de minério de ferro [Evaluation of CMC reagents application in cationic flotation of iron ore]. In *Encontro Nacional de Tratamento de Minérios e Metalurgia Extrativa*, pages 229–234, Natal, RN, Brazil.

Ceperley, D. M. and Alder, B. J. (1980). Ground state of the electron gas by a stochastic method. *Physical Review Letters*, 45(7):566–569.

Chapman, D. L. (1913). A contribution to the theory of electrocapillarity. *The London, Edinburgh, and Dublin Philosophical Magazine and Journal of Science*, 25(148):475–481.

Chen, J.-h., Long, X.-h., Zhao, C.-h., Kang, D., and Guo, J. (2014). DFT calculation on relaxation and electronic structure of sulfide minerals surfaces in presence of H_2O molecule. *Journal of Central South University*, 21(10):3945–3954.

Chen, Y., Bylaska, E. J., and Weare, J. H. (2017). Weakly bound water structure, bond valence saturation and water dynamics at the goethite (100) surface/aqueous interface: ab initio dynamical simulations. *Geochemical Transactions*, 18(1):3.

Chernyshova, I. V., Ponnurangam, S., and Somasundaran, P. (2011). Adsorption of fatty acids on iron (hydr)oxides from aqueous solutions. *Langmuir*, 27(16):10007–10018.

Cooke, S., Iwasaki, I., , and Choi, H. (1960). Effect of temperature on soap flotation of iron ores. *Trans. AIME*, 217:491–498.

Cooper, T. and de Leeuw, N. (2003). A combined ab initio and atomistic simulation study of the surface and interfacial structures and energies of hydrated scheelite: introducing a cawo4 potential model. *Surface Science*, 531(2):159 – 176.

Cooper, T. G. and de Leeuw, N. H. (2004). A computer modeling study of the competitive adsorption of water and organic surfactants at surfaces of the mineral scheelite. *Langmuir*, 20(10):3984–3994.

Cornell, R. M. and Schwertmann, U. (1996). *The iron oxides : structure, properties, reactions, occurrence, and uses*. Weinheim ; New York : VCH.

Corona-Esquivel, R., Tritlla, J., Henriquez, F., Morales-Isunza, A., Luz Portugal, J., and Nava-Perez, N. (2009). *Geología y mineralización del Yacimiento de hierro Peña Colorada, Colima [Geology and mineralization of the Peña Colorada iron deposit, Colima].* Asociación de Ingenieros de Minas, Metalurgistas y Geólogos de México y Servicio Geológico Mexicano, Mexico.

Crabtree, E. and Vincent, J. (1962). Historical outline of major flotation developments. Froth Flotation. 50th Anniversary. *Rocky Mountain Fund Series AIME*, page 51.

Davis, J. A. (1982). Adsorption of dissolved organic matter at oxide-water interface. *Geochimica et Cosmochimica Acta*, 46(11):2381–2393.

de Leeuw, N. H. and Cooper, T. G. (2002). A computational study of the surface structure and reactivity of calcium fluoride. *Journal of Materials Chemistry*, 13(1):93–101.

de Leeuw, N. H. and Cooper, T. G. (2003). The layering effect of water on the structure of scheelite. *Phys. Chem. Chem. Phys.*, 5:433–436.

de Leeuw, N. H. and Cooper, T. G. (2007). Surface simulation studies of the hydration of white rust $Fe(OH)_2$, goethite - FeO(OH) and hematite - Fe_2O_3. *Geochimica et Cosmochimica Acta*, 71(7):1655–1673.

de Leeuw, N. H. and Parker, S. C. (1997). Atomistic simulation of the effect of molecular adsorption of water on the surface structure and energies of calcite surfaces. *J. Chem. Soc., Faraday Trans.*, 93:467–475.

de Leeuw, N. H. and Parker, S. C. (1998). Surface structure and morphology of calcium carbonate polymorphs calcite, aragonite, and vaterite: An atomistic approach. *The Journal of Physical Chemistry B*, 102(16):2914–2922.

de Leeuw, N. H., Purton, J. A., Parker, S. C., Watson, G. W., and Kresse, G. (2000). Density functional theory calculations of adsorption of water at calcium oxide and calcium fluoride surfaces. *Surface science.*, 452:9–19.

Deer, W., Howie, R., and Zussman, J. (2010). *Minerais constituintes das rochas [Constituent minerals of rocks].* Fundação Calouste Gulbenkian, Lisboa.

Deju, R. and Bhappu, R. B. (1966). A chemical interpretation of surface phenomena in silicate minerals. *Society of Mining Engineers*, (December):329–332.

Du, Z. and de Leeuw, N. H. (2006). Molecular dynamics simulations of hydration, dissolution and nucleation processes at the -quartz (0001) surface in liquid water. *Dalton Transactions*, (22):2623–2634.

Edwards, M., Benjamin, M. M., and Ryan, J. N. (1996). Role of organic acidity in sorption of natural organic matter (nom) to oxide surfaces. *Colloids and Surfaces A: Physicochemical and Engineering Aspects*, 107:297 – 307. A collection of papers presented at the Symposium on Colloidal and Interfacial Phenomena in Aquatic Environments.

Ekmekçi, Z., Bradshaw, D., Allison, S., and Harris, P. (2003). Effects of frother type and froth height on the flotation behaviour of chromite in UG2 ore. *Minerals Engineering*, 16(10):941 – 949.

Erdemoğlu, M. and Sarikaya, M. (2006). Effects of heavy metals and oxalate on the zeta potential of magnetite. *Journal of Colloid and Interface Science*, 300(2):795–804.

Escamilla-Roa, E., Sainz-Díaz, C. I., Huertas, F. J., and Hernández-Laguna, A. (2013). Adsorption of molecules onto (1014) dolomite surface: An application of computational studies for microcalorimetry. *The Journal of Physical Chemistry C*, 117(34):17583–17590.

Espiritu, E., da Silva, G., Azizi, D., Larachi, F., and Waters, K. (2018). The effect of dissolved mineral species on bastnäsite, monazite and dolomite flotation using benzohydroxamate collector. *Colloids and Surfaces A: Physicochemical and Engineering Aspects*, 539:319–334.

Espiritu, E., da Silva, G., Azizi, D., Larachi, F., and Waters, K. (2019). Flotation behavior and electronic simulations of rare earth minerals in the presence of dolomite supernatant using sodium oleate collector. *Journal of Rare Earths*, 37(1):101–112.

Evans, J. D., Fraux, G., Gaillac, R., Kohen, D., Trousselet, F., Vanson, J.-M., and Coudert, F.-X. (2017). Computational chemistry methods for nanoporous materials. *Chemistry of Materials*, 29(1):199–212.

Evans, L. T. and Russel, E. W. (1959). The adsorption of humic and fulvic acids by clays. *Journal of Soil Science*, 10(1):119–132.

Filippov, L. O., Duverger, A., Filippova, I. V., Kasaini, H., and Thiry, J. (2012). Selective flotation of silicates and Ca-bearing minerals: The role of non-ionic reagent on cationic flotation. *Minerals Engineering*, 36–38:314–323.

Filippov, L. O., Javor, Z., Piriou, P., and Filippova, I. V. (2018). Salt effect on gas dispersion in flotation column – Bubble size as a function of turbulent intensity. *Minerals Engineering*, 127(July):6–14.

Filippov, L. O., Joussemet, R., and Houot, R. (2000). Bubble spargers in column flotation : Adaptation to precipitate flotation. *Minerals Engineering*, 13(1):37–51.

Filippov, L. O., Severov, V. V., and Filippova, I. V. (2013). Mechanism of starch adsorption on Fe-Mg-Al-bearing amphiboles. *International Journal of Mineral Processing*, 123:120–128.

Filippov, L. O., Severov, V. V., and Filippova, I. V. (2014). An overview of the beneficiation of iron ores via reverse cationic flotation. *International Journal of Mineral Processing*, 127:62–69.

Flint, I. M., Wyslouzil, H. E., Lima Andrade, V. L., and Murdock, D. J. (1992). Column flotation of iron ore. *Minerals Engineering*, 5(10-12):1185–1194.

Fornasiero, D. and Ralston, J. (2005). Cu(II) and Ni(II) activation in the flotation of quartz, lizardite and chlorite. *International Journal of Mineral Processing*, 76(1-2):75–81.

Foucaud, Y., Badawi, M., Filippov, L. O., Filippova, I. V., and Lebègue, S. (2018a). Surface Properties of Fluorite in Presence of Water: An Atomistic Investigation. *Journal of Physical Chemistry B*, 122(26):6829–6836.

Foucaud, Y., Lebègue, S., Filippov, L. O., Filippova, I. V., and Badawi, M. (2018b). Molecular insight into fatty acid adsorption on bare and hydrated (111) fluorite surface. *The Journal of Physical Chemistry B*, 122(51):12403–12410.

Frommer, D. (1967). Iron ore flotation: Practice, problems, and prospects. *Journal of the American Oil Chemists Society*, 44(4):270–274.

Fuerstenau, D. W. and Pradip (2005). Zeta potentials in the flotation of oxide and silicate minerals. *Advances in Colloid and Interface Science*, 114-115:9–26.

Fuerstenau, M. C. and Palmer, B. R. (1976). Anionic flotation of oxides and silicates. in: Flotation : A. M. Gaudin memorial volume. *New York : American Institute of Mining, Metallurgical, and Petroleum Engineers*, pages 148–196.

Fuerstenau, M. C., Palmer, B. R., and Gutierrez B (1977). Mechanisms of flotation of selected iron-bearing silicates. *Trans. SME/AIME*, 262:234–236.

Fujimoto, J. and Petri, D. F. S. (2001). Adsorption behavior of carboxymethylcellulose on amino-terminated surfaces. *Langmuir*, 17(1):56–60.

Gabe, E. J., Ponthelue, J. C., and Whitlow, S. H. (1973). A reinvestigation of the epidote structure: Confirmation of the lron location. *American Mineralogist*, 58(3):218–223.

Gaines, R. V., Skinner, H. C. W., Foord, E. E., Mason, B., and Rosenzweig, A. (1997). *Dana's New Mineralogy: The System of Mineralogy of James Dwight Dana and Edward Salisbury Dana*. Wiley-Interscience.

Gao, Z., Fan, R., Ralston, J., Sun, W., and Hu, Y. (2019). Surface broken bonds: An efficient way to assess the surface behaviour of fluorite. *Minerals Engineering*, 130:15 – 23.

Gao, Z., Li, C., Sun, W., and Hu, Y. (2017). Anisotropic surface properties of calcite: A consideration of surface broken bonds. *Colloids and Surfaces A: Physicochemical and Engineering Aspects*, 520:53 – 61.

Gao, Z., Sun, W., and Hu, Y. (2014). Mineral cleavage nature and surface energy: Anisotropic surface broken bonds consideration. *Transactions of Nonferrous Metals Society of China*, 24(9):2930 – 2937.

Gao, Z., SUN, W., HU, Y., and LIU, X. (2012). Anisotropic surface broken bond properties and wettability of calcite and fluorite crystals. *Transactions of Nonferrous Metals Society of China*, 22(5):1203 – 1208.

Gao, Z., Sun, W., HU, Y., and Liu, X. (2013). Surface energies and appearances of commonly exposed surfaces of scheelite crystal. *Transactions of Nonferrous Metals Society of China*, 23(7):2147 – 2152.

Gong, G., Han, Y., Liu, J., Zhu, Y., Li, Y., and Yuan, S. (2017). In situ investigation of the adsorption of styrene phosphonic acid on cassiterite (110) surface by molecular modeling. *Minerals*, 7(10):181.

Gouy, M. (1910). Sur la constitution de la charge électrique à la surface d'un électrolyte [On the constitution of the electric charge on the surface of an electrolyte]. *J. de Phys.*, pages 457–468.

Goverapet Srinivasan, S., Shivaramaiah, R., Kent, P. R. C., Stack, A. G., Riman, R., Anderko, A., Navrotsky, A., and Bryantsev, V. S. (2017). A comparative study of surface energies and water adsorption on Ce-bastnäsite, La-bastnäsite, and calcite via density functional theory and water adsorption calorimetry. *Phys. Chem. Chem. Phys.*, 19:7820–7832.

Grimme, S. (2006). Semiempirical hybrid density functional with perturbative second-order correlation. *The Journal of Chemical Physics*, 124(3):034108.

Grotendorst, J., editor (2000). *Modern methods and algorithms of quantum chemistry: Winterschool, 21-25 February 2000, Forschungszentrum Jülich, Germany : proceedings*, volume 1. of *NIC series*. John von Neumann Inst. for Computing, Jülich. Record converted from JUWEL: 18.07.2013.

Gu, B., Schmitt, J., Chen, Z., Liang, L., and McCarthy, J. F. (1995). Adsorption and desorption of different organic matter fractions on iron oxide. *Geochimica et Cosmochimica Acta*, 59(2):219–229.

Haas, P. (1913). *An Introduction To The Chemistry Of Plant Products. Vol II: Metabolic Processes*. Longmans, Green Co.

Haider, S., Roldan, A., and de Leeuw, N. H. (2014). Catalytic dissociation of water on the (001), (011), and (111) surfaces of violarite, feni2s4: A dft-d2 study. *The Journal of Physical Chemistry C*, 118(4):1958–1967.

Hallimond, A. F. (1944). Laboratory apparatus for flotation tests. *Mining Magazine*, 70:87–91.

Hanna, H. S. (1974). *Adsorption of some Starches on Particles of Spar Minerals*, pages 365–374. Springer US, Boston, MA.

He, G.-C., Xiang, H.-M., Jiang, W., Kang, Q., and Chen, J.-H. (2014). First-principles theory on electronic structure and floatability of spodumene. *Rare Metals*, 33(6):742–748.

Helmholtz, H. (1879). *Wiss. Abh. Phy. Tech. Reichsanst 1, 925.*

Henriques, A., Peres, A. E., Correa de Araujo, A., and M Almeida, T. (2009). Caracterização de hematita e estudo do potencial zeta [Hematite characterization and study of zeta potential]. In *XXIII Encontro Nacional de Tratamento de Minérios e Metalurgia Extrativa*, number January, pages 15–22, Gramado.

Henriques, A. B. (2012). *Caracterização e estudo das propriedades eletrocinéticas dos minerais de ferro: hematita, goethita e magnetita [Characterization and study of the electrokinetic properties of iron minerals: hematite, goethite and magnetite].* PhD thesis, Universidade Federal de Minas Gerais, Belo Horizonte, 223pp (in Portuguese).

Hey, M. H. (1954). A new review of the chlorites. *Mineralogical Magazine and Journal of the Mineralogical Society*, 30(224):277–292.

Heydari, H., Elahifard, M., and Behjatmanesh-Ardakani, R. (2019). Role of oxygen vacancy in the adsorption and dissociation of the water molecule on the surfaces of pure and Ni-doped rutile (110): a periodic full-potential DFT study. *Surface Science*, 679:218–224.

Hohenberg, P. and Kohn, W. (1964). Inhomogeneous electron gas. *Physical Review*, 136(3B):B864–B871.

Holland-Batt, A. (1998). Gravity separation: a revitalized technology. *SME Preprint 98*, page 45.

Hoogendam, C. W., de Keizer, A., Cohen Stuart, M. A., Bijsterbosch, B. H., Batelaan, J. G., and van der Horst, P. M. (1998a). Adsorption mechanisms of carboxymethyl cellulose on mineral surfaces. *Langmuir*, 14(14):3825–3839.

Hoogendam, C. W., de Keizer, A., Cohen Stuart, M. A., Bijsterbosch, B. H., Smit, J. A. M., van Dijk, J. A. P. P., van der Horst, P. M., and Batelaan, J. G. (1998b). Persistence length of carboxymethyl cellulose as evaluated from size exclusion chromatography and potentiometric titrations. *Macromolecules*, 31(18):6297–6309.

Houot, R. (1983). Beneficiation of iron ore by flotation — review of industrial and potential applications. *International Journal of Mineral Processing*, 10(3):183 – 204.

Hu, Y., Gao, Z., Sun, W., and Liu, X. (2012). Anisotropic surface energies and adsorption behaviors of scheelite crystal. *Colloids and Surfaces A: Physicochemical and Engineering Aspects*, 415:439 – 448.

Hung, A., Yarovsky, I., and Russo, S. P. (2003). Density-functional theory studies of xanthate adsorption on the pyrite FeS_2(110) and (111) surfaces. *The Journal of Chemical Physics*, 118(13):6022–6029.

Hung, A., Yarovsky, I., and Russo, S. P. (2004). Density-functional theory of xanthate adsorption on the pyrite FeS2(100) surface. *Philosophical Magazine Letters*, 84(3):175–182.

Hunter, R. (1989). *Foundations of colloid science*. Oxford University Press, Oxford.

Hur, J. and Schlautman, M. A. (2003). Molecular weight fractionation of humic substances by adsorption onto minerals. *Journal of Colloid and Interface Science*, 264(2):313 – 321.

Ikumapayi, F., Makitalo, M., Johansson, B., and Hanumantha, K. (2012). Recycling of process water in sulphide flotation : Effect of calcium and sulphate ions on flotation of galena. *Minerals Engineering*, 39:77–88.

Illés, E. and Tombácz, E. (2003). The role of variable surface charge and surface complexation in the adsorption of humic acid on magnetite. *Colloids and Surfaces A: Physicochemical and Engineering Aspects*, 230(1):99 – 109. Second IACIS Conference Interfaces Against Pollution.

Illés, E. and Tombácz, E. (2006). The effect of humic acid adsorption on pH-dependent surface charging and aggregation of magnetite nanoparticles. *Journal of Colloid and Interface Science*, 295(1):115 – 123.

Irannajad, M., Ejtemaei, M., and Gharabaghi, M. (2009). The effect of reagents on selective flotation of smithsonite-calcite-quartz. *Minerals Engineering*, (22):766–771.

Iwasaki, I. (1990). Iron ore flotation - historical perspective and future prospects, in: Parekh. B. K., Miller J.D. (Eds). *Advances in Flotation Technology*, pages 231–243.

Iwasaki, I., Cooke, S., and Choi, H. (1960). Flotation characteristics of hematite, goethite, and activated quartz with 18-carbon aliphatic acids and related compounds. *Trans. AIME*, 217:237–244.

Jane, J.-l. (1994). Properties of granular cold-water-soluble starches prepared by alcoholic-alkaline treatments properties of granular cold-water-soluble starches prepared by alcoholic-alkaline treatments. *Cereal Chemistry*, 71(6):623–626.

Janeček, J., Netz, R. R., Flörsheimer, M., Klenze, R., Schimmelpfennig, B., and Polly, R. (2014). Influence of hydrogen bonding on the structure of the (001) corundum–water interface. density functional theory calculations and monte carlo simulations. *Langmuir*, 30(10):2722–2728.

Jardine, P. M., McCarthy, J. F., and Weber, N. L. (2010). Mechanisms of dissolved organic carbon adsorption on soil. *Soil Science Society of America Journal*, 53(5):1378.

Jiao, F., Qin, W., Liu, R., and Wang, X. (2015). Adsorption mechanism of 2-mercaptobenzothiazole on chalcopyrite and sphalerite surfaces: Ab initio and spectroscopy studies. *Transactions of Nonferrous Metals Society of China*, 25(7):2388–2397.

Jones, M. N. and Bryan, N. D. (1998). Colloidal properties of humic substances. *Advances in Colloid and Interface Science*, 78(1):1 – 48.

Jordens, A., Marion, C., Kuzmina, O., and Waters, K. E. (2014). Physicochemical aspects of allanite flotation. *Journal of Rare Earths*, 32(5):476–486.

Jucker, C. and Clark, M. M. (1994). Adsorption of aquatic humic substances on hydrophobic ultrafiltration membranes. *Journal of Membrane Science*, 97(C):37–52.

Kangal, O., Sirkeci, A., and Güney, A. (2005). Flotation behaviour of huntite ($Mg_3Ca(CO_3)_4$) with anionic collectors. *International Journal of Mineral Processing*, 75(1):31 – 39.

Kerisit, S., Bylaska, E. J., and Felmy, A. R. (2013). Water and carbon dioxide adsorption at olivine surfaces. *Chemical Geology*, 359:81–89.

Khatib, R., Backus, E. H. G., Bonn, M., Perez-Haro, M.-J., Gaigeot, M.-P., and Sulpizi, M. (2016). Water orientation and hydrogen-bond structure at the fluorite/water interface. *Scientific Reports*, 6:24287 EP –. Article.

Khosla, N. K. and Biswas, A. K. (1984). Mineral-collector-starch constituent interactions. *Colloids and Surfaces*, 9:219–235.

Khraisheh, M., Holland, C., Creany, C., Harris, P., and Parolis, L. (2005). Effect of molecular weight and concentration on the adsorption of CMC onto talc at different ionic strengths. *International Journal of Mineral Processing*, 75(3):197 – 206.

King, R. P. (1994). Comminution and liberation of minerals. *Minerals Engineering*, 7(August 1993):129–140.

Kittel, C. (2004). *Introduction to Solid State Physics*. Wiley, 8th edition.

Klein, C. (2007). *Manual of Mineral Science*. Wiley, Nex York.

Kohn, W. and Sham, L. J. (1965). Self-consistent equations including exchange and correlation effects. *Physical Review*, 140(4A):A1133–A1138.

Kolarik, L., Dixon, D., Freeman, P., Furlong, D., and Healy, T. (1980). Effects of pre-treatments on the surface characteristics of a natural magnetite. In *Fine Particles Processing*, pages pp. 652–665 (chapter 34).

Kosmulski, M. (2011). The pH-dependent surface charging and points of zero charge. V. Update. *Journal of Colloid and Interface Science*, 353(1):1–15.

Kursun, I., Terzi, M., and Ozdemir, O. (2019). Determination of surface chemistry and flotation properties of rare earth mineral allanite. *Minerals Engineering*, 132:113 – 120.

Kydros, K. A., Gallios, G. P., and Matis, K. A. (1994). Modification of pyrite and sphalerite flotation by dextrin. *Separation Science and Technology*, 29(17):2263–2275.

Laskowski, J. S., Liu, Q., and Bolin, N. J. (1991). Polysaccharides in flotation of sulphides. Part I. Adsorption of polysaccharides onto mineral surfaces. *International Journal of Mineral Processing*, 33(1–4):223–234.

Laskowski, J. S., Liu, Q., and O'Connor, C. T. (2007). Current understanding of the mechanism of polysaccharide adsorption at the mineral/aqueous solution interface. *International Journal of Mineral Processing*, 84(1-4):59–68.

Lebègue, S., Pillet, S., and Ángyán, J. G. (2008). Modeling spin-crossover compounds by periodic DFT + U approach. *Physical Review B*, 78:1–6.

Leja, J. (1982). *Surface Chemistry of Froth Rotation*. New York: Plenum Press, 771p.

Li, L., Hao, H., Yuan, Z., and Liu, J. (2017). Molecular dynamics simulation of siderite-hematite-quartz flotation with sodium oleate. *Applied Surface Science*, 419:557–563.

Li, Y., Chen, J., Chen, Y., Zhu, Y., and Liu, Y. (2019). DFT Simulation on interaction of H_2O molecules with ZnS and Cu-activated surfaces. *The Journal of Physical Chemistry C*, 123(5):3048–3057.

Lima, R. (1997). *Adsorção de amido e amina na superfície da hematita e do quartzo e sua influência na flotação [Starch and amine adsorption on hematite and quartz surface and their influence on flotation]*. PhD thesis, Universidade Federal de Minas Gerais, Belo Horizonte, 238p (in Portuguese).

Lima, R. M. F. and Luz, J. A. M. d. (2001). Análise granulométrica por técnicas que se baseiam na sedimentação gravitacional: Lei de Stokes [Particle size analysis by techniques based on gravitational sedimentation: Stokes law]. *Rem: Revista Escola de Minas*, 54:155 – 159.

Liu, G., Yang, X., and Zhong, H. (2017). Molecular design of flotation collectors: A recent progress. *Advances in Colloid and Interface Science*, 246(May):181–195.

Liu, J., Wang, Y., Luo, D., Zeng, Y., Wen, S., and Chen, L. (2018). DFT study of SDD and BX adsorption on sphalerite (1 1 0) surface in the absence and presence of water molecules. *Applied Surface Science*, 450:502–508.

Liu, J., Wen, S., Deng, J., Chen, X., and Feng, Q. (2014). DFT study of ethyl xanthate interaction with sphalerite (110) surface in the absence and presence of copper. *Applied Surface Science*, 311:258–263.

Liu, Q. (1988). *The role of mineral surface composition and hydrophobicity in polysaccharide/mineral interactions*. PhD thesis, The University of British Columbia.

Liu, Q. and Laskowski, J. S. (1989). The role of metal hydroxides at mineral surfaces in dextrin adsorption, I. Studies on modified quartz samples. *International Journal of Mineral Processing*, 26(3-4):297–316.

Liu, Q. and Laskowski, J. S. (1999). On the adsorption mechanism of carboxymethyl cellulose. *Polymers in mineral processing, UBC-McGill Bi-Annual International Symposium on Fundamentals of Mineral Processing, 3, Annual Conference of Metallurgists of CIM, 38*.

Liu, Q., Zhang, Y., and Laskowski, J. S. (2000). The adsorption of polysaccharides onto mineral surfaces: An acid/base interaction. *International Journal of Mineral Processing*, 60(3-4):229–245.

Liu, S., Wang, S., Li, W., Guo, J., and Guo, Q. (2013a). Water dissociation on magnetite (001) films. *Journal of Physical Chemistry C*, 117(27):14070–14074.

Liu, T., Luo, W., Cole, D. R., and Asthagiri, A. (2019). Water adsorption on olivine(010) surfaces: Effect of alkali and transition metal cation doping. *The Journal of Chemical Physics*, 150(4):044703.

Liu, W., Moran, C. J., and Vink, S. (2013b). A review of the effect of water quality on flotation. *Minerals Engineering*, 53:91–100.

Long, X., Chen, J., and Chen, Y. (2016a). Adsorption of ethyl xanthate on ZnS(110) surface in the presence of water molecules: A DFT study. *Applied Surface Science*, 370:11–18.

Long, X., Chen, Y., Chen, J., Xu, Z., Liu, Q., and Du, Z. (2016b). The effect of water molecules on the thiol collector interaction on the galena (PbS) and sphalerite (ZnS) surfaces: A DFT study. *Applied Surface Science*, 389:103 – 111.

Lopez-Berganza, J. A., Diao, Y., Pamidighantam, S., and Espinosa-Marzal, R. M. (2015). Ab initio studies of calcium carbonate hydration. *The Journal of Physical Chemistry A*, 119(47):11591–11600. PMID: 26505205.

Luukkanen, S., Parvinen, P., Miettinen, M., Stén, P., Lähteenmäki, S., and Tuikka, A. (2003). Monitoring the composition of water of flotation slurries with an on-line analyser. *Minerals Engineering*, 16:1075–1079.

Ma, D. M. (2012). *Iron Ore Flotation*. CreateSpace Independent Publishing Platform.

Ma, X. (2008). Role of solvation energy in starch adsorption on oxide surfaces. *Colloids and Surfaces A: Physicochemical and Engineering Aspects*, 320(1):36 – 42.

Ma, X. (2010). Role of hydrolyzable metal cations in starch–kaolinite interactions. *International Journal of Mineral Processing*, 97(1):100 – 103.

Ma, X. and Bruckard, W. (2010). The effect of ph and ionic strength on starch–kaolinite interactions. *International Journal of Mineral Processing*, 94(3):111 – 114.

Ma, X., Marques, M., and Gontijo, C. (2011). Comparative studies of reverse cationic/anionic flotation of vale iron ore. *International Journal of Mineral Processing*, 100(3):179 – 183.

Ma, X., Xia, L., Wang, S., Zhong, H., and Jia, H. (2017). Structural modification of xanthate collectors to enhance the flotation selectivity of chalcopyrite. *Industrial & Engineering Chemistry Research*, 56(21):6307–6316.

Marmolejo-Rodríguez, A. J., Prego, R., Meyer-Willerer, A., Shumilin, E., and Sapozhnikov, D. (2007). Rare earth elements in iron oxy-hydroxide rich sediments from the Marabasco River-Estuary System (pacific coast of Mexico). REE affinity with iron and aluminium. *Journal of Geochemical Exploration*, 94:43–51.

Mierczynska-Vasilev, A., Ralston, J., and Beattie, D. A. (2008). Adsorption of modified dextrins on talc: Effect of surface coverage and hydration water on hydrophobicity reduction. *Langmuir*, 24(12):6121–6127. PMID: 18484762.

Miller, J. D., Laskowski, J. S., and Chang, S. S. (1983). Dextrin adsorption by oxidized coal. *Colloids and Surfaces*, 8(2):137–151.

Miller, J. D., Lin, C. L., and Chang, S. S. (1984). Coadsorption Phenomena in the Separation of Pyrite from Coal by Reserve Flotation. *Coal Preparation*, 1(1):21–38.

Mkhonto, D., Ngoepe, P. E., Cooper, T. G., and de Leeuw, N. H. (2006). A computer modelling study of the interaction of organic adsorbates with fluorapatite surfaces. *Physics and Chemistry of Minerals*, 33(5):314–331.

Montes, S., Montes Atenas, G., and Valero, E. (2007). How fine particles on haematite mineral ultimately define the mineral surface charge and the overall floatability behaviour. *Journal of the Southern African Institute of Mining and Metallurgy*, 107(11):689–695.

Montgomery, D. C. (2012). *Design and Analysis of Experiments*. John Wiley and Sons.

Morrish, A. H. (1995). *Canted Antiferromagnetism: Hematite*. World Scientific Pub Co Inc.

Mular, A. L. (1980). *The estimation of prelimary capital costs, in: Mineral Processing Plant Design*. Mular A.L. and Bhapphu, R. B., eds., SME, 2nd edition.

Murphy, E. M., Zachara, J. M., Smith, S. C., and Phillips, J. L. (1992). The sorption of humic acids to mineral surfaces and their role in contaminant binding. *Science of the Total Environment, The*, 117-118(C):413–423.

Nakatani, J., Ozawa, S., and Ogino, Y. (1990). Adsorptive interactions of glucose and carbon dioxide with basic sites over alumina. *Journal of the Chemical Society, Faraday Transactions*, 86(10):1885–1888.

Napier-Munn, T. J., Morrell, S., Morrison, R. D., and Kojovic, T. (1996). *Mineral comminution circuits: their operation and optimisation*. Julius Kruttschnitt Mineral Research Centre, University of Queensland.

Nayak, D., Varadachari, C., and Ghosh, K. (1990). Influence of organic acidic functional groups of humic substances in complexation with clay minerals. *Soil Science*, 149(5):268–271.

Nishimura, S., Hirosue, H., Shobu, K., and Jinnai, K. (1989). Analytical evaluation of locked cycle flotation tests. *International Journal of Mineral Processing*, 27(1-2):39–50.

Norrgran, D. A. and Marin, J. A. (1994). Rare earth permanent magnet separators and their applications in mineral processing. *Mining, Metallurgy & Exploration*, 11(1):41–45.

Ochs, M., Cosovic, B., and Stumm, W. (1994). Coordinative and hydrophobic interaction of humic substances with hydrophilic Al_2O_3 and hydrophobic mercury surfaces. *Geochimica et Cosmochimica Acta*, 58(2):639–650.

Oelkers, E. H., Golubev, S. V., Chairat, C., Pokrovsky, O. S., and Schott, J. (2009). The surface chemistry of multi-oxide silicates. *Geochimica et Cosmochimica Acta*, 73(16):4617–4634.

Ozdemir, O., Çelik, M. S., Nickolov, Z. S., and Miller, J. D. (2007). Water structure and its influence on the flotation of carbonate and bicarbonate salts. *Journal of Colloid and Interface Science*, 314:545–551.

Pareek, A., Torrelles, X., Angermund, K., Rius, J., Magdans, U., and Gies, H. (2008). Structure of interfacial water on fluorapatite (100) surface. *Langmuir*, 24(6):2459–2464. PMID: 18278952.

Pareek, A., Torrelles, X., Angermund, K., Rius, J., Magdans, U., and Gies, H. (2009). Competitive adsorption of glycine and water on the fluorapatite (100) surface. *Langmuir*, 25(3):1453–1458. PMID: 19118469.

Parfit, R. L., Fraser, A. R., and Farmer, V. C. (1977). Adsorption on hydrous oxides. III. fulvic acid and humic acid on goethite, gibbsite and imogolite. *Journal of Soil Science*, 28(2):289–296.

Parks, G. A. (1965). The isoelectric points of solid oxides, solid hydroxides, and aqueous hydroxo complex systems. *Chemical Reviews*, 65(2):177–198.

Partridge, A. C. and Smith, G. W. (1971). Small-sample flotation testing: A new cell. *Tansactions of the Institution of Mining and Metallutgy*, 80:C199–C200.

Pavlovic, S. and Brandao, P. R. G. (2003). Adsorption of starch, amylose, amylopectin and glucose monomer and their effect on the flotation of hematite and quartz. *Minerals Engineering*, 16(11):1117–1122.

Pearse, M. J. (2005). An overview of the use of chemical reagents in mineral processing. *Minerals Engineering*, 18(2 SPEC. ISS.):139–149.

Peng, C., Min, F., Liu, L., and Chen, J. (2016). A periodic DFT study of adsorption of water on sodium-montmorillonite (001) basal and (010) edge surface. *Applied Surface Science*, 387:308–316.

Penners, N. and Koopal, L. (1987). The effect of particle size on the stability of haematite ($\alpha-Fe_2O_3$) hydrosols. *Colloids and surfaces*, 28:67–83.

Perdew, J. P., Burke, K., and Ernzerhof, M. (1996). Generalized gradient approximation made simple. *Physical Review Letters*, 77(18):3865–3868.

Perdew, J. P. and Wang, Y. (1992). Accurate and simple analytic representation of the electron-gas correlation energy. *Physical Review B*, 45(23):13244–13249.

Perdew, J. P. and Yue, W. (1986). Accurate and simple density functional for the electronic exchange energy: Generalized gradient approximation. *Physical Review B*, 33(12):8800–8802.

Peres, A. and Correa, M. (1996). Depression of iron ores with corn starches. *Minerals Engineering*, 9(12):1227–1234.

Perrin, J. (1904). Mécanisme de l'électrisation de contact et solutions colloïdales [Mechanism of contact electrization and colloidal solutions]. *Journal de Chimie Physique*, 2:601–651.

Petteys, M. P. and Schimpf, M. E. (1998). Characterization of hematite and its interaction with humic material using flow field-flow fractionation. *Journal of Chromatography A*, 816(2):145 – 158.

Pinto, C. L., de Araujo, A. C., and Peres, A. E. (1992). The effect of starch, amylose and amylopectin on the depression of oxi-minerals. *Minerals Engineering*, 5(3-5):469–478.

Porsch, B. and Wittgren, B. (2005). Analysis of calcium salt of carboxymethyl cellulose: size distributions of parent carboxymethyl cellulose by size-exclusion chromatography with dual light-scattering and refractometric detection. *Carbohydrate Polymers*, 59(1):27 – 35.

Prigiobbe, V., Negreira, A. S., and Wilcox, J. (2013). Interaction between olivine and water based on density functional theory calculations. *The Journal of Physical Chemistry C*, 117(41):21203–21216.

Pugh, R. (1989). Macromolecular organic depressants in sulphide flotation - A review, 1. Principles, types and applications. *International Journal of Mineral Processing*, 25:101–130.

Raju, G., Holmgren, A., and Forsling, W. (1997). Adsorption of dextrin at mineral/water interface. *Journal of Colloid and Interface Science*, 193(2):215 – 222.

Ramos-Tejada, M. M., Ontiveros, A., Viota, J. L., and Durán, J. D. (2003). Interfacial and rheological properties of humic acid/hematite suspensions. *Journal of Colloid and Interface Science*, 268(1):85–95.

Rath, R. and Subramanian, S. (1999). Adsorption, electrokinetic and differential flotation studies on sphalerite and galena using dextrin. *International Journal of Mineral Processing*, 57(4):265 – 283.

Rath, S. S., Sinha, N., Sahoo, H., Das, B., and Mishra, B. K. (2014). Molecular modeling studies of oleate adsorption on iron oxides. *Applied Surface Science*, 295:115–122.

Rignanese, G.-M., Charlier, J.-C., and Gonze, X. (2004). First-principles molecular-dynamics investigation of the hydration mechanisms of the (0001) -quartz surface. *Phys. Chem. Chem. Phys.*, 6(8):1920–1925.

Rivas-Sanchez, M. L., Urrutia-Fucugauchi1, J., Arenas-Alatorre, J., Alva-Valdivia, L. M., Ruiz-Sandoval, M., and Ramos-Molina, M. A. (2006). Berthierine and chamosite hydrothermal: Genetic guides in the Peña Colorada magnetite-bearing ore deposit, Mexico. *Earth, Planets and Space*, 58(10):1389–1400.

Rohem Peçanha, E., da Fonseca de Albuquerque, M. D., Antoun Simão, R., de Salles Leal Filho, L., and de Mello Monte, M. B. (2019). Interaction forces between colloidal starch and quartz and hematite particles in mineral flotation. *Colloids and Surfaces A: Physicochemical and Engineering Aspects*, 562(August 2018):79–85.

Rosenblum, S. and K. Brownfield, I. (2000). Magnetic susceptibilities of minerals. Technical report, U. S. Geological Survey.

Santos, I. D. and Oliveira, J. F. (2007). Utilization of humic acid as a depressant for hematite in the reverse flotation of iron ore. *Minerals Engineering*, 20(10):1003–1007.

Santos, M. A., Santana, R. C., Capponi, F., Ataíde, C. H., and Barrozo, M. A. S. (2012). Influence of the Water Composition on the Selectivity of Apatite Flotation. *Separation Science and Technology*, 47:4:606–612.

Sarvaramini, A., Azizi, D., and Larachi, F. (2016a). Hydroxamic acid interactions with solvated cerium hydroxides in the flotation of monazite and bastnäsite—experiments and DFT study. *Applied Surface Science*, 387:986–995.

Sarvaramini, A. and Larachi, F. (2017). Understanding the interactions of thiophosphorus collectors with chalcopyrite through DFT simulation. *Computational Materials Science*, 132:137–145.

Sarvaramini, A., Larachi, F., and Hart, B. (2016b). Collector attachment to lead-activated sphalerite – experiments and DFT study on pH and solvent effects. *Applied Surface Science*, 367:459–472.

Schrödinger, E. (1926). An undulatory theory of the mechanics of atoms and molecules. *Physical Review*, 28(6):1049–1070.

Schulz, N. F. and Cooke, S. R. B. (1953). Froth flotation of iron ores adsorption of starch products and laurylamine acetate. *Industrial and Engineering Chemistry Fundamentals*, 45(12):2767–2772.

Schönert, K. (1988). A first survey of grinding with high-compression roller mills. *International Journal of Mineral Processing*, 22(1):401 – 412. Recent Advances in Comminution.

Scott, J. L. and Smith, R. W. (1991). Diamine flotation of quartz. *Minerals Engineering*, 4(2):141–150.

Scott, J. L. and Smith, R. W. (1993). Calcium ion effects in amine flotation of quartz and magnetite. *Minerals Engineering*, 6(12):1245–1255.

Severov, V. V., Filippov, L. O., and Filippova, I. V. (2016). Relationship between cation distribution with electrochemical and flotation properties of calcic amphiboles. *International Journal of Mineral Processing*, 147:18–27.

Sholl, D. and Steckel, J. A. (2009). *Density Functional Theory: A Practical Introduction*. Wiley-Interscience.

Shortridge, P. G., Harris, P. J., Bradshaw, D. J., and Koopal, L. K. (2000). The effect of chemical composition and molecular weight of polysaccharide depressants on the flotation of talc. *International Journal of Mineral Processing*, 59(3):215 – 224.

Shortridge, P. G., Harrris, P. J., and Bradshaw, D. J. (1999). The influence of ions on the effectiveness of polysaccharide depressants in the flotation of talc. *Polymers in mineral processing, UBC-McGill Bi-Annual International Symposium on Fundamentals of Mineral Processing, 3, Annual Conference of Metallurgists of CIM, 38*, page 155.169.

Shrimali, K., Atluri, V., Wang, Y., Bacchuwar, S., Wang, X., and Miller, J. D. (2018). The nature of hematite depression with corn starch in the reverse flotation of iron ore. *Journal of Colloid and Interface Science*, 524:337–349.

Shrimali, K., Yin, X., Wang, X., and Miller, J. D. (2017). Fundamental issues on the influence of starch in amine adsorption by quartz. *Colloids and Surfaces A: Physicochemical and Engineering Aspects*, 522:642–651.

Skelton, A. A., Wesolowski, D. J., and Cummings, P. T. (2011). Investigating the quartz (1010)/water interface using classical and ab initio molecular dynamics. *Langmuir*, 27(14):8700–8709.

Slater, J. C. (1930). Note on Hartree's method. *Physical Review*, 35(2):210–211.

Somasundaran, P. (1969). Adsorption of starch and oleate and interaction between them on calcite in aqueous solutions. *Journal of Colloid And Interface Science*, 31(4):557–565.

Sondi, I., Bišćan, J., and Pravdić, V. (1996). Electrokinetics of pure clay minerals revisited. *Journal of Colloid and Interface Science*, 178(2):514–522.

Souvi, S. M., Badawi, M., Paul, J. F., Cristol, S., and Cantrel, L. (2013). A DFT study of the hematite surface state in the presence of H_2, H_2O and O_2. *Surface Science*, 610(November 2017):7–15.

Srinivasan, S. G., Shivaramaiah, R., Kent, P. R. C., Stack, A. G., Navrotsky, A., Riman, R., Anderko, A., and Bryantsev, V. S. (2016). Crystal structures, surface stability, and water adsorption energies of La-Bastnäsite via density functional theory and experimental studies. *The Journal of Physical Chemistry C*, 120(30):16767–16781.

Stack, A. G., Stubbs, J. E., Srinivasan, S. G., Roy, S., Bryantsev, V. S., Eng, P. J., Custelcean, R., Gordon, A. D., and Hexel, C. R. (2018). Mineral–water interface structure of xenotime (YPO_4) {100}. *The Journal of Physical Chemistry C*, 122(35):20232–20243.

Steenberg, E. and Harris, P. J. (1984). Adsorption of carboxymethylcellulose, guar gum, and starch onto talc, sulfides, oxides, and salt-type minerals. *South African Journal of Chemistry*, 37(3):85–90.

Stern, O. (1924). The theory of the electrolytic double layer. *Z. Elektrochem.*, 30:508–516.

Stevenson, F. J. (1994). *Humus Chemistry: Genesis, Composition, Reactions*. Wiley.

Svoboda, J. (1994). The effect of magnetic field strenght on the efficiency of magnetic separation. *Minerals Engineering*, 7(5):747 – 757.

Taggart, A. F. (1948). *Handbook of mineral dressing*. Wiley, New York, NY.

Tan, H., Skinner, W., and Addai-Mensah, J. (2012). Leaching behaviour of low and high Fe-substituted chlorite clay minerals at low pH. *Hydrometallurgy*, 125-126:100–108.

Tartaj, P., Cerpa, A., García-González, M. T., and Serna, C. J. (2000). Surface instability of serpentine in aqueous suspensions. *Journal of Colloid and Interface Science*, 231(1):176–181.

Thomas, F., Michot, L., Vantelon, D., Montargès, E., Prélot, B., Cruchaudet, M., and Delon, J. (1999). Layer charge and electrophoretic mobility of smectites. *Colloids and Surfaces A: Physicochemical and Engineering Aspects*, 159(2):351 – 358.

Tian, M., Gao, Z., Han, H., Sun, W., and Hu, Y. (2017). Improved flotation separation of cassiterite from calcite using a mixture of lead (II) ion/benzohydroxamic acid as collector and carboxymethyl cellulose as depressant. *Minerals Engineering*, 113(August):68–70.

Tian, M., Zhang, C., Han, H., Liu, R., Gao, Z., Chen, P., He, J., Hu, Y., Sun, W., and Yuan, D. (2018). Novel insights into adsorption mechanism of benzohydroxamic acid on lead (II)-activated cassiterite surface: An integrated experimental and computational study. *Minerals Engineering*, 122:327–338.

Tipping, E. (1981). The adsorption of aquatic humic substances by iron oxides. *Geochimica et Cosmochimica Acta*, 45(2):191–199.

Tombácz, E., Libor, Z., Illés, E., Majzik, A., and Klumpp, E. (2004). The role of reactive surface sites and complexation by humic acids in the interaction of clay mineral and iron oxide particles. *Organic Geochemistry*, 35(3):257–267.

Tombácz, E., Libor, Z., Illés, E., Majzik, A., and Klumpp, E. (2004). The role of reactive surface sites and complexation by humic acids in the interaction of clay mineral and iron oxide particles. *Organic Geochemistry*, 35(3):257 – 267. Selected papers from the Eleventh International Humic Substances Society Conference.

Tritlla, J., Camprubí, A., Centeno-García, E., Corona-Esquivel, R., Iriondo, A., Sánchez-Martínez, S., Gasca-Durán, A., Cienfuegos-Alvarado, E., and Morales-Puente, P. (2003). Estructura y edad del depósito de hierro de Peña Colorada (Colima): Un posible equivalente fanerozoico de los depósitos de tipo IOCG. *Revista Mexicana de Ciencias Geologicas*, 20(3):182–201.

Turrer, H. D. G. and Peres, A. E. C. (2010). Investigation on alternative depressants for iron ore flotation. *Minerals Engineering*, 23(11-13):1066–1069.

Ulian, G., Moro, D., and Valdrè, G. (2018). Probing the interaction of (001) carbonated hydroxylapatite surfaces with water: a density functional investigation. *Micro & Nano Letters*, 13(1):4–8.

US Geological Survey (2018). Mineral Commodity Summaries 2018. Technical report, US Geological Survey, Reston, Virgina, USA.

Valdivieso, A. L., Cervantes, T. C., Song, S., Cabrera, A. R., and Laskowski, J. S. (2004). Dextrin as a non-toxic depressant for pyrite in flotation with xanthates as collector. *Minerals Engineering*, 17(9-10):1001–1006.

Valdivieso, A. L., López, A. S., Song, S., Martínez, H. G., and Almada, S. L. (2007). Dextrin as a regulator for the selective flotation of chalcopyrite, galena and pyrite. *Canadian Metallurgical Quarterly*, 46(3):301–309.

Veloso, C. H., Filippov, L. O., Filippova, I. V., Ouvrard, S., and Araujo, A. C. (2018). Investigation of the interaction mechanism of depressants in the reverse cationic flotation of complex iron ores. *Minerals Engineering*, 125(May):133–139.

Vermeer, A. W. P., van Riemsdijk, W. H., and Koopal, L. K. (1998). Adsorption of humic acid to mineral particles 1. Specific and electrostatic interactions. *Langmuir*, 14(10):2810–2819.

Walker, J. R. and Bish, D. L. (1992). Application of Rietveld refinement techniques to a disordered IIb Mg-Chamosite. *Clays and Clay Minerals*, 40(3):319–322.

Wang, J., Kalinichev, A. G., Kirkpatrick, R. J., and Cygan, R. T. (2005). Structure, energetics, and dynamics of water adsorbed on the muscovite (001) surface: a molecular dynamics simulation. *The Journal of Physical Chemistry B*, 109(33):15893–15905.

Wang, J. and Somasundaran, P. (2005). Adsorption and conformation of carboxymethyl cellulose at solid-liquid interfaces using spectroscopic, AFM and allied techniques. *Journal of Colloid and Interface Science*, 291(1):75–83.

Wang, L., Sun, W., and qing Liu, R. (2014). Mechanism of separating muscovite and quartz by flotation. *Journal of Central South University*, 21(9):3596–3602.

Wang, X., Zhang, Q., Li, X., Ye, J., and Li, L. (2018). Structural and electronic properties of different terminations for quartz (001) surfaces as well as water molecule adsorption on it: A first-principles study. *Minerals*, 8(2):58.

Wechsler, B. A., Lindsley, D. H., and Prewitte, C. T. (1984). Crystal structure and cation distribution in titanomagnetites (Fe_{3-x},Ti_x,O_4). *American Mineralogist*, 69:754–770.

Weisseborn, P. K., Warren, L. J., and Dunn, J. G. (1995). Selective flocculation of ultrafine iron ore. 1. Mechanism of adsorption of starch onto hematite. *Colloids and Surfaces A: Physicochemical and Engineering Aspects*, 99(1):11–27.

Whittaker, E. J. W. (1982). Cleavage energies of minerals. *Mineralogical Magazine*, 46(340):398–399.

Wie, J. M. and Fuerstenau, D. W. (1974). The effect of dextrin on surface properties and the flotation of molybdenite. *International Journal of Mineral Processing*, 1(1):17 – 32.

Wills, B. A. and Napier-Munn, T. (2005a). 12 - Froth flotation. In Wills, B. A. and Napier-Munn, T., editors, *Wills' Mineral Processing Technology (7th)*, pages 267 – 352. Butterworth-Heinemann, Oxford, 7th edition.

Wills, B. A. and Napier-Munn, T. (2005b). 4 - Particle size analysis. In Wills, B. A. and Napier-Munn, T., editors, *Wills' Mineral Processing Technology (7th)*, pages 90 – 107. Butterworth-Heinemann, Oxford, 7th edition.

Wungu, T. D. K., Agusta, M. K., Saputro, A. G., Dipojono, H. K., and Kasai, H. (2012). First principles calculation on the adsorption of water on lithium–montmorillonite (Li–MMT). *Journal of Physics: Condensed Matter*, 24(47):475506.

Xia, L., Zhong, H., Liu, G., and Li, X. (2009). Electron bandstructure of kaolinite and its mechanism of flotation using dodecylamine as collector. *Journal of Central South University of Technology*, 16(1):73–79.

Xia, S., Pan, G., Cai, Z.-L., Wang, Y., and Reimers, J. R. (2007). The manganite-water interface. *The Journal of Physical Chemistry C*, 111(28):10427–10437.

Xie, J., Li, X., Mao, S., Li, L., Ke, B., and Zhang, Q. (2018). Effects of structure of fatty acid collectors on the adsorption of fluorapatite (0 0 1) surface: A first-principles calculations. *Applied Surface Science*, 444:699–709.

Xu, L., Peng, T., Tian, J., Lu, Z., Hu, Y., and Sun, W. (2017a). Anisotropic surface physicochemical properties of spodumene and albite crystals: Implications for flotation separation. *Applied Surface Science*, 426:1005–1022.

Xu, L., Tian, J., Wu, H., Deng, W., Yang, Y., Sun, W., Gao, Z., and Hu, Y. (2017b). New insights into the oleate flotation response of feldspar particles of different sizes: Anisotropic adsorption model. *Journal of Colloid and Interface Science*, 505:500–508.

Xu, Y., Liu, Y.-L., He, D.-D., and Liu, G.-S. (2013). Adsorption of cationic collectors and water on muscovite (001) surface: A molecular dynamics simulation study. *Minerals Engineering*, 53:101–107.

Yin, W.-Z., Wang, J.-Z., and Sun, Z.-M. (2014). Structure–activity relationship and mechanisms of reagents used in scheelite flotation. *Rare Metals*, 34(12):882–887.

Yin, X., Gupta, V., Du, H., Wang, X., and Miller, J. D. (2012). Surface charge and wetting characteristics of layered silicate minerals. *Advances in Colloid and Interface Science*, 182:43–50.

Yu, F., Wang, Y., Wang, L., and Xie, Z. (2014). Investigation on different behavior and mechanism of Ca^{2+}, Fe^{3+} adsorption on spodumente surface., journal = Physicochemical Problems of Mineral Processing. 50:535–550.

Yu, F., Wang, Y., Zhang, L., and Zhu, G. (2015). Role of oleic acid ionic-molecular complexes in the flotation of spodumene. *Minerals Engineering*, 71:7–12.

Zahn, D. and Hochrein, O. (2003). Computational study of interfaces between hydroxyapatite and water. *Phys. Chem. Chem. Phys.*, 5:4004–4007.

Zhang, Y., Kallay, N., and Matijevic, E. (1985). Interaction of metal hydrous oxides with chelating agents. 7. Hematite-oxalic acid and -citric acid systems. *Langmuir*, 1(2):201–206.

Zhao, G., Peng, J., Zhong, H., Wang, S., and Liu, G. (2016). Synthesis of novel ether thionocarbamates and study on their flotation performance for chalcopyrite. *Minerals*, 6(3):97.

Zhao, G., Zhong, H., Qiu, X., Wang, S., Gao, Y., Dai, Z., Huang, J., and Liu, G. (2013). The DFT study of cyclohexyl hydroxamic acid as a collector in scheelite flotation. *Minerals Engineering*, 49:54–60.

Zheng, X. and Smith, R. (1997). Dolomite depressants in the flotation of apatite and collophane from dolomite. *Minerals Engineering*, 10(5):537 – 545.

Zhu, G., Wang, Y., Wang, X., Yu, F., and Miller, J. D. (2018). States of coadsorption for oleate and dodecylamine at selected spodumene surfaces. *Colloids and Surfaces A: Physicochemical and Engineering Aspects*, 558:313–321.

Zürcher, L., Ruiz, J., and Barton, M. D. (2001). Paragenesis, elemental distribution, and stable isotopes at the Peña Colorada Iron Skarn, Colima, Mexico. *Economic Geology*, 96(3):535–557.

Appendix A

X-ray diffractograms of pure minerals

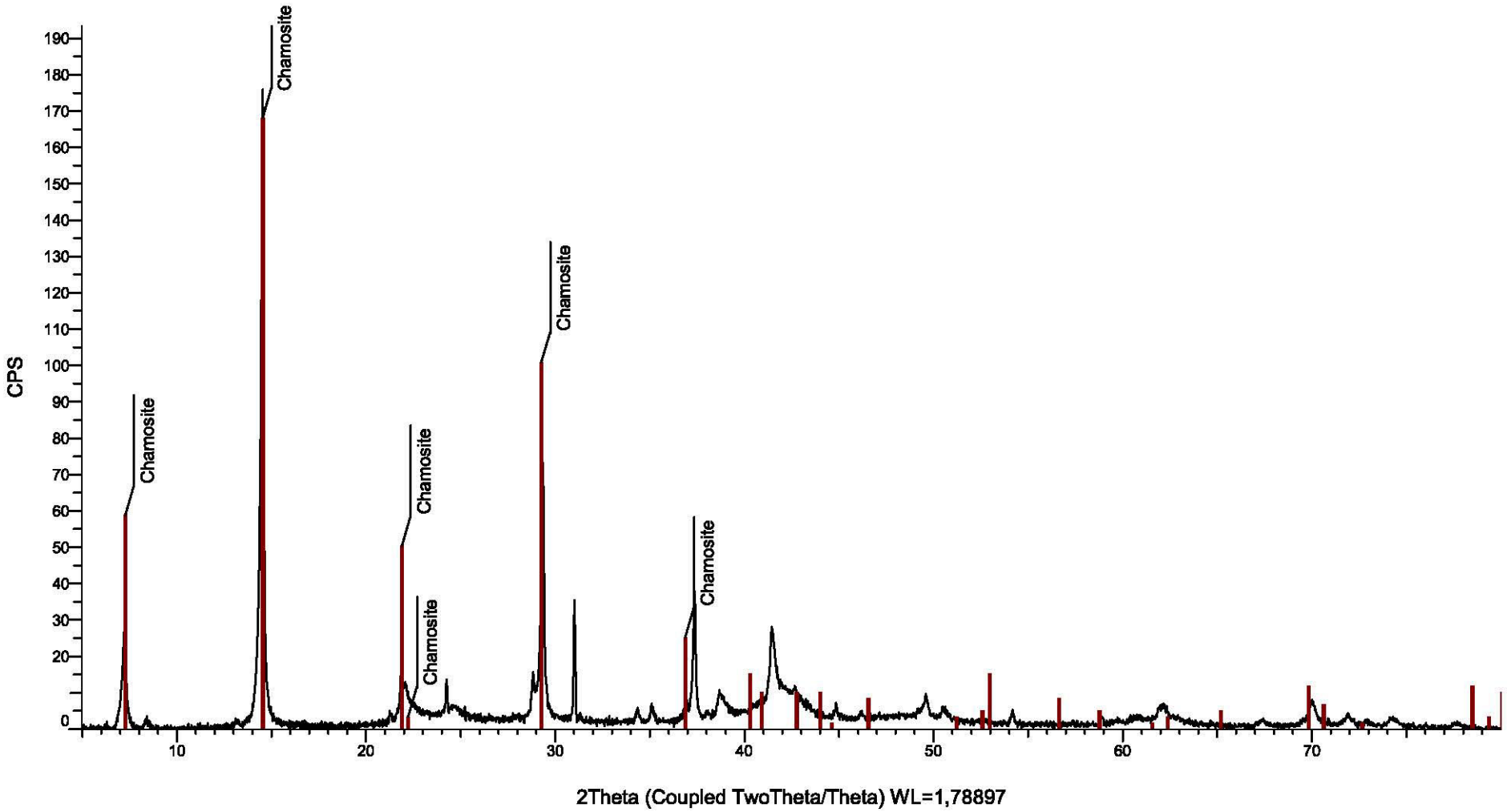

Fig. A.1 – X-ray diffractogram of chamosite in the size fraction between 106 µm and 38 µm.

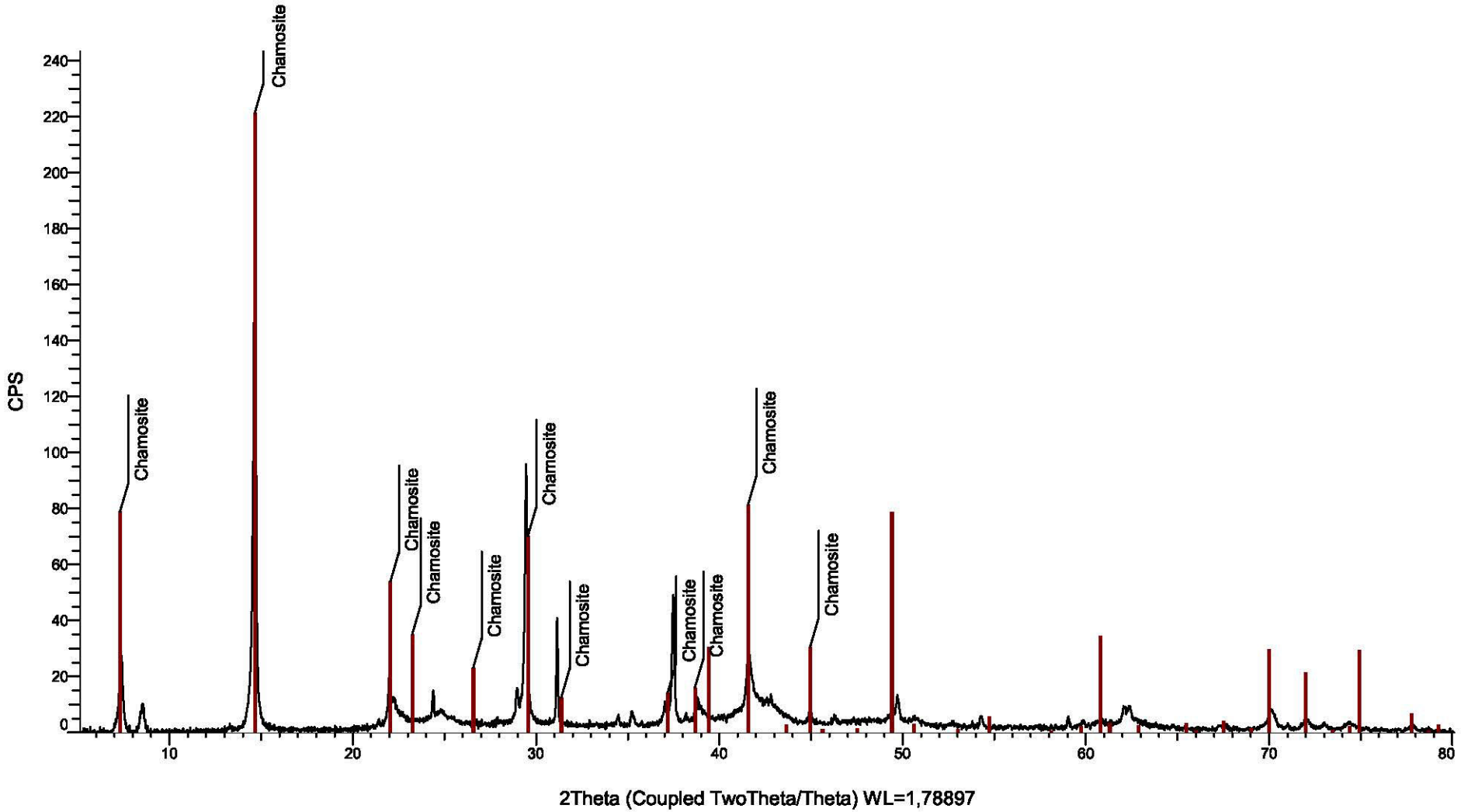

Fig. A.2 – X-ray diffractogram of chamosite in the size fraction below 38 µm.

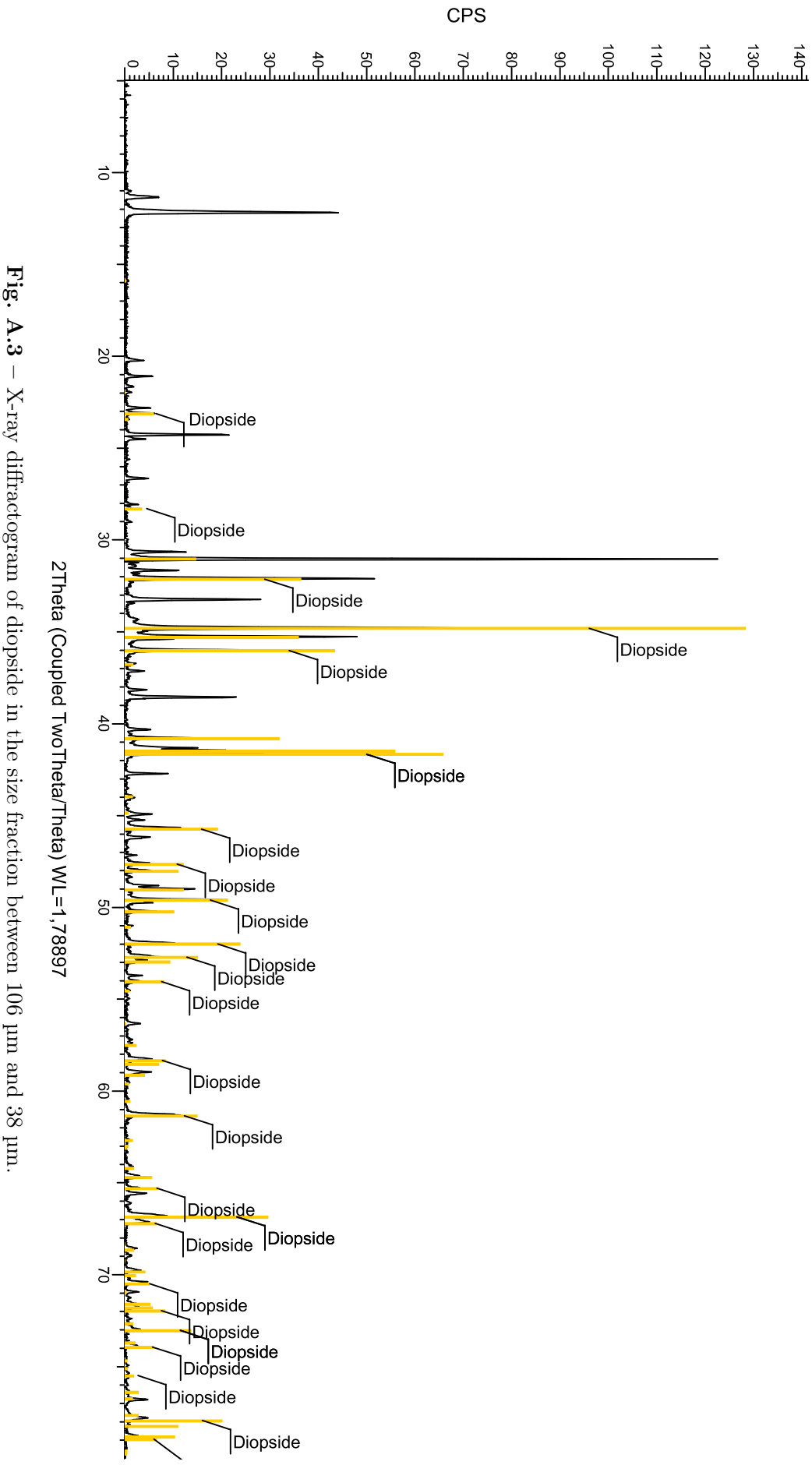

Fig. A.3 – X-ray diffractogram of diopside in the size fraction between 106 µm and 38 µm.

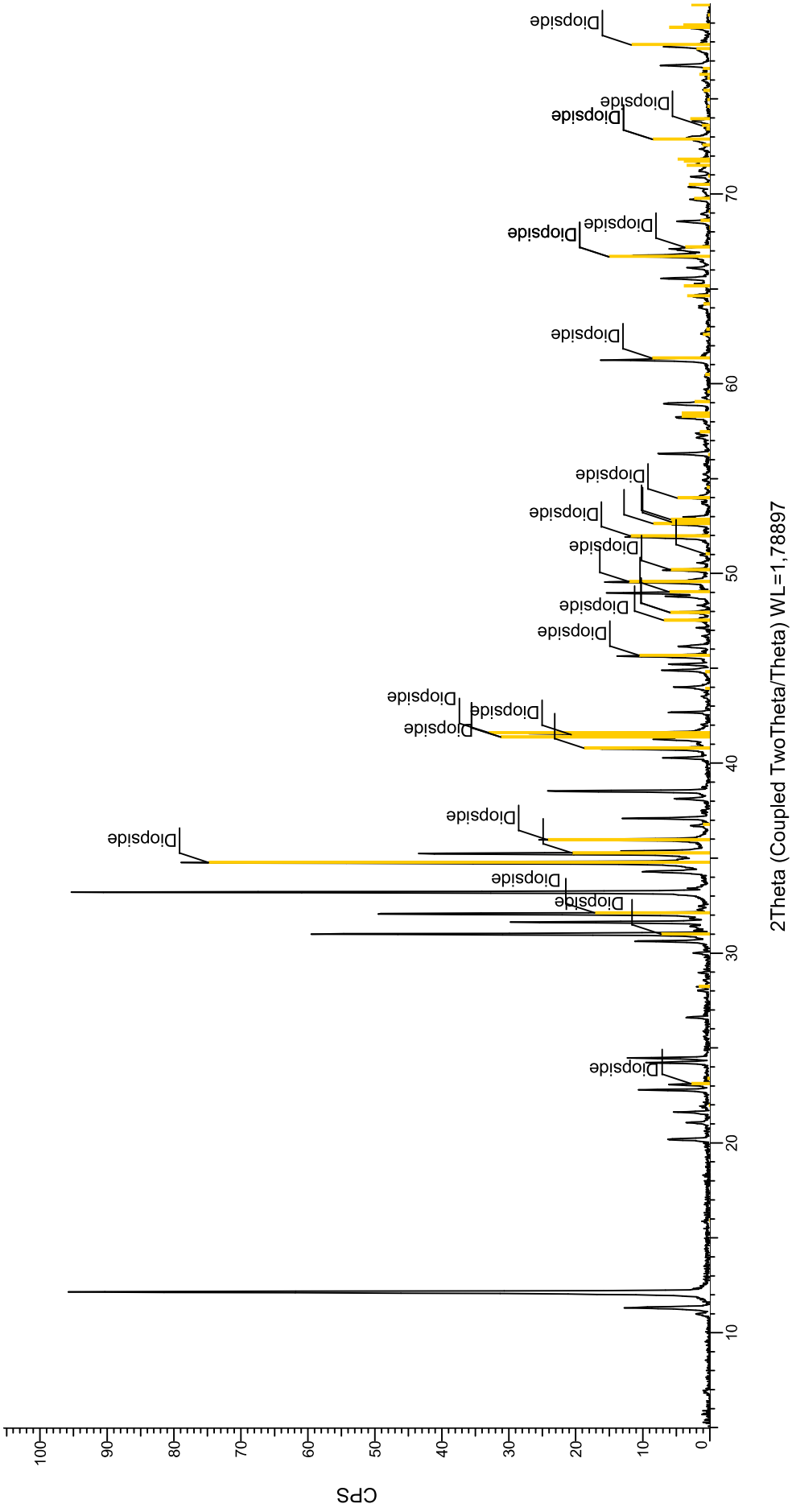

Fig. A.4 – X-ray diffractogram of diopside in the size fraction below 38 µm.

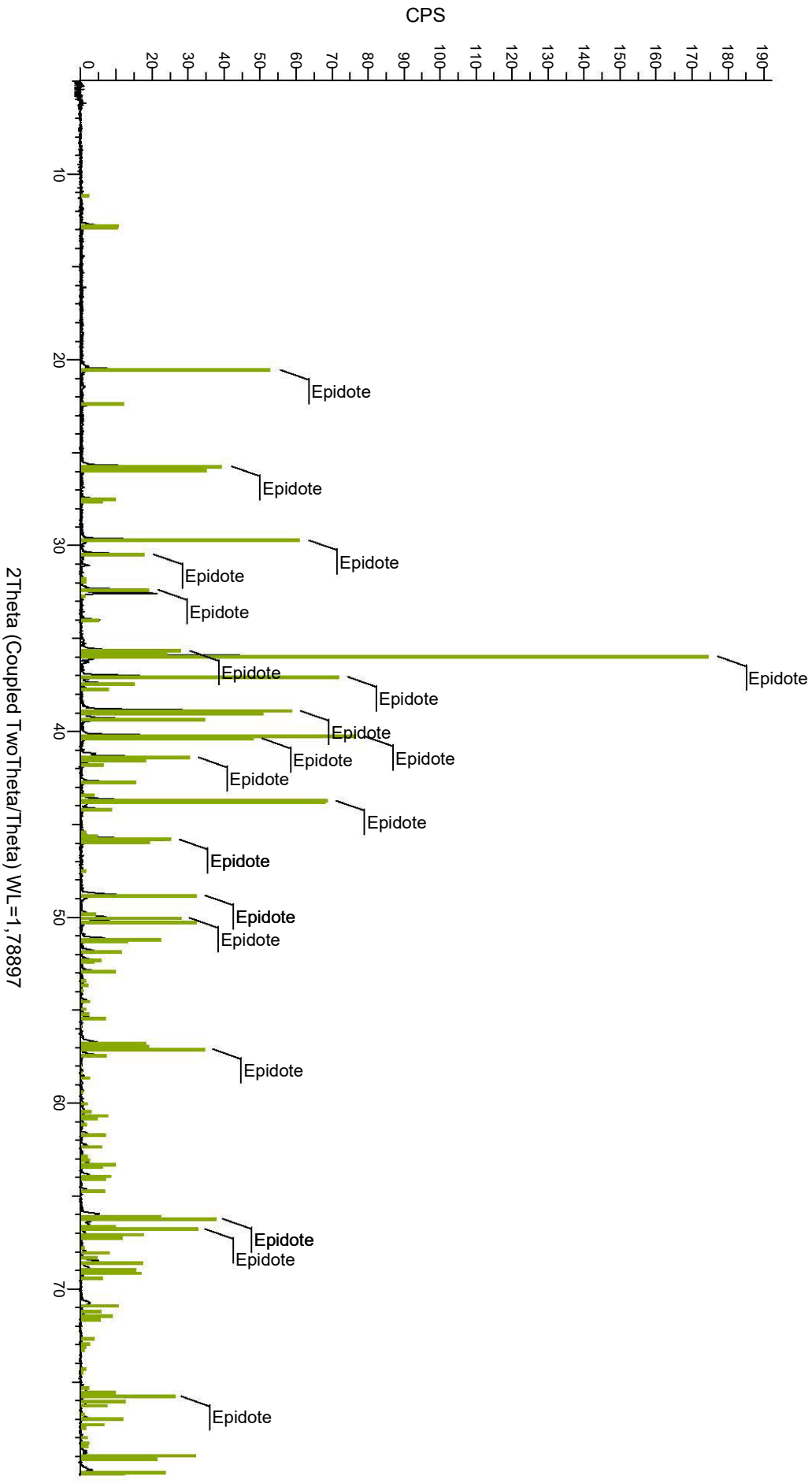

Fig. A.5 – X-ray diffractogram of epidote in the size fraction between 106 µm and 38 µm.

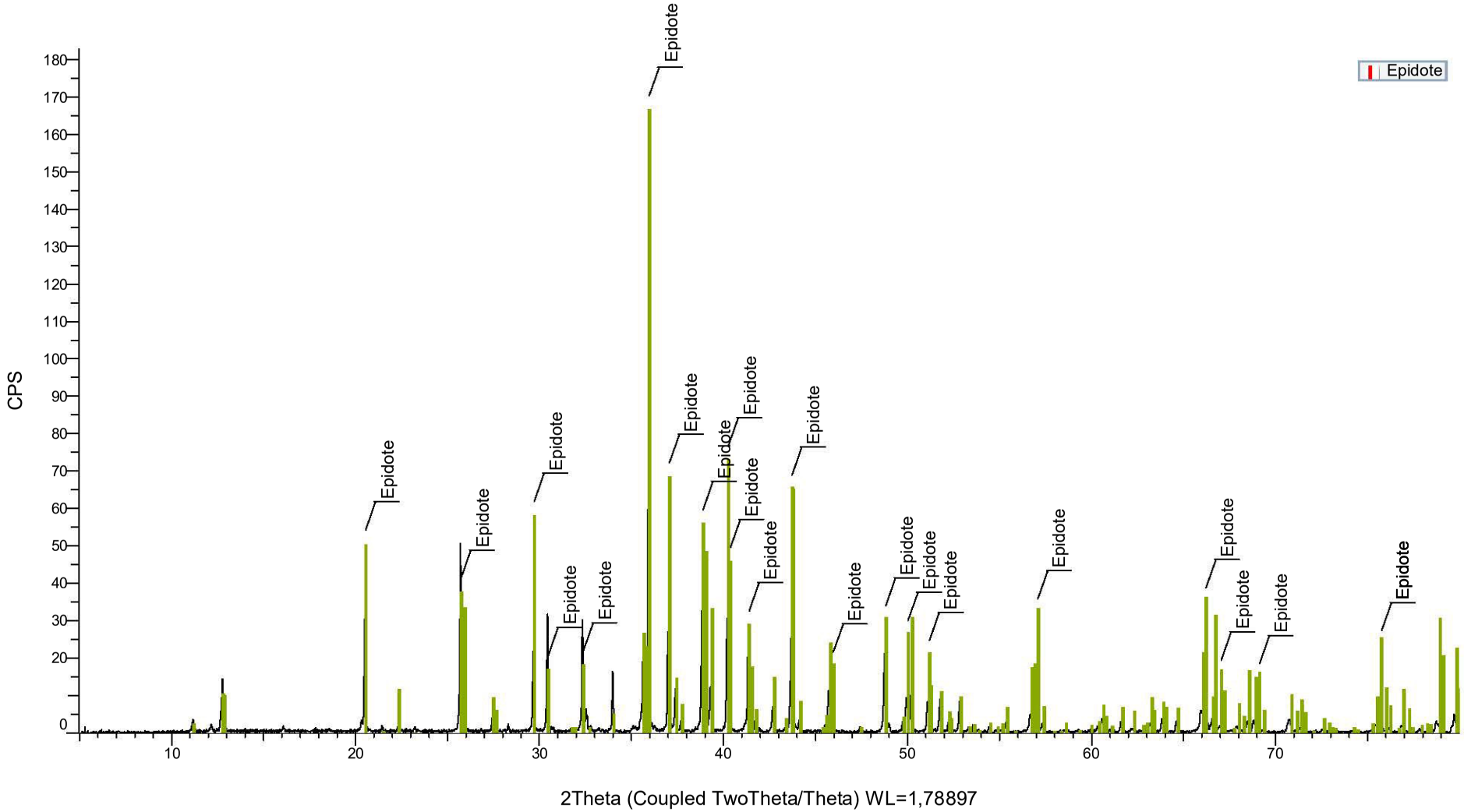

Fig. A.6 – X-ray diffractogram of epidote in the size fraction below 38 µm.

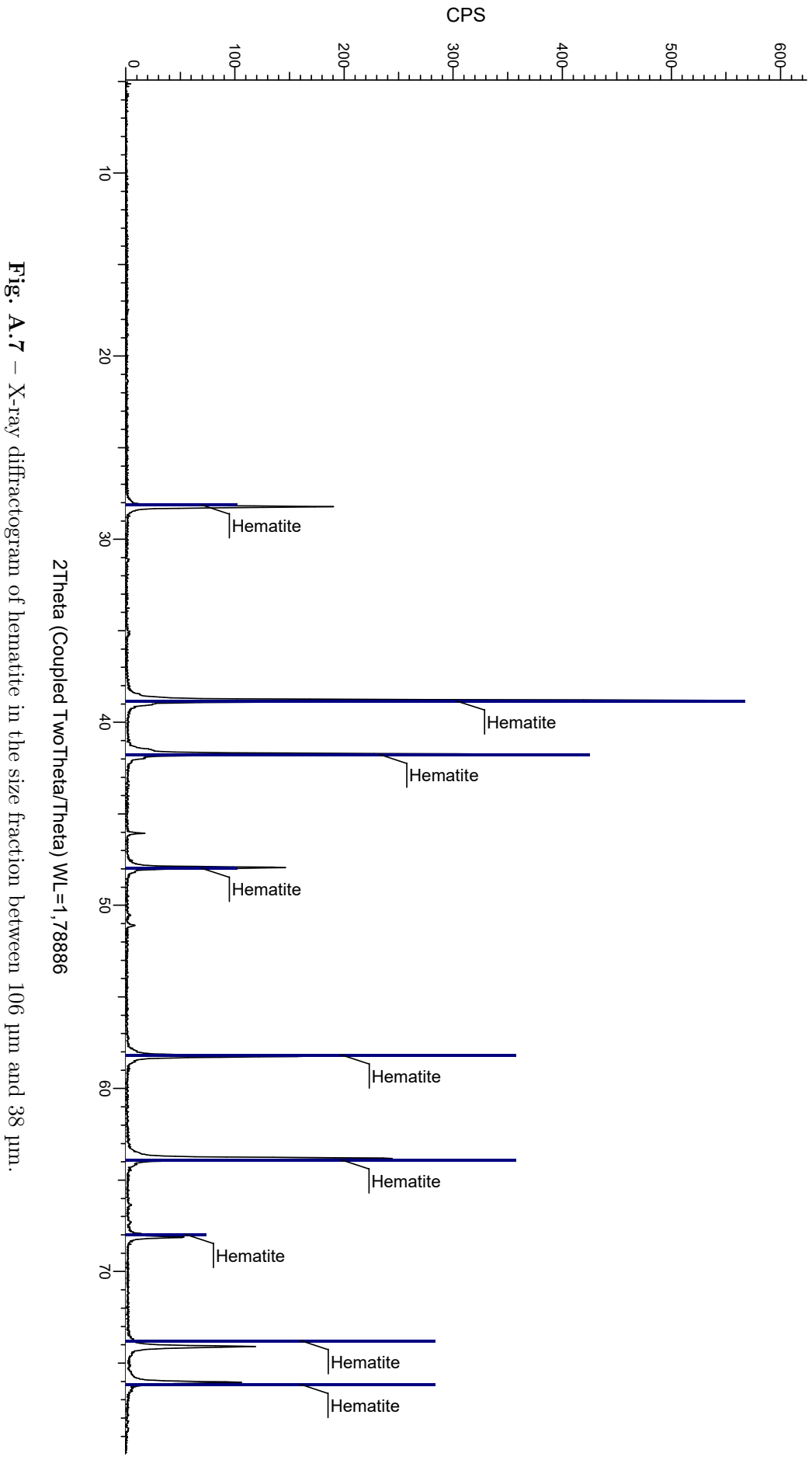

Fig. A.7 – X-ray diffractogram of hematite in the size fraction between 106 µm and 38 µm.

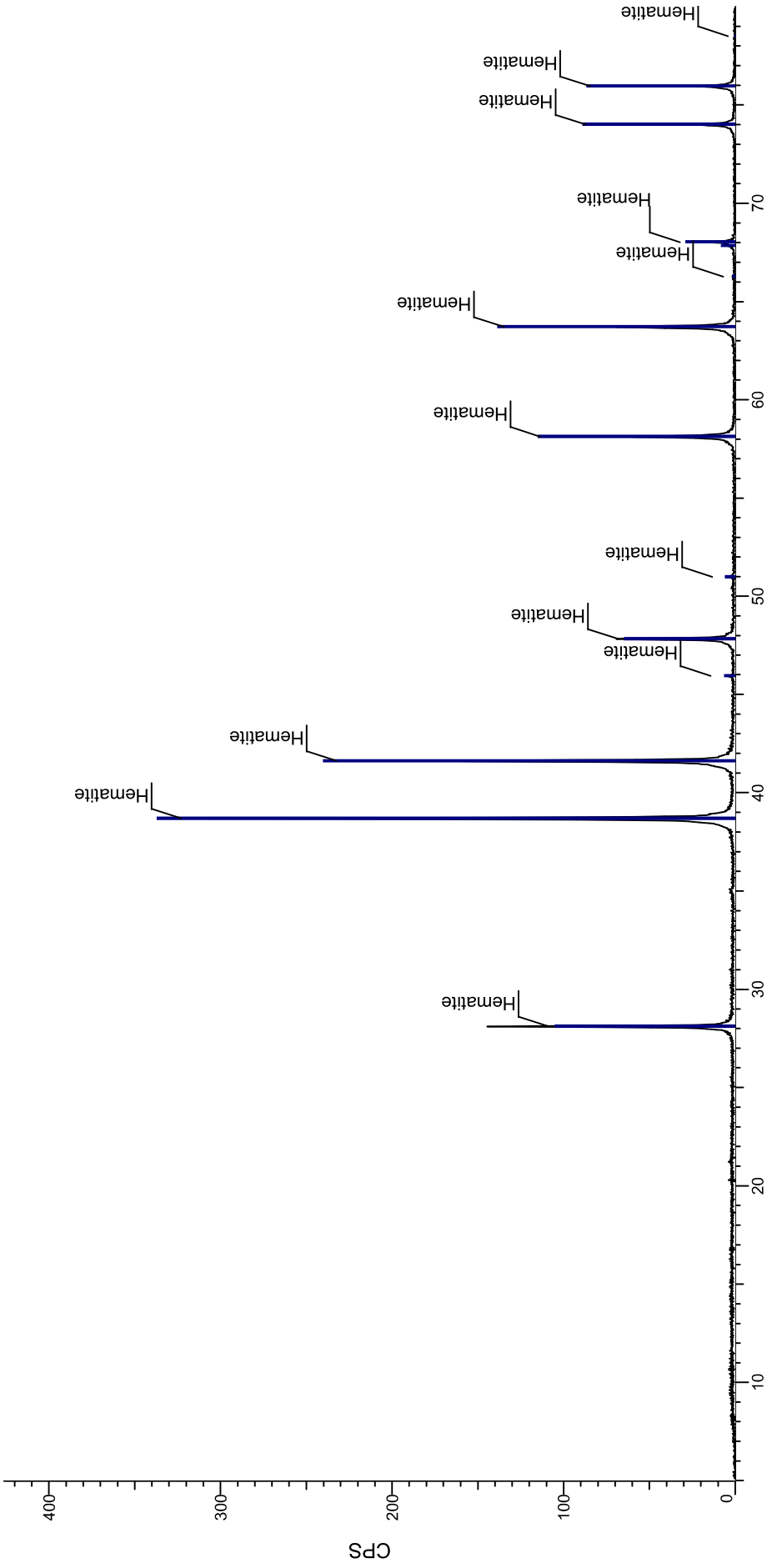

Fig. A.8 – X-ray diffractogram of hematite in the size fraction below 38 µm.

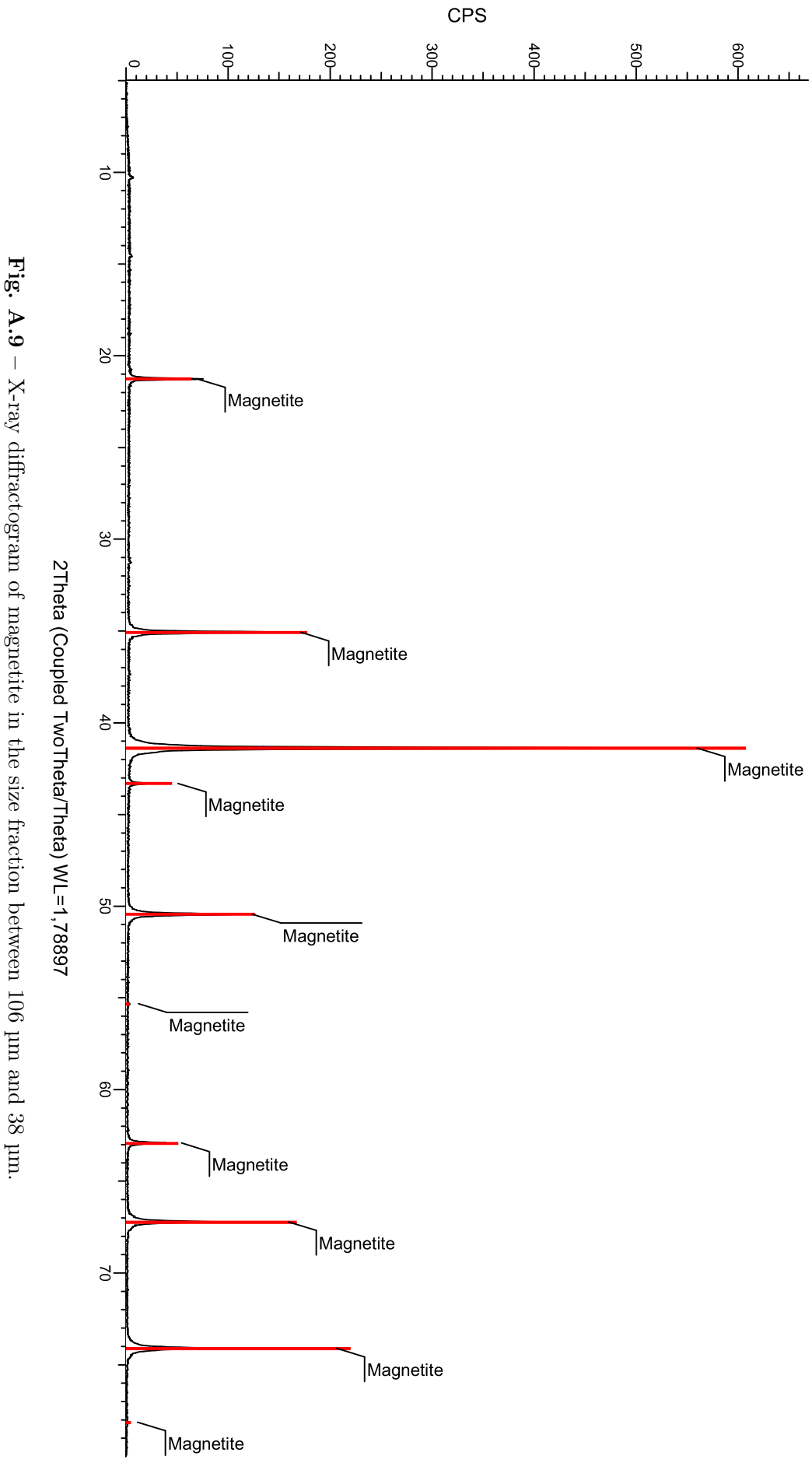

Fig. A.9 – X-ray diffractogram of magnetite in the size fraction between 106 µm and 38 µm.

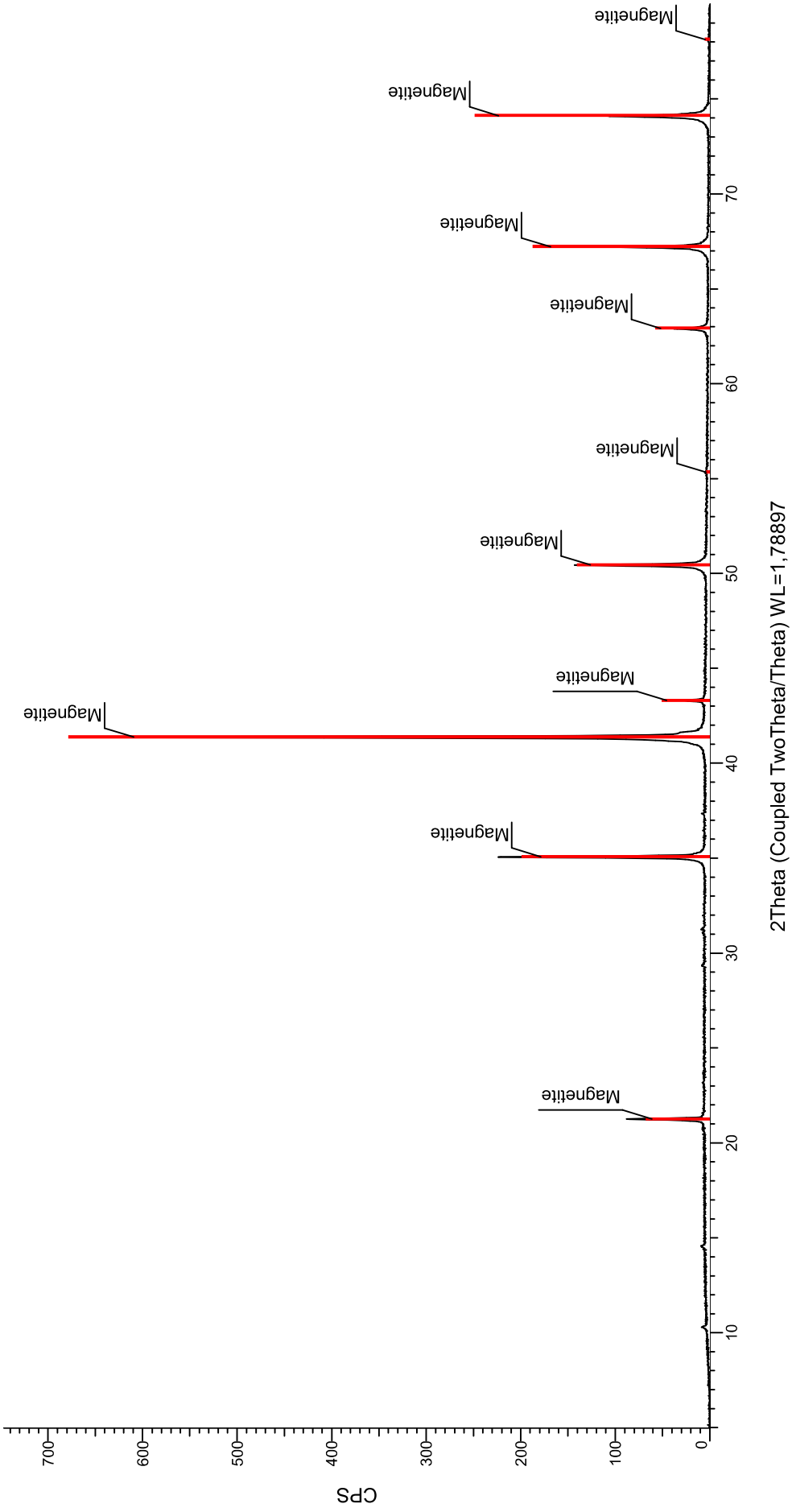

Fig. A.10 – X-ray diffractogram of magnetite in the size fraction below 38 µm.

Appendix B

ATR-IR spectrum of the neutralised ether-amine

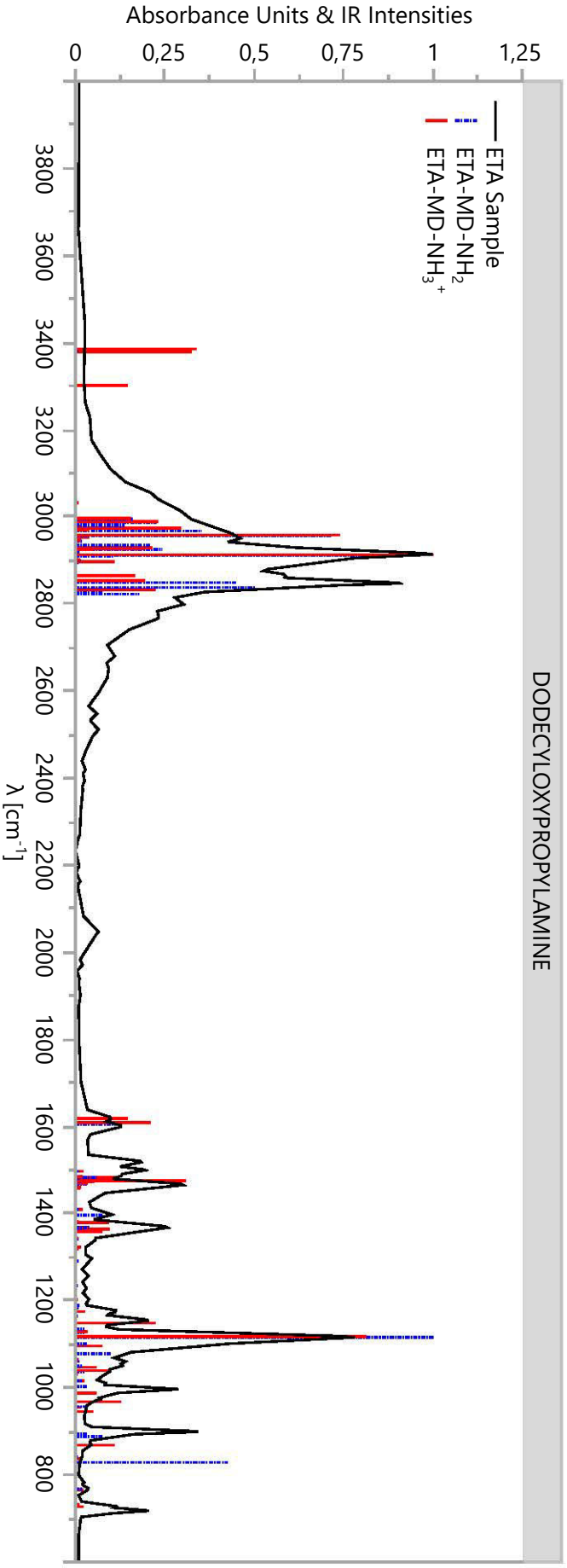

Fig. B.1 – ATR-IR spectrum of the neutralised ether-amine compared with ionic and molecular state of the molecule. Blue lines: molecular state of ETA and red lines: ionic state of ETA, were calculated by the software Orca.

Appendix C

X-ray diffractograms of samples 1 and 2

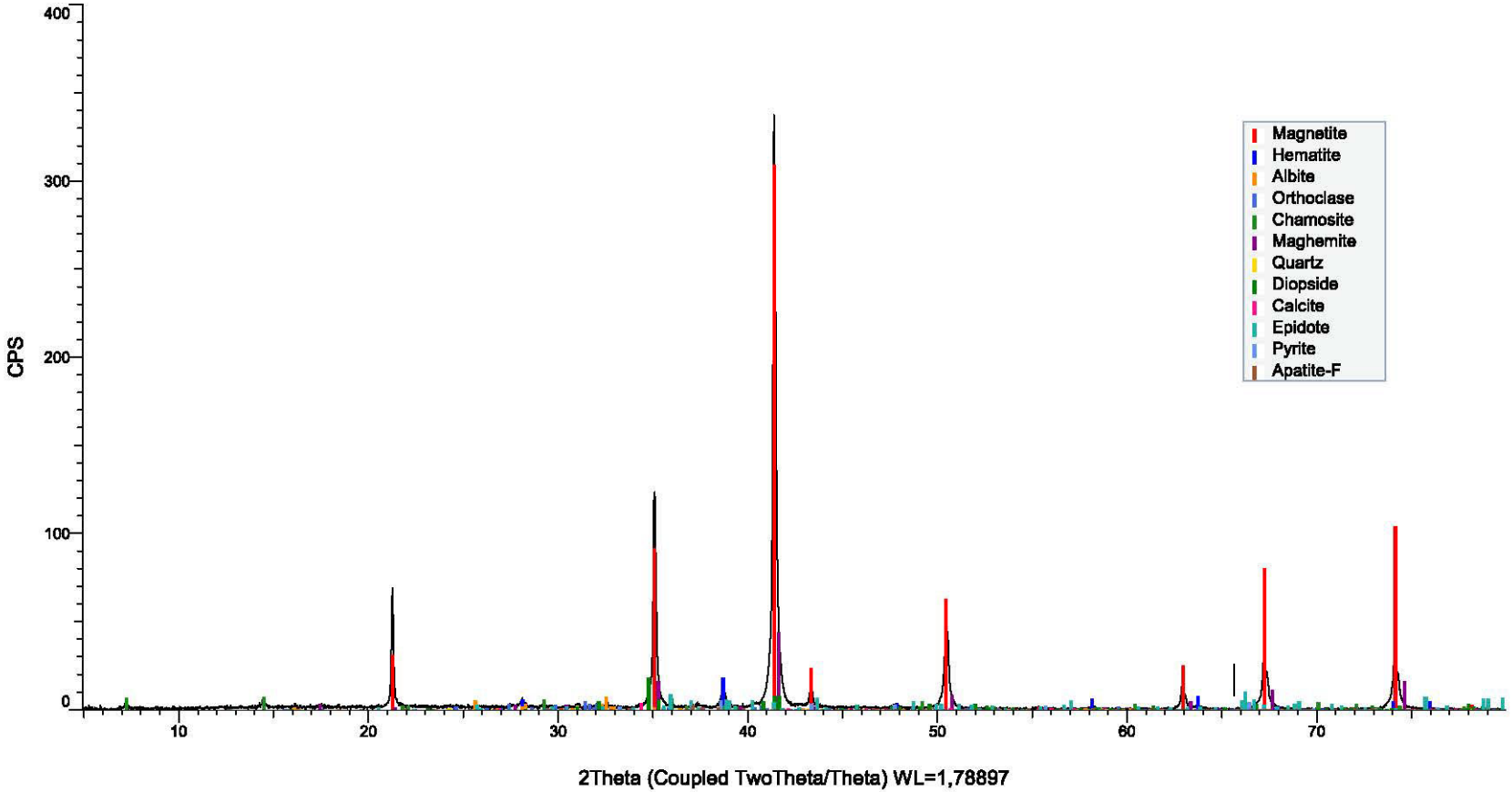

Fig. C.1 – Qualitative mineralogical composition of sample 1 through X-ray diffraction.

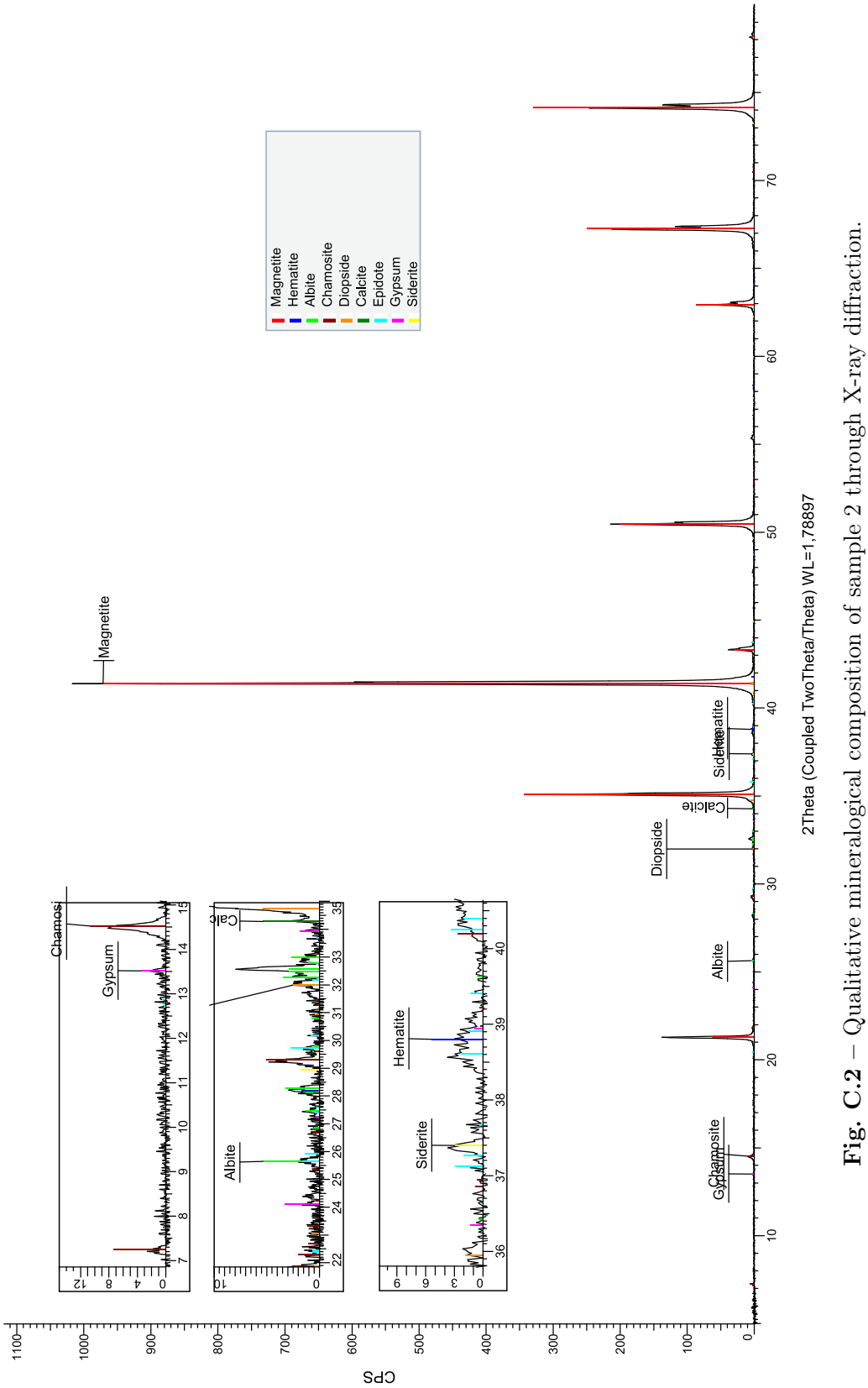

Fig. C.2 – Qualitative mineralogical composition of sample 2 through X-ray diffraction.

Appendix D

Locked cycle tests data

D.1 Locked cycle 1

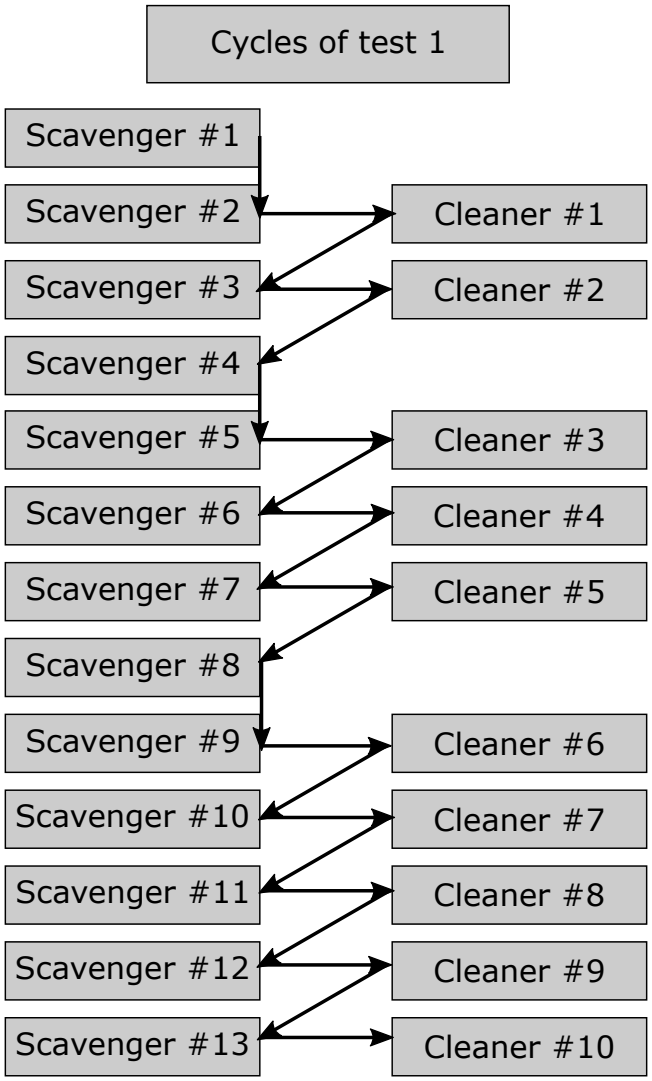

Fig. D.1 – Locked cycle 1 order of flotation test cycles.

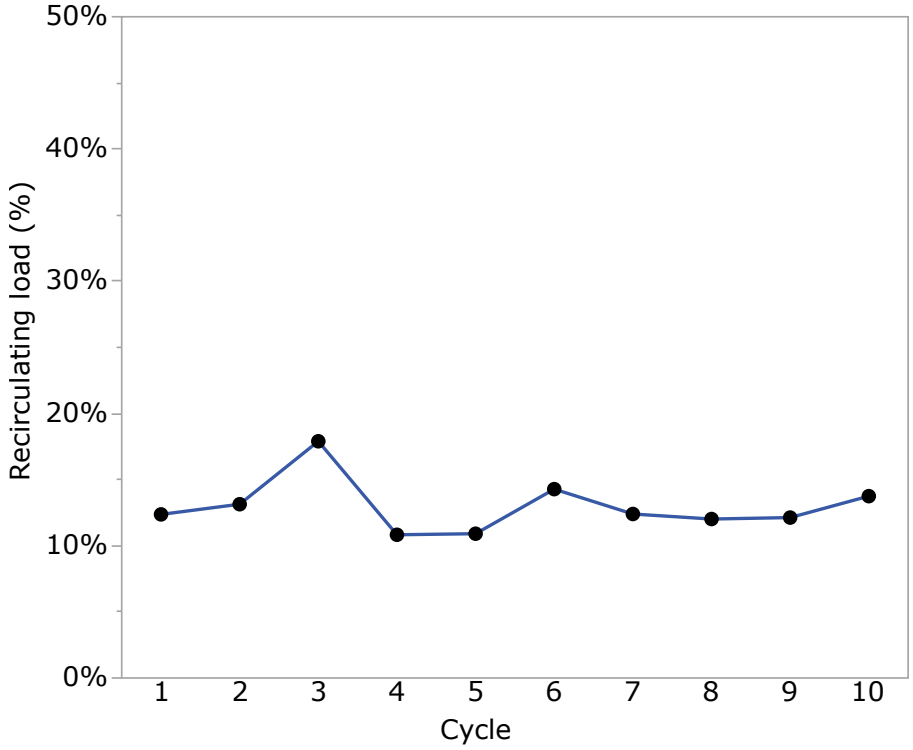

Fig. D.2 – Locked cycle 1 recirculated mass stabilization for cleaner stage.

D.2 Locked cycle 2

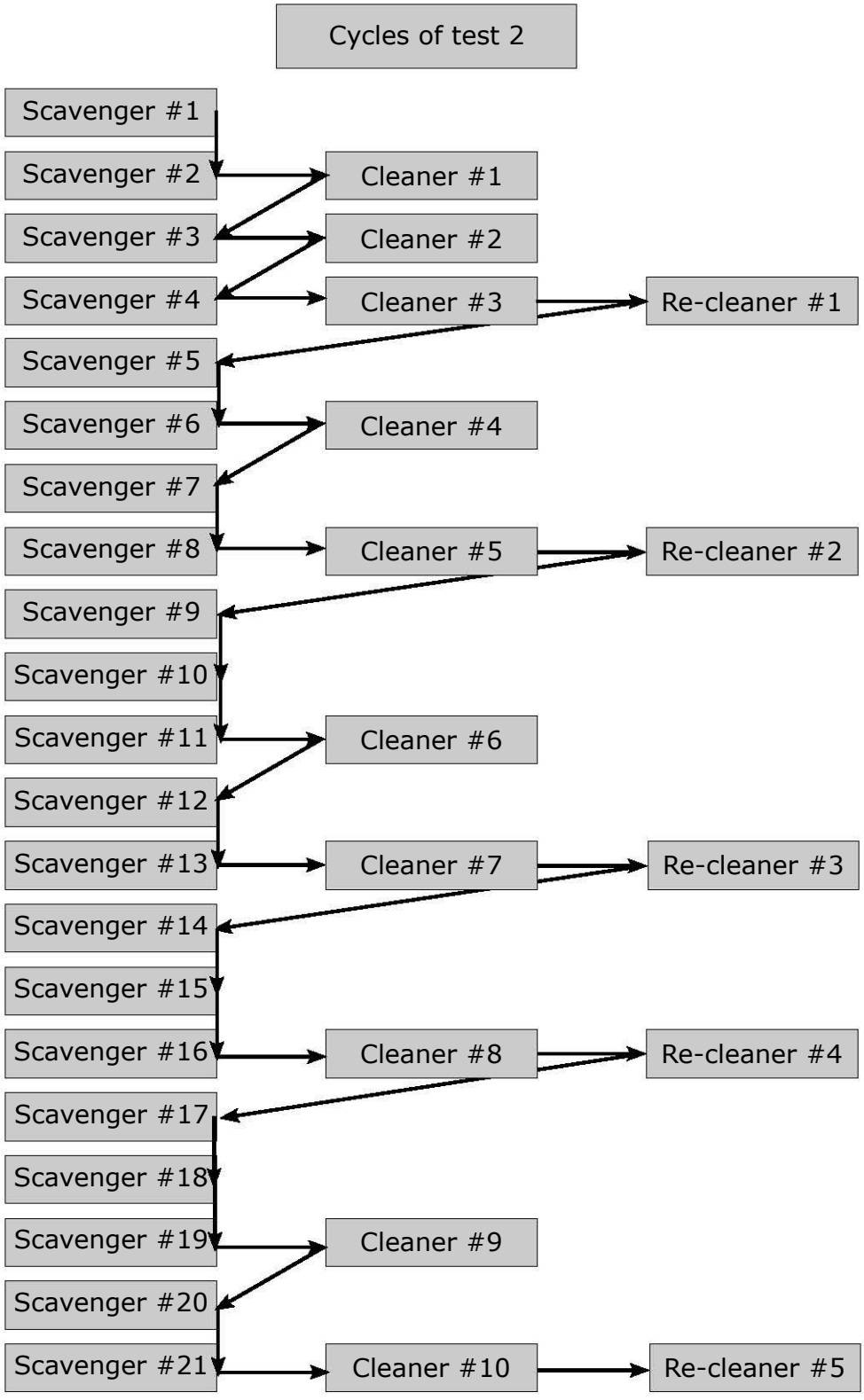

Fig. D.3 – Locked cycle 2 order of flotation test cycles.

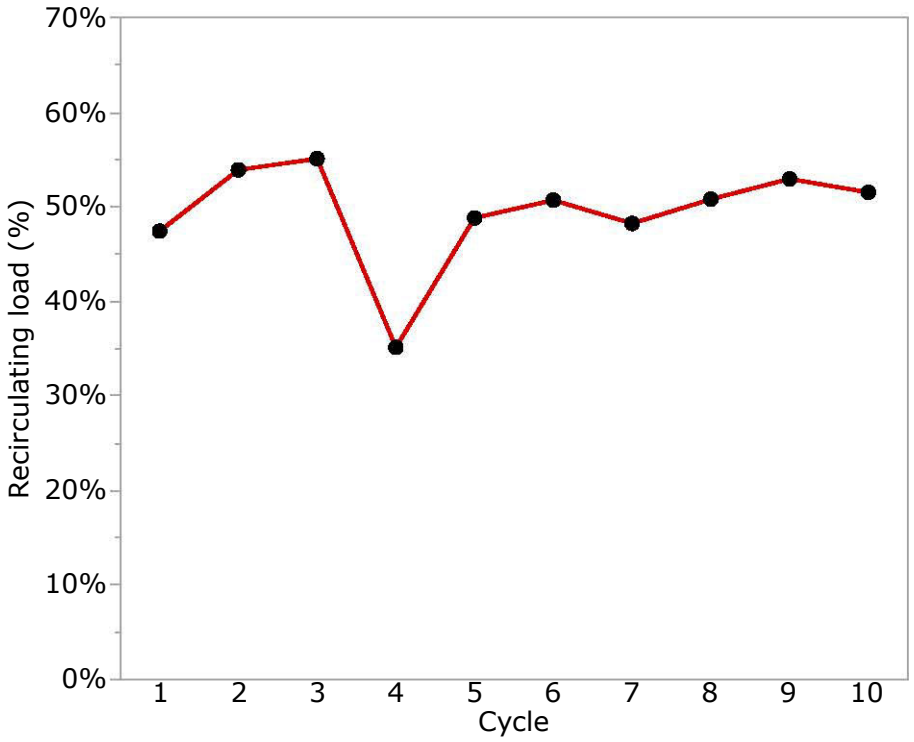

Fig. D.4 – Locked cycle 2 recirculated mass stabilization for cleaner stage.

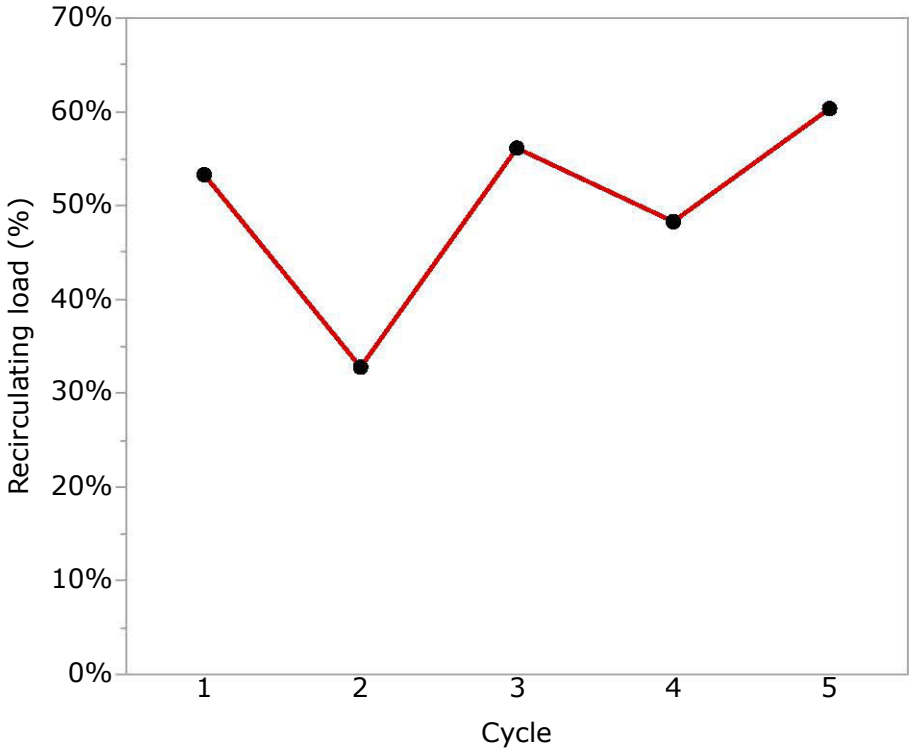

Fig. D.5 – Locked cycle 2 recirculated mass stabilization for re-cleaner stage.

Appendix E

Value creation study cash flow

Project cash flow													
Year	**2020**	**2021**	**2022**	**2023**	**2024**	**2025**	**2026**	**2027**	**2028**	**2029**	**2030**	**2031**	**2032**
Earnings	0	0	37,185,794	37,185,794	37,185,794	37,185,794	37,185,794	37,185,794	37,185,794	37,185,794	37,185,794	37,185,794	0
Operational costs	0	0	-5,332,492	-5,332,492	-5,332,492	-5,332,492	-5,332,492	-5,332,492	-5,332,492	-5,332,492	-5,332,492	-5,332,492	0
Maintenance	0	0	-375,300	-375,300	-375,300	-375,300	-375,300	-375,300	-375,300	-375,300	-375,300	-375,300	0
Lost of production	0	0	-14,240,000	-14,240,000	-14,240,000	-14,240,000	-14,240,000	-14,240,000	-14,240,000	-14,240,000	-14,240,000	-14,240,000	0
EBITDA	0	0	17,238,002	17,238,002	17,238,002	17,238,002	17,238,002	17,238,002	17,238,002	17,238,002	17,238,002	17,238,002	0
Depreciation	0	0	-1,356,040	-1,356,040	-1,356,040	-1,356,040	-1,356,040	-1,356,040	-1,356,040	-1,356,040	-1,356,040	-1,356,040	0
Base for taxes	0	0	17,238,002	15,881,962	15,881,962	15,881,962	15,881,962	15,881,962	15,881,962	15,881,962	15,881,962	15,881,962	-1,356,040
Taxes	0	0	-4,654,261	-4,288,130	-4,288,130	-4,288,130	-4,288,130	-4,288,130	-4,288,130	-4,288,130	-4,288,130	-4,288,130	366,131
Social outcomings	0	0	0	0	0	0	0	0	0	0	0	0	0
Investiments	-668,000	-19,288,500	0	0	0	0	0	0	0	0	0	0	0
Other deductions	0	0	0	0	0	0	0	0	0	0	0	0	0
De-investiments	0	0	0	0	0	0	0	0	0	0	0	0	0
Agregaded value	-668,000	-19,288,500	12,583,742	12,949,872	12,949,872	12,949,872	12,949,872	12,949,872	12,949,872	12,949,872	12,949,872	12,949,872	366,131
Total	-668,000	-19,288,500	-7,372,758	5,577,114	18,526,986	31,476,859	44,426,731	57,376,603	70,326,476	83,276,348	96,226,220	109,176,093	109,542,224

Fig. E.1 – Cash flow for the implementation and operation of fine screening and reverse cationic flotation of silicates.

The challenges of multi-mineral assemblages in the reverse cationic flotation of iron ores

Abstract

Iron ore is the main raw material for the steel production and generally it must be processed to reach the specifications required by the steel industry. The iron ore mining industry is now facing increasingly lean-grade deposits with complex mineral assemblages. This study addresses the upgrade of a magnetic concentrate from Peña Colorada mine in Mexico by reverse cationic flotation. Peña Colorada deposit is an iron skarn with an average iron content of 36%. It is composed by several mineral phases that were identified in a detailed mineralogical characterisation programme. Iron-bearing silicates such as chamosite and epidote are the problematic minerals to draw attention to. They present certain properties that are like the iron oxides. The current processing of this ore is made by magnetic separation and yet the silica content of the final concentrate remains between 4 and 5%, too high for the upstream process. Traditional techniques like magnetic separation or gravity separation are not capable to promote further separation. The intrinsic properties of these minerals do not have enough contrast and the liberation is reached only at micrometre sizes. Flotation is proposed in this study as a technique capable of playing with those properties to make this separation possible. The surface chemistry study of the minerals coupled with comparative adsorption isotherms with depressants, has shown that corn starch does not promote selectivity for such a complex iron ore, adsorbing on all minerals. The testing of alternative depressants highlighted humic acid as a viable depressant to sponsor the required level of selectivity in the separation by flotation. Micro-flotation experiments with pure minerals show that chamosite behaves very similar to iron oxides, not presenting good floatability with amines, like the other two silicates. Bench flotation tests with a material previously screened at 53 µm leads to a high-quality concentrate with 1.82% of silica and 84% of iron recovery, when humic acid is selected as depressant. Locked cycle tests trying to simulate a continuous process gave an excellent response of a concentrate with 2.78% of silica and 85% of iron recovery, with an altered natural polysaccharide as depressant. Pilot tests also confirmed the feasibility of the method with a concentrate with 2.06% of silica content and 64% of iron recovery, that should be improved by the addition of more scavenger stages. The use of column flotation for this stage is entirely possible, considering that its tests indicated a high iron recovery of 96%. A concentration route combining fine screening at 53 µm and reverse cationic flotation of silicates using alternative depressant as humic acid or altered natural polysaccharides has proven to be effective in achieving the desired quality levels for the iron concentrate at high iron recovery levels. Finally, molecular modelling identified that the strange behaviour of chamosite is mainly because it is less hydrophilic than the other minerals involved in flotation.

Keywords – Iron ore, iron-bearing silicates, flotation, depressants, humic acid

Les défis des assemblages multi-minéraux dans la flottation cationique inverse des minerais de fer

Résumé

Le minerai de fer est la principale matière première utilisée dans la production d'acier et doit en général être traité de manière à répondre aux spécifications requises par l'industrie de l'acier. L'industrie du minerai de fer fait désormais face à des gisements de plus en plus pauvres avec des assemblages de minéraux complexes. L'objective de cette étude est de valoriser un concentré magnétique de la mine de Peña Colorada (Mexique) via flottation cationique inverse. La mine de Peña Colorada est un gisement de type skarn ayant une teneur moyenne en fer de 36%. Il est composé de plusieurs phases minérales identifiées dans un programme détaillé de caractérisation minéralogique. Les silicates de fer tels que la chamosite et l'épidote sont les minéraux les plus problématiques car ils présentent certaines propriétés proches des oxydes de fer. Le traitement actuel de ce minerai se fait par séparation magnétique et pourtant la teneur en silice du concentré final reste comprise entre 4 et 5%, ce qui est trop élevé pour le traitement en amont. Les techniques traditionnelles telles que la séparation magnétique ou la séparation par gravité ne peuvent pas entrainer une séparation plus poussée. Les propriétés physiques de ces minéraux associés à la libération fine, atteinte seulement au niveau du micromètres, n'ont pas assez de contraste pour que cette séparation aye lieu. La flottation est proposée dans cette étude comme une technique capable de jouer plus finement avec ces propriétés pour rendre cette séparation possible. L'étude de la chimie de surface des minéraux, associée à des isothermes comparatifs d'adsorption avec des déprimants, a montré que l'amidon de maïs ne favorise pas la sélectivité pour un minerai de fer aussi complexe, puisqu'il s'adsorbe sur tous les minéraux. L'essai de déprimants alternatifs a montré que l'acide humique était un déprimant viable permettant de garantir le niveau de sélectivité requis dans la séparation par flottation. Des expériences de micro-flottation avec des minéraux purs montrent que la chamosite se comporte de manière très similaire aux oxydes de fer, ne présentant pas de bonnes capacités de flottabilité avec les amines, comme les deux autres silicates. Les tests de flottation à l'échelle du laboratoire avec un matériau préalablement tamisé à 53 µm conduisent à un concentré de haute qualité avec 1,82% de silice et 84% de récupération de fer, lorsque l'acide humique est sélectionné comme déprimant. Des essais en circuit fermé (locked cycle test) tentant de simuler un processus continu ont donné une excellente réponse d'un concentré contenant 2,78% de silice et 85% de récupération de fer, avec un polysaccharide naturel modifié comme déprimant. Des essais pilotes ont également confirmé la faisabilité de la méthode avec un concentré contenant 2,06% de silice et 64% de récupération de fer, ce qui devrait être amélioré en ajoutant davantage d'étapes d'épuisage. L'utilisation de la flottation en colonne pour cette étape est tout à fait possible, étant donné que ses tests ont indiqué une récupération de fer élevée de 96%. Une voie de concentration combinant un tamisage fin à 53 µm ainsi qu'une flottation cationique inverse des silicates en utilisant un déprimant alternatif comme l'acide humique ou des polysaccharides naturels modifiés s'est révélée efficace pour atteindre les niveaux de qualité souhaités pour le concentré de fer à des taux de récupération élevés. Enfin, la modélisation moléculaire a révélé que le comportement particulier de la chamosite est principalement dû au fait qu'elle est moins hydrophile que les autres minéraux impliqués dans la flottation.

Mots-clés – Minerai de fer, silicates de fer, flottation, déprimants, acide humique